UNIVERSITY OF BIRMINGHAM

Development of Fluorophore-Tagged DNA Probes for Cellular Imaging Applications

Rosemary Anne Bamford

A thesis submitted to the University of Birmingham for the degree of Doctor of Philosophy

School of Chemistry

College of Engineering and Physical Sciences

The University of Birmingham

October 2015

Contents

Acknowledgments

Thank you to my supervisor Prof. Jim Tucker for giving me the opportunity to work in his group. I appreciate all the help and support he gave me. I always enjoyed the discussions and his unwavering enthusiasm.

Thank you to Prof. Roy Bicknell for welcoming me into his group. I thank him for all the support and interesting discussion.

Thank you to Prof. Gerard Nash for all the help and (brutal) honesty. Thank you to Dr. Vicky Heath for help throughout but especially with the plasmid studies.

I also thank my other supervisors Dr. John Wilkie, Dr. Hamid Dehghani and mentor Prof. Chris Thomas. I thank Prof. Mike Hannon in PSIBS; Dr. Iain Styles for computational help and Dr. Neil Hotchin for microinjection assistance.

Thank you to analytical staff in Chemistry (Dr. Chi Tsang and Dr. Jonathon Snelling) and Dr. Rob Shaw for microscope assistance.

I am thankful for all the support from those in PSIBS, especially my academic buddy Ting. Special thanks to David and Ryan for all the discussion, collaboration and for keeping me grounded. I thank all my PSIBS project students.

I thank all past and present members of Tucker group- Gemma, James, Jack, John, Jean-Louis, David, Haydn, Huy, Jon, Antoine, Pete, Holly, Andrea, Michel and the Nina sequence. I particularly thank Simon who was a fantastic project student. I thank all past and present members of the Bicknell group.

Thank you to all the friends who have helped me along the way: Emma, Katherine, Sanaz, Mike, Matt and lunch club.

I thank my family (Mum, Dad, Granny, Catriona and Jack) for all their love and support.

Finally, I would like to thank John for his love and encouragement throughout; I couldn't have done it without you. Well, maybe I could have but it wouldn't have been so much fun.

Declarations

I declare that the work presented in this thesis is my own except where stated otherwise, and was carried out entirely at the University of Birmingham, during the period October 2011 to September 2014, under the supervision of Prof. Jim Tucker. The research reported here has not been submitted, either wholly or in part, in this or any other academic institution for admission to a higher degree.

Oligonucleotides were synthesised by members of the Tucker group: Dr. John Zhao, Gemma Bullen and James Carr-Smith.

Initial fluorescence and melting studies on DNA sensing in Chapter 3 were carried out by Dr. Jean-Louis Duprey and Gemma Bullen from the Tucker group. The DNA studies described in Chapter 3 were done as a repeat to verify the results in advance of comparing with RNA. The CDKN1A DNA studies, including anthracene probe synthesis and initial quantitative measurements, were carried out by Gemma Bullen.

The work in Chapter 4 and Appendix B is based on a paper accepted by PLOS ONE entitled 'Electroporation and microinjection successfully deliver single-stranded and duplex DNA into live cells as detected by FRET measurements' (DOI: 10.1371/journal.pone.0095097).

DNA synthesis and deprotection of DNA acridine probes in Chapter 5 was carried out by Dr. John Zhao and Ryan Brown. The design and production of the GMM algorithm was carried out by Ryan Brown (PSIBS Doctoral Centre).

The work in Chapter 7 and Appendix E was done in conjunction with MChem project student Simon Perry (project entitled 'Anthracene-based fluorescent oligonu-

cleotide probes for detection of single nucleotide polymorphisms').

Other contributions based on this thesis:

- The 10th Nucleic Acids Forum, July 2014, Poster presentation: *Delivery of single-stranded and duplex DNA into live cells as detected by FRET measurements*;
- XXI Round Table on Nucleosides, Nucleotides and Nucleic Acids, Poznan, Poland, August 2014, Poster presentation: *Ratiometric SNP sensing with an anthracene FRET probe.*

Abstract

Single nucleotide polymorphisms (SNPs) are single base variations in DNA which give genetic variation. However, SNPs can also be linked to the development of certain diseases. Modified oligonucleotides used to probe biological changes and processes have become an important focus of scientific research. Fluorescent tagging of DNA can be used to sense SNPs in DNA targets through differences in emission intensity on the formation of a duplex.

An anthracene-tagged DNA probe developed by Tucker *et al.* is able to discriminate between a fully complementary DNA target sequence and one with a single base difference. This thesis describes how SNP sensing with anthracene-tagged DNA has been extended to SNPs in RNA targets and sequences associated with Alzheimer's disease. A novel method of quantitative SNP sensing of heterozygous SNP targets is also described.

Current SNP detection methods often involve converting RNA extracted from cells into cDNA. In order to move towards detecting SNPs in biological samples, it would be advantageous to target RNA directly. This work describes the experimental and analysis steps involved in testing the anthracene-tagged DNA probes and their target sequences in fixed and living cells in order to achieve *in vitro* SNP sensing. Further investigation was carried out to target endogenous RNA expressed in cells using plasmids.

Cell delivery techniques were tested using fluorophore-tagged DNA which is capable of Förster resonance energy transfer (FRET) if the duplex is formed. Finally, a new dual fluorophore DNA probe was designed for SNP sensing via FRET.

Abbreviations

A	adenine
Amp	ampicillin
APS	ammonium persulphate
bp	base pair
BDF	base discriminating fluorophore
BSA	bovine serum albumin
C	cytosine
CD	circular dichroism
cDNA	complementary DNA
CHO	chinese hamster ovary
Cy3/5	cyanine 3/5
DEA	diethylamine
DIPEA	N,N-diisopropylethylamine
DMAP	N,N-dimethylaminopyridine
DMEM	Dulbecco's Modified Eagle's Medium

DMF	N,N-dimethylformamide
DMTr	dimethoxytrityl
DNA	deoxyribonucleic acid
dsDNA/RNA	double stranded DNA/RNA
E.coli	*Escherichia coli*
EDTA	ethylenediaminetetraacetic acid
EtOH	ethanol
ϵ	extinction coefficient
FACS	fluorescence-activated cell sorting
FBS/FCS	fetal bovine/calf serum
FISH	fluorescent *in situ* hybridisation
FRET	Förster resonance energy transfer
G	guanine
GMM	Guassian Mixture Modelling
HEK 293T	human embryonic kidney 293T
HBTU	O-Benzotriazole-N,N,N′,N′-tetramethyl-uronium-hexafluoro-phosphate
HPLC	high performance liquid chromatography
LB broth/agar	Luria Bertani broth/agar
LNA	locked nucleic acid
(ES)-MS	(electrospray)-mass spectrometry
mRNA	messenger RNA

MeOH	methanol
Me	methyl
miRNA	micro RNA
mM, μM, μl	millimole, micromole, microlitre
M	molar
MB	molecular beacon
MMT	monomethoxytrityl
nm, ns	nanometer, nanosecond
NMR	nuclear magnetic resonance
OD	optical density
ODN	oligodeoxynucleotide
PBS	phosphate buffered saline
PCR	polymerase chain reaction
PEI	polyethylenimine
PMT	photomultiplier tube
PNA	peptide nucleic acid
PSO	Particle Swarm Optimisation
qPCR	quantitative polymerase chain reaction
RCA	rolling circle amplification
RNA	ribonucleic acid
ROI	region of interest

RT	room temperature
SDS-PAGE	sodium dodecyl sulphate polyacrylamide gel electrophoresis
siRNA	short interfering RNA
SNP	single nucleotide polymorphism
ssDNA/RNA	single stranded DNA/RNA
T	thymine
TAE	tris base/acetic acid/EDTA
TB/TBE	tris/borate/EDTA
TBAF	tetra-n-butylammonium fluoride
TEA	triethylamine
TEAA	triethylammonium acetate
TEMED	tetramethylethylenediamine
T_M	melting temperature
U	uracil
UV-vis	ultraviolet-visible
λ	wavelength
λ_{ex}	excitation wavelength
λ_{em}	emission wavelength
w/v, v/v	weight/volume per volume
wt	wildtype

Chapter 1

Introduction

1.1 Nucleic acids

1.1.1 DNA and RNA

Deoxyribonucleic acid (DNA) is a nucleic acid that contains all the instructions for the make-up and functioning of all living organisms. DNA is a double helix formed of two strands bound by hydrogen bonds (Figure 1.1). The two DNA strands consist of nucleoside bases (Figure 1.2); the purines (adenine, guanine) and pyrimidines (cytosine, thymine). There are specific base pairing rules: adenine and thymine bind together by two hydrogen bonds; guanine and cytosine bind together by three hydrogen bonds (Figure 1.3). The nucleoside bases form bonds with deoxyribose sugars, which are held in place by a carbon-oxygen-phosphorus (phosphodiester) repeating scaffold which forms a polymer strand (Figure 1.4). The DNA double helix has a sugar-phosphate backbone, hence the outer surface of DNA is negatively charged. [1] In the double helix the nucleobases are nearly perpendicular to the backbone since they stack on top of each other. However, the stacked bases must twist, roll and slide in order to accommodate the helical twist and stay in direct π-π van der Waals contact with neighbouring bases. There are three main secondary structures for DNA double helices: A-DNA, B-DNA and Z-DNA

(Figure 1.5). The differences are largely based upon variations in the sugar pucker and helical twist. [2]

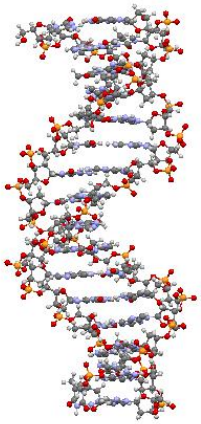

Figure 1.1: DNA oligonucleotide double helix.

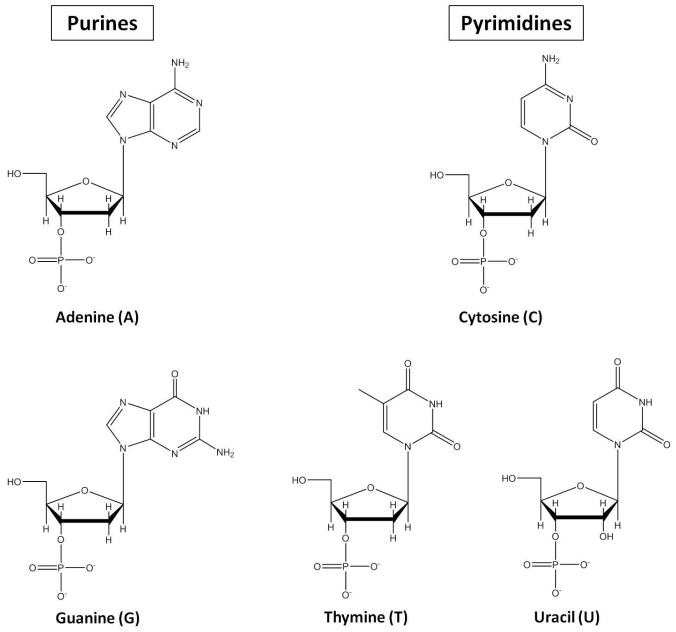

Figure 1.2: Nucleotides that occur naturally in the DNA and RNA.

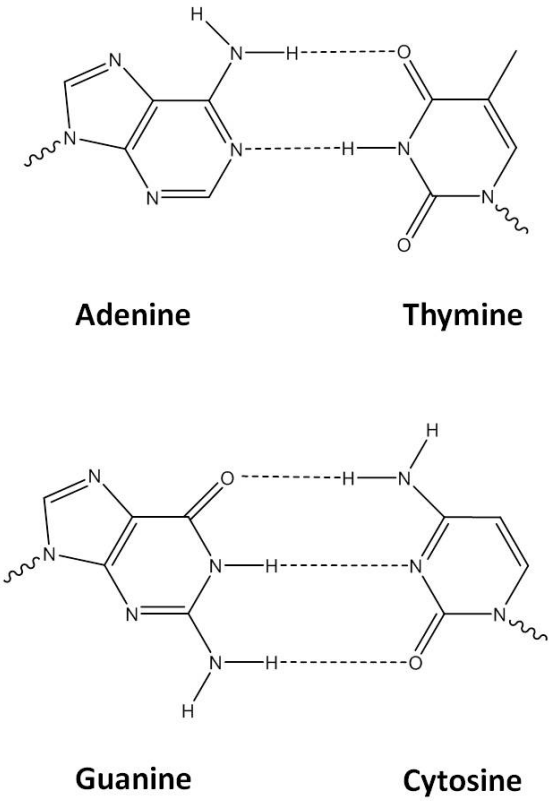

Figure 1.3: Hydrogen bonding between base pairs.

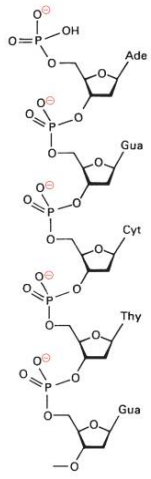

Figure 1.4: Phosphodiester bonds forming the backbone of DNA. [2]

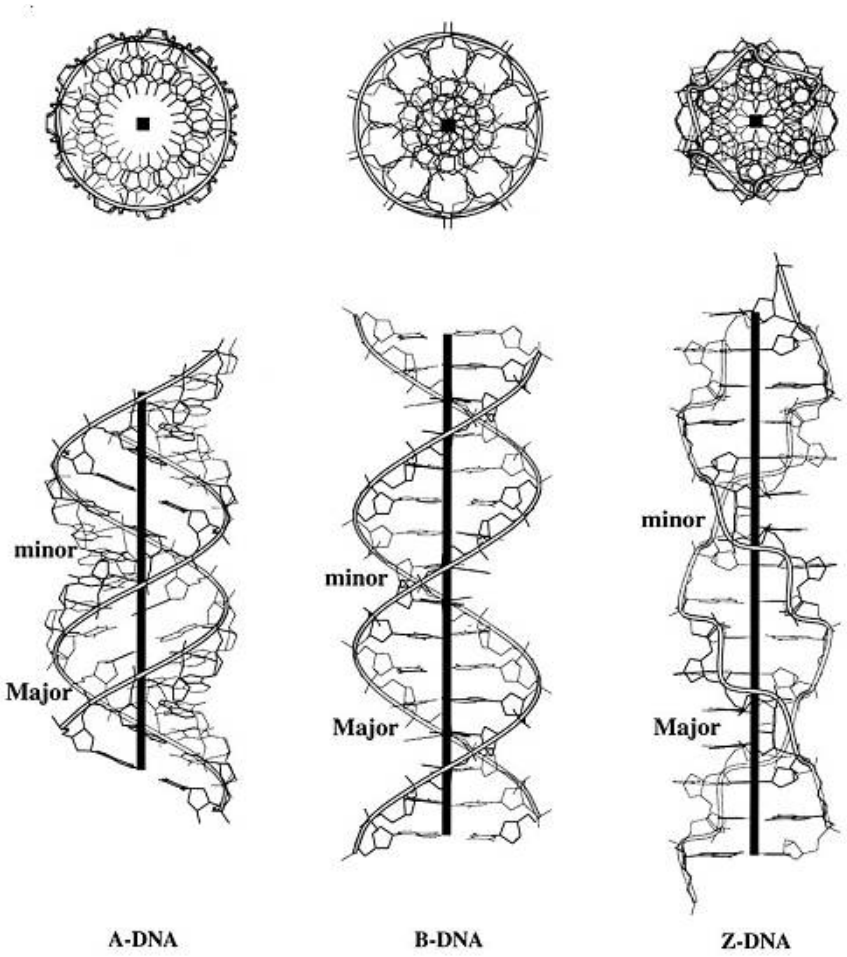

Figure 1.5: Secondary structures of DNA duplexes. Image adapted from 3DNA, http://x3dna.org

Ribonucleic acid (RNA) differs from DNA in three ways: RNA is mainly single-stranded; contains uracil instead of thymine bases and features an extra 2′-hydroxyl group. The presence of the 2′-hydroxyl group causes RNA helices to adopt the A-DNA conformation. Base-pairing rules apply to RNA: adenine and uracil bind together by two hydrogen bonds; guanine and cytosine bind together by three hydrogen bonds.

The stability of duplexes is RNA:RNA > RNA:DNA > DNA:DNA, although stability is also sequence dependent. [3] DNA is generally more stable in comparison to

RNA, especially upon duplex formation, due to the presence of the 5-methyl group on thymine.

Whilst DNA and RNA can be synthesised in a lab environment, nucleic acids should also be considered in the natural setting of cells (Figure 1.6). Each cell nucleus contains two copies of DNA, one originating from each parent. DNA sequences coding for specific genes are transcribed in the cell nucleus to yield heterogeneous nuclear RNA. Primary RNA transcripts are processed into mature RNA, which are then exported to the cytoplasm. Ribosome-based protein synthesis takes place and the proteins are used for the structure, function and regulation of the body's tissues and organs. A 'mistake' in any part of this process or components can have serious consequences.

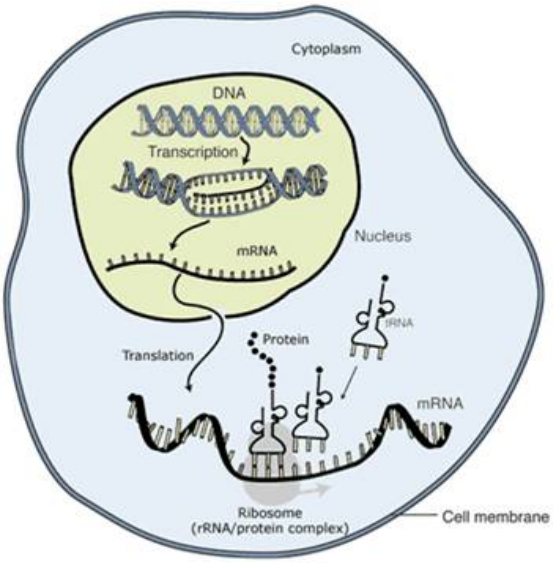

Figure 1.6: Schematic diagram of cell processes. Image adapted from National Human Genome Research Institute.

1.1.2 Modified nucleic acids

The fundamental structure of DNA can be modified in terms of the backbone, bases and sugar. Modifications are usually purpose-driven, for example, to impart nuclease-resistance or for electrochemistry.

Nucleotide modifications

Locked nucleic acids (LNA) are nucleotide analogs that contain an ethylene linkage between the 2' oxygen and the 4' carbon of the ribose ring (Figure 1.7). They generate the most stable hybrids measured with RNA (10 °C per modification. [4]) This may allow LNA oligonucleotides to hybridise with complex RNA structures plus they possess high nuclease resistance. [5]

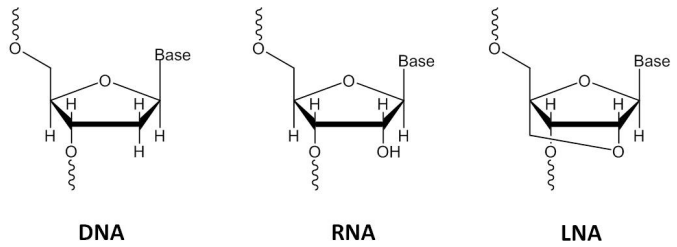

Figure 1.7: Schematic representation of the sugar chemical structure adopted by DNA, RNA and LNA monomer.

Nucleoside modifications

Saito and co-workers introduced base-discriminating fluorescent (BDF) nucleosides, designed primarily for SNP analysis. [6] This is carried out by attaching a BDF to the complementary section of the DNA proximal to the SNP site and measuring the subsequent modified output. Further fluorescent nucleoside analogs are described in a review by Sinkeldam *et al.* [7]

Nucleobase modifications

An example of a nucleobase analog is the 7-aminoquinazoline-2,4-(1*H*,3*H*)-dione which is incorporated into a DNA oligonucleotide and senses mismatched pairing by displaying G-specific fluorescence enhancement. [8] This is particularly impressive since most fluorophores are quenched in proximity to guanine residues. They suggest the key is to introduce a heterocycle which is similar to native nucleobases and are capable of Watson-Crick pairing. Further to that, a red-shifted absorption spectra relative to native nucleosides, permitting selective excitation, is highly desirable.

Sugar modification

2′OMe RNA has an extra methyl group on the 2′ position compared to RNA. It is a naturally occurring modification found in RNA which has increased binding affinity to RNA target since the 2′OMe modified ribose sugars prefer to adopt a C3'-endo conformation. [9] 2′OMe RNA is popular for cell studies since it has increased nuclease stability. They also bind well to regions of dsRNA, and therefore may have the ability to efficiently hybridise to folded RNA in living cells. [10] There are studies into the potential therapeutic benefits of 2′-O-alkyl oligoribonucleotides. [11]

Popular modifications, such as streptavidin, are to prevent probes migrating to the nucleus and to help uptake by cells. [10] The most common modification to oligonucleotides is the addition of fluorophores. Fluorescence is a powerful tool that can allow oligonucleotides to be tracked and interactions be monitored. [12–14] Oligonucleotides with a covalently bound fluorophore inserted within its sequence can exhibit different fluorescence properties depending on whether the DNA is single stranded, duplexed to a matching or mismatching sequence. [6–8, 15, 16] For example, thiazole orange (TO) is a popular choice of fluorophore modification for oligonucleotides. [17–20] TO is popular for two reasons; first it fluoresces only upon hybridisation (intercalates between base pairs), and second, unlike many other fluorophores, its fluorescence is not greatly quenched by

nearby guanine bases.

Fluorophores do not have to be covalently attached to the nucleic acid backbone to enable sensing with oligonucleotide-based probes. Alternative binding modes include intercalation, groove-binding, end-stacking or electrostatic interactions. In most cases, the fluorophores are non-emissive unless bound to DNA. Common examples include ethidium bromide, SYBR Green I and DAPI. [21]

Förster resonance energy transfer (FRET) is the nonradiative transfer of excitation energy between distinct chromophores, typically referred to as donors and acceptors. [22] This results in either an increase in fluorescence intensity or quenching, which is the loss of fluorescence intensity. There are many literature examples of FRET and quenching being utilised in nucleic acid studies. [23–28] Chapter 4 describes FRET in further detail.

Backbone modification

Xeno nucleic acid (XNA) is the general term for synthetic alternatives to DNA or RNA. [29, 30] Peptide nucleic acids (PNA) have peptide rather than sugar-phosphate backbones (Figure 1.8). Therefore, unlike DNA, PNA have a neutral-charged backbone. PNA are good candidates for targeting RNA in living cells because they have been shown to form extremely stable hybrids with complementary DNA as well as RNA. However, PNA is a rigid molecule and therefore expected to have poor access to highly folded RNA structures, precluding hybridisation to complementary structures. [31] Seitz *et al.* has utilised PNA probes for sensing with huge effect, in/out of cells and with DNA/RNA targets (further discussed in Section 1.5).

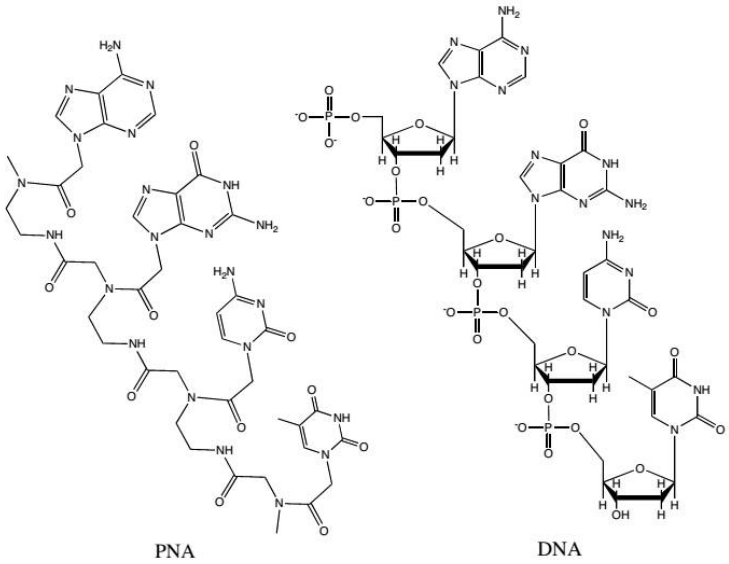

Figure 1.8: Comparison between PNA and DNA backbones. Image adapted from [32] and [33].

FcNA is a new metal-based DNA where the sugar-phosphate-sugar unit is replaced with a synthetic ferrocene nucleic acid mimic (Figure 1.9).

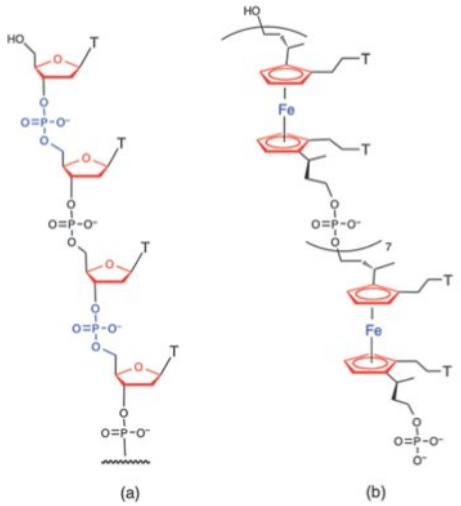

Figure 1.9: The structure of (a) DNA (b) a form of FcNA, $(Fc\text{-}TT)_8$, where T represents the nucleobase thymine. [34]

The redox properties of ferrocene can provide useful electrochemical behaviour

for probing binding mechanisms of various biologically relevant analytes such as proteins, DNA, RNA and metals. Additionally the binding strength can be controlled by manipulating the redox state of these metallocene nucleic acid motifs. [34, 35] A further review of biorganometallic nucleic acid chemistry can be found. [36]

1.2 Oligonucleotide Synthesis and Characterisation

Chemists have been able to develop oligonucleotide synthesis in order to produce high yields of pure DNA in the lab. An oligonucleotide is a short single-stranded chain consisting of a number of nucleoside units linked together by phosphodiester bridges. Generally, in oligonucleotide synthesis, phosphodiesters are formed between a $3'$-hydroxyl group bearing a phosphate derivative and a $5'$-hydroxyl group of another nucleoside. [2] Phosphoramidite oligonucleotide synthesis has inherently high coupling efficiency and stable starting materials. Synthesis always begins on the $3'$ and usually on a solid support. RNA and modified oligonucleotide synthesis have added complications and often require more protecting groups to prevent side-reactions. Further details can be found in Chapter 2.

Oligonucleotides are commonly characterised by HPLC and mass spectrometry. High performance liquid chromatography (HPLC) purifies oligonucleotides by separating a mixture using a buffer gradient on a column. Mass spectrometry measures the mass-to-charge ratio of a sample in order to determine the content. An alternative method of purification is gel electrophoresis, which separates DNA, RNA and proteins based on size and charge.

Gel electrophoresis can also be used as a method of studying interactions since it can distinguish between double-stranded and single-stranded oligonucleotides (native gel). Alternatively, secondary structure can be lost and constituents be analysed (denaturing gel). The latter is useful for analysing digested samples.

Oligonucleotides have a strong absorption spectra and concentration can be calculated from it. UV-vis melting studies involve monitoring absorption over a range of temperatures (several ramps). The transition between double and single stranded DNA can be observed since the absorption of single stranded DNA is greater (Figure 1.10). The point where 50% of DNA is single and double stranded is known as the melting temperature (T_M). Melting temperatures allow the stability of oligonucleotides to be quantified.

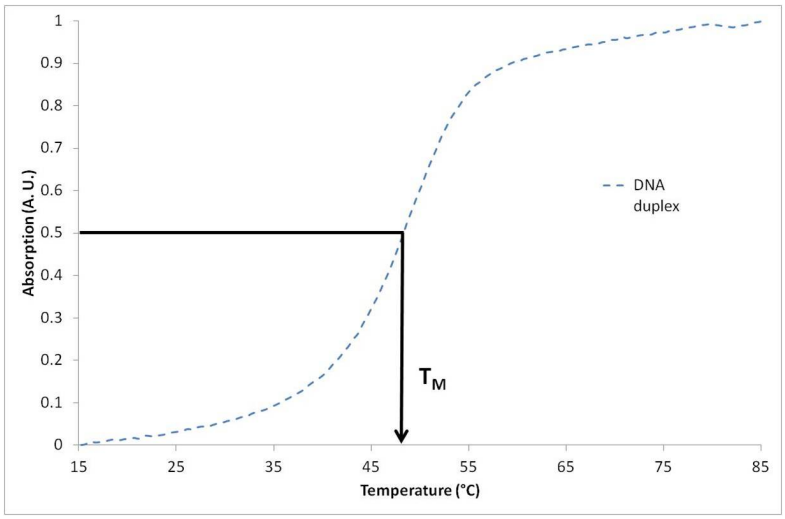

Figure 1.10: UV-vis melting study of a duplex structure transitioning to single strands. The black line represents the point where the absorption is 0.5 i.e. 50% of the DNA is single-stranded and 50% is double-stranded. This absorption is defined as the melting temperature (T_M).

Fluorophore-tagged oligonucleotides can be tested using steady-state fluorescence spectroscopy. This means that upon excitation of a chromophore (typically at its absorption maximum) with a light source providing a constant photon flow, an emission spectrum is recorded, revealing the energy maximum and intensity of emission. [7] The quantum yields of the tagged oligonucleotide can also be measured. The quantum yield of a radiation-induced process is the number of times a specific event occurs per photon absorbed by the system. The event in this case is fluorescence. It can also be described

as the emission efficiency of a fluorophore. Although steady-state measurements are useful in detecting changes in fluorescence intensity, their spectra give an average emission profile of all excited fluorophores present in the sample. Therefore, this technique cannot distinguish between individual fluorophores found in a heterogenous population, such as those associated with different conformational states. Time-resolved measurements give excited state lifetimes and insight into decay pathways of excited chromophores. Like steady-state, time-resolved fluorescence spectroscopy also gives an averaged profile of the excited chromophores in a sample. With deconvolution, however, it is possible to resolve more than one decay pathway, each of which represents an average across a population. Section 7.5 discusses time-resolved measurements in the context of fluorophore-tagged oligonucleotides. Other fluorescent measurement techniques exist such as fluorescence anisotropy and microscopy. [7]

The structure of oligonucleotides can be studied using circular dichroism (CD). Optically active matter absorbs left and right hand circular polarised light slightly different. Right circular polarised light absorption is subtracted from left circular polarised light absorption as a function of wavelength. Therefore the overall signal can be positive or negative. The CD signal of DNA is not a sum of the CD spectra of the bases, but is influenced by the 3D structure of the DNA. The benefits of CD that it requires very little sample; non-destructive; and effects such as pH, denaturants, temperature on the structure can be monitored. The drawbacks include solvent absorption interference in the UV region and few buffers are non-absorbing below 200 nm. [37]

Additional techniques to study oligonucleotides include modelling, nuclear magnetic resonance (NMR) and electrochemistry.

1.3 Single Nucleotide Polymorphisms (SNPs)

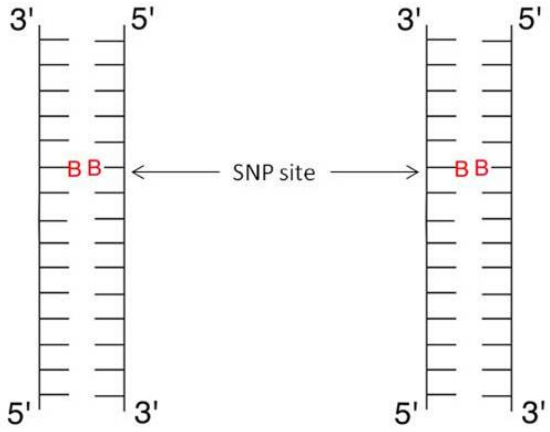

Figure 1.11: Schematic example of SNPs in DNA.The majority of SNPs in humans are bi-allelic, which means for one base pair there could be two combinations. One or more of these combinations can be associated with the development of a disease.

Each cell contains two copies of DNA called alleles; one from each parent. In some regions, or for particular bases, the two alleles can be the same or different (Figure 1.11). This is referred to as homozygous or heterozygous respectively. The allelic contribution varies, which has an impact on human development and characteristics. For two people, >99% of their DNA sequence is the same, with variations occurring every 1000 bases in at least 1% of the population. [38] Single nucleotide polymorphisms (SNPs) are natural variations of a single base within the genome and are chiefly responsible for genetic diversity across the population. [39–41] SNPs are wide-ranging, and stable which makes them exploitable for use in DNA research. [42] Although SNPs are beneficial in terms of gene variation they are linked to diseases that have a genetic component (e.g. cancer [43, 44] and Alzheimer's disease [45, 46]). SNPs are not thought to cause disease directly but increase the likelihood of a person developing the disease. [47] For example, there are three versions of a gene (allele) that codes for a protein associated with Alzheimer's

disease development; the two with SNPs increase the likelihood of the disease developing. Therefore, it is of great interest to identify SNPs since they are molecular markers for genetic diseases. [48] The majority of SNPs in humans are bi-allelic, which means for one base pair there could be two combinations. The purines can either switch to the other purine, and the same for pyrimidines. This is called transition. The alternative is a purine switching to a pyrimidine and vice versa. This is called transversion. Two thirds of human SNPs are of the transition variety, even though there is more opportunity for a transversion to occur. [41]

In addition, there are insertion and deletion polymorphisms which cause a great deal of genetic diversity. [49, 50] Base modifications, known as epigenetic changes, are also commonly found in the genome. [51] Cytosine methylation at the 5 position is a common epigenetic modification, but if misregulated can result in hyper- and hypomethylated sites, which are associated with cancer development. [44] The newly detected 5-hydroxymethylcytosine is also causing interest in genetic studies. [52] A final example of a mutation is the conversion of guanine to 7,8-dihydro-8-oxoguanine (8-oxoG). This causes DNA polymerase into base-pairing adenosine with 8-oxoG instead of its expected cytosine base, since 8-oxoG mimics thymine. The subsequent guanine to thymine transversion mutation can increase susceptibility to diseases and ageing, but also as a biomarker for oxidative stress. [51]

1.3.1 Current SNP detection assays

Whole genome sequencing seems to be the answer to all SNP detection problems. Unfortunately, this technology is currently too expensive and time-consuming for the average patient. Therefore it has become important to develop a method that can detect SNPs without requiring sequencing of the entire genome.

Rapid methods for detecting single nucleotide polymorphisms (SNPs) are of importance to allow high throughput screening for genetic diseases. [40, 53] There is a high

level of interest in developing convenient methods for detecting and quantifying a specific sequence of DNA, in particular SNPs.

Engle *et al.* summarises common commercial techniques for detecting SNPs in the genome. [54] Interest lies particularly in fluorescence-based detection methods. [38] Fluorescence is a proven sensitive technique which is an effective reporter even at low concentrations ($< \mu$M). It requires relatively simple equipment and many fluorescent systems have been successfully commercialised. A selection of the most common SNP detection techniques currently available shall now be described.

HyBeacon probes

When the HyBeacon probe hybridises to its complementary target there is a measurable elevation in probe fluorescence emission (Figure 1.12). SNP sequences may be discriminated by measuring the melting temperatures (T_M) of various probe/target duplexes and exploiting the differences in T_M that exist between different duplexes. The signal is also allelic discriminatory since homozygous samples generate single melt peaks and heterozygous samples generate multiple peaks. The disadvantages of this system are that it requires heating and therefore could not be carried out *in vitro*. [55]

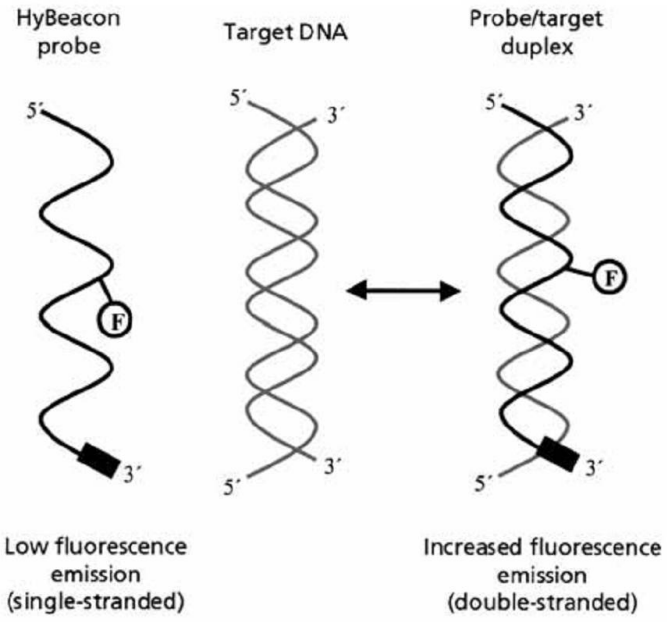

Figure 1.12: Schematic of HyBeacon probes and target detection. HyBeacons consist of oligonucleotide sequences with fluorophore moieties (F) attached to internal nucleotides and 3′-end blockers to prevent PCR extension. The fluorescence emission is greater on formation of duplexes, compared to single-stranded probes, allowing detection of target sequences. [55]

Binary probes

Binary probes consist of two oligonucleotides which must bind adjacent to one another on the target so that FRET can occur between the fluorophores attached to them respectively (Figure 1.13). [56, 57] By having two oligonucleotides which require binding in order to produce a fluorescent signal, this increases the sensitivity and specificity of the system. However, the hybridisation kinetics can be a lot slower. Sandwich probes have a similar concept to binary probes. Two quencher displacement reactions must take place on two probes, in order to allow the fluorophore in the centre probe to fluoresce. [58]

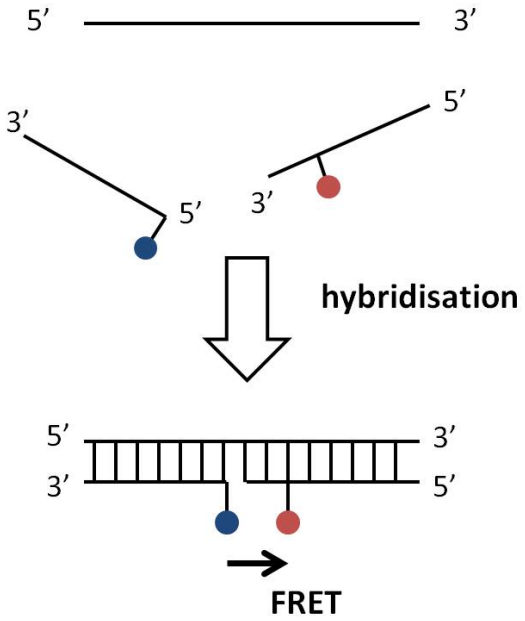

Figure 1.13: Schematic of binary probes target detection.

Molecular beacons

Molecular beacons (MB) are a popular choice for DNA and RNA detection. [59–62] They consist of an oligonucleotide which forms a stem loop with a fluorophore and quencher at either end of the strand (Figure 1.14). When MB's are in single stranded conformation, the fluorophore and quencher are in close proximity and the fluorescence signal is quenched. When in a duplex, the fluorophore and quencher are separated and fluorescence emission increases. MB's rely entirely on the thermodynamics of binding and are therefore not ideal for detecting minor changes in the DNA sequence such as SNPs. [63]

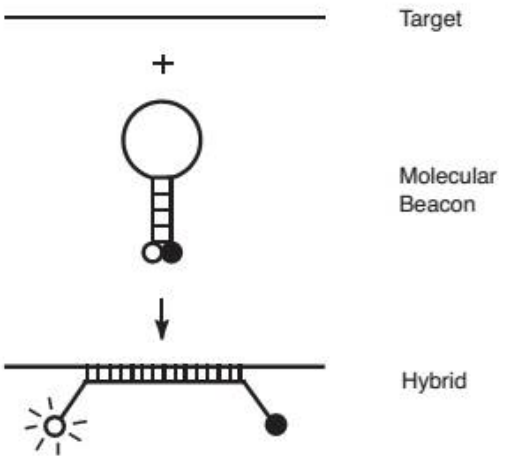

Figure 1.14: Schematic of molecular beacon probe target detection. The fluorescence is quenched until the MB opens to hybridise to its target. [59]

Polymerase Chain Reaction (PCR)

Before DNA detection takes place, there must be enough DNA for analysis. An important method in the field is polymerase chain reaction (PCR) which amplifies the specific region of DNA or RNA under investigation. Figure 1.15 gives the general cycle of PCR, which involves denaturing the DNA; annealing short strands of DNA called primers to each strand; heating the system to extend the primer along the template DNA using deoxynucleotides (dNTPs) and DNA polymerase to produce double-stranded DNA, and then the process repeats resulting in an exponential increase in product. This can also be carried out in real-time and quantitatively (RT-qPCR) using fluorophore-tagged primers. [64] PCR-based techniques are limited by the fidelity of reverse transcription. Although sensitive, PCR is time and labour intensive, and often error prone (1.3×10^{-4} - 3×10^{-6} error rate (errors/base)). [65, and references therein] A further requirement is that the original DNA/RNA is extracted and amplified outside of the cell. New developments with padlock probes and rolling circle amplification (RCA) have been described as PCR within the cell.

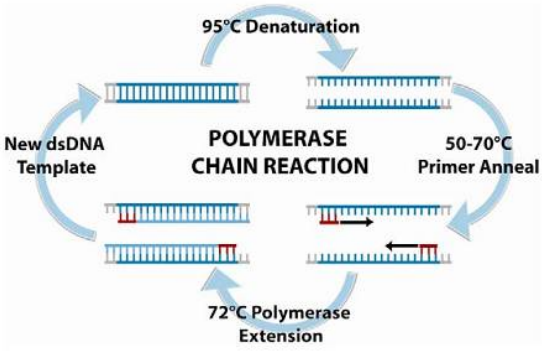

Figure 1.15: Schematic of the polymerase chain reaction. [66]

TaqMan probes

TaqMan® (Applied Biosystems) is a relatively cheap PCR based technique. Although used to monitor PCR in real time, TaqMan can be adapted for the analysis of polymorphisms. [67, 68] The TaqMan probe consists of an oligonucleotide, complementary to the sequence of interest, located directly over the SNP. A fluorophore is covalently attached to the 5′ and a quencher at the 3′. When the probe is intact, the proximity of the quencher to the fluorophore reduces the fluorescence signal observed. During PCR, as the forward primer extends, the target specific probe is degraded by the 5′-3′ exonuclease activity of the DNA Taq polymerase, releasing the fluorescence of the fluorophore. With each round of amplification, there is an exponential increase in the fluorescence intensity related to the accumulation of PCR product. Genotypes can be determined according to the ratio of fluorescence attributable to each fluorophore on allele-specific oligonucleotide probes, compared to controls. The TaqMan probe only binds when it is a fully matching system, and is temperature dependent. The disadvantages of TaqMan assays are that they are only suitable for genotyping one polymorphism at a time since there is a limit to the number of fluorophore probes that can be read at once. PCR clearly plays an important role in the TaqMan assay, however PCR in itself is error prone. [65]

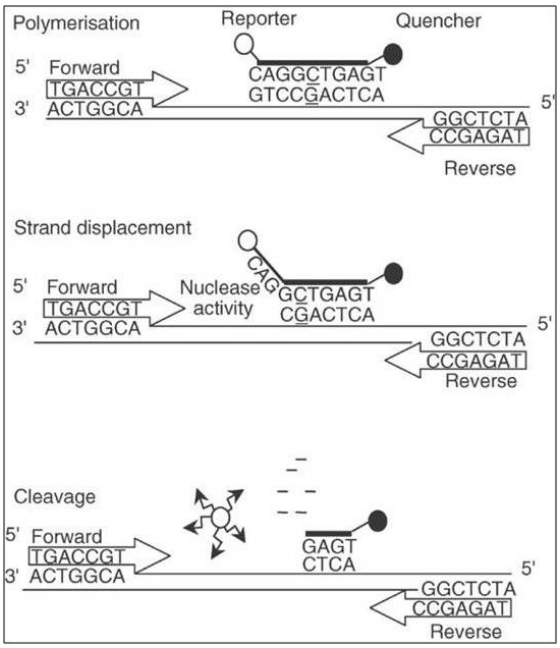

Figure 1.16: Schematic of TaqMan probe mechanism. [67]

Fluorescence *in situ* hybridisation (FISH)

Fluorescent *in situ* hybridisation (FISH) uses fluorophore-tagged oligonucleotides to detect and bind to specific DNA (chromosomes) and mRNA targets in individual cells with high resolution. [69, 70] They are used in a variety of applications, such as gene expression analysis. Novel probe designs, such as ECHO probes, are often tested in cells using FISH-based techniques. [71] FISH is not ideal for SNP sensing since a single base difference is not enough to disfavour an incorrect FISH probe from binding. [72] The reliance on a high degree of complementarity causes strictly controlled conditions to be implemented such as elevated temperature windows (Figure 1.17). Conventional FISH protocols are cumbersome, time-consuming and not suitable for live cells, although improvements are being made.

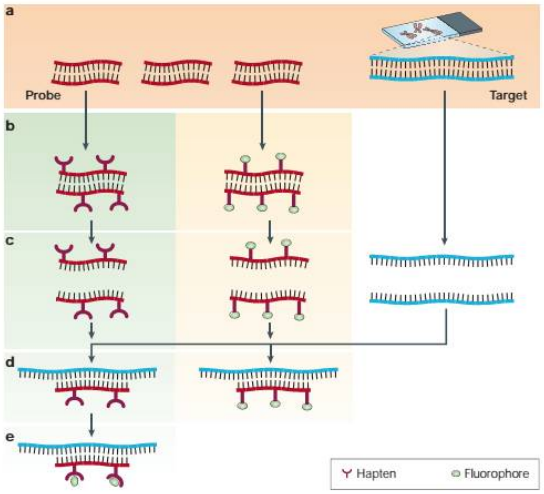

Figure 1.17: Schematic of FISH: (a) DNA probe and target are required; (b) the DNA probe is labelled before hybridisation; (c) the labelled DNA probe and the target DNA are denatured (will require fixation of cell or tissue first); (d) the denatured probe finds the target and anneals if they are complementary DNA sequences, the remaining unbound probe shall be washed away. Adapted from reference [73].

1.3.2 Future of SNP detection

Most sensing methods rely entirely on the thermodynamics of binding and are therefore not necessarily capable of detecting minor changes in the DNA sequence such as SNPs at room temperature. [63] The majority of the techniques described above rely on hybridisation alone and require strict temperature windows. Therefore, this restricts the temperatures at which sensing can be carried out, and hence limits applicability to live cell studies.

Current transcript analysis often involves reverse transcription of mRNA to cDNA. Alternatively, genetic screening involves extracting DNA from a patient. Fluorescent techniques, such as the examples described above, are then used in both scenarios.

The majority of probes only differentiate between wildtype and variant, and provide no information on the variant identity. For example, TaqMan probes simply distinguish homozygous from heterozygous DNA and are not set up for quantitative

analysis. Allelic ratios can be determined by other techniques, but like so many techniques described in this Introduction, they are not routine, quick or cheap.

Overall the current methods are lacking sensitivity and capability to do allelic discrimination. There are several improvements required for current SNP detection technologies:

- SNP sensing could be carried out using DNA samples (e.g. saliva) to save patients having to undergo a tissue extraction. Most current SNP detection assays are carried out at elevated temperatures which cannot be easily applied to a biological environment. A method which can be used at room temperature and cell temperatures is required.

- Fluorescence sensing has been utilised for *in vitro* detection of DNA and RNA sequences, however, a single probe capable of discriminating between single DNA or RNA bases in a cellular environment, has not been presented.

- Identifying SNPs within mRNA transcripts gives an idea of the role of gene expression in disease development. It requires a more accurate analysis of SNPs than those carried out for genomic DNA. For example, in the analysis of a SNP locus within a heterozygous nucleic acid sample, at the DNA level this is 50-50 by definition, but at the RNA level, this can vary from 0-100%, depending on the amount of mRNA transcribed from each allele; such a variation may be crucial to understanding and curing a particular condition. Further to that, mRNA targets within the cell are more accessible and significantly more abundant than DNA targets.

- Fluorescent probes should ideally associate fluorescence enhancement with positive identification of a mismatch, rather than quenching. [8] Therefore, "switch on" or ratiometric (described later) are the most desirable sensing systems. [21]

- Finally, SNPs could be detected using a single probe which indicates and quantifies base variations by fluorescence differences. The probe has the ability to detect a single base difference in a complementary strand of DNA and does not rely on differences

in thermal hybridisation efficiency. SNP sensing which can determine base differences and also has capabilities to discriminate between alleles has been demonstrated by the Tucker group. This work shall now be described.

1.4 Anthracene

1.4.1 Anthracene and DNA

Anthracene is a polycyclic aromatic hydrocarbon (Figure 1.18). Anthracene derivatives are well-known as intercalators and good fluorescent indicators. [74]

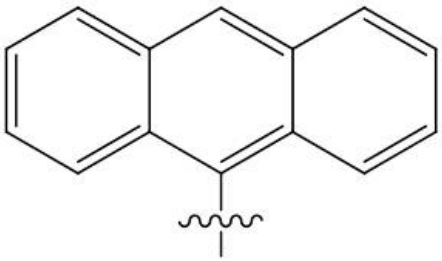

Figure 1.18: Anthracene molecule

Anthracene is a simple, versatile, and useful fluorophore used for tagging oligonucleotides because it has well characterised properties such as its ability to form excimers and undergo [4π+4π] photocycloaddition. [75–77] The main disadvantage of anthracene is its excitation/emission spectra overlaps with the autofluorescence caused by amino acids such as tryptophan in biological samples. [78] This means light absorption and emission at wavelengths that can interfere with the anthracene fluorescence signal. However, there are microscopy and image analysis techniques to help overcome these problems, which shall be discussed later.

Anthracene has been previously used as a sugar modification in oligonucleotides with the addition of 2′-anthracene-modified uridine. [79] The modified oligonucleotides bind to both DNA and RNA targets, proven by UV-vis melting studies. In fact, the an-

thracene stabilised the duplex compared to an unmodified duplex control. This strongly suggests that the anthracene intercalates in between base pairs in the DNA causing stability. Interestingly, a similar effect was not observed with RNA targets, although RNA targets give a higher fluorescence emission response than equivalent DNA targets.

The main advantage of using anthracene as a fluorophore tag is because it is relatively easy to fix anthracene to a specific position in the DNA. The simplest method is to incorporate the anthracene monomer into the oligonucleotide backbone. [80] Incorporation of anthracene monomer was first carried out using a serinol linker. [81] However, prochiral serinol caused a mixture of diastereomeric oligonucleotides to be produced. Although these isomers could be separated, the linker stereochemistry was difficult to assign with complete certainty. Subsequently a threoninol linker has been used for anthracene incorporation. Threoninol has been used for other functionalised oligonucleotide studies, and as an enantiopure starting material, removes the problem of generating diastereomers. [80, 82, 83] Molecules attached to the threoninol can be incorporated at any position into oligonucleotides as base surrogates. This allows intercalation of the molecule between base pairs upon hybridisation to an unmodified oligonucleotide. [84]

The advantages of anthracene-derived monomers in DNA synthesis are solubility in organic solvent and incorporation into oligonucleotides on the synthesiser with high yields. Once incorporated into DNA the anthracene emission signal is centred on 426 nm upon excitation at 350 nm (Figure 1.19). The Stokes shift is therefore 76 nm which is big enough to observe a difference between the excitation and emission, but not too big that there is an energy loss.

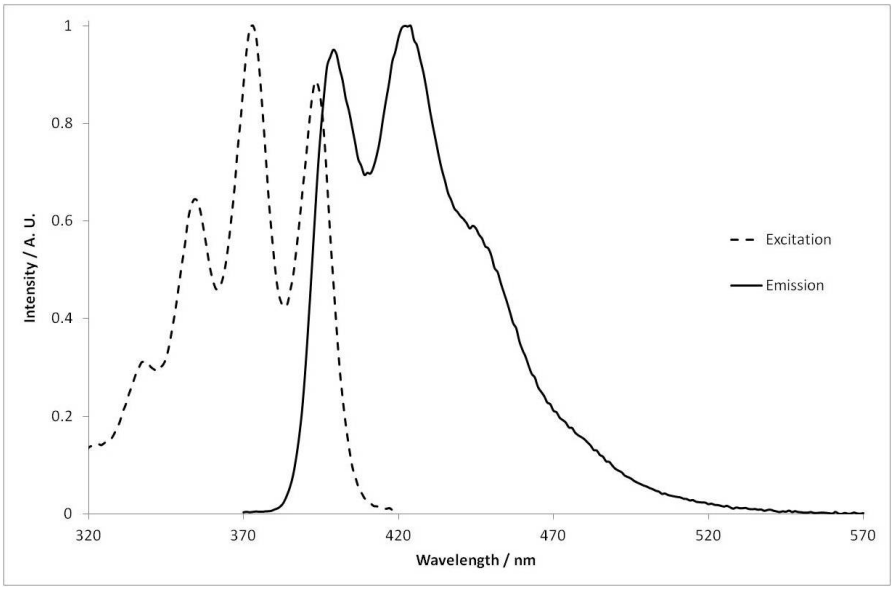

Figure 1.19: Anthracene incorporated into DNA excitation (dashed line) and emission spectra (solid line). $\lambda_{em} = 426$ nm and $\lambda_{ex} = 350$ nm, respectively.

Pyrene has also been used which is second to anthracene in simplicity, although it is a slightly bigger molecule (Figure 1.20). [6, 85]

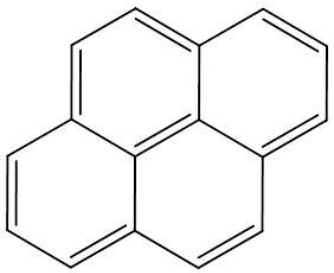

Figure 1.20: Pyrene molecule

Saito *et al.* is the pioneer of nucleoside fluorophores, first developing a pyrene-labelled 7-deaza-2′-deoxyadenosine (^{Py}A). [85] An oligonucleotide containing ^{Py}A gives fluorescence quenching upon duplex formation which can be measured to discriminate a thymine base on the target DNA. All other base mismatches opposite ^{Py}A cause an increase in fluorescence emission. The decreased fluorescence emission is due to

the pyrene chromophore intercalating into the duplex, which was verified via modelling studies and melting temperature measurements.

The insertion of two pyrene moieties into oligonucleotides was used to detect deletion polymorphisms. [82] When the wild type oligonucelotide is hybridised, both pyrene moieties intercalate and thus interaction between the two pyrenes is suppressed by the intervening base-pair. Therefore, there is only monomer emission. For a deletion mutant that lacks one nucleotide, a three-base bulge (including two pyrene moieties) will be formed. In this case, two pyrene moieties should be close enough to exhibit excimer emission (Figure 1.21).

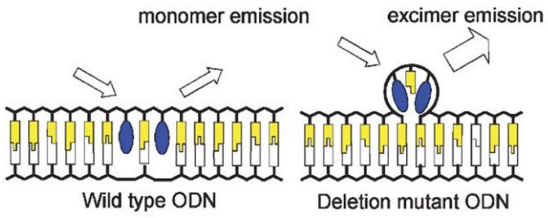

Figure 1.21: Two pyrenes are able to discriminate between a deletion polymorphism. [82]

1.4.2 SNP sensing using anthracene

Given the properties of anthracene, a DNA probe with anthracene as a fluorescent tag has been a focus of research for Tucker *et al.*. [81, 86] An alternative method is adopted, compared to the H-bonding nucleoside derivatives described in Section 1.1.2, through the use of an anucleoside linker group which can provide more versatility and synthetic accessibility for the sensing of different SNPs.

The anthracene monomer is prepared from anthrone, according to standard procedures. [86, 87] The two anthracene monomers, L and D, are stereoisomers caused by the threoninol unit (Figure 1.22).

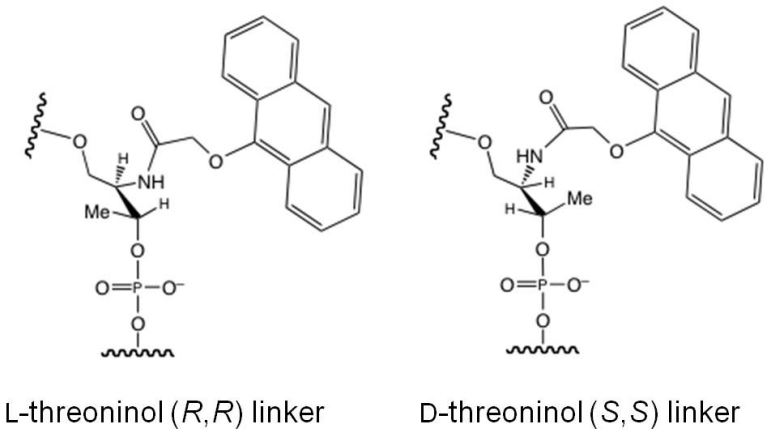

Figure 1.22: Anthracene steroisomer monomers

The anthracene monomer can be incorporated into oligonucleotides (details given in Chapter 2). Once DNA anthracene probes are synthesised they can be used to sense SNPs in DNA target sequences. There are two SNP sensing strategies, which shall be fully explained in Chapter 3. The general SNP sensing idea is given in Figure 1.23. The DNA anthracene probe can detect SNPs when a duplex is formed by distinct fluorescence emission profiles.

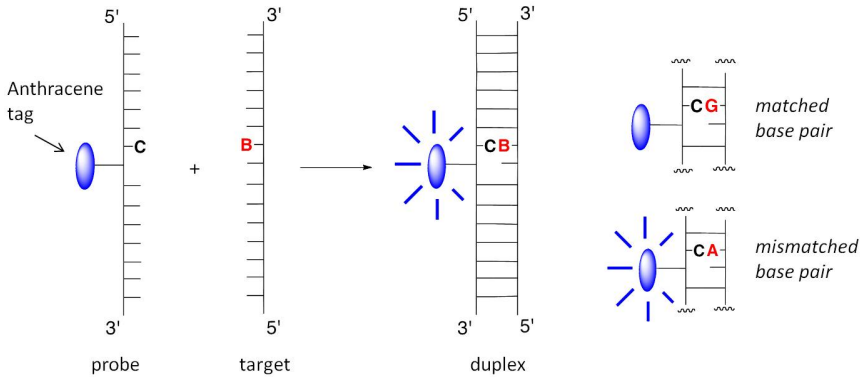

Figure 1.23: Anthracene SNP sensing

Further to SNPs the DNA anthracene probes are also able to detect epigenetic changes such as methylated cytosine bases opposite the anthracene tag in comparison to a cytosine base. [86]

The DNA anthracene probes have minimal hybridisation efficiency requirements, depending only on duplex formation. It is crucially different to other hybridisation-based probes in two ways: 1) analysis is based on the strength of the signal generated upon duplex formation not on how well the duplex forms to give a signal. This means the assay can be done at room temperature and obviates the need to use narrow temperature windows to ensure only one transcript binds. 2) There is no need to generate multiple expensive fluorescent tagged DNA strands for the sensing process. By varying the linker length between anthracene and the phosphodiester, different sensing capabilities between the same target sequences are realised. [86] It has been shown to be biologically compatible and applicable, since it has been shown to probe sequences with SNPs associated with prostate cancer. [88]

It should be emphasised that the system is universal and can be tailored to target SNPs. This has been unavailable to date and has great clinical and commercial potential. In comparison to other commercial solutions, the DNA anthracene probe is sensitive at low levels, no need for excessive amounts of DNA target, and doesn't require the use of tightly controlled thermodynamic conditions.

Aside from DNA anthracene probes there are other base discriminating fluorophore oligonucleotide probes being used for SNP sensing described in the literature. Notable advances include work by Seitz *et al.* on thiazole orange (TO) probes. Having previously focussed on PNA based probes [89] the group have switched to DNA FIT (forced intercalation) probes as they move towards cellular work. [90] TO provides an emissive long wavelength fluorescence which is well suited to cell work because it does not interfere with autofluorescence. However, the DNA TO probe (unlike the PNA TO probe) can only detect if a target sequence is present or not and therefore is not suitable for discriminating SNPs. Similar in terms of intercalation are the linear DNA probes designed by Asanuma *et al.* [84] Multiple perylene molecules are incorporated into the DNA backbone using D-threoninol, which quench each other in the single strand form,

but intercalate and are highly emissive upon rapid hybridisation. The probes have been further optimised for cell work and nuclease stability with 2′OMe RNA nucleotides and anthraquinone quencher. Based upon the high signal to noise ratio, the authors claim "this may be the most sensitive linear probe ever reported". [91]

1.5 RNA SNP sensing

SNP genotyping in DNA is becoming easier with next-generation technologies becoming more common. However, establishing SNP identity at the RNA level is crucial since this allows the functional consequences of gene expression to be probed. For example, for a particular heterozygous (i.e. 50/50) SNP locus in a DNA sequence associated with a particular disease, it is the allelic ratio within the resulting mRNA transcripts that can determine the phenotypic expression of the disease. [92]

At present, RNA sensing is carried out indirectly using reverse transcription of the extracted RNA from cells to form cDNA. This is because RNA is inherently unstable and degrades quickly outside of the cell. [93]

Seitz *et al.* have used FIT-PNA probes to target RNA in a cuvette environment, in preparation for targeting mRNA in live influenza infected cells. [94] The thiazole orange (TO) PNA probe gives 11-fold emission on binding to a complementary RNA target. This is specific since emission does not change on binding to a 'semi-complementary' strand however their system is not capable of SNP detection. A dual fluorophore PNA FIT probe was next developed, which is used to target both DNA and RNA in a cuvette. [95]

Dahan *et al.* tested both synthetic and extracted endogenous RNA in a spectrometer. Binary FRET probes were used (see Section 1.3.1), which were composed of both 2′OMe RNA and LNA residues with phosphorothioate internucleotide linkage. Several probes were designed to discriminate SNPs based on hybridisation. They were

later used in live cell studies. [96]

1.6 Nucleic acid sensing in cells

Detecting a single base difference in nucleic acids is difficult enough within a cuvette environment. The added complexity of a cellular environment introduces a whole new level of challenges, but is worth attempting. Targeting DNA/RNA directly in the cell avoids extraction and reverse transcription/amplification which are time-consuming and often include inaccurate additional steps. Localisation and time-lapse information of cellular processes such as RNA interference can be gained from *in vitro* studies.

The majority of cell studies are in fixed cells, not live cells. There are many examples of probes targeting DNA/RNA in the cell; a selection of examples shall be described. Oligonucleotide probe design and delivery are also important considerations that shall be discussed.

1.6.1 Targeting DNA in cells

Targeting DNA directly in the cell is ambitious since there are only two copies and they are relatively inaccessible in the nucleus. Fluorescence *in situ* hybridisation (FISH), previously introduced, is commonly used in detection and localisation of DNA *in situ*. [69, 97]

'Not enough target' is a common issue in sensing targets in cells and tissue. This can be solved by amplifying the signal compared to background. One of the most exciting solutions in the literature, initially developed by Nilsson *et al.*, is being deemed as PCR in the cell. The primary development was padlock probes, which are highly selective probes that are converted into circular molecules only when the probes are able to match and hybridise to a target sequence. [98] Rolling circle amplification (RCA) was conceived from the idea of padlock probes being used to amplify target DNA (Figure 1.24). [99, 100] RCA

can replicate circularised oligonucleotide probes using DNA polymerase and a single primer in order to generate a linear DNA molecule of up to 1000 copies of tandemly linked copies. Padlock probes and RCA have been added to a cellular environment so that DNA target can be amplified inside the cell. [101]

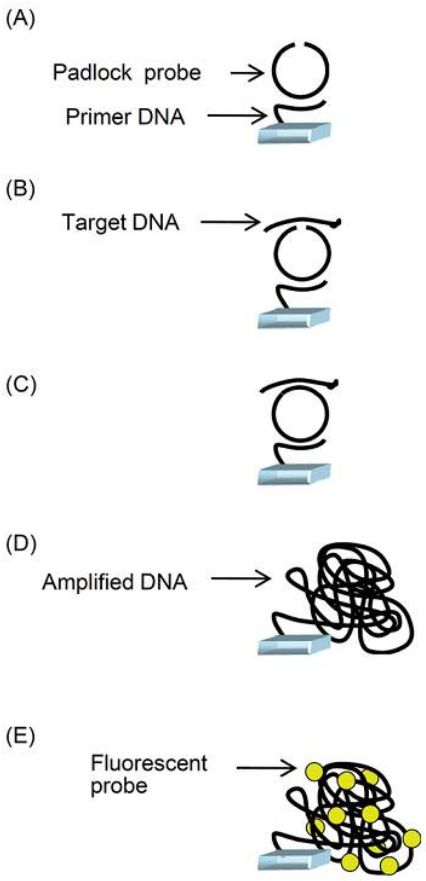

Figure 1.24: Schematic of padlock probe and RCA sensing on a microchannel glass surface. (A) Padlock probe introduced and hybridises to an immobilised primer DNA; (B) target DNA introduced and hybridises to the padlock probe; (C) ligation of the padlock probe; (D) RCA using polymerase; (E) fluorescent labelling by hybridisation of fluorescently labelled DNA. [102]

1.6.2 Targeting RNA in cells

Targeting RNA in cells is preferable to DNA since RNA is more abundant and accessible in the cytoplasm. [103, 104] However, RNA does tend to have a high level of secondary structure, and is often shrouded by proteins and enzymes. RNA also has a short lifetime due to degradation, which is a natural cell process since more RNA is transcribed than is ever accumulated. [93]

FISH can be used to target RNA in the cell. Detection of mRNA *in vitro* requires either probes labelled with multiple fluorophores or multiple probes with single fluorophores. [59, 70, 103]

There are many examples of oligonucleotide probes being used to probe RNA in the cell. [105–107]. Thiazole orange (TO) PNA probes, previously mentioned, have been used to target mRNA in live influenza infected cells. [94] Prior to cell work, the FIT-PNA probes were thoroughly tested for stability at elevated temperatures in cell lysates and in the presence of calf thymus DNA. The dual fluorophore PNA FIT probe has also been used to target RNA in cells. [95] Simultaneous multicolour detection of multiple targets is achieved by using more than one fluorophore probe (with distinguishable emission wavelengths). PNA FIT probes were used for dual imaging of two viral mRNA targets in live cells. [108] Simply, two different fluorescent probes were used to target two different mRNA targets. This work does not provide any real advances aside from extra spatial and temporal information. Crucially, the difficulty of delivering PNA probes into cells is acknowledged.

Kubota *et al.* studied the targeting of intracellular RNA using doubly-labelled TO nucleosides and probes (ECHO probes) respectively. [18, 109] The doubly-labelled nucleoside causes a quenched fluorescence in the single-strand DNA probe, but upon hybridisation to RNA target (including endogenous RNA in cells) causes a high level of fluorescence emission. ECHO probes are capable of single mismatch detection, however complex structural demands have often caused probe malfunctions in detecting endoge-

nous RNA. The progression to cell work was always at the forefront since earlier work switched the backbone to 2′OMe in order to increase tolerance of nucleases.

RNA sensing in cells often takes inspiration from siRNA knockdown and antisense therapeutics. [110] RNA interference (RNAi) is a natural response within living (eukaryotic) cells to double-stranded RNA which leads to control over how active genes are. Small interfering RNA (siRNA), short double-stranded RNA, is known to trigger gene silencing by interacting with and degrading mRNA. This can prevent translation of potentially damaging proteins. Järve *et al.* tagged opposing strands of siRNA with fluorophores capable of FRET in order to monitor siRNA degradation upon entry to and within cells. [111] It was found to be a non-invasive monitoring technique and compatible with RNAi.

There have been further advances for RCA and padlock probes. mRNA has now been used as the target, although the first step in the protocol is the conversion of mRNA to cDNA (complementary DNA). [112] RCA *in vitro* localises target molecules and amplifies the mRNA in the cell for further probing. The padlock probe/RCA method has the potential to distinguish between SNPs. [113] As with other probes the mismatch is distinguished through a lack of binding/ligation of the padlock probe to the target.

1.6.3 Live cell work

Live cell DNA and RNA targeting is becoming increasingly popular. [18, 71, 114, 115] Live cell work allows the understanding of complex dynamic cellular processes, for example, detect and track specific endogenous RNAs in a living cell. Live cell work has more logistical problems than fixed cell work. However, fixed cell work has some disadvantages which have not yet been discussed. Fixed cells provide static rather than dynamic views on oligonucleotide localisation. Cell fixation procedures may cause redistributions or loss of target nucleic acid sequences. Fixation artifacts may interfere with *in situ* hybridisation and/or analysis. [31]

Fluorescence methods are popular in order to detect and track DNA and RNA in living cells. [31] The challenge for fluorescent nucleic acid probes is the unbound probe which cannot be easily washed away and causes background fluorescence. [109] FISH in live cells is able to detect specific endogenous RNA species in living cells. [116, 117] This works well in theory since RNA is mainly in a single-stranded state. DNA is more difficult since it is double-stranded and requires denaturation (not compatible with live cell studies). A more intrusive method to visualise DNA/RNA in living cells is by incorporating fluorescent nucleotides using the cell's own replication or transcription machinery [118], or through binding of DNA or RNA-associating fluorescent dyes. [119] This results in an overall labelling of cellular DNA or RNA *in vitro*, but does not allow for the detection of defined DNA sequences or specific RNA molecules.

The live cell environment is very different to the cuvette and fixed cell. The oligonucleotide probe design and delivery is crucial and shall now be discussed.

1.6.4 Delivery of oligonucleotide probes

The cellular plasma membrane is quite lipophilic and restricts the transport of various molecules. Nucleic acid probes, as hydrophilic molecules, cannot freely traverse the plasma membrane. [120] Therefore, nucleic acid probes require extra help in order to be internalised to the cell intact. Several delivery methods such as microinjection and electroporation are discussed in Chapter 4.

Migration to the nucleus is often an issue (especially if you are targeting RNA in the cytoplasm). At minimum, the resident time of the probe in the cytoplasm needs to be increased. One popular technique is binding biotin and streptavidin to probes to prevent passage through nuclear pores. [57, 121]

Once the probe is inside the cell and intact, the next hurdle is to locate its target and bind with it. As already mentioned, targeting DNA is difficult since it is in the nucleus and is double-stranded. If RNA is to be probed, then the target gene should

be chosen carefully. The target should be transcribed and present in the cell cytoplasm, ready for probing. Initial steps such as using plasmids to over-express the target can be used to ensure the probing is successful. This can be carried out using lentivirus, which means the target RNA is present in next generation cells. [70, 122] An accessible mRNA target should ideally be chosen (RNAfold Webserver) e.g. a loop rather than a stem. Binding is also dependent on RNA secondary structure and proteins which bind along its structure.

1.6.5 Probe design for cell work

The design of the oligonucleotide probe can help to alleviate the delivery issues described above. Delivery and targeting have already been discussed but there are two remaining important requirements for probes in cells: stability and detectability.

Oligonucleotide probes are at risk of digestion upon delivery and once within the cell. This is the cell's defence to attack foreign material using enzymes and nucleases. Modified DNA, as discussed in Section 1.1.2, such as PNA, 2′OMe RNA and LNA, are highly resistant to enzyme degradation. However, this can cause a change to thermodynamics. Alternatively, attachment to nanomaterials such as nanoparticles (NPs) can increase stability. Stability of oligonucleotide probes are particularly important when fluorophores are involved, because digestion can cause false signals and high background.

In terms of detectability, fluorescent nucleic acid probes are a popular choice. [116, 123] In general, long wavelength, high intensity, long lifetime fluorophores are best suited for cellular work since they are differentiable from the background. Dyes which easily photobleach should be avoided (irreversible alteration causing loss of fluorescence). Finally, the fluorescence output of the probe must be compatible with the instrumentation that is to be used for detection.

Wang *et al.* uses a combination of the above approaches in order to image mRNA expression in live cells. The mRNA is targeted by PNA:DNA duplexes, which are de-

livered into live cells attached to nanoparticles. The neutrally-charged PNA is shorter than the DNA and is able to displace to bind to the mRNA with kinetic and thermo-favorability. Finally, a fluorophore/quencher pair are attached to the duplex so binding can be monitored in real-time. [124]

1.7 Quantitative SNP sensing and allelic discrimination in cells

Current methods of SNP detection, including DNA anthracene probes, are able to determine whether a SNP is present or not. However, humans have two copies of DNA (alleles) which means there are several base pair combination possibilities. The homozygous case occurs when the base pairs are the same. In the majority of cases the base pairs are different; the heterozygous case. Most methods of SNP detection are unsuitable for the hetereozygous case, and essentially require double the effort with a probe required for each eventuality.

An interesting example of quantitative and allelic-specific FISH sensing by Hansen *et al.* is provided. Single-molecule FISH (smFISH) uses multiple short oligonucleotides to target specific mRNA sequences. [70, 125] Hansen *et al.* extends this to detect allele-specific expression of mRNA and quantification of SNPs in mRNA within fixed cells. [126] Fluorophore-tagged probes were designed to target either the maternal or paternal gene. Therefore, despite SNPs being detected, multiple probes were required.

A further challenge for SNP sensing is allelic percentage contribution determination from mixtures of DNA and RNA targets respectively. This has been reported very little in the literature. One example used rolling circle amplification for SNP sensing, and was able to determine the allele frequency from mixtures of mutant-type and wild-type DNA. [127] The mutant-type and wild-type DNA (fragments of human p53 gene) were mixed at different ratios ranging from 0-100%. The padlock probes were designed to

ligate for mutant-type DNA, which results in dsDNA and a high level of SYBER Green I (an intercalating dye) fluorescence emission. The wild-type DNA acts as background signal since the ssDNA RCA product does not attract SYBER Green I binding. The resultant mutant-type DNA to wild-type DNA fluorescence signal ratio is approximately 6:1. Therefore, when mutant-type and wild-type DNA are added in different ratios, a fluorescence intensity graph can be produced where the % of alleles can be determined (Figure 1.25).

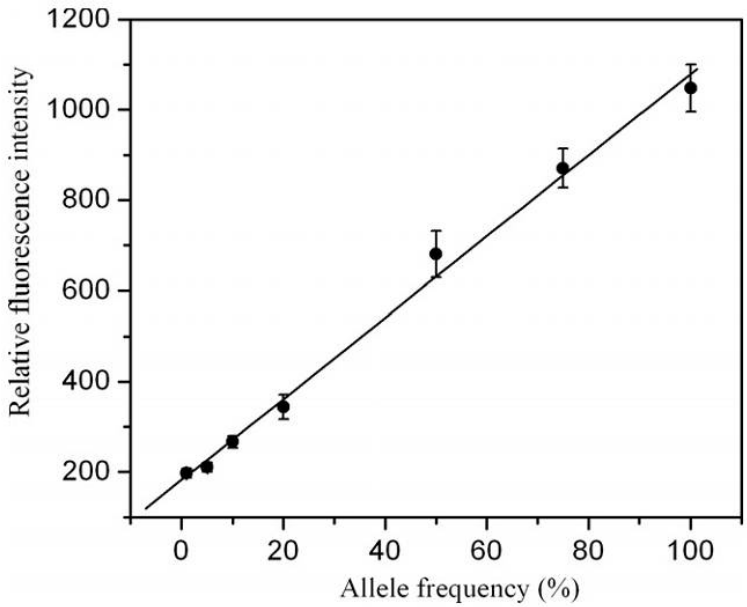

Figure 1.25: Relationship between allele frequencies and relative fluorescence intensities of the samples of mixed mutant-type and wild-type DNA with various ratios. [127]

Many probes are influenced by probe concentration, environment, excitation intensities etc. Ratiometric measurements based upon the intensity ratios at two wavelengths alleviates most of these problems. [128, 129] Ratio SNP sensing can also help with quantitative determination. [111, 130]

1.8 Aims of the project

Single nucleotide polymorphisms (SNPs) provide important genetic diversity to the human genome but are also associated with common diseases. There is ongoing interest in developing convenient methods for distinguishing between different bases within a particular sequence of DNA. Commercially, SNPs can be thought of as molecular markers for genetic diseases. Current SNP detection methods often involve converting RNA extracted from cells into cDNA, which is error prone and time-consuming. In order to move towards detecting SNPs in biological samples, it would be advantageous to target RNA directly.

The DNA anthracene probes described herein (Chapter 3) have been previously shown to detect single base differences in DNA targets. [81, 86] The DNA anthracene probes emission intensity upon hybridisation depends upon whether the target sequence contains one base or another at a particular site.

The key questions for this project are:

1) Can DNA *in situ* studies be repeated in a cellular environment?

2) Can the anthracene DNA probes sense RNA?

Question 1) focuses on establishing the extent to which the DNA anthracene SNP sensing effect developed by Tucker *et al.* can be observed in cells. This was with the aim to carry out novel *in vitro* sensing by adding the fluorescent probes to fixed and live cells. Cell loading conditions must be optimised so that variations in emission intensity can be observed in cells. This includes testing to ensure duplexes are forming within the cell (Chapters 4 and 5). It is important to establish that duplexes form within the cell since the SNP sensing mechanism of the DNA anthracene probe relies upon this. Finally, functionalised probes with two different fluorophores may be required to facilitate quantitative measurements (Chapter 7).

Question 2) opens up the possibility of detecting RNA in a sequence selective

manner using DNA anthracene probes (Chapter 3). A better understanding of the properties of the system would allow targeting RNA *in vitro*, including in live cells. The delivery of the probe into cells in order to target endogenous RNA would be a big final step. This could be carried out using plasmid DNA and transfection (Chapter 6). There are two DNA and RNA sequences that will be used as targets in studies: a well-studied sequence for proof of principle, and a biologically relevant sequence associated with Alzheimer's disease.

In summary, the main aims of the project are to:

- To optimise design of fluorophore-tagged oligonucleotide probes that function through changes in fluorescence emission upon DNA duplex formation (Chapter 3 and Chapter 7).
- To develop imaging methods based on match- or mismatch-pairs to accurately screen patients' DNA for SNPs associated with diseases such as Alzheimer's, or to quantify specific mRNA strands on a cell-by-cell basis (Chapter 3). These measures have not been available to date and have great clinical and commercial potential.
- To optimise regimes for loading probes into cells, imaging their location and quantifying their fluorescence (Chapter 4).
- To develop a novel imaging strategy for quantifying and localising specific DNA or mRNA in living cells (Chapter 5 and Chapter 6).

Chapter 2

Materials and methods

2.1 Oligonucleotide synthesis

Unless otherwise stated, solvents and reagents were purchased from commercial suppliers and used without further purification. Degassed HPLC-grade or MilliQ water was used in all syntheses and studies of oligonucleotides.

Common equipment:

- Savant SPD131DDA SpeedVac Concentrator (Thermo Scientific);
- Dry block heating system (QBD1 Grant instruments, Cambridge);
- Biofuge Pico Heraeus centrifuge for 1.5 ml microfuge tubes with up to 16,060 x g (Kendro Laboratory Products GmbH, Langenselbad, Germany);
- Lab dancer shaker (IKA).

Common buffers:

- 0.1 M pH 7.0 phosphate buffer (0.2 M mono-sodium $NaH_2PO_4.2H_2O$ and 0.2 M di-sodium Na_2HPO_4)
- 5 M NaCl.

2.1.1 Anthracene monomer synthesis

Anthracene monomer was required for insertion into the DNA sequence in order to synthesise fluorescent probes. Synthesis of anthracene monomer is given in Figure 2.1.

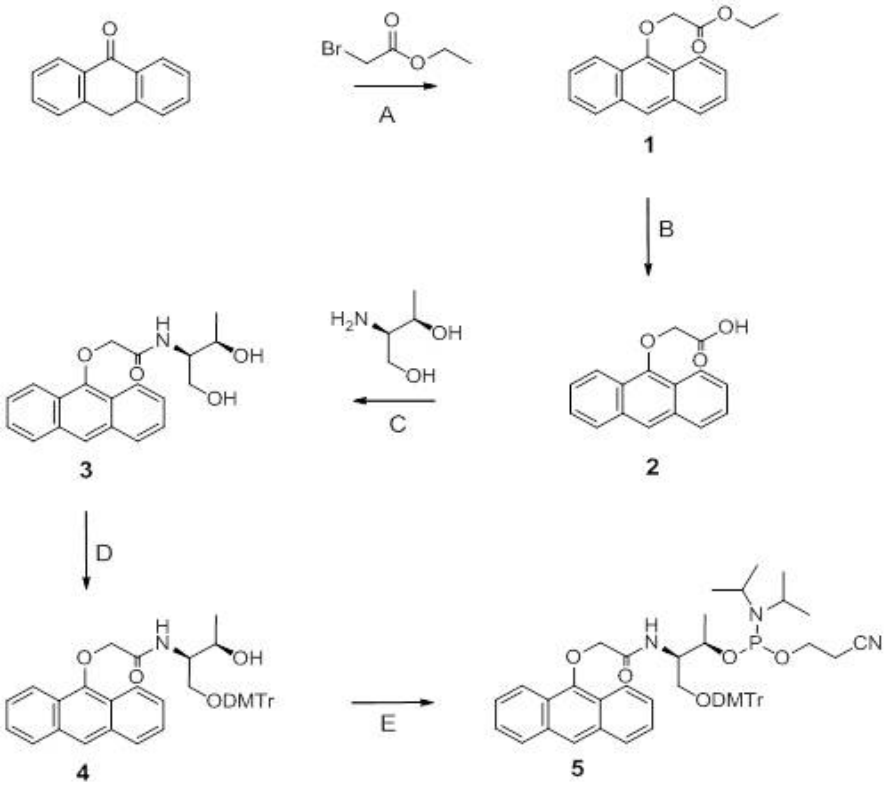

Figure 2.1: Synthesis of the L-anucleosidic anthracene monomer. Reagents and conditions: A) K_2CO_3, acetone, reflux o/n, 33%; B) i. 10% NaOH aq./EtOH (1:1), reflux o/n; ii. conc. HCl, 92%; C) HBTU, DIPEA, DMF, 40 °C o/n, 36%; D) DMTrCl, DMAP, pyridine, o/n, 22% E) $(i-Pr_2N)_2PClO(CH_2)_2CN$, DIPEA, anhy. DCM, 3h, 63%

Commercially available anthrone was reacted with ethyl bromoacetate to generate the anthracene ester (**1**, Figure 2.1). Subsequent saponification yielded the corresponding anthracene carboxylic acid **2** following acidification. Condensation of **2** with L-threoninol and coupling agent HBTU yields the corresponding amide **3** bearing a 1, 3-bis alcohol. Using standard reaction protocols, these alcohol functions were sequentially tritylated to the mono-protected racemate **4**, and then phosphitylated to generate the desired

anthracene-tagged anucleosidic unit **5**. A similar approach was used to generate alternate tethered anthracene with threoninol configurations (L/D) or with various carbon linker lengths. Modified anthracene monomer **5** was introduced into the central position of a 15-mer oligonucleotide via solid phase synthesis on a 1.0 mmol scale with a stepwise coupling yield of over 98%.

Unmodified and tagged oligonucleotides were synthesised as previously described using the phosphoramidite method (Applied Biosystems 394). [77] Oligonucleotide reagents and chemicals used were purchased from Link Technologies (Glasgow, UK), unless otherwise stated. Standard DNA phosphoramidites used were Bz-A-CE, Ac-C-CE, dmf-G-CE and U-CE. RNA 2′-OTBDMS phosphoramidites used were Bz-A-CE, Ac-C-CE, dmf-G-CE and U-CE. DNA SynBase^{TM} CPG functionalised supports and RNA SynBase^{TM} CPG columns were used respectively. The addition of protecting groups to all other functional groups in the nucleosides prevents undesired side reactions. Once oligonucleotide assembly was complete, all the protecting groups must be removed; a process known as deprotection. DNA was deprotected on the synthesiser by the addition of ammonia. This also cleaves the DNA from the solid support and into aqueous solution. The solution was heated for 6 hours at 55 °C to carry out base deprotection as well as phosphate deprotection.

2.1.2 DNA purification and characterisation

DNA is purified by reversed-phase HPLC (high pressure liquid chromatography) preparatory using a buffer gradient of acetonitrile and water on a C18 generation packed axia column. The buffer is removed using a rotary evaporator. The DNA is eluted with 1.5 ml HPLC-grade water which is then passed through a NAP-10 column (GE Healthcare) to remove any salts. HPLC analytical can then be used to confirm the purity of the DNA (see Appendix F for HPLC buffer, program details and results).

Electrospray negative time-of-flight (ESI TOF) mass spectrometry can be used

to characterise the DNA by comparing it to the calculated theoretical molecular mass (see Appendix F for mass spectrometry results).[1]

DNA concentration can be calculated using a Shimadzu UV-Vis 1800 spectrophotometer. The UV absorbance value was measured at 260 nm for a diluted sample of DNA in water. 1 ml volume, 1 cm pathlength, quartz absorption cuvettes were used. The concentration of the DNA can be calculated using the Beer Lambert law (Equation 2.1). Extinction coefficients were found at IDT Biophysics[2] and Ribotask Oligo Calculator.[3] Anthracene extinction coefficient at 260 nm is $\epsilon = 52000\ \mathrm{M}^{-1}$ [33], Cy3 $\epsilon = 4930\ \mathrm{M}^{-1}$, Cy5 $\epsilon = 10000\ \mathrm{M}^{-1}$ and acridine $\epsilon = 39500\ \mathrm{M}^{-1}$.[4]

$$c = \frac{A}{\epsilon l} \tag{2.1}$$

2.1.3 RNA synthesis

RNA synthesis is similar to DNA; however there are two main differences. RNA nucleotides have a $2'$ hydroxyl group, and thymine is replaced with uracil. Therefore synthesis requires alternative phosphoramidites and the extra hydroxyl group causes a more stringent deprotection process. [131] The RNA remains on the column until released manually by 3:1 ammonia : ethanol solution. It was then heated for 6 hours at 55 °C to carry out base and phosphate deprotection as before. The solvents were evaporated prior to overnight tetra-n-butylammonium fluoride (TBAF) treatment, which removes the TBDMS protecting group on the $2'$-OH. A NAP-10 column was used to remove salts. Isoproponal precipitation was carried out to concentrate the RNA and remove any further salts. Finally, purification and characterisation were carried out as for DNA. Single-strand RNA is highly susceptible to degradation by nucleases; therefore extra precaution was taken during the deprotection and purification stages. This included:

[1] Mongo Oligo Mass Calculator v2.06, http://library.med.utah.edu/masspec/mongo.htm
[2] IDT, http://biophysics.idtdna.com/UVSpectrum.html
[3] Ribotask, www.ribotask.com
[4] Glen Research Corporation, http://www.glenresearch.com/Technical/Extinctions.html

working in a sterile flow hood; nuclease decontamination spray (RNAse AWAY®) used on all equipment; gloves at all times and autoclaved MilliQ water.

The synthesis and experimental details of modified Cy3 and Cy5 tagged DNA is presented in Chapter 4.

2.2 Fluorescence and lifetime studies

The fluorescence emission of the DNA probes can be measured using a Shimadzu RF-5301 PC spectrofluorophotometer. 1 μM DNA probe samples are prepared in 1 ml of buffer solution (10 mM phosphate, 100 mM NaCl, pH 7.0). 1 ml volume, 1 cm path-length, quartz emission cuvettes were used. The target is titrated in 0.5 equivalence steps in order to observe any differences in emission. An excess of target is added to ensure there is 1:1 binding. 5-10 minutes between titration's allows the DNA strands to anneal. DNA anthracene probe excitation (λ_{ex}) is 350 nm and the emission is measured over a range of 370-570 nm (370-680 nm for Cy3 modified probes). The spectrofluorophotometer slit widths are 3 nm for excitation and 5 nm for emission, unless otherwise stated. The percentage change in emission compared to the probe alone is measured at the wavelength 426 nm, which is the peak emission wavelength of anthracene, unless otherwise stated. Excitation scans monitor emission at 426 nm (570 nm for Cy3 modified probes) using an excitation slit width of 1.5 nm and emission slit width of 3 nm.

The quantum yield of DNA anthracene probes were measured using 1 μM DNA probe, 100 mM NaCl, 10 mM pH 7.0 sodium phosphate buffer, λ_{ex} = 350 nm. The slit widths were 3 nm for excitation and 10 nm for emission. Quantum yields (Φ) were determined relative to quinine sulphate ($\Phi_f = 0.546$).

Lifetime measurements are carried out with an Edinburgh Instruments FLS920 spectrometer. The laser used was an Edinburgh Instruments EPL-376 pulsed diode laser with a 50 ns pulse excitation wavelength of 376 nm and the emission was detected using

a Hamamatsu R928 PMT. The multi-exponential decays were fitted using Edinburgh Instruments F900 or FAST software. An exponential function was fitted with optimised parameters by minimising χ^2 values. Data was corrected using an IRF file (50 μl LUDOX® TM-40 colloidal silica (Sigma-Aldrich) in 1 ml water).

2.3 Melting studies

The melting temperature (T_m) of duplex DNA were obtained on a Varian Cary-5000 by measurement of the change in absorbance at 260 nm as a function of temperature. The melting temperature T_m is defined as the temperature at which 50% of the DNA is part of a duplex and 50% is single-stranded. 5 μM samples of DNA probe and target were prepared in 500 μl of buffer solution (10 mM phosphate, 100 mM NaCl, pH 7.0). 500 μl volume, 1 cm pathlength, quartz absorption cuvettes were used. The sample was heated from 15 °C to 85 °C and vice versa, repeatedly. The absorbance was measured at increments of 0.5 °C at a wavelength of 260 nm. Sufficient time is allowed between each temperature change to allow stabilisation of the sample. The melting temperature error values are limited to the instrumental error (0.5 °C).

2.4 Circular dichroism

Spectra were recorded on a Jasco J-810 spectropolarimeter between 200 and 400 nm (200-680 nm for Cy3 modified probes). Other settings were: data pitch 0.2 nm; continuous scans at 200 nm/min; bandwidth 1; slitwidth 1000 μm; 1 second response; scan accumulation 10. The sample solutions were as follows: 5 μM each DNA strand, 10 mM pH 7.0 phosphate buffer, 100 mM NaCl. 1 ml volume, 1 cm pathlength, quartz absorption cuvettes were used. Scans were baseline corrected with buffer solution.

2.5 Nuclease studies

To test the stability and specificity of the DNA it was incubated at 37 °C in cell lysate extracted from CHO cells (see below), and emission spectra collected at intervals over a 2 hour period. To test degradation, DNA was incubated with DNase I (Sigma-Aldrich) for 2 hours, added to CHO cell lysate and emission spectra collected.

2.6 Cell culture

Reagents and chemicals used were purchased from Sigma-Aldrich (Gillingham, UK), unless otherwise stated.

Common equipment:

- Biofuge Pico Heraeus centrifuge for 1.5 ml microfuge tubes with up to 16,060 x g (Kendro Laboratory Products GmbH, Langenselbad, Germany);
- Hettich Mikro 22R refrigerated centrifuge for 1.5 ml microfuge tubes with up to 21,910 x g (Andreas Hettich GmbH, Tuttlingen, Germany);
- Biofuge Primo Heraeus centrifuge for up to 50 ml tubes with up to 2576 x g (Thermo Electron Corporation, Waltham, USA);
- Sanyo CO_2 incubator (Sanyo Electric CO, Japan);
- Leica DM IL inverted microscope (Leica Microsystems, USA);
- CellStar incubator (Borolabs Ltd. Basingstoke, UK);
- Sanyo/Gallenkamp orbital shaker (Loughborough, UK).

Common buffers:

- Tris-Acetate-EDTA (TAE) buffer (40 mM Tris-base, 20 mM glacial acetic acid, 1 mM EDTA);

- Phosphate-Buffered Saline (PBS) (137 mM NaCl, 2.7 mM KCl, 10 mM Na_2HPO_4, 1.76 mM KH_2PO_4 pH 7.4);
- NP40 (Igepal) Lysis buffer (1% (v/v) NP40, 10 mM Tris pH 7.5 (Fisher Scientific), 150 mM $NaCl$, 1 mM EDTA pH 8, 0.01% (w/v) sodium azide and 1x protease inhibitor cocktail (Roche)).

Human embryonic kidney (HEK), Chinese hamster ovary (CHO) and HeLa cells were cultured for use. HEK/CHO cells were supplied by Cancer Research UK and HeLa cells were a gift from Dr. Nik Hodges. They were grown at 37 °C in a humidified atmosphere of 5% CO_2. Cells were maintained by regular passage in DMEM (Sigma-Aldrich). This medium was supplemented with 10% heat-inactivated fetal bovine serum (FBS), 2 mM L-glutamine, 100 U/ml penicillin and 50 U/ml streptomycin (gibco® by Life Technologies).

Cell lysate: Confluent plates (10 cm diameter) of CHO cells were washed with PBS and lysed on plates by adding 200 μl of lysis buffer. Cells were scraped quickly with a cell scraper (Fisher Scientific) and transferred into 1.5 ml microfuge tubes. The cells were lysed for 10 mins on ice and centrifuged for another 10 min (21,910 x g, 4 °C). The supernatant was used directly in different assays or stored at −80 °C in 10% (v/v) glycerol.

2.7 Transfection

2.7.1 Fixation

For cell fixation, 3 x 10^5 CHO cells were seeded in DMEM on Mattek dishes (P35G-1.5-20-C, MatTek Corp.). The cells were fixed and permeabilised using −20 °C methanol for 5-10 minutes. 0.025 μg/μl DNA in PBS was added to cells for 1 hour and then rinsed with PBS solution. If DNA was added sequentially the next strand was added for

a subsequent 1 hour and then rinsed with PBS solution. Alternative fixatives include formaldehyde with or without triton.

2.7.2 Lipid based transfection

For chemical transfection, CHO cells were grown on ϕ13 mm coverslips for 24 hours in complete DMEM. Transfection was carried out using 100 μM DNA, Opti-MEM® medium (Life Technologies) and Lipofectamine™ RNAiMAX (Life Technologies). Transfection was carried out over 4 hours at 37 °C. Cells were fixed with 4% formaldehyde and nuclei stained with Bisbenzamide (Sigma-Aldrich) for imaging purposes. Cells were allowed to recover between sequential transfections. Bafilomycin A1 (Sigma-Aldrich) was dissolved in DMSO and added to the transfection medium (final concentration 100 nM) as above.

2.7.3 Microinjection

For microinjection, 1.5 x 10^5 CHO cells were seeded in DMEM on Mattek dishes. Prior to microinjection, the medium was replaced with HEPES supplemented DMEM. Microinjection was performed using a micromanipulator (model 5171, Eppendorf) and transjector (model 5246 Plus/Basic, Eppendorf). A DNA concentration of 100 μg/μl was microinjected into the cytoplasm of cells.

2.7.4 Electroporation

For electroporation, 8 x 10^5 CHO cells were added to serum free DMEM and 0.025 μg/μl DNA in a 4 mm gap electroporation cuvette (Geneflow) for 10 minutes at room temperature. Electroporation was carried out at 400 V and 25 μF (BioRad Gene Pulsar® II). The cells were left for 5 minutes at room temperature and then for 5 minutes on ice. The cells were then seeded in DMEM on Mattek dishes and allowed to recover for 12 hours.

2.8 Microscopy

Anthracene fluorescence images were acquired on a Nikon A1R inverted confocal microscope using a 40x oil immersed objective lens and 402 nm laser. Emission range for anthracene probe emission was 425-475 nm. Acridine fluorescence images required a 457 nm laser with emission range 465-500 nm. A z-stack of images was acquired to ensure the image at the correct focal plane was taken for further analysis. Images were collected at 1 μm intervals.

All Cy3/Cy5 cell imaging, excluding transfected cells, was carried out on an inverted confocal microscope (Zeiss); Cy3 (543 nm laser, beam splitter (MBS) 488/543/633, em 515-613 nm) and Cy5 (633 nm laser, MBS 488/543/633, em 698-754 nm). Transfected cells were imaged on an axiovert UV confocal microscope (Zeiss); BB (364 nm, 351 nm laser, MBS UV/488/543/633, em BP 385-470 nm), Cy3 (543 nm laser, MBS UV/488/543/633, em BP 560-615 nm) and Cy5 (633 nm laser, MBS UV/488/543/633, em LP 650 nm).

Emission microscopy was carried out on a spectral imaging inverted confocal microscope (Leica); Cy3 (543 nm laser, MBS UV/488/543/633, em 556-615 nm) and Cy5 (633 nm laser, MBS UV/488/543/633, em 641-750 nm).

2.9 Computational analysis

All analysis was performed offline in Matlab 2009b and ImageJ. Section C.6 contains a detailed explanation of the particle-swarm optimisation algorithm.

2.10 Statistical analyses

For the Cy3/Cy5 DNA statistical analysis (Chapter 4), data is plotted with error bars representing the standard error of the mean (s.e.m.). Emission intensity values were

taken from ROI in cell images, with at least ten cells analysed. In order to compare Cy5 intensity values between using both the 543 nm and 633 nm lasers, and the 543 nm laser only, the Mann-Whitney test was performed. For the anthracene DNA probes in fixed cell analysis (Chapter 5), s.e.m. on intensity values from GMM analysis were combined between images to give error on the percentage change in emission values. ImageJ analysis (s.e.m. error) was performed as for Cy3/Cy5 DNA. In order to compare intensity values between images, the Mann-Whitney test was performed.

2.11 Manipulation of DNA material

Reagents, enzymes and their compatible buffers used in cloning were purchased from New England Biolabs (NEB) (Herts, UK), unless otherwise stated.

2.11.1 DNA oligonucleotides and plasmids

Thank you to Professor Steve Lee for the plasmid (mp71 retroviral vector), and Dr. Alan Zhuang for his advice. The plasmid is ampicillin resistant. There is more detail on the plasmid, including a diagram, in Chapter 6. DNA oligonucleotides for insertion were purchased from IDT. The complementary oligos were annealed upon combination of 1 μl of each oligo (100 μM) and 98 μl elution buffer (10 mM Tris pH 8 buffer). The mixture was heated at 100 °C for 5 minutes then cooled at room temperature. The plasmid and inserts required no further amplification or purification.

2.11.2 Digestion of DNA with restriction enzymes

Plasmid was cut at two restriction sites, ClaI and NotI, using corresponding restriction enzymes (NEB). 5 μg of plasmid was incubated in 50 μl of digestion solution containing: 5 μl of 10x CutSmart NEBuffer (NEB), 2.5 μl of each restriction enzyme (20,000 U/ml) and water. Digestion was carried out for 2 hours at room temperature.

2.11.3 DNA agarose-gel electrophoresis

DNA agarose-gel electrophoresis was performed using equipment for horizontal electrophoresis (Jencons Scientific Ltd., VWR division, East Grinstead, UK). Gels were prepared by dissolving 0.8-1.5% (w/v) agarose (VWR International, Lutterworth, UK or Sigma-Aldrich) in TAE buffer and stained with SybrSafe (Invitrogen). A loading dye (NEB) and ladder (GeneRuler, Thermo Scientific) were also used. Gels were visualised and imaged using Gene Genius Bio Imaging System (Syngene, Cambridge, UK).

2.11.4 DNA gel purification

DNA bands were cut from the gel and DNA was extracted using GeneJET^{TM} Gel Extraction Kit (Fermentas) according to the manufacturers instructions. Plasmids were stored at $-20\,^{\circ}$C.

2.11.5 DNA ligations

Inserts were ligated with the plasmid using T4 Ligase as follows. A 20 μl ligation solution containing 2 μl of 400,000 U/ml T4 DNA Ligase enzyme (NEB) and 2 μl 10x T4 Ligase buffer (NEB) is added to a 16 μl insert/vector mixture prepared in a ratio of 4:1. Ligations were performed at RT for 2 hours.

2.11.6 Heat shock transformation of bacteria

The chemically competent *Escherichia coli (E.coli)* strains (Bioline, α-select Gold efficiency competent cells) were used for transformations with the plasmid. Chemically competent *E.coli* (20-50 μl) was mixed with 5 μl ligation mix and incubated on ice for 30 minutes. The bacteria were heat shocked at $42\,^{\circ}$C for 45 seconds then incubated on ice for a further 2 minutes. All bacteria were cultured in Luna Bertani (LB) broth or LB agar (Sigma Aldrich) with appropriate antibiotic. The final concentration of antibiotic was 0.1 mg/ml ampicillin (Amp). Transformed bacteria mix was diluted into 150 μl

of pre-warmed antibiotic-free liquid LB medium bacteria and incubated in the orbital shaking incubator at 37 °C for 1 hour. Subsequently bacteria were added to LB-agar containing ampicillin plates for overnight incubation at 37 °C. Larger colonies were selected from the agar plate and added to 2 ml LB broth/ampicillin. Bacteria was grown overnight in the orbital shaking incubator at 37 °C.

2.11.7 Plasmid purification

Large scale preparation of plasmids was performed from bacterial cultures using the Qiagen Plasmid Maxi Kit (Qiagen, Crawley, UK) or GeneJET^{TM} plasmid Maxiprep Kit (Thermo Scientific, UK) according to the manufacturer's protocols. For small-scale plasmid preparations DNA was isolated using the GeneJET^{TM} plasmid Miniprep Kit (Thermo Scientific, UK). Final DNA concentration was measured with the NanoDrop ND-1000 Spectrophotometer (Labtech, Ringmer, UK).

2.11.8 Colony PCR screen

Colony PCR was used to screen for successful ligation of vector and insert. A 20 μl PCR reaction was prepared for each colony screened by adding: 2x PCR mix (ReadyMix^{TM} REDTaq PCR Reaction Mix with $MgCl_2$, Sigma-Aldrich); 100 μM of each primer (Table 2.1); water and bacterial colony sample. Prior to mixing with the PCR mix, a replica plate was set up containing samples of each colony screened. The PCR reaction was performed as follows: initial denaturation (96 °C, 3 mins) then 34 cycles of denaturation (96 °C, 30 s); annealing (55 °C, 30 s); and elongation (72 °C, 30 s, 1 min/1 kb of amplicon). A final DNA elongation step of 72 °C for 5 mins was carried out. (MJ Research, PTC-225 Peltier Thermal Cycler). PCR products were visualised by DNA gel electrophoresis. Colonies which gave positive results were used for small or large scale plasmid preparations as described above.

Table 2.1: Primer sequences used for PCR and sequencing (Eurogentec).

Oligonucleotide	Sequence (5' to 3')
RBShortF	Forward `AACTTTGATCTGCTGAAGCTGGCC`
RBLongF	Forward `ATTGCTCTTCTCATTGTCTAGG`
RBShortR	Reverse `GGCCGCTGGACTCTCTCAATGCTAGAT`
RBLongR	Reverse `ATTGCTCTTCTCATTGTCTAGG`

2.11.9 Sequencing and storage of plasmids

All constructed plasmids were verified by sequencing by the Functional Genomics and Proteomics Laboratory (School of Biosciences, University of Birmingham, UK). All constructs were stored as glycerol stocks at $-80\,^{\circ}$C. These were prepared by mixing the saturated bacterial cultures with an equal volume of 30% (v/v) glycerol.

2.12 DNA plasmid transfection

Plasmids were added to cells via PEI transfection, which was performed for a 10 cm plate of 80% confluent cells as follows:

- 18 μg of DNA added to 1 ml Opti-MEM® medium (Life Technologies) in a 1.5 ml tube. Mixed by flicking tube.
- 27 μl PEI stock solution (1 mg/ml) added, mixed by gently vortexing (half speed) and left for 10 minutes at room temperature to allow DNA/PEI complexes to form.
- The DNA/PEI is gently added to the cells and mixed by slow movements of the plate.

2.13 Flow cytometry

Cells were removed from plates using cell dissociation buffer (10 mM EDTA in PBS), centrifuged at 2000 rpm for 4 mins and resuspended in FACS buffer (PBS, 0.5% BSA, 0.1% sodium azide). Antibodies were added (1 in 50) and cells kept on ice for 1 hour. Isotype controls were also carried out (non-specific antibody with Cy5 tag). Flow cytometry was carried out using a Becton Dickinson FACSCalibur machine with settings: (P1, FSC, E-1, 7.00 lin); (P5, FL3, 535, 1.00, log). Settings for PRan plasmid: (P3, FL1, 366). BDFACSFlow (azide free) buffer and CellQuest software were used with the machine. Antibody was 0.2 mg/ml Cy5-tagged αhCD34 (PE-Cy5 conjugate) (R&D Systems AF4968). Isotype was Cy5-tagged anti-mouse IgG1 (Dako #x0931). PRan plasmid was a HA-Clec14A pc52 human plasmid. PRan plasmid required anti-clec14A antibody with secondary anti-sheep.

Chapter 3

DNA and RNA SNP sensing with DNA anthracene probes

3.1 Introduction

SNP sensing has an important role now and in the future of disease screening. Oligonucleotide probes can be used for single base discrimination through hybridisation and fluorescence emission. Tucker *et al.* SNP sensing work has been focussed on detecting single base differences in DNA systems. [81, 86, 88] This was briefly discussed in Chapter 1 (Section 1.4.2) but shall be described fully, including its mechanism, within this chapter. In order to expand the potential biological utility of the system, experiments were carried out to determine whether DNA anthracene probes could detect single base differences in RNA targets in a similar manner to DNA. To analyse SNPs in RNA, RNA is extracted from cells and tissues and is subjected to reverse transcription to become cDNA before being amplified by PCR. However, direct targeting of extracted RNA would be quicker and more accurate. Targeting RNA can lead to *in vitro* and *in vivo* studies since RNA is more abundant and accessible in a cellular environment. The initial question was therefore, could the Tucker group SNP sensing be applied to sensing

RNA directly? Using the same sequence used for DNA sensing, various RNA targets were synthesised and purified, which were then hybridised with the DNA anthracene probes (of varying linker length and stereochemistry). Their properties were then investigated using a combination of UV-vis, fluorescence and CD spectroscopy. It is described below that DNA anthracene probes are able to discriminate SNPs in RNA targets by modulation of the fluorescence emission. However, the results do not exactly replicate those for DNA targets, indicating that although the general sensing mechanism is the same there are subtle changes associated with conformation for some RNA targets. The trends observed can be explained by results obtained from sensing 2′OMe RNA targets. Finally, the biological relevance of the DNA anthracene probes is demonstrated through sensing of a SNP sequence within an RNA or DNA strand associated with Alzheimer's disease. This provides inspiration for an assay to determine the percentage of allelic contribution (Section 1.3) within a particular sample.

3.2 Results and discussion

3.3 DNA sensing

The SNP sensing mechanisms using DNA anthracene probes were described briefly in Section 1.4.2, Chapter 1. They shall now be described in detail and a summary of the main results discussed.

3.3.1 DNA probe design

The anthracene phosphoramidites were synthesised from the known anthracene carboxylic acid via a DMT protected diol (Section 2.1.1, Chapter 2). DNA anthracene probes were prepared by automated solid phase synthesis using conventional phosphoramidite chemistry, as reported previously. [77] Unmodified oligonucleotide strands were also synthesised by this route. Table 3.1 lists the DNA oligonucleotides used in the

Table 3.1: DNA sequences synthesised. X denotes the anthracene monomer. n is the carbon linker length and L/D denotes the stereochemistry.

Oligonucleotide	Sequence (5' to 3')
DN	TGGACTCTCTCAATG
P(n)(L/D)	TGGACTCXCTCAATG
DT1	CATTGAGAAGAGTCCA
DT2	CATTGAGGGAGTCCA
DT3	CATTGAGCGAGTCCA
DT4	CATTGAGTGAGTCCA
DT5	CATTGAGAAAGTCCA

studies described in this section. A full list of oligonucleotides is given in Table G.1, Appendix G. DN is the unmodified DNA probe compared to P(n)(L/D), which represent anthracene modified oligonucleotides, with (n) denoting the carbon linker length (n = 1 - 7, excluding n = 2) and L/D denoting the stereochemistry (Figure 3.1 includes the anthracene monomer structure).

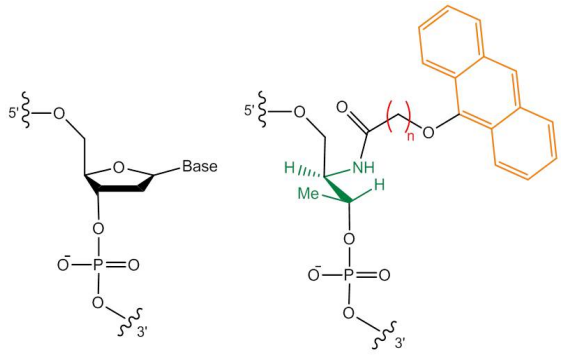

Figure 3.1: Left: A standard nucleotide with sugar phosphate backbone. Right: Anthracene monomer. The anthracene molecule is seen in yellow; the red (n) is the carbon linker length and the green threoninol molecule denotes the stereochemistry (L shown here).

The probes P1L and P6D are focussed on here but the complete results for all probes are shown in Appendix A. A list of the single-stranded probe quantum yield val-

ues is also included for reference. DT(1 - 5) are DNA targets which are complementary to DN, P1L and P6D, but for one base difference. Oligonucleotides were purified by RP-HPLC and characterised by mass spectrometry (Appendix F). Although the chosen 15 base sequence does not contain a SNP from the human genome, it has been extensively studied by *Tucker et al.*. All melting studies show the DNA anthracene probes to be stable duplexes with the DNA targets at room temperature. See Appendix A for full results, including examples of DNA anthracene probe duplex melting curves (Figure A.1). DNA anthracene probes give good sensing results in two different strategies, which shall now be described.

3.3.2 DNA SNP sensing

The DNA anthracene probe is used to sense one base difference in target DNA based on changes in emission. There are two sensing systems: base adjacent and base opposite sensing.

3.3.3 DNA base adjacent sensing

Melting and fluorescence studies

In this strategy, the emission from the anthracene is found to increase or decrease depending on whether the duplex base-pair immediately adjacent on the 5′ side with respect to the probe is matching or mismatching. Here, the match adjacent target is DT1 and the mismatch adjacent target is DT5 (Figure 3.2).

P(*n*) (L/D)	5′	TGGACTCXCTCAATG 3′
DT1	3′	ACCTGAGAGAGTTAC 5′
DT5	3′	ACCTGAAAGAGTTAC 5′

Figure 3.2: DNA base adjacent sensing system. X denotes the anthracene monomer. n is the carbon linker length and L/D denotes the stereochemistry. Bases underlined denote the single base difference.

The base adjacent system is only sensitive to a change in base pair identity for anthracene with a short carbon linker ($n = 1$) and L stereochemistry i.e. DNA anthracene probe P1L (Figure 3.1). The 1D linker and longer linkers (L or D) are not effective sensors since they cause the anthracene emission for both targets to change to the same degree respectively.

The mismatch adjacent target (DT5) causes the P1L anthracene emission to increase significantly at $\lambda_{em} = 426$ nm (+77%) compared to the probe alone. However, the matching base adjacent target (DT1) causes the emission to decrease (-70%) (Figure 3.3).

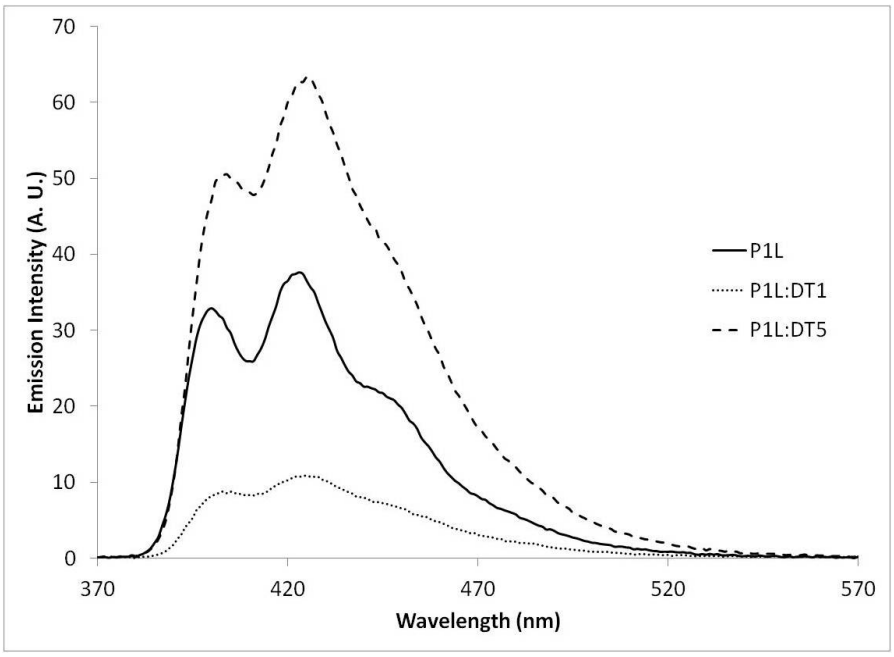

Figure 3.3: Fluorescence spectra showing the change in emission upon hybridisation of anthracene probe P1L with targets DT1 and DT5 respectively. 1 μM DNA, 100 mM NaCl, 10 mM pH 7.0 sodium phosphate buffer, $\lambda_{ex} = 350$ nm.

The anthracene tag was seen to stabilise the duplex despite the lack of hydrogen bonding in the central base pair (Table 3.2). The 1L anthracene must intercalate reasonably well since the T_M for duplex P1L:DT1 is only 2 °C less than the unmodified duplex DN:DT1 T_M. The duplex P1L:DT5 is more stable than DN:DT5 which, in agreement

with model studies, indicates that the anthracene is able to partake in π-stacking with proximate base pairs. [86, 132] This will be described in more detail later.

Table 3.2: Melting temperatures (°C) of DNA targets and DNA anthracene probes. 5 μM DNA, 100 mM NaCl, 10 mM pH 7.0 sodium phosphate buffer.

Probe/Target	DT1	DT5
DN	55	42
P1L	53	46
P1D	48	35

The hypothesis is that having the mismatch target adjacent allows space for the anthracene to intercalate effectively into a more hydrophobic environment. On the contrary, when there is a matching base pair adjacent to the anthracene, the hydrogen bonding remains intact and there is less space for the anthracene. In both cases, the anthracene does not remain in a single state but is dynamic. The anthracene in the match case therefore spends more time located outside of the duplex since it cannot access a hydrophobic environment so effectively. This is also shown by lifetime data which shall be discussed in Chapter 7. As shown in Figure 3.3, when anthracene intercalates into DNA, a bathochromic shift of 3 nm is observed in the fluorescence bands compared to the probe alone. This bathochromic shift is also present in absorption spectra between P1L and duplexes. The base pair mismatch has a larger effect on the $5'$ side of the probe because the anthracene is closer to the base than on the $3'$ side. [87] The binding is specific since there is no change in emission on the addition of a non-complementary target. Titrations of target DNA showed no further change in emission was observed in the presence of excess target. This indicates the formation of a 1:1 complex, which is consistent with DNA duplex formation. This was applicable for both sensing systems (Section 3.3.4). An example of a titration graph is shown in Figure 3.4 for base adjacent sensing with P1L.

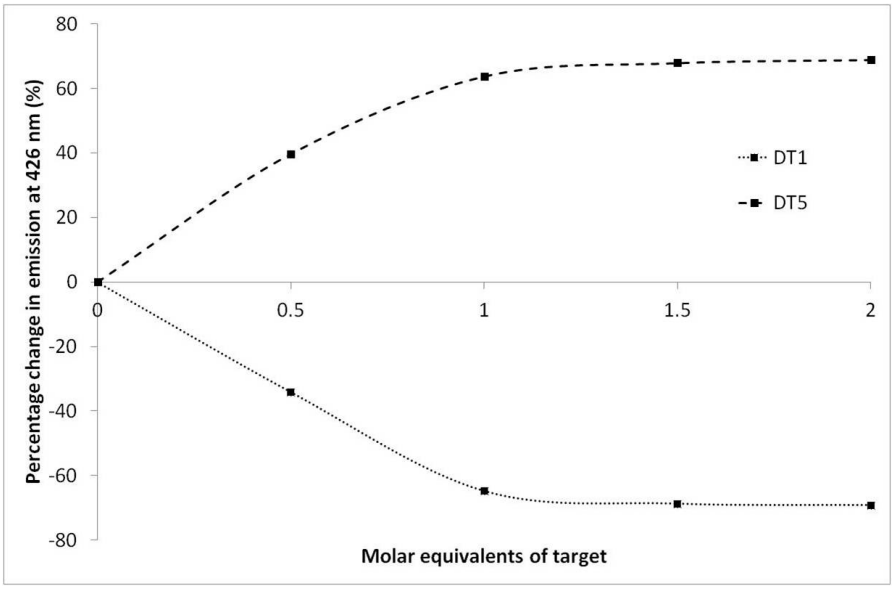

Figure 3.4: Fluorescence titrations of up to 2 equivalents of DNA target into probe P1L. The binding is shown to be 1:1 since the emission does not change beyond 1 equivalent of target. Percentage change in emission is calculated at λ_{em} = 426 nm, compared to the probe alone. 1 μM DNA, 100 mM NaCl, 10 mM pH 7.0 sodium phosphate buffer, λ_{ex} = 350 nm.

3.3.4 DNA base opposite sensing

Melting and fluorescence studies

In the alternative base opposite sensing strategy, the anthracene emission is found to change as a function of the base directly opposite it (Figure 3.5).

P(*n*) (L/D)	5′ TGGACTCXCTCAATG 3′
DT(1-4)	3′ ACCTGAGBGAGTTAC 5′

Figure 3.5: DNA base opposite sensing system. X denotes the anthracene monomer. n is the carbon linker length and L/D denotes the stereochemistry. B = A, C, G, T.

DNA base opposite sensing is an effective strategy since each target forms a duplex with similar affinity as evidenced by T_M values (i.e. there are no duplexes formed with mismatching base pairs). The anthracene tag was once again seen to stabilise the

Table 3.3: Melting temperatures (°C) of DNA targets and DNA anthracene probes. 5 μM DNA, 100 mM NaCl, 10 mM pH 7.0 sodium phosphate buffer.

Probe/Target	DT1	DT4
DN	55	48
P6D	48.5	50.5

duplex despite the lack of hydrogen bonding in the central base pair (Table 3.3).

This system only works with longer linker lengths to the anthracene monomer (n = 3 - 7, where stereochemistry is either L or D) (Figure 3.1). For example, in Figure 3.6 the emission changes are shown upon addition of base opposite targets to P6D probe. P6D was found to be a particularly effective probe based on its base discriminating ability and changes in absolute fluorescent emission.

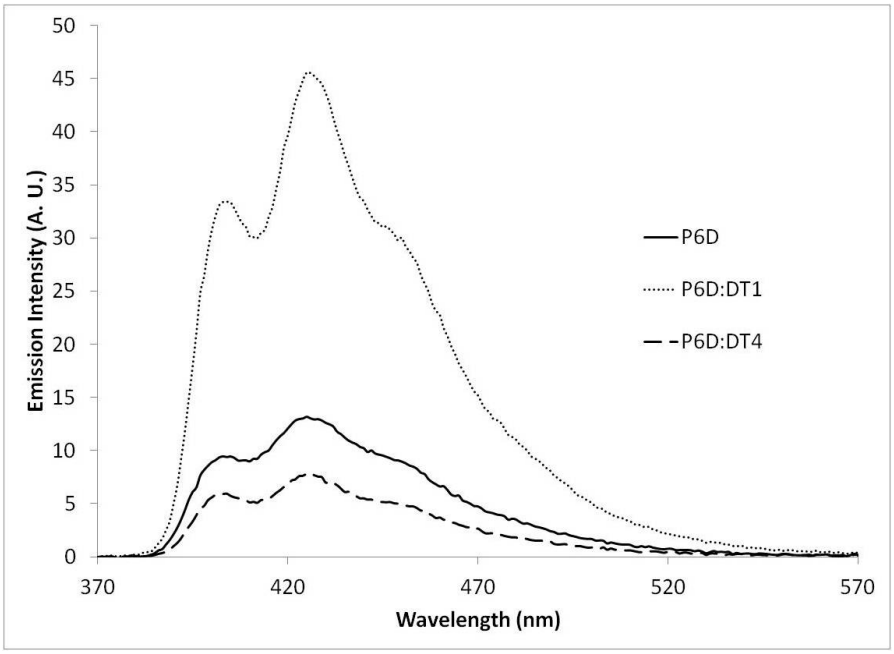

Figure 3.6: Fluorescence spectra showing the change in emission upon hybridisation of anthracene probe P6D with targets DT1 and DT4 respectively. 1 μM DNA, 100 mM NaCl, 10 mM pH 7.0 sodium phosphate buffer, λ_{ex} = 350 nm.

Adenine opposite the anthracene causes the emission to increase by the high-

est amount at λ_{em} = 426 nm for P6D (+244%), relative to the probe alone. Conversely, thymine opposite anthracene causes the emission to decrease (-41%). In general, the emission trend for the DNA base opposite sensing is purines>pyrimidines. This is thought to be caused by the size of the nucleobase opposite the anthracene, and how much the anthracene is able to intercalate into the duplex. There is also emission variation caused by the probe linker length (n) and stereochemistry (L/D), but for simplicity the P6D probe shall be discussed (full results can be seen in Appendix A).

3.3.5 DNA circular dichroism studies

Duplex DNA typically adopts a B-DNA conformation, which has characteristic features in CD spectra. There is a positive peak at 280 nm from the helical twist and a negative peak at 245 nm from base stacking. [133] This is seen for all unmodified DNA duplexes. CD spectroscopy studies show the DNA anthracene probe and DNA target duplex to be B-DNA (Figure 3.7). There is also a notable positive shoulder peak at approximately 255 nm from the induced anthracene signal. A CD signal is induced from the anthracene chromophore upon its interaction with neighbouring base pairs. [74, 132, 134] At high concentrations of DNA anthracene probe, the anthracene CD signal can be observed between 320 and 420 nm. Mismatches in the duplex cause distortions to the structure, which is observed in the CD spectra. [33]

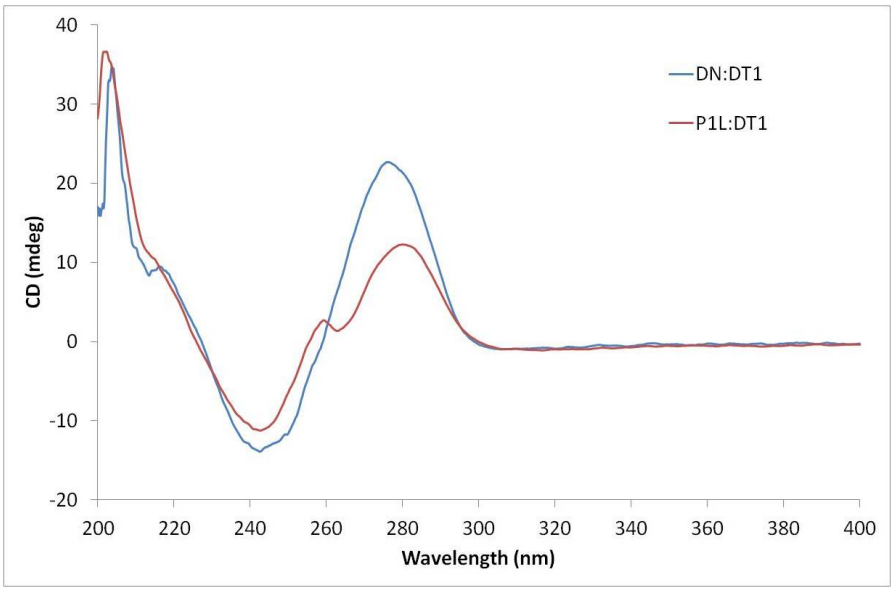

Figure 3.7: Circular dichroism spectra of unmodified DNA and P1L duplexes. 5 μM DNA, 100 mM NaCl, 10 mM pH 7.0 sodium phosphate buffer.

3.4 RNA sensing

3.4.1 RNA synthesis, deprotection and purification

One of the main objectives of the project was to synthesise and study RNA targets for sensing with the DNA anthracene probes. RNA synthesis was carried out using phosphoramidite chemistry as for DNA (Chapter 2). During synthesis there was a 10 minute coupling time on each base as opposed to 25 s for its DNA equivalent. A reduced concentration of iodine (0.05 M) was used for a milder oxidation step. There were further considerations during deprotection. RNA deprotection was carried out off-column since milder conditions were required. The deprotection protocol required improvement to provide optimal yields. Extending the TBAF incubation time to up to 36 hours enhanced efficiency of protecting groups removal. Replacing ethanol with isoproponal increased the level of precipitation, but crucially using a refrigerated centrifuge ensured the pellet remained intact. Purification was carried out via RP-HPLC and characterisation by mass

Table 3.4: RNA Sequences. X denotes the anthracene monomer. n is the carbon linker length and L/D denotes the stereochemistry.

Oligonucleotide	Sequence (5' to 3')
DN	TGGACTCTCTCAATG
P(n)(L/D)	TGGACTCXCTCAATG
RT1	CAUUGAGAGAGUCCA
RT2	CAUUGAGGGAGUCCA
RT3	CAUUGAGCGAGUCCA
RT4	CAUUGAGUGAGUCCA
RT5	CAUUGAGAAAGUCCA
RanR	CAUAAGAAGACCCUU

spectrometry as before. Table 3.4 gives the RNA oligonucleotides used in this study; the sequence is the same as DNA. A full list of oligonucleotides is given in Table G.1, Appendix G. RT(1 - 5) are RNA targets that are complementary to DN, P1L and P6D, but for one base difference. RanR is a random mismatching RNA sequence.

3.4.2 RNA SNP sensing

The RNA SNP sensing capabilities were tested in the same way as for the DNA. The same DNA anthracene probes were used with the RNA targets. All probes and targets were tested and the full results are shown in Appendix A. A summary of the base adjacent sensing results for DNA and RNA targets are presented in Figures 3.8, 3.9 and base opposite results in Figures 3.10, 3.11. The T_M values of the duplex combinations are shown in full within Appendix A. The P1L and P6D probes are reported here for consistency to represent the base adjacent and base opposite sensing results respectively.

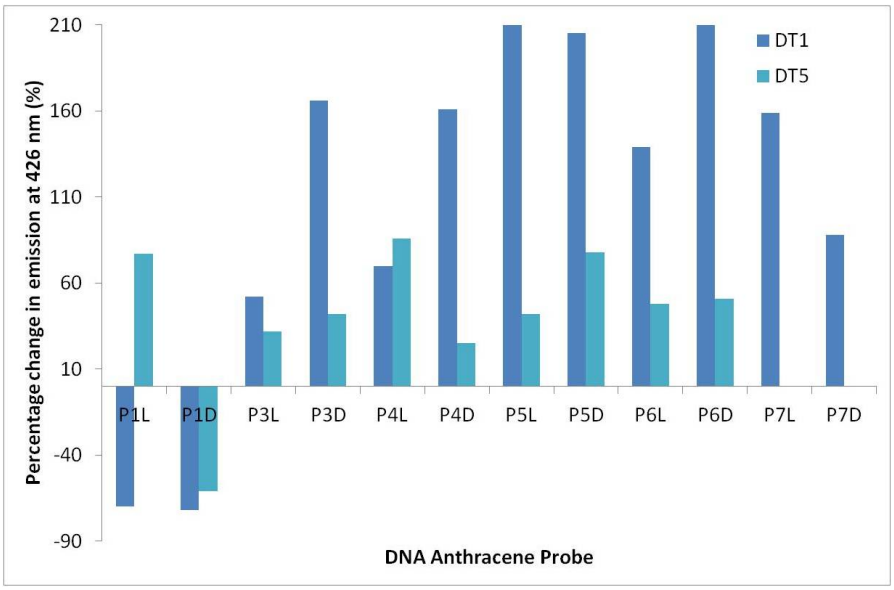

Figure 3.8: Summary of percentage change in emission for DNA base adjacent sensing targets for all DNA anthracene probes. Percentage change in emission is calculated at λ_{em} = 426 nm, compared to the probe alone. 1 μM DNA, 100 mM NaCl, 10 mM pH 7.0 sodium phosphate buffer, λ_{ex} = 350 nm.

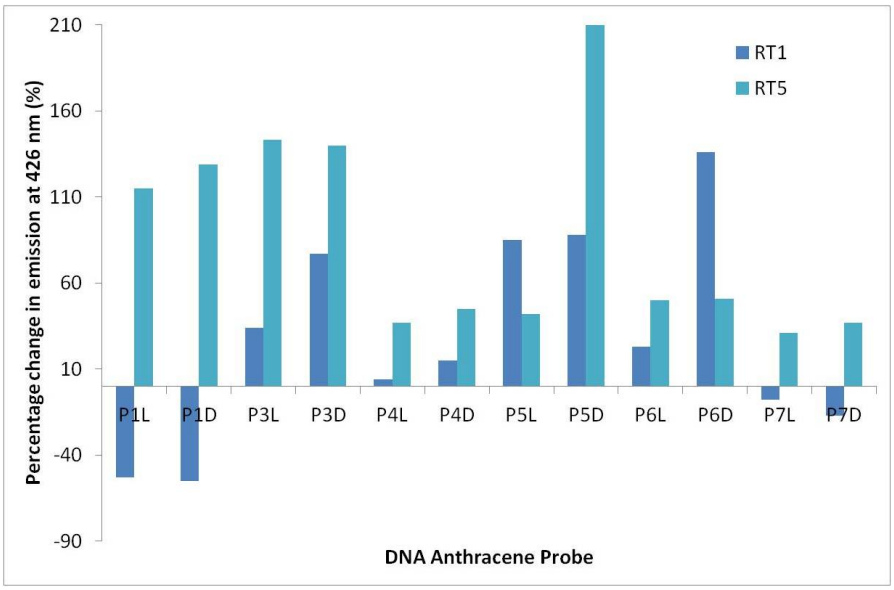

Figure 3.9: Summary of percentage change in emission for RNA base adjacent sensing targets for all DNA anthracene probes. Percentage change in emission is calculated at λ_{em} = 426 nm, compared to the probe alone. 1 μM DNA/RNA, 100 mM NaCl, 10 mM pH 7.0 sodium phosphate buffer, λ_{ex} = 350 nm.

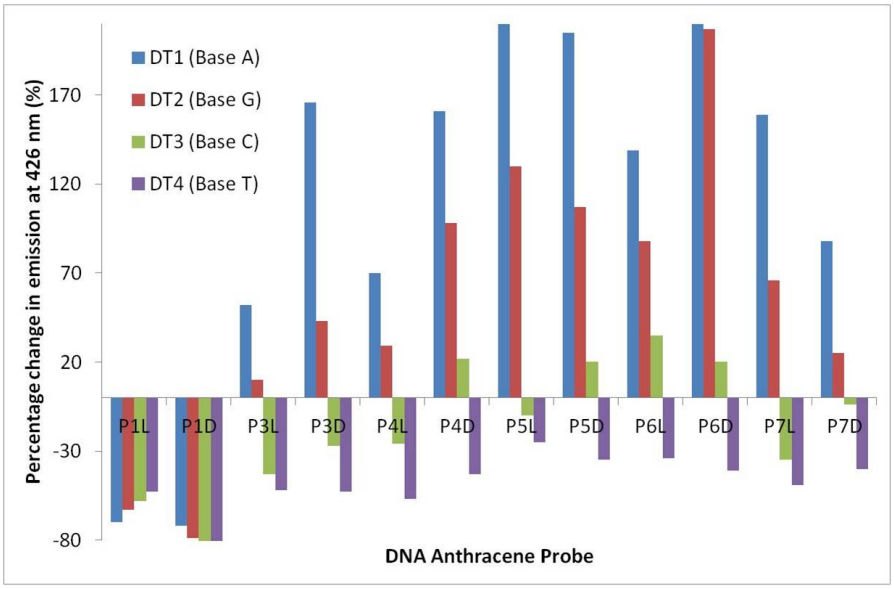

Figure 3.10: Summary of percentage change in emission for DNA base opposite sensing targets for all DNA anthracene probes. Percentage change in emission is calculated at λ_{em} = 426 nm, compared to the probe alone. 1 μM DNA, 100 mM NaCl, 10 mM pH 7.0 sodium phosphate buffer, λ_{ex} = 350 nm.

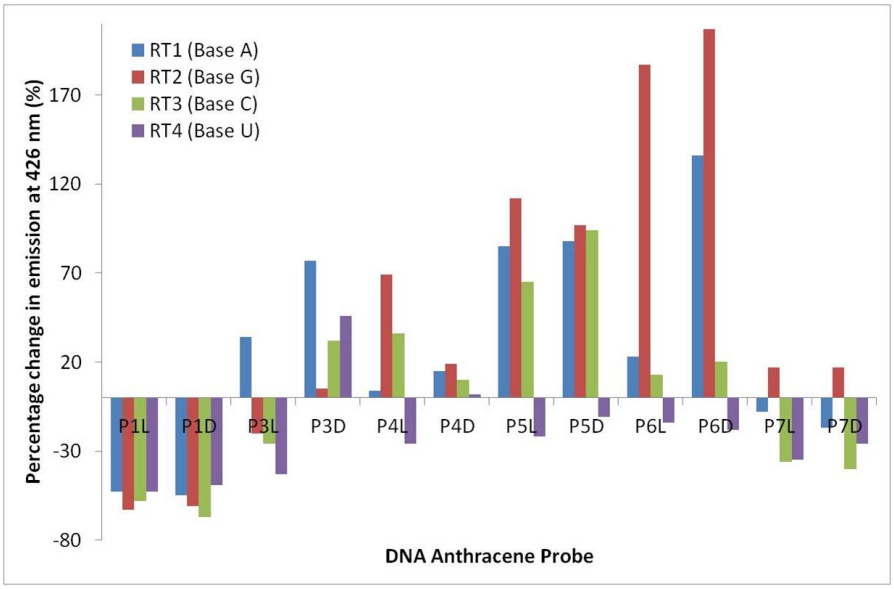

Figure 3.11: Summary of percentage change in emission for RNA base opposite sensing targets for all DNA anthracene probes. Percentage change in emission is calculated at λ_{em} = 426 nm, compared to the probe alone. 1 μM DNA/RNA, 100 mM NaCl, 10 mM pH 7.0 sodium phosphate buffer, λ_{ex} = 350 nm.

Table 3.5: Melting temperatures (°C) of DNA anthracene probes and RNA targets, plus controls. 5 μM DNA, 100 mM NaCl, 10 mM pH 7.0 sodium phosphate buffer.

Probe/Target	RT1	RT2	RT3	RT4	RT5
DN	60	56	46	47.5	45
RN	71	66	60	60.5	54
P1L	51	48	51	52	41
P1D	49.5	45.5	45.5	46	38

3.4.3 RNA base adjacent sensing

Melting and fluorescence studies

Unmodified DNA (DN) and its complementary target (DT1) provide a standard (55 °C) which can be used to compare melting temperatures to (Table 3.5). The equivalent RNA duplex version (RN:RT1) gives a significantly higher melting temperature of 69 °C under the same conditions. For DNA and RNA hybrids, DN:RT1 and RN:DT1, the melting temperatures are 60 °C and 53 °C respectively. This trend in melting temperatures is conformation dependent and agrees with literature. [3, 135]

The complexity now increases if there is a DNA anthracene probe with an RNA target (P1L:RT1) which gives a melting temperature of 51 °C, whereas the DNA anthracene probe with a DNA target (P1L:DT1) gives 53 °C. Melting studies confirmed that all the duplexes formed between the DNA anthracene probes and RNA targets were duplexes at room temperature (Table 3.5).

It has been previously observed that 1L anthracene (Figure 3.1) is able to intercalate into the DNA, which stabilises the duplex. [33] There is some evidence of this here, with modified duplexes having higher T_M values compared to their unmodified counterparts. As discussed previously, the duplex case of P1L:DT5 has a higher T_M (T_M = 46 °C) compared to DN:DT5 (T_M = 42 °C), indicating the anthracene intercalates and stabilises the duplex. The trend is not replicated with P1L:RT5 (T_M = 41 °C) versus

DN:RT5 ($T_M = 45\,°C$) or RN:RT5 ($T_M = 54\,°C$). It is understandable in the RN:RT5 comparison since RNA/RNA duplexes are fundamentally more stable than DNA/RNA duplexes. Overall this suggests that the 1L anthracene does not intercalate as much into the RNA duplex compared to the DNA duplex. However, the differences in melting temperatures between the P1L and unmodified duplexes show that the mismatch duplex retains more intercalation compared to the match duplex.

Fluorescence spectroscopy measurements were carried out for RNA target strands RT1 and RT5 that were added to DNA anthracene probe P1L (Figure 3.12).

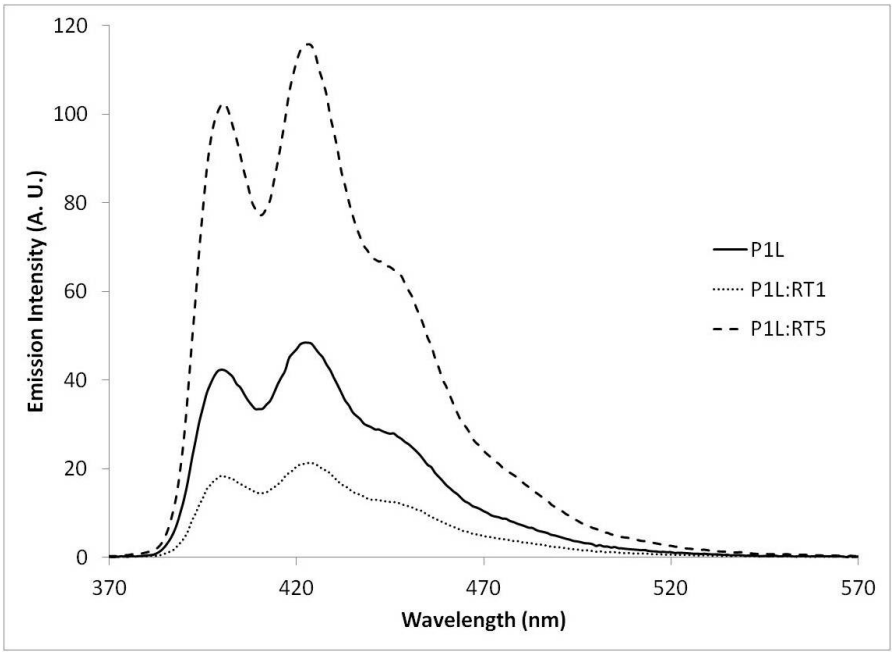

Figure 3.12: Fluorescence spectra showing the change in emission upon hybridisation of anthracene probe P1L with targets RT1 and RT5. 1 μM DNA/RNA, 100 mM NaCl, 10 mM pH 7.0 sodium phosphate buffer, $\lambda_{ex} = 350$ nm.

It was observed that the emission intensity decreased as the matching RNA target RT1 was added, yet the mismatching RNA target RT5 caused the emission to increase. The addition of the matching target RT1 caused a 55% decrease in emission at $\lambda_{em} = 426$ nm, with respect to the probe alone. However, the mismatching target RT5 caused an

increase in emission of 115%. For the equivalent DNA targets, the percentage emission differences, compared to the probe alone, are a 70% decrease for the matching target and a 77% increase for the mismatching target. Clearly the percentage values between RNA and DNA targets vary, but interestingly the ON/OFF sensing trend remains the same between matching and mismatching targets. As described for the DNA base adjacent sensing, P1L was the only probe able to discriminate between DT1 and DT5. However in the case of RNA, there is an exception to this rule. Interestingly the P1D also has the same ON/OFF sensing trend for the base adjacent targets RT1 and RT5 (Table A.4), which was not observed for the analogous DNA system. From previous studies, it is suggested that there is a weaker interaction between the anthracene and DNA bases in the 1D isomer system. [87] This is attributed to the D stereochemistry creating an unfavourable alignment angle between the anthracene and the base pair stack which results in less intercalation. Previous model studies have shown the 1L isomer to fit into the duplex like a base, whereas the 1D isomer duplex is more deformed due to the different orientation of the anthracene towards the minor groove. This causes the large difference in melting temperatures between the 1L and 1D isomer systems (Table 3.6). However in the case of RNA, the melting temperatures show that the 1D isomer now stacks better with the RNA target compared to the analogous DNA target. Therefore the 1D isomer has a better alignment for intercalation of the anthracene into the duplex, which leads to the ON/OFF sensing observed in the fluorescence studies. In comparison the 1L isomer does not stack as well with RNA, however the stacking seen with DNA is very optimal.

In both cases the fluorescence emission intensity was shown not to change beyond one equivalent of RNA target being added (Figure A.2). This shows that there is 1:1 DNA/RNA binding. As expected, there was no significant change in emission intensity when random mismatching target RanR was titrated into the probe (Figure A.2).

Table 3.6: Difference in melting temperatures (°C) of DNA anthracene probes and DNA/RNA targets, compared to the unmodified complementary DNA duplex (DN:DT1 = 55 °C). 5 μM DNA, 100 mM NaCl, 10 mM pH 7.0 sodium phosphate buffer.

Probe/Target	DT1	DT5	RT1	RT5
DN	55	-13	+5	-10
P1L	-2	-9	-4	-14
P1D	-7	-20	-5.5	-21

3.4.4 RNA base opposite sensing

Melting and fluorescence studies

The T_M values of the duplex combinations are shown in full within Appendix A. The longer linker probe P6D causes some stabilisation compared to the unmodified duplex but not in all cases (Table 3.7).

Table 3.7: Melting temperatures (°C) of DNA anthracene probes and RNA targets, plus controls. 5 μM DNA, 100 mM NaCl, 10 mM pH 7.0 sodium phosphate buffer.

Probe/Target	RT1	RT2	RT3	RT4	RT5
DN	60	56	46	47.5	45
RN	71	66	60	60.5	54
P6D	48	49	48.5	48.5	39.5

Similarly for the base opposite system, fluorescence spectroscopy measurements were carried out on addition of RNA target strands to the probe P6D (Figure 3.13).

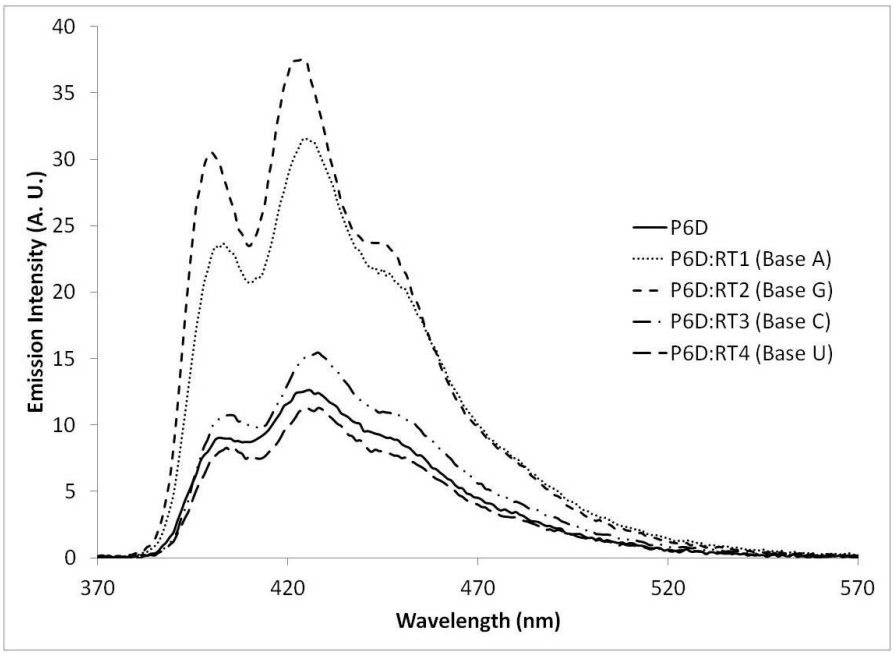

Figure 3.13: Fluorescence spectra showing the change in emission upon hybridisation of anthracene probe P6D with targets RT1 - RT4 (RT5 in Appendix A) respectively. 1 μM DNA/RNA, 100 mM NaCl, 10 mM pH 7.0 sodium phosphate buffer, λ_{ex} = 350 nm.

Since P6D has a longer carbon linker (Figure 3.1), it is possible it can discriminate base opposite variations better than probes with shorter linker lengths. It was observed that the emission intensity increased/decreased depending on the base opposite in the RNA target added. The addition of RT2 (G base opposite) causes the greatest increase in emission at λ_{em} = 426 nm (+207%) with respect to the probe alone and RT4 (U base) is the only RNA target to cause a decrease in emission (-18%). In direct comparison to the base adjacent system the target RT1 (A base) now causes an increase in emission (+136%), rather than a decrease. This sensing result mirrors previous DNA linker studies [86], which show the purine bases cause a significant increase in emission. The pyrimidines cause little change in emission (cytosine) or a decrease in emission (thymine, analogous to uracil). This result again suggests that the nucleobase opposite the anthracene has an effect on how efficiently the anthracene is able to intercalate into the duplex.

Despite there being some small trend differences between the RNA and DNA target sensing systems, these results clearly show that the probe P6D can indeed discriminate between the RNA bases located opposite to the anthracene. In all cases the fluorescence emission intensity was shown not to change beyond one equivalent of RNA target being added (Figure A.3). This again shows that there is 1:1 DNA/RNA binding. As expected there was no significant change in emission intensity when random mismatching target RanR was titrated into the probe (Figure A.3).

3.4.5 RNA circular dichroism studies

Circular dichroism (CD) spectroscopy was additionally used to observe the interaction of the anthracene within the duplex. DNA duplexes have a B-DNA conformation, whereas RNA duplexes are A-DNA. The difference between the conformations lies in the RNA duplex being a thicker right-handed duplex with a shorter distance between base pairs. Characteristic features for B-DNA in CD spectra are a roughly equal positive peak centred at 280 nm and negative peak at 245 nm, whereas for A-DNA it has a dominant positive peak at 260 nm and negative peak at 210 nm. [133] The unmodified DNA/RNA and RNA/DNA duplexes closely resemble the A-DNA conformation with a negative peak at 210 nm and positive peak at 265 nm. However, there is also a small negative peak at 245 nm, which is a B-DNA feature (Figure 3.14). It has been described in the literature as a homologous conformation. [3, 136, 137]

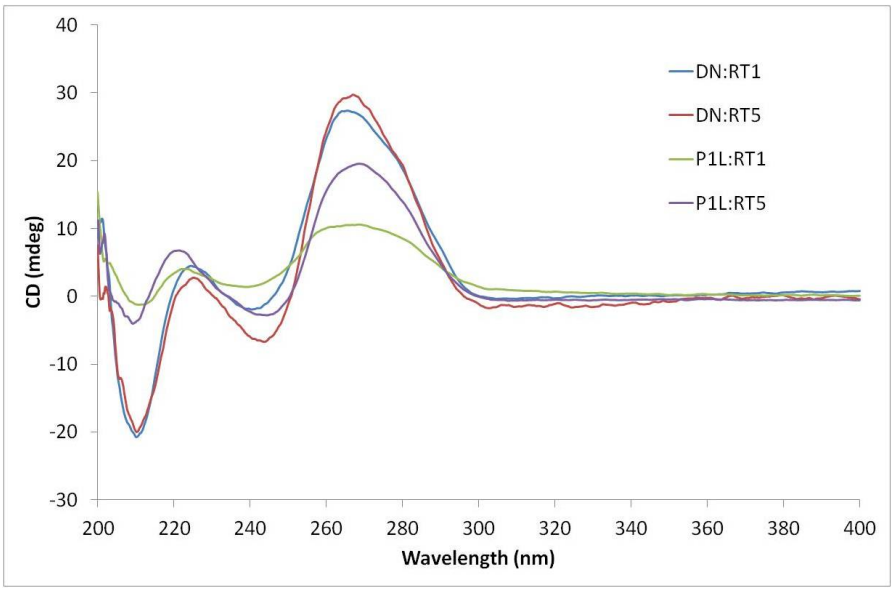

Figure 3.14: Circular dichroism spectra of unmodified (DN) and modified (P1L) duplexes. 5 μM DNA/RNA, 100 mM NaCl, 10 mM pH 7.0 sodium phosphate buffer.

Previous studies of P1L with DNA targets have shown features in CD spectra which indicate interactions between anthracene and nearby bases. [87] In this study no shoulder peak at approx. 250 nm was observed which indicated less interaction between anthracene and the adjacent RNA bases. This suggests the anthracene does not stack well in the P1L and RNA target duplexes, and would also explain the lower melting temperatures compared to the controls. CD spectra for the other RNA targets with P1L can be seen in Appendix A. The P6D:RNA duplex CD spectra are also included (Figure A.7) and display DNA/RNA hybrid CD characteristics.

3.5 2′OMe RNA SNP sensing

2′OMe RNA is an analogue oligonucleotide often used in cell studies due to its duplex stability and its greater resistance to nucleases. [11, 138] It was therefore decided to carry out preliminary sensing experiments using 2′OMe RNA. The structure of 2′OMe RNA can be seen in Figure 3.15.

Table 3.8: 2′OMe RNA Oligonucleotide Sequences

Oligonucleotide	Sequence (5' to 3')
2OMeRN	UGGACUCUCUCAAUG
2OMeT1	CAUUGAGAAGAGUCCA
2OMeT4	CAUUGAGUUGAGUCCA
2OMeT5	CAUUGAGAAAAGUCCA

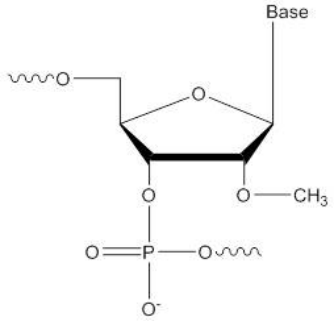

Figure 3.15: 2′OMe RNA structure

Compared to RNA, 2′OMe RNA has an extra methyl group on the 2′ position. In general, 2′ modifications enhance the biostability and affinity of the oligonucleotide towards their target *in vitro* and *in vivo*. [139] The 2′OMe RNA sequences synthesised can be seen in Table 3.8. The 2′OMe RNA oligonucleotides were prepared similarly to DNA (Chapter 2). The deprotection was performed using milder conditions by reducing the temperature to 69 °C for 1 - 2 hours, or alternatively, leaving at room temperature for 5 hours. The 2′OMe RNA sensing results can be used to reinforce the RNA sensing trends that have been discussed so far.

Melting and fluorescence studies

Melting studies show that all duplexes are stable at room temperature (Table 3.9). The unmodified duplex T_M values agree with literature trends. [140–142] The unmodified 2′OMe RNA duplex with methylation on both strands causes a very high melting tem-

Table 3.9: Melting temperatures (°C) of 2′OMe RNA targets and DNA anthracene probes. 5 μM each oligonucleotide, 100 mM NaCl, 10 mM sodium phosphate pH 7.0.

Probe/Target	2OMeT1	RT1	DT1
2OMeRN	79	72	52.5
DN	62	60	55
RN	74.5	69	53

perature of 79 °C, clearly indicating that the 2′ modification causes a significant increase in binding affinity. Table 3.9 shows that 2′OMe RNA oligonucleotides have a higher affinity for RNA complementary targets than analogous DNA, which agrees with literature. [141] The 2′OMe RNA:RNA duplex is more stable than DNA:RNA, which in turn is more stable than DNA:DNA. Therefore using 2′OMe RNA in future sensing experiments is important in terms of thermodynamic stability. Some preliminary fluorescence measurements between DNA anthracene probes and 2′OMe RNA target strands were carried out (Table 3.10). The emission spectra are given in Figures A.8 and A.9, Appendix A.

The trends were similar to those for DNA and RNA target sensing i.e. the ON/OFF sensing for base adjacent system and variable for the base opposite system. In terms of values, the P1L results are very similar to the RNA values (Table A.4). The melting temperature trends for the 1L modified duplexes are very similar to those observed for RNA (Table 3.11). The 1L anthracene stabilises less for both RNA and 2′OMe RNA targets, compared to the unmodified probes. This is to be expected since the fluorescence

Table 3.10: Percentage differences in emission on addition of 2′OMe RNA targets to DNA anthracene probes, relative to the probe alone. Percentage change in emission is calculated at λ_{em} = 426 nm, compared to the probe alone. 1 μM DNA, 100 mM NaCl, 10 mM pH 7.0 sodium phosphate buffer, λ_{ex} = 350 nm.

Probe/Target	2OMeT1	2OMeT4	2OMeT5
P1L	-57%	-52%	+122%
P6D	+178%	+6%	+48%

Table 3.11: Melting temperatures (°C) of 2′OMe RNA targets and DNA anthracene probes. 5 μM each oligonucleotide, 100 mM NaCl, 10 mM sodium phosphate pH 7.0.

Probe/Target	2OMeT1	2OMeT5	RT1	RT5	DT1	DT5
2OMeRN	79	64	72	63.5	52.5	41
DN	62	47.5	60	45	55	42
RN	74.5	60.5	69	54	53	35
P1L	53	43.5	51	41	53	46

results between RNA and 2′OMe RNA show similarities.

The P6D values are similar to both the DNA and RNA results (Table A.4), however one noticeable difference was a small positive value for 2′OMe GUG rather than the previously observed negative value in all cases. A possible explanation would be that the anthracene is able to intercalate more effectively since the uracil, with its 2′OMe modification, is larger and less able to stack efficiently (Table 3.12). This explains why the RT4 targets (U base opposite) caused less of a decrease compared with analogous DNA. As extra modifications occur the base opposite allows the anthracene to intercalate more, which has already been observed for the purines in DNA sensing (Section 3.3.4). This ties in well with the 2′OMe RNA and RNA targets (2OMeT4 and RT4 respectively) causing a bathochromic shift. This suggests the anthracene is able to intercalate more compared to the equivalent DNA target DT4, which shows no peak shift. [143, 144]

Table 3.12: Melting temperatures (°C) of 2′OMe RNA targets and DNA anthracene probes. 5 μM each oligonucleotide, 100 mM NaCl, 10 mM sodium phosphate pH 7.0.

Probe/Target	2OMeT1	2OMeT4	RT1	DT1
2OMeRN	79	69	72	52.5
DN	62	52	60	55
RN	74.5	58.5	69	53
P6D	50.5	52	48	49

Circular dichroism studies

2′OMe RNA duplexes give an A-form conformation like RNA rather than the B-form DNA (Appendix A, Figure A.10). In fact, it only takes a couple of 2′OMe RNA modifications to DNA to cause a transition from B-form to A-form. [145] It would be expected that hybrid duplexes between 2′OMe RNA and RNA would be A-form also. They are shown to be very similar (Appendix A, Figure A.11). It was also assumed that 2′OMe RNA and DNA would also be A-form given that 2′OMe RNA has such a domineering impact on the structure. However, Figure A.11 shows the hybrids to be homologous between the A-form and B-form. This was seen before with RNA and DNA hybrids, and on closer inspection, the CD spectra are very similar. The 2OMeRN:DT1 and RN:DT1, and vice versa DN:2OMeRN and DN:RT1, have the same features as described for hybrids previously (Figure A.4). The DNA anthracene probe with 2′OMe RNA targets causes similar CD spectra as previously seen with analogous RNA targets (Figure 3.16), which is pleasing since the unmodified cases are so similar.

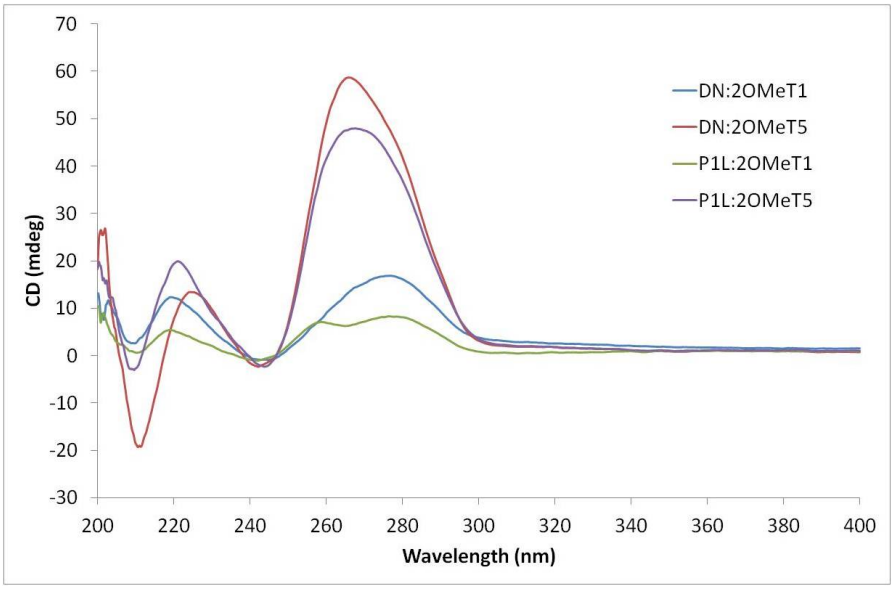

Figure 3.16: Circular dichroism spectra of unmodified (DN) and modified (P1L) 2′OMe RNA duplexes. 5 μM DNA/RNA, 100 mM NaCl, 10 mM pH 7.0 sodium phosphate buffer.

Table 3.13: CDKN1A oligonucleotide sequences. X denotes the anthracene monomer. n is the carbon linker length and L/D denotes the stereochemistry.

Oligonucleotide	Sequence (5' to 3')
ZDN	AGTCGCGTCTCAGCT
ZP(n)(L/D)	AGTCGCGXCTCAGCT
ZDT1	AGCTGAGCCGCGACT
ZDT2	AGCTGAGACGCGACT
ZRT1	AGCUGAGCCGCGACU
ZRT2	AGCUGAGACGCGACU

In the P1L:RNA CD spectra seen before (Figure 3.14), it was observed that the anthracene did not stack well since there was a lack of dominant shoulder peak at approx. 250 nm. An exception is observed for the P1L:2OMeT1 duplex. This is at the expense of the helical twist though, with the positive peak at 270 nm much reduced compared to the P1L:2OMeT5 case. The differences in CD spectra are expected since earlier DNA studies showed that even single base mismatches caused distortions to the duplex. [33]

3.6 CDKN1A gene SNP sensing

An advancement was to test the DNA anthracene probe against a naturally occurring SNP sequence. The CDKN1A gene sequence chosen is associated with Alzheimer's disease. [45] Although it is a different sequence from studies discussed so far, there is a one base difference, C to A, for wildtype and variant respectively. Initial work with sequence-specific DNA anthracene probes (with varying linker length and stereochemistry as before) were used to sense the wildtype/variant DNA targets. The wildtype/variant RNA target equivalents were synthesised (Table 3.13) and tested in the same way. The C and A SNP's (underlined) correspond to the wildtype and variant targets respectively.

One of the more exciting and promising results of the CDKN1A study was testing

mixtures of targets. This involved adding the DNA anthracene probe to known percentage mixtures of the two targets. Collectively the emission results were used to generate a calibration line, which could then allow quantitative measurements from unknown samples. Initial studies using DNA show this to be possible.

3.6.1 CDKN1A gene DNA SNP sensing

All of the sequence-specific DNA anthracene probes were tested with the wildtype/variant DNA targets. In general the variant ZDT2 (A SNP) caused the emission to increase at $\lambda_{em} = 426$ nm (+124%) and the wildtype ZDT1 (C SNP) caused the emission to decrease (-39%), relative to the ZP5L probe only. It is pleasing to note the ON/OFF sensing observed for the non-biological sequence studies is reproduced here. It was found that ZP5L gave the biggest percentage difference between the two SNP targets and was used for further studies. The choice of a base opposite sensing system over base adjacent was due to the smaller difference in melting temperatures between the two targets.

3.6.2 CDKN1A gene RNA SNP sensing

Melting studies showed that all DNA/DNA and DNA/RNA duplexes were stable at room temperature (Table 3.14). For full results see Table A.7, Appendix A. Circular dichroism studies showed all unmodified and modified duplexes have B-DNA conformation (for example, Figure A.13). All DNA anthracene probes were tested with the RNA targets and full results can be seen in Table A.6, Appendix A. Overall, the ON/OFF

Table 3.14: Melting temperatures (°C) of CDKN1A DNA and RNA targets with DNA anthracene probes, plus controls. 5 μM DNA, 100 mM NaCl, 10 mM pH 7.0 sodium phosphate buffer.

Probe/Target	ZDT1	ZDT2	ZRT1	ZRT2
ZDN	73	67	70	67
ZP5L	63	60	57	55.5

sensing trend for the wildtype/variant is replicated for RNA as it was for DNA i.e. the ZRT2 (A SNP) causes emission to increase and ZRT1 (C SNP) to decrease, relative to the probe only. The increase in emission for ZRT2 was seen to be not as great compared to ZDT2, and in some cases little or no change was seen. The greatest percentage difference between RNA targets was for ZP4D (Δ = 75%). For consistency the ZP5L was focussed on to allow comparison to previous CDKN1A DNA work within the group. The ZRT2 target caused a 12% increase in emission and the ZRT1 target a 47% decrease in emission at λ_{em} = 426 nm, relative to the probe alone (Figure 3.17). In both cases the fluorescence emission intensity was shown not to change beyond one equivalent of RNA target being added (Figure A.12). This again shows that there is 1:1 DNA/RNA binding.

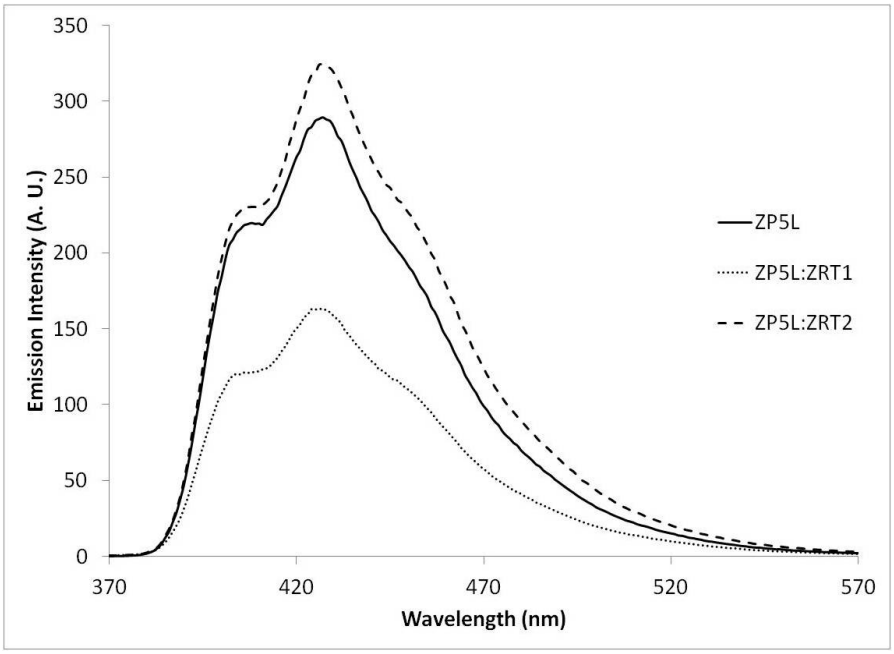

Figure 3.17: Fluorescence spectra showing the change in emission upon hybridisation of anthracene probe ZP5L with targets ZRT1 (C SNP) and ZRT2 (A SNP) respectively. 1 μM DNA/RNA, 100 mM NaCl, 10 mM pH 7.0 sodium phosphate buffer, λ_{ex} = 350 nm.

Overall there is a 59% change in emission between the RNA targets (approx. av-

erage for all the probes tested), which although significantly less than the 163% change between analogous DNA targets, is still worth pursuing for future sensing experiments. Comparisons between the CDKN1A sensing system and the non-biological sequence sensing previously discussed does not yield anything of relevance beyond purines opposite anthracene causing the emission to increase and pyrimidines causing emission to decrease. Previous work has shown that neighbouring bases to the central base have a significant impact on emission, despite the respective probes both having a 5L linker. [33]

3.6.3 CDKN1A gene RNA quantitative SNP sensing

In most biological cases, SNPs occur heterozygously rather than homozygously (Section 1.3, Chapter 1). Previously only the homozygous case was considered (although a 50:50 mixture of targets was tested in a previous study [88]). If there were mixtures of the two SNP targets would the fluorescence response be linear? Could this lead to quantitative measurements of unknown mixtures being determined from a calibration graph? This was shown to be possible with mixtures of CDKN1A DNA targets and ZP5L anthracene probe carried out at a probe concentration of 1 μM (Figure 3.18). The results were shown to be reproducible with ZP5L and RNA target mixtures (Figure 3.19).

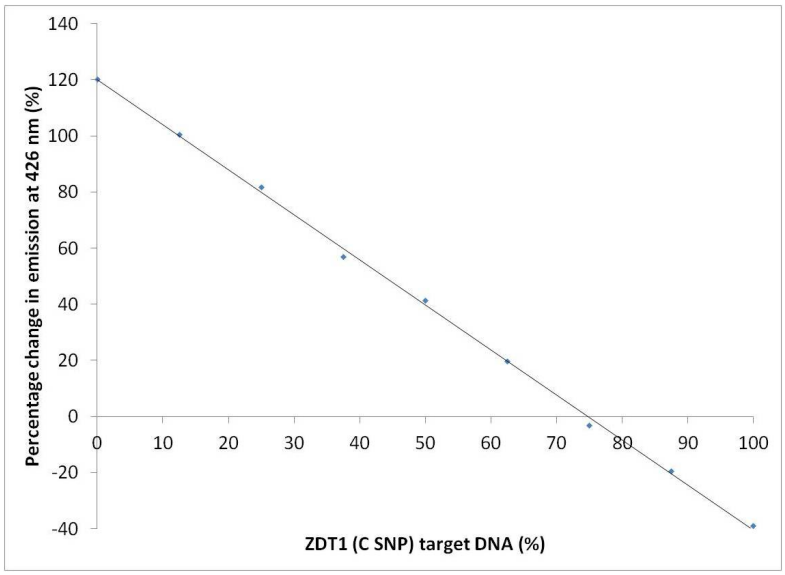

Figure 3.18: Percentage difference in emission of ZP5L at λ_{em} = 426 nm, with respect to probe alone, upon addition of mixtures of DNA targets. The percentage of ZDT1 (C SNP) is quoted: the remaining percentage is made up of ZDT2 (A SNP). 1 μM DNA, 100 mM NaCl, 10 mM pH 7.0 sodium phosphate buffer, λ_{ex} = 350 nm. A linear regression fit of the data is added (y = -0.6383x + 122.63, R^2 = 0.9989).

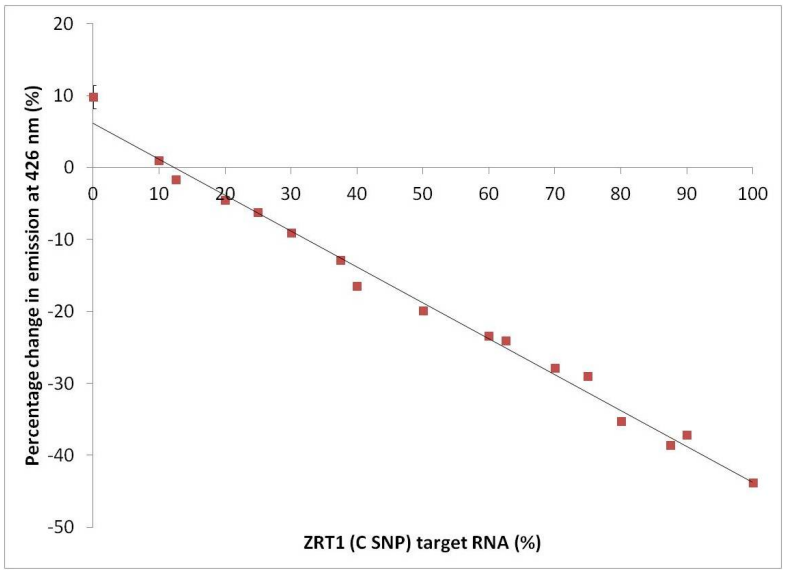

Figure 3.19: Percentage difference in fluorescence of ZP5L at λ_{em} = 426 nm, with respect to probe alone, upon addition of mixtures of RNA targets. The percentage of ZRT1 (C SNP) is quoted: the remaining percentage consists of ZRT2 (A SNP). 1 μM DNA/RNA, 100 mM NaCl, 10 mM pH 7.0 sodium phosphate buffer, λ_{ex} = 350 nm. A linear regression fit of the data is added (y = -0.499x + 6.1796, R^2 = 0.9902)

.

If there is a significant difference in melting temperatures for the two targets with a probe then kinetics will affect the emission of target mixtures. The melting temperatures of ZP5L with RNA targets (Table 3.14) showed a difference of approximately 1.5 °C which is small enough not to cause significant preferential binding.

3.7 Conclusion

DNA SNP sensing has been shown to be successful in discrimination of single base differences based on emission and not relying solely on hybridisation. RNA SNP sensing can be carried out in the same way using DNA anthracene probes. Both base adjacent and base opposite sensing strategies are replicated. Differences in emission trends are caused by the change in conformation of the hybrid duplex and the efficiency of anthracene

intercalation into the duplex. This will be further investigated through modelling and NMR studies within the group. The 2′OMe RNA sensing results extrapolate from those results observed for RNA targets. The results also show promise for a full or partial 2′OMe RNA anthracene probe which could show resistance to cell degradation. 2′OMe RNA probes have already shown promise in targeting miRNA due to their increased stability of duplexes; faster kinetics of hybridisation and ability to bind in conditions that DNA cannot. [10, 146] Although interesting, an RNA anthracene probe would be difficult to synthesise and more susceptible to nucleases. The DNA and RNA SNP sensing strategies discussed in this chapter shall be further investigated within a cellular environment in Chapter 5. The ON/OFF RNA SNP sensing result for a sequence associated with Alzheimer's disease also opens the door for future assay developments. Finally, mixtures of targets give a linear response with RNA targets, allowing unknown alleic contributions to be determined.

Chapter 4

Optimising Cy3 and Cy5 tagged DNA delivery to cells

4.1 Introduction

An important goal of this project was to replicate the SNP sensing strategies described in Chapter 3 in a cellular environment. This is further discussed in Chapter 5. However there were several issues that needed to be considered before using this approach, centred around first the most effective method for delivery and second the fate of the DNA once it is introduced into the cell. As far as the latter is concerned, several strategies [78, 121, 147] have been employed to mitigate factors such as susceptibility to degradation by nucleases [148], non-specific binding to proteins and unwanted migration to the nucleus if the interaction with non-nuclear targets is required. [149]

The most popular technique for effecting non-viral delivery of DNA into cells (i.e. transfection as opposed to transduction) is to use chemical reagents that facilitate the passage of polyanionic DNA through the membrane bilayer. [150] DNA modification has also been shown to enhance cell delivery, with attached peptides facilitating chemical transfection [151, 152] and Locked Nucleic Acids (LNA) shown to have been taken up

without the use of transfection reagents. [153] Another uptake methodology is microinjection, which has been used in a study comparing the cell stability of phosphodiester and phosphorothioate oligonucleotides. [154, 155] A common alternative to microinjection is electroporation, which uses a rapid and high-voltage electric pulse that causes pore formation in the membrane. [156] Nevertheless there is a sparsity of literature that compares different transfection methodologies and their possible effect on intracellular DNA stability. This chapter describes a controlled fundamental study that was undertaken to compare the various techniques for transfection of DNA into cells, to include invasive methods such as microinjection and electroporation, and non-invasive methods such as chemical transfection.

Fluorescence microscopy was chosen as the method for monitoring cell transfection through the use of fluorophore-tagged DNA strands [106], which is by far the most common way of tracking cellular processes *in vitro*. Doubly tagged single strands or duplexes were chosen to allow transfection to be monitored by Förster resonance energy transfer (FRET). FRET is the physical process that occurs when the excited-state energy of a donor fluorophore is transferred nonradiatively to an acceptor in the excited state [22], which results in quenching of the donor fluorophore and excitation of the acceptor (Figure 4.1).

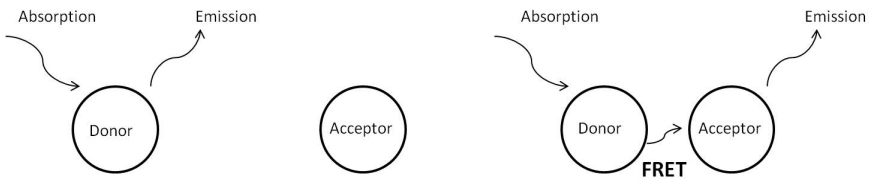

Figure 4.1: Schematic diagram of FRET. The donor fluorophore is able to donate energy to the acceptor fluorophore if they in close proximity. The donor emission must also overlap with the acceptor excitation spectra.

The efficiency of energy transfer depends on the spectral overlap of the emission and absorption spectra of the donor and acceptor respectively, as well as their

respective distance and orientation. The distance dependence of FRET can monitor differences over the range of 10-100 Å, which is ideal for macromolecules such as nucleic acids. [13, 157] FRET can be used to detect and quantify sequences extracted from biological samples [158–160] including real-time PCR assays. [161–163] It has also been widely used to detect hybridisation of donor- and acceptor-labelled complementary nucleic acid strands. [59, 164–166] This in turn can allow the integrity of a duplex to be monitored on entry to the cell, which is relevant to this study. As for the choice of FRET pair, fluorophores Cy3 (donor) and Cy5 (acceptor) are commonly used in nucleic acid experiments due to their easy attachment to DNA, high FRET efficiency, relatively low photobleaching and long emission wavelengths away from the autofluorescence region of cells. [57]

As described below, having confirmed that Cy3-Cy5-tagged DNA displays FRET in a cuvette in its single stranded and duplex form, a comparison of the effectiveness of delivery of intact DNA to cells using FRET is then described, via various techniques that include chemical transfection, microinjection and electroporation. The fundamental work demonstrates how the choice of technique is crucial for optimising the stability of DNA strands and duplexes in a cellular environment.

4.2 Results

4.2.1 Synthesis and characterisation of DNA probes

Table 4.1 shows the main oligonucleotides synthesised for this study. There are two further control sequences in Table B.1, Appendix B.

Tagged DNA strands were prepared by automated solid phase synthesis using conventional phosphoramidite chemistry, as described previously in Chapter 2. Cy3 and Cy5 phosphoramidites (Glen Research) were tagged to the 5′ and 3′ termini. Complementary strands S1 and S2 containing respectively a Cy3 and a Cy5 fluorophore at the

Table 4.1: Cy3 and Cy5 tagged DNA sequences synthesised.

Oligonucleotide	Sequence (5' to 3')
Cy3 strand (S1)	Cy3-TGGACTCTCTCAATG
Cy5 strand (S2)	Cy5-CATTGAGAAGAGTCCA
Cy3 and Cy5 strand (S3)	Cy5-TGGACTCTCTCAATG-Cy3

5′ terminus were prepared for duplex studies, in addition to a strand containing the fluorophores at each end (S3). Each strand was purified by reversed phase HPLC and characterised by mass spectrometry, with UV melting studies confirming that the S1:S2 duplex was stable at both room temperature and at 37 °C in salt conditions (110 mM - 10 mM sodium, respectively) appropriate for cell studies (Table B.2, Appendix B).

4.2.2 Cuvette fluorescence spectroscopy

For the strand S3 as well as the S1:S2 duplex, the Cy3-Cy5 fluorophore pair was expected to be in close enough proximity to display FRET (Figure 4.2). Figure B.1, Appendix B gives the normalised excitation and emission spectra of Cy3 and Cy5-tagged DNA, with the area of overlap labelled. This demonstrates the suitability of Cy3 and Cy5 as a FRET pair when tagged on DNA.

FRET was indeed evidenced by fluorescence spectroscopy studies in a cuvette (10 mM sodium phosphate buffer, 100 mM NaCl, pH 7.0, 1 μM strand concentration) in which the emission intensity from the Cy3 and Cy5 tags was monitored over the range 500-800 nm, when exciting only the Cy3 chromophore directly. In particular a titration study involving the addition of S2 to S1 indicated that the Cy3 signal at 570 nm decreased, while the signal for Cy5 at 670 nm increased, with no further increases observed after the addition of one molar equivalent of the target, consistent with 1:1 duplex formation (Figure 4.3).

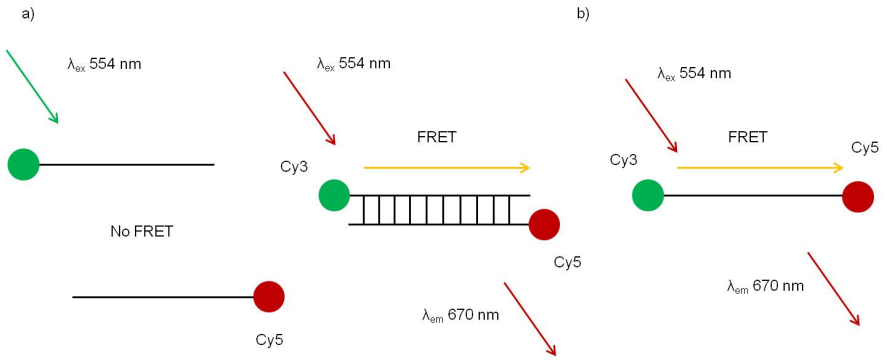

Figure 4.2: Schematic of Cy3 and Cy5 tagged DNA. a) Complementary DNA strands are individually tagged with Cy3 and Cy5 fluorophores. When in close enough proximity the Cy3 can donate energy to Cy5 through FRET. In this case, FRET can only occur when the two complementary strands form a duplex. b) Single strand DNA can be tagged at either end with Cy3 and Cy5. FRET can occur as long as the single strand remains intact.

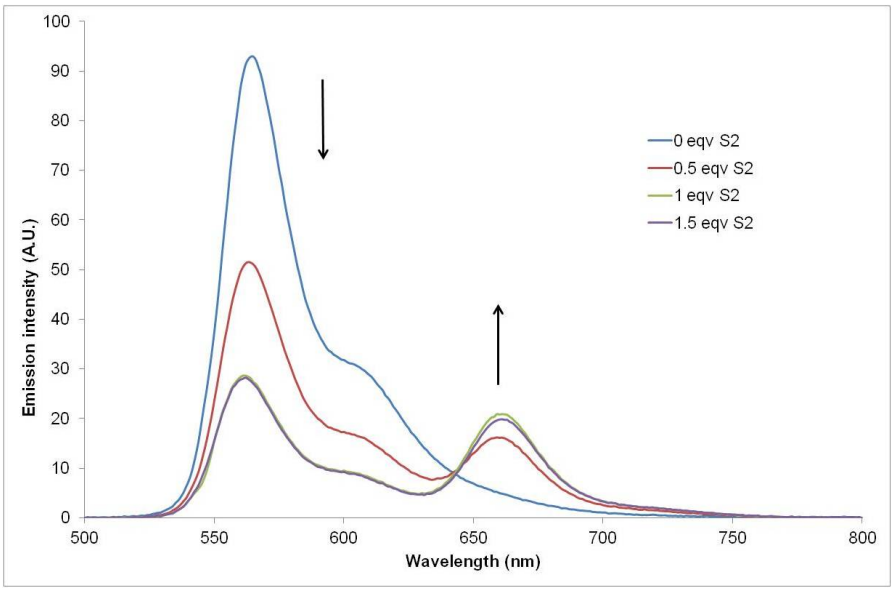

Figure 4.3: Emission spectra of Cy3 and Cy5 DNA. Titration of Cy5 tagged DNA (S2) into Cy3 tagged DNA (S1), showing resulting Cy5-Cy3 FRET upon duplex formation (λ_{ex} = 554 nm). The emission intensities centred at 570 nm and 670 nm correspond to emission from Cy3 and Cy5 respectively (conditions: 1 μM DNA, 100 mM NaCl, and pH 7.0 sodium phosphate buffer). The spectra are background subtracted, including the spectrum of S2 at 554 nm, which gave a small signal caused by direct excitation of the Cy5 chromophore.

Control studies indicated little or no emission at 670 nm when S2 was irradiated alone in the absence of S1 at 554 nm under the same conditions. Similar results and trends were obtained for the doubly-tagged strand S3. The FRET signal from the S1:S2 duplex and S3 were then studied in Chinese hamster ovary (CHO) cell lysate at 37 °C in the absence and presence of DNase (Figures B.2 and B.3 respectively, Appendix B). In cell lysate alone, over a period of 2 hours, only small changes in the emission spectra were observed. However as expected, the addition of nuclease brought about a rapid decrease in the FRET signal for both systems, indicating backbone cleavage of the DNA in either its single-stranded or duplex form. [59]

4.2.3 Fluorescence microscopy on fixed cells

Having observed the desired FRET effect under cuvette conditions, the same strands were then exposed to Chinese hamster ovary (CHO) cells that had previously been fixed using methanol, to allow the strands to readily permeate into the cell, which was otherwise not possible with live cells. Other fixatives were tested (Section 2.7.1, Chapter 2) but were not as effective as methanol. The successful transfection of S1:S2 as an intact duplex was evidenced by FRET (Figure 4.4) at room temperature using scanning laser confocal microscopy.

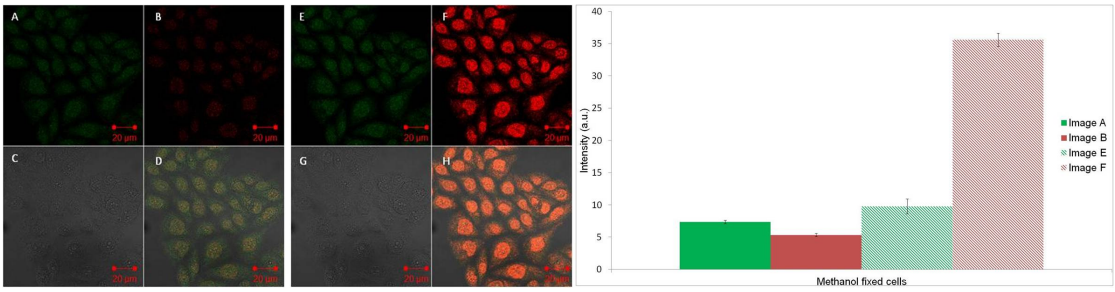

Figure 4.4: Fixed cell confocal microscopy images. Left: Cy3 and Cy5 tagged DNA duplex (S1:S2) added to fixed/permeabilised cells and imaged using confocal microscopy. Images A/E represents the Cy3 channel; B/F the Cy5 channel; C/G the bright field channel and D/H an overlay of all the channels. Images A-D are excited with the 543 nm laser. Images E-H are excited with both the 543 and 633 nm lasers. Right: Intracellular fluorescence intensity from images A/B and E/F. Data are expressed as mean ± s.e.m from at least ten cells ($p<0.001$).

The key result was the observation of a signal in image B (Cy5 channel) upon excitation at the Cy3 absorption wavelength, with a control study indicating no emission observed under these conditions when fixed cells were transfected with S2 alone (Figure B.4). Quantitative data extracted from the intensities of the cell images in Figure 4.4 also showed significant FRET based on the ratio between the Cy5 intensity and Cy3 intensity upon excitation at the Cy3 absorption wavelength only (Figure 4.4, first two bars on chart). The *in vitro* formation of a duplex was also indicated by FRET when the strands were added sequentially (S1 followed by S2) in order to replicate the cuvette experiment and show that the sequences were able to find each other in a cell environment (Figure B.5, Appendix B). A similar FRET signal was also seen on the addition of S3 to fixed cells but as expected, non-complementary Cy3 and Cy5 tagged DNA strands, added either together or sequentially, were shown not to display FRET (Figures B.6 and B.7 respectively, Appendix B). To enable a closer comparison with the cuvette studies, emission spectra were also recorded in fixed cell samples using spectral imaging inverted confocal microscopy (Figure B.8, Appendix B), and these gave broadly similar profiles, confirming the presence of FRET in fixed cells within both the S1:S2

duplex and the S3 strand.

4.2.4 Live cell fluorescence microscopy

Whereas fixed cells could be readily transfected by simple exposure to a PBS solution of the modified DNA strands in their single stranded or duplex forms, as expected, established transfection methodologies were required to transfect live cells, as described below.

Chemical transfection

The preformed S1:S2 duplex in PBS was treated with the chemical transfection agent Lipofectamine. FRET was still observed for the complex between DNA and Lipofectamine (Figure B.9, Appendix B) prior to incubation with CHO cells and visualisation by confocal microscopy as before. Once again, excitation of the Cy3 and Cy5 fluorophores at their excitation wavelengths indicated that they were both present within cells and co-localised. However this time when only the Cy3 laser was turned on i.e. only Cy3 excitation, no Cy5 signal was observed, and hence no FRET was occurring (Image C, Figure 4.5).

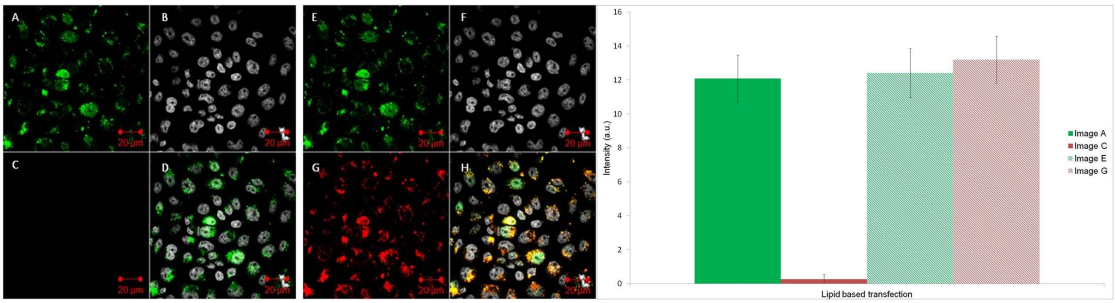

Figure 4.5: Chemical transfection confocal microscopy images. Left: Cy3 and Cy5 tagged DNA duplex (S1:S2) added to cells via chemical transfection using Lipofectamine and imaged using confocal microscopy. Images A/E represents the Cy3 channel; B/F the nuclear stain channel; C/G the Cy5 channel and D/H an overlay of all the channels. Images A-D are excited with a 543 nm laser only. Images E-H are excited with both the 543 and 633 nm lasers. Right: Intracellular fluorescence intensity from images A/C and E/G. Data are expressed as mean ± s.e.m from at least ten cells ($p<0.001$).

Quantitative data in Figure 4.5 clearly shows negligible Cy5 signal compared to Cy3 signal upon excitation at the Cy3 absorption wavelength only (Figure 4.5, first two bars on chart). Similar results were observed for the chemical transfection of S3, which meant that the absence of FRET being ascribed to dissociation of the duplex in the cellular environment could be essentially ruled out. Emission spectra were also measured for chemically transfected cell samples using spectral imaging inverted confocal microscopy (Figure B.11, Appendix B), which confirmed the absence of a FRET signal under these conditions. It was observed that the Cy3 and Cy5 fluorescence was to some extent co-localised in a punctate pattern rather than being evenly distributed. These results were consistent with the tagged DNA being unable to be released from endosomes once within the cell and subsequently digested by nucleases. [152, 167, 168] It is hypothesised that the tagged oligonucleotides, whether in their single strand or duplex forms are being degraded within vesicles on entry to the cell via endocytosis. When strands S1 and S2 were transfected into cells individually under these conditions, there was shown to be no crosstalk between the Cy3 and Cy5 channels, since upon excitation, only signals from their respective channels were observed (Figure B.12, Appendix B).

As expected, non-complementary Cy3 and Cy5 oligonucleotides added either together or sequentially via chemical transfection were also shown not to display FRET (Figure B.13, Appendix B).

Microinjection

Cy3 and Cy5 oligonucleotides S1 and S2 were then added to cells via microinjection as a preformed duplex. Under these conditions and in contrast to the chemical transfection study, this time when only the Cy3 chromophore was excited using a 543 nm laser, a signal was observed in the Cy5 channel, confirming the occurrence of FRET (Image B, Figure 4.6).

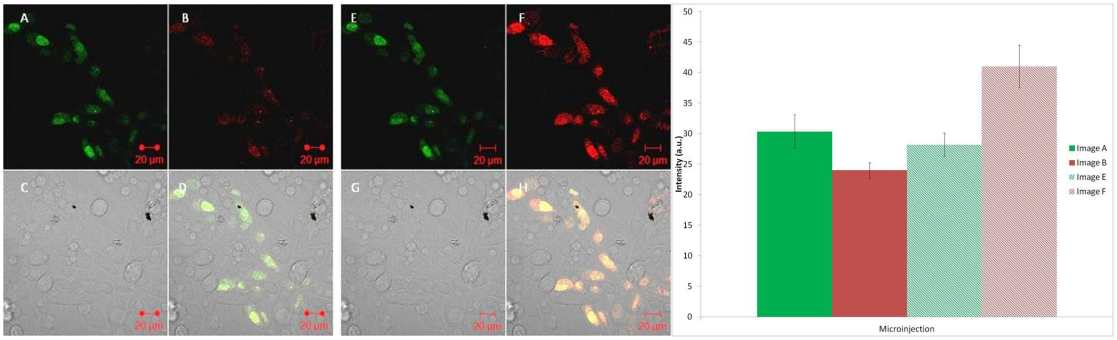

Figure 4.6: Microinjection confocal microscopy images. Left: Cy3 and Cy5 tagged DNA duplex (S1:S2) added to cells via microinjection and imaged using confocal microscopy. Images A/E represents the Cy3 channel; B/F the Cy5 channel; C/G the bright field channel and D/H an overlay of all the channels. Images A-D are excited with the 543 nm laser. Images E-H are excited with both the 543 and 633 nm lasers. Right: Intracellular fluorescence intensity from images A/B and E/F. Data are expressed as mean ± s.e.m from at least ten cells ($p<0.001$).

Quantitative data in Figure 4.6 clearly shows significant Cy5 signal compared to Cy3 signal upon excitation at the Cy3 absorption wavelength only (Figure 4.6, first two bars on chart). Once again the control study involving the microinjection of the Cy5 strand S2 only and excitation at 543 nm gave a negligible signal, which confirmed that the FRET signal was genuine (Figure B.14, Appendix B). Other control studies,

which included the microinjection of the doubly-tagged S3 strand and that of a non-complementary strand pair, gave the expected results, with FRET only occurring for the S3 system (Figures B.15 and B.17 respectively, Appendix B).

Electroporation

Cy3 and Cy5 oligonucleotides (S1 and S2) were next added to cells via electroporation. The results were similar to the microinjection studies in that when the Cy3 chromophore in the S1:S2 duplex was excited using a 543 nm laser, a signal present in the Cy5 channel was observed (Image B, Figure 4.7) to indicate FRET, which was again supported by control studies on S2 alone.

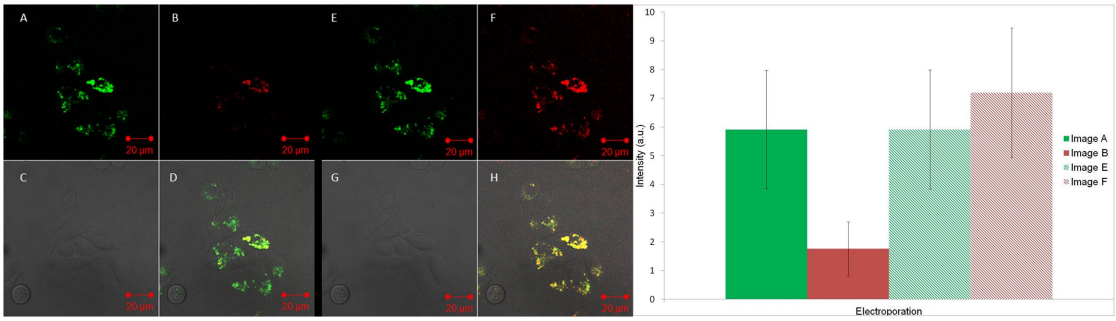

Figure 4.7: Electroporation confocal microscopy images. Left: Cy3 and Cy5 tagged DNA (S1:S2) duplex added to cells via electroporation and imaged using confocal microscopy. Images A/E represents the Cy3 channel; B/F the Cy5 channel the nuclear stain channel; C/G the bright field channel and D/H an overlay of all the channels. Images A-D are excited with a 543 nm laser only. Images E-H are excited with both the 543 and 633 nm lasers. Right: Intracellular fluorescence intensity from images A/B and E/F. Data are expressed as mean ± s.e.m from at least ten cells (p=0.001 to 0.01).

Quantitative analysis of the cell images in Figure 4.7 confirmed the FRET signal, although the ratio of the Cy5 signal to Cy3 signal was smaller than for microinjection. Sequential studies involving the addition of S1 and S2 were less conclusive, possibly due at least in part to the damaging effect of physically perturbing the live cell environment more than once. Once again the addition of non-complementary strands gave no FRET signal, which was consistent with the S1:S2 duplex being intact inside cells (Figure B.21,

Appendix B). Compared to microinjection, the fluorescence was seen to be not as evenly distributed throughout each cell. This would suggest that the DNA strands show a tendency to accumulate in distinct areas.

4.3 Discussion

The results from the cuvette studies clearly indicate that energy transfer via FRET can occur both intramolecularly in the case of S3 and intermolecularly upon formation of the S1:S2 duplex. Melting studies confirmed the stability of the duplexes under cellular conditions. Furthermore cell lysate studies demonstrate that these systems can in principle remain intact over a period of a few hours if they are not exposed to degrading nucleases. However results on these systems in cells clearly indicate that the type of technique employed and the status of the cell (fixed or live) have a strong bearing on the degree to which FRET imaging can be successfully observed. Cells are commonly fixed and permeabilised with alcohols or formaldehyde. However this is incompatible with live cell imaging and the effect of fixation on DNA in cells is uncertain. Nevertheless, these studies clearly indicate that DNA can easily enter fixed/permeabilised cells, as evidenced by the observation of a strong FRET signal when tagged DNA is added either as a duplex or sequentially. That DNA duplexes of this length can remain intact from either simultaneous or sequential addition to fixed cells is clearly shown from these studies, with no FRET observed when using non-complementary strands under the same conditions. The transfection of live cells with DNA was certainly found to be more challenging, with generally less material entering compared to fixed cells. Despite these strands being relatively small in size, the hydrophilicity and negative charge of the DNA backbone prevents it from crossing biological membranes of live cells unaided. Although chemical transfection has been reported as being relatively inefficient ($<80\%$) [167, 169] and slow (delivery times $\sim$4 hours), it is well established that lipid-

based chemical transfection reagents help to mask the negative charge, which allows binding to the cell membrane, uptake by receptor-mediated endocytosis and deposition into endosomes. [170] The studies indicate that this technique does indeed facilitate cell transfection of single or double stranded DNA. However in each case, no FRET signal was observed, even though the respective fluorophores were shown to be co-localised. Furthermore the bright spots of fluorescence from both fluorophores suggest that the DNA is not released from the endocytotic vesicles that are formed, which is consistent with nuclease degradation and supports similar findings in previous studies. [152, 167, 171] This interpretation was supported by repeating the transfection experiments on the S1:S2 duplex and S3 in the presence of bafilomycin, which is known to block degradation by preventing the acidification of the endosomal vesicles. [172, 173] It was interesting to note that under these conditions, DNA was found to be still internalised into vesicles but no longer degraded, with a FRET signal now observed (Figure B.22, Appendix B). Alternative live cell transfection techniques tested, which were also unsuccessful, were chloroquine transfection [174], calcium phosphate transfection [175, 176] and the physical method of scrape loading. [177] In contrast to chemical transfection, degradation of DNA in cells does not appear to be a major issue when microinjection or electroporation is used as the transfection technique. In each case, when the DNA was added, the S1:S2 duplex and the S3 single strand stayed intact, as evidenced by the observation of a FRET signal. In the case of microinjection, the fluorescence signal was generally evenly distributed throughout the cell. Microinjection can precisely add a controlled dose of material to a single cell, either to the nucleus or cytoplasm. [178, 179] However as found here, despite the high transduction efficiency, microinjection typically only treats a small proportion of cultured cells and also can lead to physical stress. [180] By comparing the quantitative data in Figures 4.6 and 4.7, it can be seen that the FRET efficiency, defined here as the ratio between the Cy5 and Cy3 intensity upon excitation at the Cy3 absorption wavelength only, is approximately halved for electroporation compared to

microinjection. Despite this, electroporation is a less cumbersome technique, although under the conditions used here, the cell distribution was less uniform than found using microinjection, which indicates a possible accumulation of the DNA in vesicles. However although FRET was not widely observed across a large number of cells, it appears that any vesicles that may form are less primed to degrade the DNA than those formed via the endocytotic pathway.

In conclusion, this work represents a relatively rare example of a controlled study that compares a range of different DNA transfection techniques using both fixed and live cells. The work underlines the issues that surround the stability and viability of DNA delivered into live cells by lipid-based transfection, whether the DNA is single or double stranded. In the field of nucleic acid chemistry, it appears that this technique is a more viable option when using other types of nucleic acid (e.g. siRNA) that are capable of entering the cell intact via endocytotic pathways. [181] Otherwise suitable inhibitors have to be used (e.g. bafilomycin) or chemical modifications to the nucleic acid structure have to be made to mitigate nuclease degradation. [182–184] On the other hand, the studies here indicate that the techniques of microinjection and electroporation are both viable as alternative methods for transfecting cells with single-stranded or duplex DNA. The work provides a further example of the power of FRET in probing the fate of DNA duplexes in cells and as such is relevant to related hybridisation studies in living cells. [104, 185, 186] Continued work in this area using different nucleic acids, targets, fluorophores, delivery techniques and conditions will only increase our understanding of how DNA and its derivatives may be delivered into cells efficiently and effectively. Finally this work provides a basis of understanding in the techniques to be used for advancing the DNA anthracene probes and SNP sensing systems (Chapter 3) for use in a cellular environment.

Chapter 5

Quantification of SNP sensing in a cellular environment with DNA anthracene probes

5.1 Introduction

Oligonucleotide probes are a popular choice for targeting DNA and RNA. These probes are commonly designed for cellular imaging purposes, and in particular for the direct targeting of mRNA *in vitro*. [18, 90] This is because the extraction of RNA, reverse transcription to cDNA and amplification are time-consuming and prone to error. [65] However, targeting DNA and RNA in a live cell also brings complications such as probe stability and temperature restrictions (Section 1.6). A common compromise is the fixation of cells and tissue. This provides a cellular environment but has none of the degradation issues since enzymes are deactivated. One of the key aims of this project was to test the SNP sensing protocol using the DNA anthracene probes in a cellular environment.

As discussed in Section 1.4.2, Chapter 1, the DNA anthracene probes developed

by Tucker *et al.* give a robust and reliable SNP sensing method at room temperature. The method has been shown to be biologically compatible and can test probe sequences with SNPs associated with prostate cancer. [88] Although the cell delivery of DNA probes had been optimised as described in the previous chapter, it was unclear whether the signal from a DNA anthracene probe would be detectable in a cellular environment since its emission overlaps with short wavelength (visible spectrum) autofluorescence. Other considerations were whether changes in emission caused by a single base variation could be detected in a cellular environment and whether changes in emission for the DNA anthracene probe upon hybridisation could be quantified and match those found in a cuvette.

Given the concerns over the excitation/emission of anthracene in a cellular environment, an alternative probe was designed to emit at a longer wavelength. Acridine is a known DNA intercalator and cell-permeant used in cell-cycle studies and as a lysosomal dye. [187, 188] It has a longer excitation wavelength (maximum λ_{ex} = 446 nm in ethanol) [189] than anthracene (350 nm in water (5% MeCN)) but a similar structure makes base-dependent emission possible. [190] Commercially available acridine yellow phosphoramidite was therefore chosen for incorporation into oligonucleotides (Figure 5.1). [190]

In this chapter, the quenching mechanisms for the two fluorescent probes are compared both in and out of a cellular environment. Oligonucleotide delivery to methanol fixed/permeabilised cells was performed and analysed by scanning laser confocal microscopy. SNP sensing trends were analysed and quantified computationally in a cellular environment. An innovative application of an evolutionary algorithm to quantify SNP sensing in a cellular environment was also developed. This involves an adapted method for quantifying intensity in fluorescence images based on Gaussian Mixture Modelling. Applying this model results in the identification of single base changes from fluorescent cell images.

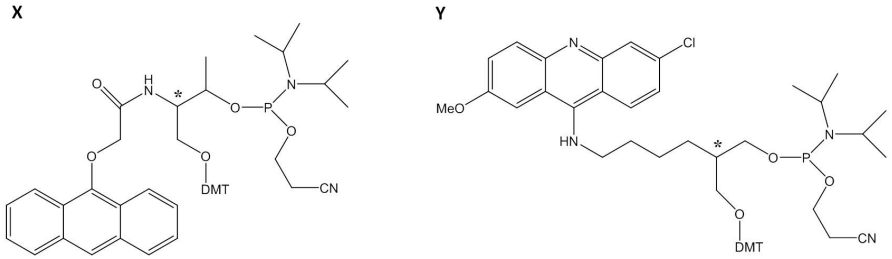

Figure 5.1: **X**: Synthesised anthracene phosphoramidite (Tucker *et al.*) **Y**: Commercially available acridine yellow phosphoramidite (Glen Research).

5.2 Synthesis

The DNA anthracene probes and DNA targets described in Chapter 3 were used again here. DNA acridine probes (PAcr) were synthesised using acridine yellow phosphoramidite (Glen Research) (Figure 5.1) which was inserted centrally in DNA. The DNA acridine probe was deprotected with 0.4 M methanolic sodium hydroxide for 17 hours at room temperature and then removed from the solid support and neutralised with 2 M TEAA. DNA acridine probes were a racemic mixture. General DNA synthesis and purification details are described in Chapter 2. Table 5.1 lists all the modified and unmodified DNA oligonucleotides used. A full list of oligonucleotides used in the thesis can be seen in Table G.1.

Table 5.1: DNA sequences synthesised. X denotes the anthracene monomer. Y denotes the acridine monomer. n is the carbon linker length and L/D denotes the stereochemistry.

Oligonucleotide	Sequence (5' to 3')
DN	TGGACTCTCTCAATG
P(n)(L/D)	TGGACTCXCTCAATG
PAcr	TGGACTCYCTCAATG
DT1	CATTGAGAGAGTCCA
DT5	CATTGAGAAAGTCCA
RanD	GTATTCCTCTGGGAA

5.3 Melting studies

Thermal melting studies were undertaken to confirm DNA duplex formation and duplex stability at room temperature (Table 5.2). The explanation for differences in T_M between the DNA anthracene probes versus unmodified probes was discussed in Chapter 3. Acridine also gives some stability to the fully matched duplex PAcr:DT1 despite the loss of hydrogen bonding in the central sequence position. This indicates a similar interaction to the base opposite sensing anthracene system with the acridine intercalating into the duplex (Section 3.3.4). In fact, acridine is known from the literature to bind nucleic acids via an intercalative mode and to stabilise DNA duplexes. [191] For the PAcr:DT5 duplex there is less evidence of intercalation since the T_M is lower than the equivalent unmodified duplex DN:DT5.

Table 5.2: Melting temperatures (°C) of DNA anthracene and acridine probes with DNA targets, plus controls. 5 μM DNA, 100 mM NaCl, 10 mM pH 7.0 sodium phosphate buffer.

Probe/Target	DT1	DT5
DN	55	42
P1L	53	46
PAcr	53	41.5

5.4 Fluorescence studies

Excitation and emission spectra for PAcr and P1L were recorded under the usual conditions (1 μM DNA, 100 mM NaCl, 10 mM pH 7.0 sodium phosphate buffer) and are displayed in Figure 5.2. P1L and PAcr have similar Stokes shift; 76 nm and 73 nm respectively.

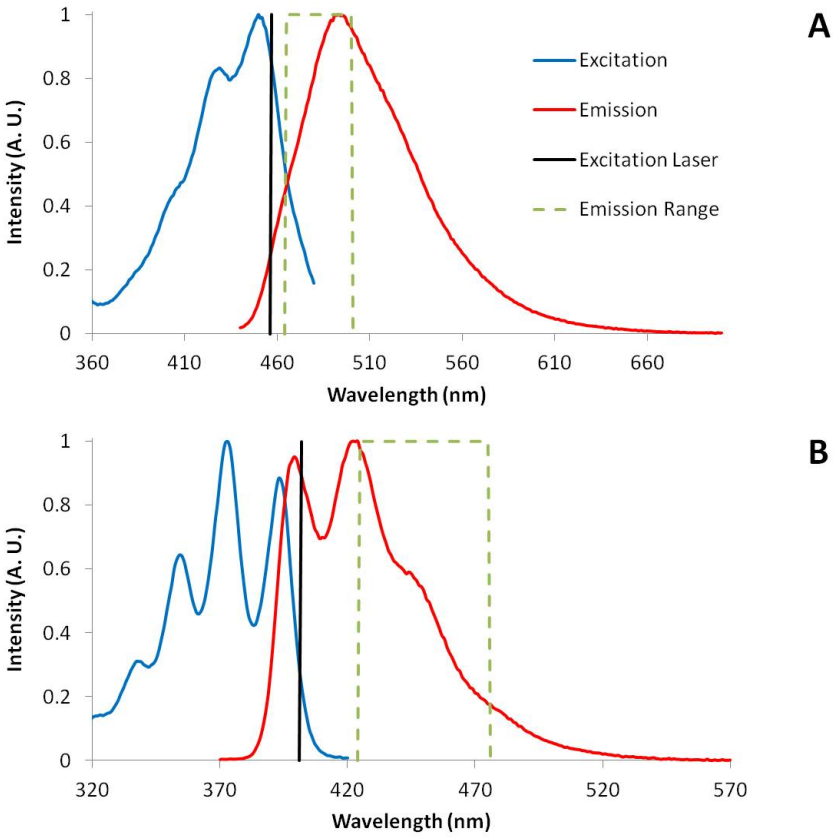

Figure 5.2: (A) Probe PAcr: Excitation spectrum (blue) with λ_{em} = 494 nm. Emission spectrum (red) with λ_{ex} = 421 nm. (B) Probe P1L: Excitation spectrum (blue) with λ_{em} = 426 nm. Emission spectrum (red) with λ_{ex} = 350 nm. Black line indicates the microscope laser excitation wavelength (PAcr = 457 nm, P1L = 402 nm). Green dashed line indicates the emission range collected on the microscope (PAcr = 465-500 nm, P1L = 425-475 nm). Data is normalised to λ_{max} values. 1 μM DNA, 100 mM NaCl, 10 mM pH 7.0 sodium phosphate buffer.

Upon their successful incorporation into oligonucleotides the characteristic fluorescence properties of anthracene and acridine were retained, allowing titration studies to be undertaken. As already described and rationalised earlier in Chapter 3, P1L emission decreased upon addition of matching target (DT1) and increased with mismatching target (DT5) (Figure 5.3).

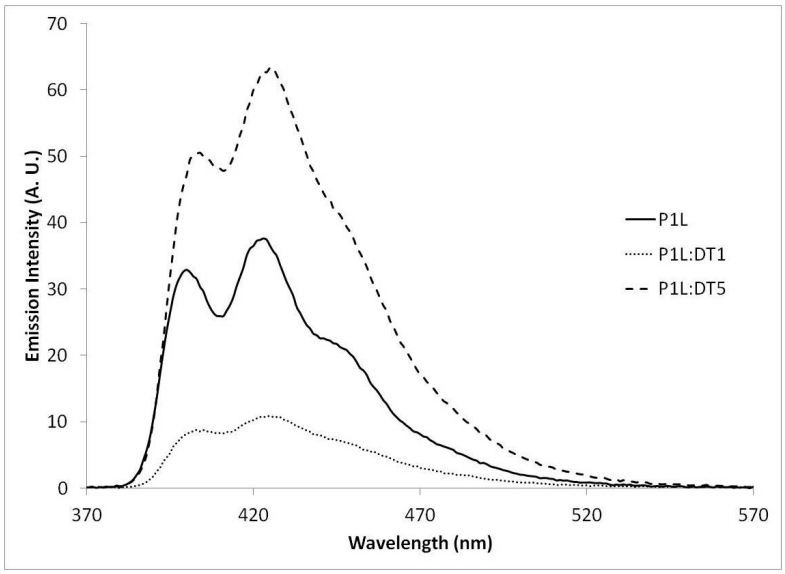

Figure 5.3: Emission spectra showing the change in emission upon hybridisation of anthracene probe P1L with targets DT1 and DT5 respectively. 1 μM DNA, 100 mM NaCl, 10 mM pH 7.0 sodium phosphate buffer, $\lambda_{ex} = 350$ nm. Emission range = 370-570 nm.

In the case of the acridine system, the titrations of PAcr with the complementary target strand DT1 resulted in almost complete quenching of the acridine emission signal. The addition of mismatching target (DT5) to PAcr also caused quenching, but to a lesser degree (Figure 5.4). This initially seems similar to the base opposite sensing anthracene system (Section 3.3.4). A summary table of percentage changes in emission for both probes is shown in Table 5.3. For both probes, no further changes in emission were observed in the presence of excess target (Figure C.1). This indicates the formation of a 1:1 complex, which is consistent with DNA duplex formation (Figure 3.4). The binding is specific since as expected there was no change in emission upon the addition of the non-complementary target RanD.

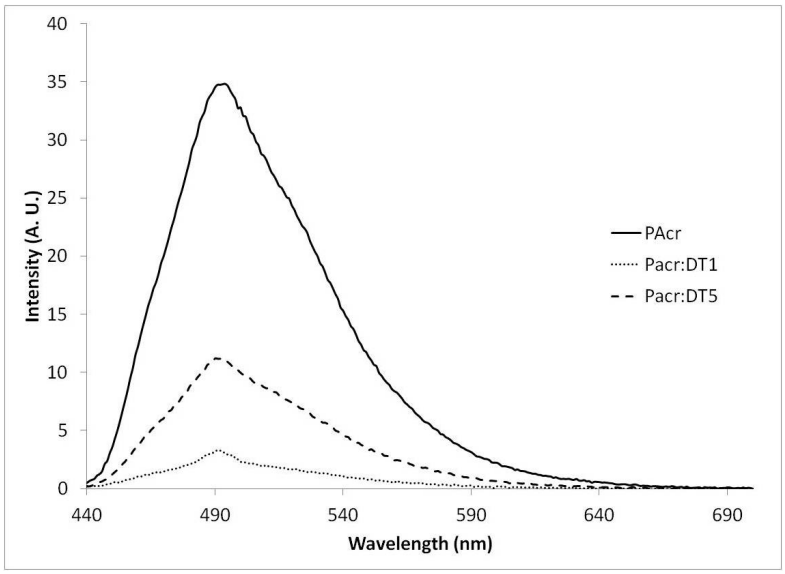

Figure 5.4: Emission spectra showing the change in emission upon hybridisation of DNA acridine probe PAcr with targets DT1 and DT5 respectively. 1 μM DNA, 100 mM NaCl, 10 mM pH 7.0 sodium phosphate buffer, λ_{ex} = 421 nm. Emission range = 440-700 nm.

To enable a quantitative comparison with the fluorescence images (*vide infra*), the excitation and emission wavelength ranges in the titration studies were replicated to the microscope settings (Figure 5.2). The percentage changes in emission were now calculated from the areas under the curves, to correspond to the integrated emission ranges captured by the microscope, with PAcr now excited at 457 nm and P1L at 402 nm (Figure 5.5). Percentage changes in emission intensity are displayed in Table 5.4. A comparison of the data in Tables 5.3 and 5.4 shows that the system change in excitation

Table 5.3: Percentage change in emission on addition of target to probe, relative to probe only. 1 μM DNA, 100 mM NaCl, 10 mM pH 7.0 sodium phosphate buffer. PAcr λ_{ex} = 421 nm, P1L λ_{ex} = 350 nm. Percentage changes calculated from emission intensity at P1L = 426 nm and PAcr = 494 nm.

Probe/Target	DT1	DT5
P1L	-70%	+77%
PAcr	-91%	-68%

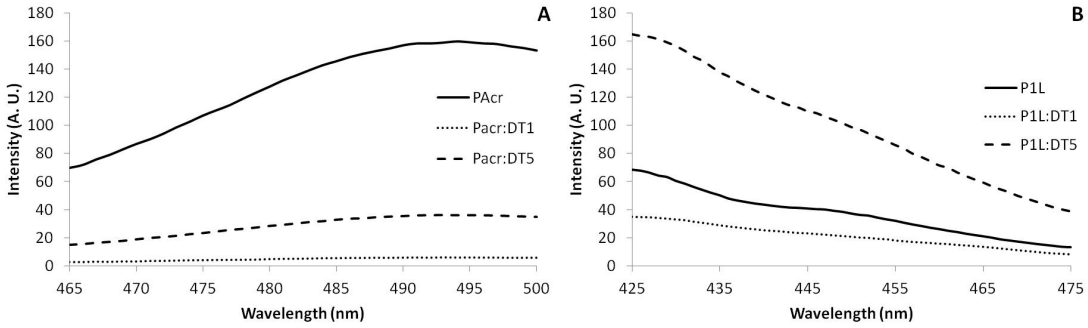

Figure 5.5: Emission spectra showing the change in emission upon hybridisation of (A) DNA acridine probe PAcr and (B) DNA anthracene probe P1L with targets DT1 and DT5 respectively. 1 μM DNA, 100 mM NaCl, 10 mM pH 7.0 sodium phosphate buffer, **PAcr λ_{ex} = 457 nm, P1L λ_{ex} = 402 nm.** Emission ranges correspond to microscope settings (PAcr = 465-500 nm, P1L = 425-475 nm.)

Table 5.4: Percentage change in integrated emission on addition of target to probe, relative to probe only. 1 μM DNA, 100 mM NaCl, 10 mM pH 7.0 sodium phosphate buffer. **PAcr λ_{ex} = 457 nm, P1L λ_{ex} = 402 nm.** Emission ranges: PAcr = 465-500 nm, P1L = 425-475 nm.

Probe/Target	DT1	DT5
P1L	-43%	+168%
PAcr	-96%	-78%

wavelength has less impact on the PAcr result due to the high degree of quenching observed in each case. There are previous examples in the literature of this approach, i.e. where spectral study wavelengths (excitation and emission ranges) have been chosen to match laser sources on confocal microscopes. [57, 111, 192]

Due to the change in excitation wavelength the percentage change values in emission do not match those from Chapter 3, although the ON/OFF sensing is retained. The difference in values result from varying degrees of absorption (Figure 5.6).

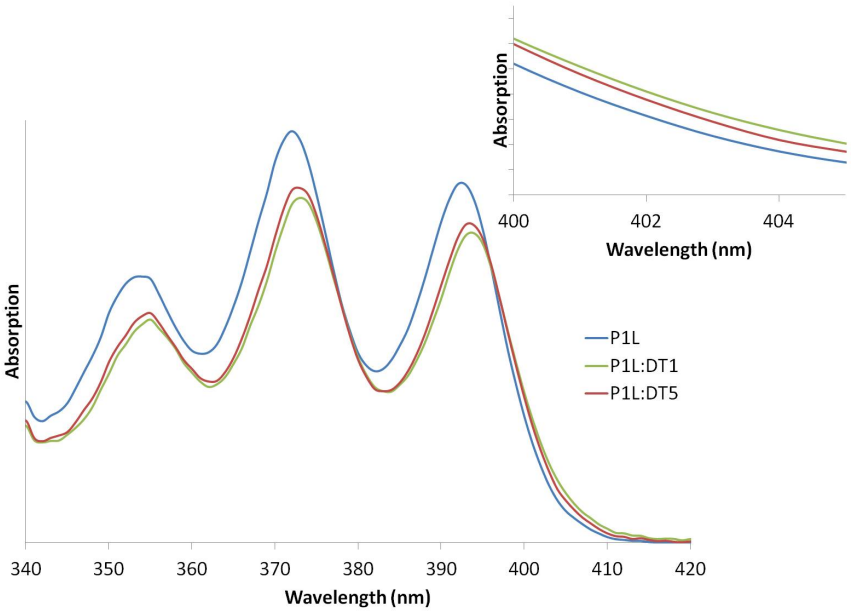

Figure 5.6: Absorption spectra of P1L in the region of anthracene. It can be seen that the single stranded P1L absorbs more than P1L duplexes upon 350 nm excitation. However the inverse is true upon 402 nm excitation (inset).

The melting temperature data indicates that acridine intercalates, which would bring the acridine unit into closer proximity with adjacent and opposing nucleobases, which is likely to be responsible for the observed quenching in DT1 case. Acridine intercalates less into the duplex than anthracene does, especially in the DT5 case. This is likely due to acridine distorting the duplex upon intercation since it is more bulky. Therefore, one reason quenching is caused is by reduced acridine intercalation. The second reason is that the adjacent SNP target DT5 has one less adjacent guanine residue than the base opposite target DT1 (Table 5.1). The phenomenon of fluorescence quenching via photo-induced electron transfer (PET) (Figure 5.7) from guanine bases to acridine is well documented in the literature and would appear to be the explanation. [83, 193] Anthracene is also reduced but not as easily as acridine- it is certainly not the driving force in the anthracene SNP sensing system. [88]

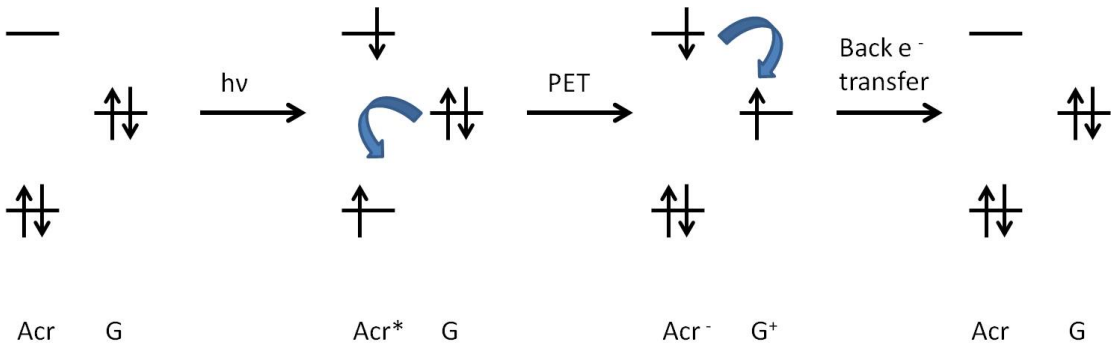

Figure 5.7: Photo-induced electron transfer (PET). When the electrons of the fluorophore are photoexcited, electron transfer occurs from a higher donor orbital, which results in quenching of the fluorescence.

Since $E_2 > E_1$ (Equations 5.1 and 5.2 respectively), then Equation 5.3 is true. In thermodynamic terms, PET between guanine and acridine is favourable due to the large difference in reduction potentials leading to ΔG = -0.46 eV.

$$Acr^* + e^- \rightarrow Acr\ (E_2) \tag{5.1}$$

$$G^* + e^- \rightarrow G\ (E_1) \tag{5.2}$$

$$Acr^* + G \rightarrow Acr^- + G^+ \tag{5.3}$$

Using the Rehm-Weller equation [194], the Gibbs free energy of electron transfer was calculated in our system yielding ΔG^0_{ET} = -0.47 eV (Equation 5.4).

$$\Delta G^0_{ET} = E^0\left(\frac{D^{+\cdot}}{D}\right) - E^0\left(\frac{A}{A^{-\cdot}}\right) - E_{0,0}(D) + \Delta G^0(\epsilon) \tag{5.4}$$

$E_{0,0}(D)$ is the excited state energy of the donor obtained from the crossing point wavelength of the absorption and emission spectra, in this case 465 nm (Figure 5.2). $\Delta G^0(\epsilon)$ is a coulombic interaction term between the oxidised donor and the reduced acceptor. The kinetics of electron transfer are also favourable: the lifetime of guanine-acridine PET has been previously found to be in the femtosecond regime, which is significantly faster than

fluorescence and therefore likely to dominate in these studies. [195] Overall, the DNA acridine probe was successful in DNA sensing applications and can detect variations of a single base in the sequence. However, unlike the anthracene system, the success of this sensing process appears to be based on the number of proximal guanine bases due to quenching via PET. This would therefore only make it useful in detecting SNPs in which a nearby guanine is the varying base. In addition, the ideal sensing mechanism is ON/OFF emission. This is the case with the DNA anthracene probe P1L with the emission going either up or down (Figure 5.5).

As mentioned earlier, optimal excitation of anthracene in cells is a drawback of these probes since UV lasers are not common in confocal microscopes (due to phototoxicity effects and high absorption by bioorganic matter). The absorption at 402 nm is significantly reduced compared to the previously used excitation wavelength of 350 nm. It also encroaches on the emission spectrum although emission is only collected beyond that point.

5.5 Quantitative *in vitro* SNP sensing

The benefits of *in vitro* sensing assays were discussed in Chapter 1. The development of an *in vitro* assay requires the sensing achieved in a cuvette to be replicated in a cellular environment. Adding oligonucleotide probes to live cells is no easy task, as was discussed in Chapter 4. The oligonucleotides were therefore added to fixed cells to prevent degradation upon delivery (demonstrated by fluorescent-tagged DNA in Chapter 4). The aim was to visualise the fluorescent probes in fixed cells and differentiate between SNP targets based on emission intensity comparisons. To simplify matters initially, the probes were added either as single strands or in a pre-formed duplex with the targets. The probe-target combinations listed in Table 5.1 were introduced into the fixed cells, with a view to replicating the emission trends found in fluorescence emission studies.

5.5.1 Cell fixation and imaging

Methanol is used as a cell fixative but also has a further effect on cells in that membranes are permeabilised, thus providing a simple method for the uptake of intact oligonucleotides into cells. This protocol (Chapter 2) successfully introduces intact P1L and PAcr, with and without targets, into the cells. After a short incubation time, the cells are washed with PBS. The cells could then be visualised using confocal microscopy. Images were acquired in the z-direction to ensure that 1) the fluorescent DNA was within the cell, and 2) that an optimal in-focus image of the fluorescent DNA in cells could be taken for further analysis. An example collection of z-stack images is shown in Appendix C. All settings on the confocal microscope were consistent for various image acquisitions for a particular probe, thereby ensuring that any observed changes in intensity were due to the probe rather than the imaging system.

Qualitatively, the level of brightness of cells treated with DNA anthracene probe P1L, with and without targets DT1 and DT5, suggested that the trend found in emission studies had been reproduced (Figure 5.8) i.e. the mismatching duplex P1L:DT5 had a greater emission in cells compared with the matching duplex P1L:DT1. Fixed cell results for PAcr and its duplexes also replicated trends in the cuvette (full results for PAcr are shown in Appendix C). These qualitative observations suggested that *in vitro* sensing with base-discriminating fluorophores had been achieved. Control experiments were carried out; adding no oligonucleotides or non-complementary duplex (Figure 5.9).

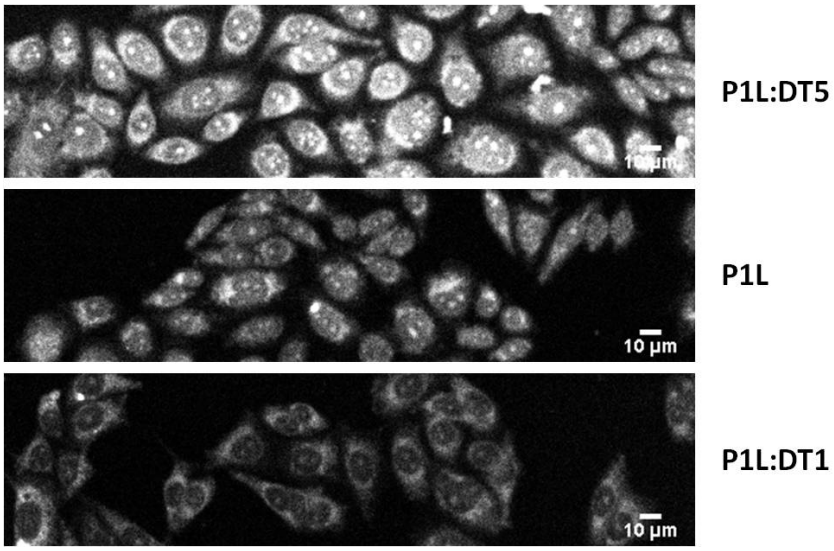

Figure 5.8: P1L:DT5; P1L; P1L:DT1 (top to bottom) added to fixed/permeabilised CHO cells and imaged using confocal microscopy. 402 nm laser excitation. Emission range: 425-475 nm.

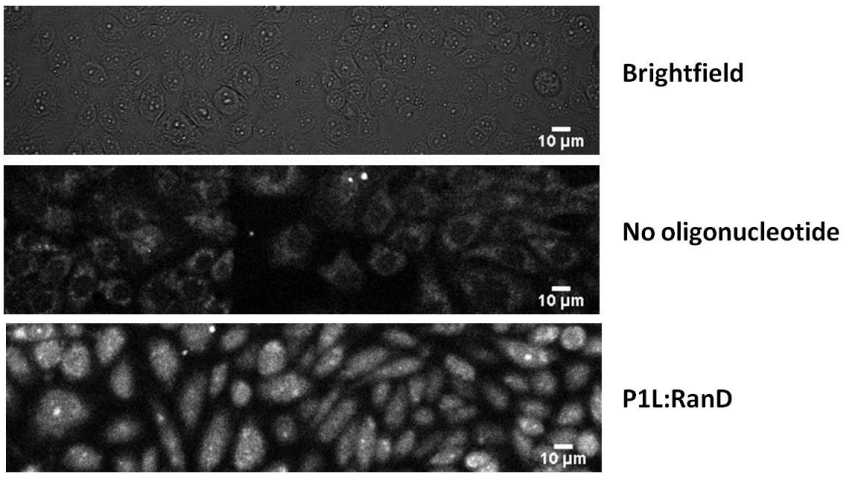

Figure 5.9: Top: Brightfield image of CHO cells; Centre: No oligonucleotide added; Bottom image: P1L:RanD, added to fixed/permeabilised CHO cells and imaged using confocal microscopy. 402 nm laser excitation. Emission range: 425-475 nm.

The majority of fluorescence appears in the cytoplasm of the cell, although, bright spots of fluorescence also accumulate in the nucleus. The bright spots do not appear in the blank control (Figure 5.9) and vary in intensity depending on the oligonucleotides

added which indicates that they are caused by the probes and not the cell. Nuclear accumulation is common for oligonucleotides added to cells and appear as punctate concentrations on nuclear bodies. [149] Access to the nucleus is mainly by diffusion and is not a function of cell fixation. [196]

Although trends may have been reproduced qualitatively, quantitative information from images is an important aim for assay development purposes. Quantification would allow percentage differences in emission from images to be compared to cuvette values. This was approached in two ways: standard image analysis software and an adapted method for quantifying fluorescence intensity from images based on Gaussian Mixture Modelling. Typically, the mean intensity of an image or regions of interest is measured using image analysis software such as ImageJ. Although easy to calculate, the mean intensity of an image also contains contributions from the cells and background (which are both variable). The intensity contribution from the DNA anthracene probe (and targets) within the cell is only of interest here. Calculating intensities from regions of interest (ROI) removes the background contribution only, but is a hugely time-consuming and user-dependent task. As a means of comparison, ImageJ analysis was carried out and the results are displayed in Table 5.5. Complex software involving thresholding and segmentation can also be used; however this works better for fluorophores emitting at longer wavelengths that are distinct from cell autofluorescence and background. Further quantitative techniques involving FRET (Chapter 4) and ratiometric sensing (Chapter 7) are also popular, which commonly involve a second (longer) emission wavelength.

5.5.2 Histogram analysis

The histogram of an image can be plotted, where the x-axis is the pixel intensity and the y-axis is the number of pixels (Figure 5.10). The histograms of the images in Figure 5.8 are plotted and overlaid (Figure 5.10). Shifts in the peaks in the x-axis can be seen,

which translates to differences in intensity between images. There are examples of this in the literature where emission or lifetime histograms are plotted for comparison. [111, 192]

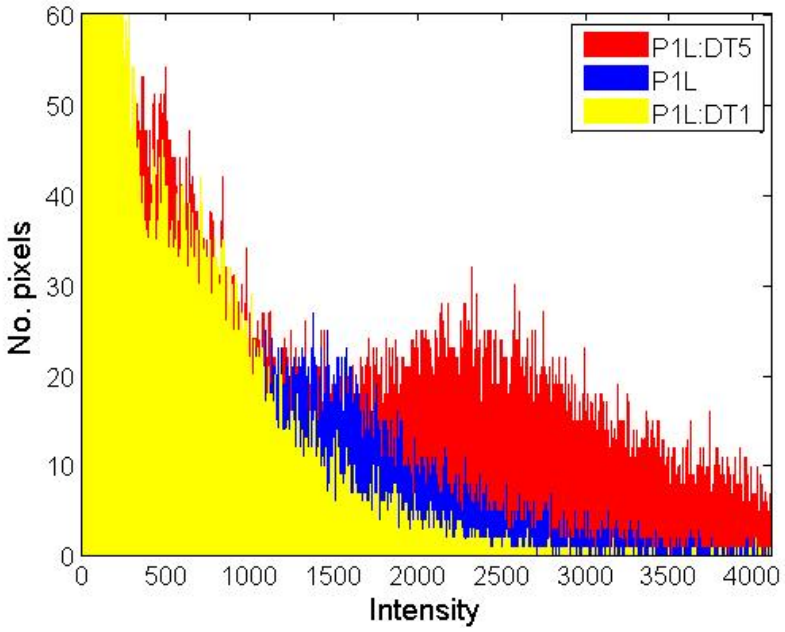

Figure 5.10: Cropped overlayed histograms for images displayed in Figure 5.8. A shift in intensity (x-axis) can be seen for images corresponding to different oligonucleotide treatment. The full scale histograms can be seen in Figure C.4, Appendix C.

Distinctive shifts are apparent between the various probe-target combinations that indicate differences in intensity, which replicate the trends seen in cuvette studies. However, these shifts alone cannot solely be used for quantitative conclusions. This is because the background and cell contribution varies between images. It was then observed that the outline of a typical image histogram can be the mixture of two Gaussian curves (Figure 5.11). This allows the different regions i.e. the background and fluorescence emission to be separable.

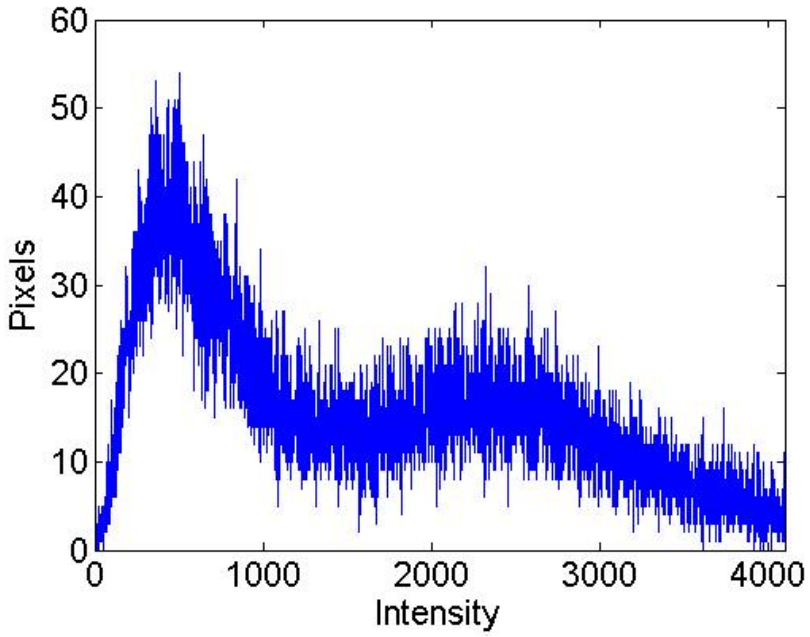

Figure 5.11: The outline of the histogram which can be the mixture of two Gaussian curves. Applying non-linear fitting to this curve results in separable background and fluorescence emission peaks for quantification purposes.

5.5.3 Gaussian Mixture Modelling (GMM)

The design and method of working of the following algorithm is first described before the analysis of the images obtained are discussed.

Image intensity was quantified using Gaussian Mixture Modelling (GMM) of histograms. [197, 198] This models the image histogram as a mixture of two Gaussian distributions, which enables the relative peak positions to be extracted. The background peak can be accounted for, resulting in measurement of the fluorescence emission signal. GMMs have been extensively used in image segmentation with histograms, where the image is automatically thresholded based on the Gaussian distributions. [199, 200] Here, the GMM application differs since the intensity correlating to the Gaussians is extracted, rather than being utilised in segmentation. As far as the author is aware GMM extraction has not been applied to cell images before now. The most similar application is found

in astronomy software such as SExtractor, which extracts quantitative information from astronomical images. [201] The Gaussian mixture model used is shown in Equation 5.5 (a full description of the model and parameters can be found in Appendix C).

$$f(x) = A \exp -\frac{(x - x_0)^2}{2\sigma^2} + A' \exp -\frac{(x - x_0')^2}{2\sigma'^2} \tag{5.5}$$

Equation 5.5 needs to be solved for parameters A, A′, x_0, x_0', σ and σ' (Figure 5.12).

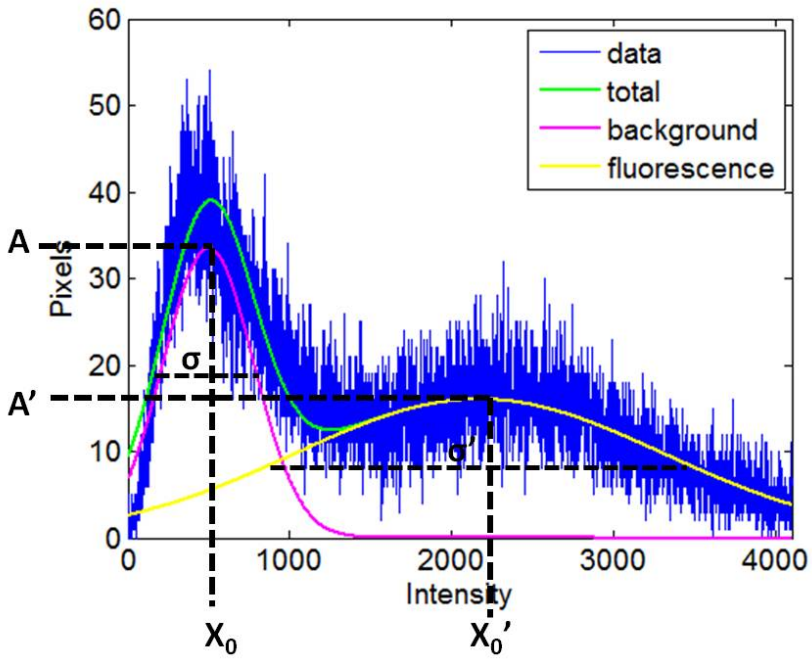

Figure 5.12: The outline of the histogram (blue) has two Gaussian curves fitted (pink and yellow) corresponding to the background and fluorescence emission contributions respectively. The unknown parameters are labelled: the peak heights A and A′, coordinates of the peak centres x_0 and x_0', and the peak widths σ and σ'. Using Gaussian Mixture Modelling (GMM) these parameters can be solved using a Particle Swarm Optimisation (PSO) algorithm. Diagram by R. Bamford.

However, Equation 5.5 is an example of a non-linear problem which cannot be solved analytically but must be optimised in a deterministic manner. The evolutionary algorithm, Particle Swarm Optimisation (PSO), was utilised for this purpose. The algo-

rithm is analogous to natural selection since the parameters are optimised by selecting the fittest members of the population. Initially this population consists of a series of random numbers for each of the six parameters given in Equation 5.5. Once the parameters of the model are known, the distributions of the background and foreground can be found for each experimental image. The difference between the centre of the background and foreground peak (x_0'-x_0) gives the true intensity due to fluorescence emission for the image. Therefore, (x_0'-x_0) values can be utilised to compare the intensity between images (Figure 5.13).

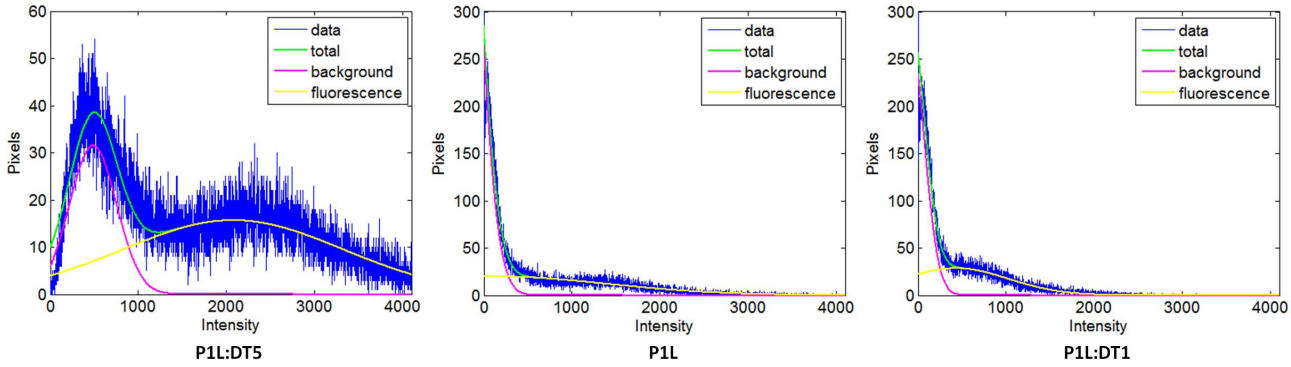

Figure 5.13: Histograms with GMM, corresponding to P1L:DT5; P1L; P1L:DT1 (left to right) cell images. GMM fits two Gaussian distributions corresponding to the background (pink) and fluorescence emission (yellow). The sum of the two Gaussian distributions (green) is shown to fit the outline of the histogram (blue).

It should be noted that the peak heights (A and A′) have no strong bearing on the results, provided that the peaks are distinguishable enough for GMM. This therefore means that the (x_0'-x_0) values are not affected by the number of cells in the image, which is an advantage to the overall analysis. The (x_0'-x_0) values for Figure 5.13 are included in the Table 5.5. As expected from the qualitative observations, the data extracted followed the fluorescence emission trends observed in cuvette studies, although the percentage values were not the same. The values don't agree with those extracted from the ImageJ analysis either. However this is most likely due to the user dependence; judging the cell

Table 5.5: Comparison of the base-discriminating fluorescence exhibited in CHO cells relative to fluorescence titrations and ImageJ analysis. Image refers to the confocal microscope image treated with probe-only or duplex systems. (x_0'-x_0) are the peak centre differences from GMM. The (x_0'-x_0) values between images can yield percentage change and s.e.m. values. These can be compared to the percentage change in integrated emission values from previous cuvette titration studies and from ImageJ image analysis, respectively. Percentage change values from ImageJ analysis are calculated from the intensity mean± s.e.m. from at least 24 cells ($p<0.001$). **PAcr λ_{ex} = 457 nm, P1L λ_{ex} = 402 nm.** Emission ranges: PAcr = 465-500 nm, P1L = 425-475 nm.

Image	(x_0'-x_0)/A.U.	% change (GMM)	% change (ImageJ)	% change (titrations)
P1L	1334	0	0	0
P1L:DT1	661	-50±1	-36±2	-43
P1L:DT5	1058	+26±2	+61±6	+168
PAcr	565	0	0	0
PAcr:DT1	274	-52±1	-30±2	-96
PAcr:DT5	323	-43±1	-20±4	-78

boundary was a difficult task.

It was noted that the background across the images increased in intensity as the image generally increased in brightness. This is due to scattering originating in the cells (turbid media), leading to higher background intensity. This effect has been previously demonstrated and has a greater contribution when the fluorescence emission intensity is higher. [202] The result is that the more emissive duplex (P1L:DT5) encounters more scattering and therefore the light collected by the PMT in the confocal microscope is comparatively less intense from inside the cell. This has a dual effect of the background being brighter in P1L:DT5 and the fluorescence emission being less intense than if no scattering were present. This can explain why the percentage changes from GMM were not as great as those found in the cuvette titrations (Table 5.5). In addition, there is likely to be a difference between the cuvette and cell percentage values when differences in environment between the cuvette and cell are considered. The cuvette titrations have a well controlled environment in terms of salt concentrations and molecular species

present, but the cellular environment has more unknowns.

Notwithstanding these issues, the scatter effect does not, however, appear to significantly hinder the ability to distinguish between bases and therefore detect SNPs present in preformed duplexes inside a cellular environment. Base discrimination *in vitro* was clearly achieved with P1L, owing to the ON/OFF sensing. Furthermore, the DNA acridine probe PAcr also exhibited quenching when in a duplex (Appendix C) and GMM was able to determine base discrimination from confocal microscopy images.

5.6 Sequential studies

The next stage was to add the target and probe sequentially to observe if they were able to find and hybridise with one another within the cell. Proof of concept was carried out for Cy3 and Cy5 tagged DNA in Chapter 4. Sequential addition is also a good test for future work which would involve adding the probe only in order to target endogenous DNA/RNA. The fixed cell protocol is the same as previously (Section 5.5.1) but here the DNA target and DNA anthracene probe are added to fixed cells sequentially with incubation and PBS washing in between. The cell image results are shown in Figure 5.14. By eye the trend in fluorescence emission is intact. However, the emission does appear lower overall than the duplex studies. This would be expected though since the PBS washing steps were doubled in number. Additionally, the incubation time may need to be extended to allow for hybridisation time. It should be emphasised that all fixed cell work is carried out at room temperature, which from previous melting studies the duplex is known to be intact.

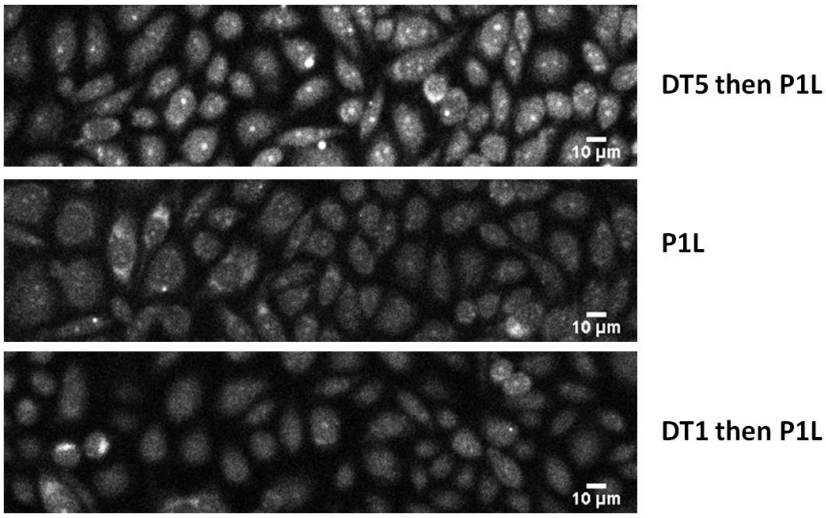

Figure 5.14: DT5 then P1L; P1L; DT1 then P1L (top to bottom) sequentially added to fixed/permeabilised CHO cells and imaged using confocal microscopy. 402 nm laser excitation. Emission range: 425-475 nm.

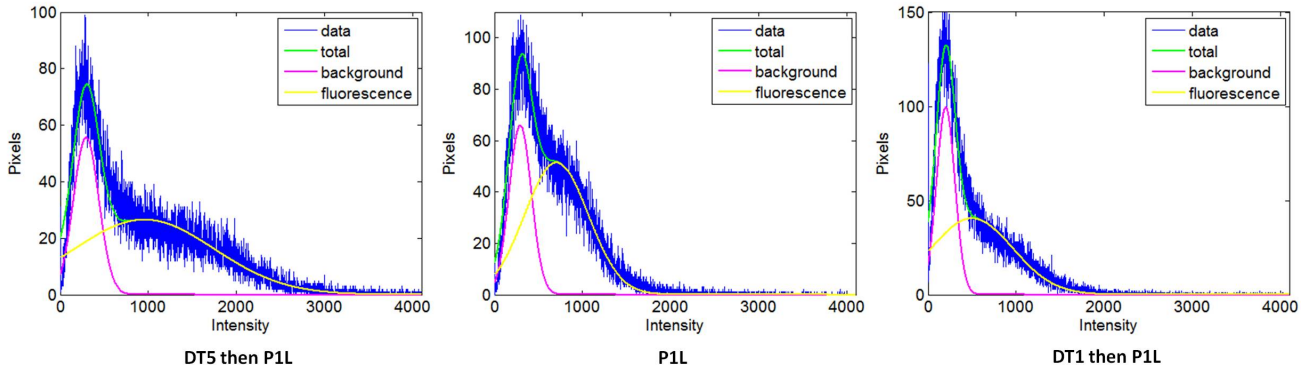

Figure 5.15: Histograms with GMM, corresponding to DT5 then P1L; P1L; DT1 then P1L (left to right) sequential images. GMM fits two Gaussian distributions corresponding to the background (pink) and fluorescence emission (yellow). The sum of the two Gaussian distributions (green) is shown to fit the outline of the histogram (blue).

GMM analysis on the sequential cell image histograms gives quantitative information (Figure 5.15). The percentage values extracted were -16% and +60% for P1L:DT1 and P1L:DT5 respectively (Table 5.6). Pleasingly, the ON/OFF sensing trend is retained. The percentage change values are not as great as those observed in cuvette

Table 5.6: Comparison of the base-discriminating fluorescence exhibited in CHO cells relative to fluorescence titrations. Image refers to the confocal microscope image treated with target DNA then DNA anthracene probe sequentially. (x_0'-x_0) are the peak centre differences from GMM. The (x_0'-x_0) values between images can yield percentage change and s.e.m. values. These can be compared to the percentage change values from previous cuvette titration studies. 402 nm laser excitation. Emission range: 425-475 nm.

Image	(x_0'-x_0)/A.U.	% change (GMM)	% change (titrations)
P1L	415	0	0
DT1 then P1L	347	-16±2	-43
DT5 then P1L	662	+60±4	+168

titration studies. The reasoning would be similar to that in the previous duplex cell study. However, the values are also shifted higher compared to the GMM percentage change values from the duplex cell study. This would suggest unbound or degraded probe causing the emission to be higher overall. The probe should not be degraded since the cells are fixed and excess probe should not be an issue since the target is in excess. However, excess DNA anthracene probe could be accounted for in the future by fitting a third Gaussian to the histogram outline. It is worth considering at this point the efficiency of delivery. For sequential studies the probe and targets are delivered as single strands and perhaps more likely to bind non-specifically. Subsequently, anthracene may intercalate into a more hydrophobic environment causing the emission to increase. This would also apply to the probe alone in the duplex studies. The preference to bind to a complementary target should overcome these non-specific interactions.

5.7 RNA studies

The duplex and sequential fixed cell studies were repeated with equivalent P1L DNA/RNA hybrids. Duplex (Figure 5.16) and sequential cell studies (Figure 5.17) also retain the ON/OFF sensing discussed in Chapter 3. The quantitative results extracted from the images using GMM analysis are shown in Table 5.7. The percentage differences from

GMM analysis show some similarity to those values from titration studies although there are discrepancies as discussed before. It is interesting that the percentage differences from GMM are higher than those from titration studies, since this is the opposite to values for DNA/DNA duplexes in fixed cells. No difference between the uptake of DNA:DNA and DNA:RNA duplexes would be expected. The initial thought when values are higher is that there is unbound DNA anthracene probe. However, probes are added as a duplex and DNA/RNA duplexes are more stable than their DNA/DNA equivalents (all experiments were carried out at room temperature). Plus, the target is in excess to the probe. RNA is more susceptible to degradation than DNA, and this could lead to unbound DNA anthracene probe. However, the likelihood of degradation is small in fixed cells.

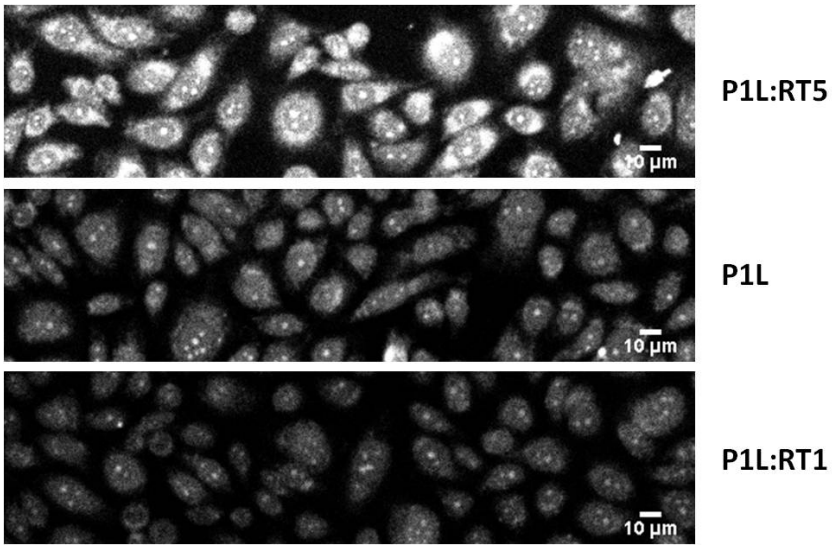

Figure 5.16: P1L:RT5; P1L; P1L:RT1 (top to bottom) added to fixed/permeabilised CHO cells and imaged using confocal microscopy. 402 nm laser excitation. Emission range: 425-475 nm.

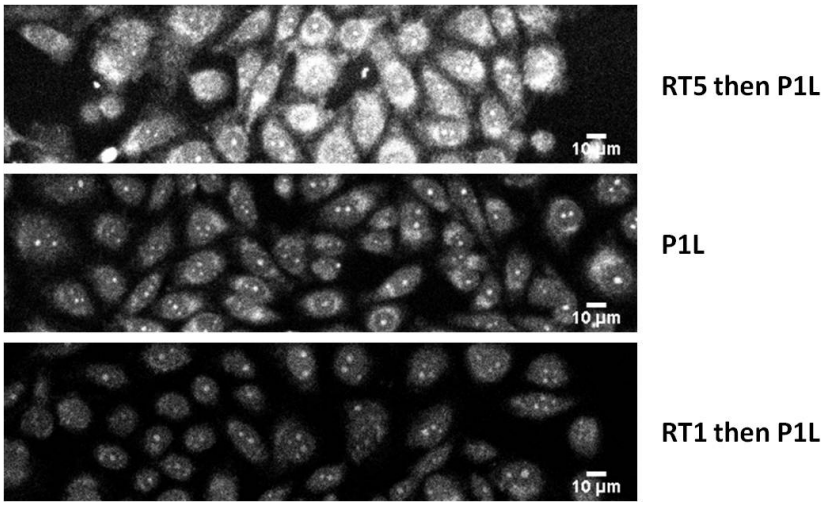

Figure 5.17: RT5 then P1L; P1L; RT1 then P1L (top to bottom) added to fixed/permeabilised CHO cells and imaged using confocal microscopy. 402 nm laser excitation. Emission range: 425-475 nm.

Table 5.7: Comparison of the base-discriminating fluorescence exhibited in CHO cells relative to fluorescence titrations. Image refers to the confocal microscope image treated with probe-only, probe-RNA duplexes or RNA-probe sequentially. (x_0'-x_0) are the peak centre differences from GMM. The (x_0'-x_0) values between images can yield percentage change and s.e.m. values. These can be compared to the percentage change values from previous cuvette titration studies. 402 nm laser excitation. Emission range: 425-475 nm.

Image	(x_0'-x_0)/A.U.	% change (GMM)	% change (titrations)
P1L	735	0	0
P1L:RT1	321	-56±1	-77
P1L:RT5	2161	+194±5	+133
P1L seq	870	0	0
RT1 then P1L	307	-65±1	-77
RT5 then P1L	1921	+121±9	+133

5.8 Base opposite and CDKN1A gene SNP sensing

Fixed cell studies were also carried out for the base opposite and CDKN1A SNP sensing (described in Chapter 3). The DNA sequences are given in Table 5.8. The GMM analysis results are given in Table 5.9. Trends observed in the cuvette are replicated in a fixed cell environment. Confocal cell images and corresponding histograms are included in Appendix C.

Table 5.8: Base opposite and CDKN1A gene sensing DNA sequences. X denotes the anthracene monomer. n is the carbon linker length and L/D denotes the stereochemistry.

Oligonucleotide	Sequence (5' to 3')
DN	TGGACTCTCTCAATG
P(n)(L/D)	TGGACTCXCTCAATG
DT1	CATTGAGAAGAGTCCA
DT4	CATTGAGTTGAGTCCA
ZP(n)(L/D)	AGTCGCGXCTCAGCT
ZDT1	AGCTGAGCCGCGACT
ZDT2	AGCTGAGAACGCGACT
ZRT1	AGCUGAGCCGCGACU
ZRT2	AGCUGAGACGCGACU

Table 5.9: Comparison of the base-discriminating fluorescence exhibited in CHO cells relative to fluorescence titrations. Image refers to the confocal microscope image treated with DNA anthracene probe (and target). (x_0'-x_0) are the peak centre differences from GMM. The (x_0'-x_0) values between images can yield percentage change and s.e.m. values. These can be compared to the percentage change in integrated emission values from previous cuvette titration studies. 402 nm laser excitation. Emission range: 425-475 nm.

Image	(x_0'-x_0)/A.U.	% change (GMM)	% change (titrations)
P6D	859	0	0
P6D:DT1	1249	+45±3	+220
P6D:DT4	493	-43±1	-35
P6D seq	853	0	0
DT1 then P6D	1274	+33±5	+220
DT4 then P6D	449	-47±2	-35
ZP5L	649	0	0
ZP5L:ZDT1	178	-73±1	-35
ZP5L:ZDT2	930	+43±3	+62
ZP5L	210	0	0
ZP5L:ZRT1	207	-1.4±2	-41
ZP5L:ZRT2	227	+8±2	+18

5.9 Conclusion

Oligonucleotides were successfully synthesised with fluorophores, anthracene and acridine, incorporated into the centre of the sequences respectively. The DNA acridine and anthracene probes show distinct base-discriminating capabilities, as shown by fluorescence emission studies which are due to different quenching and sensitising mechanisms exhibited by anthracene and acridine. DNA anthracene probe P1L possesses an effective ON/OFF sensing system whereas the DNA acridine probe PAcr discriminates between bases through distinct levels of quenching via PET to guanine bases. It has been successfully shown that the probe and target duplexes can be loaded into methanol fixed cells and base-discrimination by fluorescence emission within a cellular environment is realised, with novel application of Gaussian Mixture Modelling (GMM). GMM of the images allowed *in vitro* SNP sensing to be achieved with a simple application of the curve fitting algorithm, Particle Swarm Optimisation. Fluorescence emission intensities from the images correlated with trends seen in the cuvette environment. SNP sensing in fixed cells was shown to work for a number of systems including RNA and CDKN1A gene sequences.

Chapter 6

SNP sensing with plasmids in a cellular environment

6.1 Introduction

RNA SNP sensing using DNA anthracene probes in a cuvette was described in Chapter 3. It was proven to be as successful as the ON/OFF sensing of its DNA predecessor. This naturally progressed to adding duplexes to fixed cells in order to test if the cuvette results could be replicated in a cell environment (Chapter 5). Sequential studies carried out in Chapters 4 and 5 demonstrated probes were able to find targets which were added to the cell prior to the DNA anthracene probe. The next aim was to add DNA anthracene probe in order to target endogenous mRNA SNPs in cells.

The main benefits of targeting RNA were described previously (Chapter 3) as it meant redundancy for reverse transcription and amplification of extracted RNA into cDNA via PCR (a time consuming and often inaccurate technique). Moreover, there is a clinical need for a rapid, cheap and reliable read-out of the allelic (i.e. SNP) ratio within heterozygous mRNA transcripts directly (RNA detection in cells).

Current RNA detection in cell techniques are time-consuming, expensive and

have low sensitivity. Popular methods are TaqMan® probes and FISH (Section 1.3.1). However, they cannot resolve highly similar sequences such as allelic inactivation and splice variation since they rely on a high degree of complementarity. [97, 103] They also rely on strictly controlled conditions such as elevated temperature windows to ensure that only the fully complementary strand binds to the probe and not the SNP variant strand, which means many current techniques are non-transferable to a cellular environment anyway.

Despite the issues described above, the quest for targeting mRNA directly in a cell has its rewards. RNA is more accessible and abundant in a cell than DNA, which can lead to higher emission signals. Localisation and time-lapse information of cellular processes such as RNA interference can be gained from *in vitro* studies. As described in the Chapter 1 (Section 1.6.2), there are probes available which target RNA in cells, however there are few that can detect SNPs. Cellular RNA SNP detection could lead to quantification of specific mRNA strands and allelic ratios on a cell-by-cell basis, which could subsequently lead to screening for diseases.

Targeting endogenous mRNA in a cell brings up new challenges: (1) mRNA has a short half-life due to degradation, (2) mRNA folds into an often complex secondary structure and (3) the target may not always be accessible. Finally, the number of copies of mRNA is highly variable between sequences. Probes added to cells often exhibit nuclear migration and therefore do not have enough time to target RNA in the cytoplasm. It was observed in Chapter 5 that although there was some nuclear migration of the DNA anthracene probe, the majority remained in the cytoplasm. Therefore DNA anthracene probes should be able to target mRNA in the cytoplasm.

Overexpressing (endogenous) mRNA in a cell using plasmids is commonplace and is used here as proof of concept. [70] Also, in order to build upon previous studies (Chapters 3 and 5) which involved a non-biologically occurring sequence, it was important to use the cell's own machinery to over-express desired mRNA transcripts. This chapter

shall describe the route using plasmids to targeting endogenous mRNA SNPs in cells with DNA anthracene probes.

An initial test was to check whether the DNA anthracene probe was able to find targets that were added whilst the cell was live, rather than the sequential fixed cell case discussed in Chapter 5. The aim was then to produce multiple cell lines which will each express different versions of the non-biological SNP targets described in Chapter 3. The targets were then to be over-expressed in live cells so that a DNA anthracene probe could be added once cells were fixed and fluorescent results compared with previous *in vitro* studies.

6.2 Combined live and fixed cell studies

This section provides a link from the previous chapter where all sensing experiments were carried out in a fixed cell environment, and later in this chapter (Section 6.5) where live cells produce mRNA target, cells are fixed and DNA anthracene probe added. Here, the synthesised DNA target is added to live cells via electroporation (technique described in Chapter 4), cells are fixed and DNA anthracene probe is added (as in Chapter 5). It was found that DNA anthracene probe was degraded if chemical transfection was used for delivery to live cells (Figure D.1).

DNA targets, DT1 and DT5, were added to live CHO cells via electroporation. After a short recovery time, cells were methanol fixed and P1L DNA anthracene probe added. Controls as follows: cells electroporated but with no target, methanol fixed and half the cells DNA anthracene probe added. All images are given in Figure 6.1.

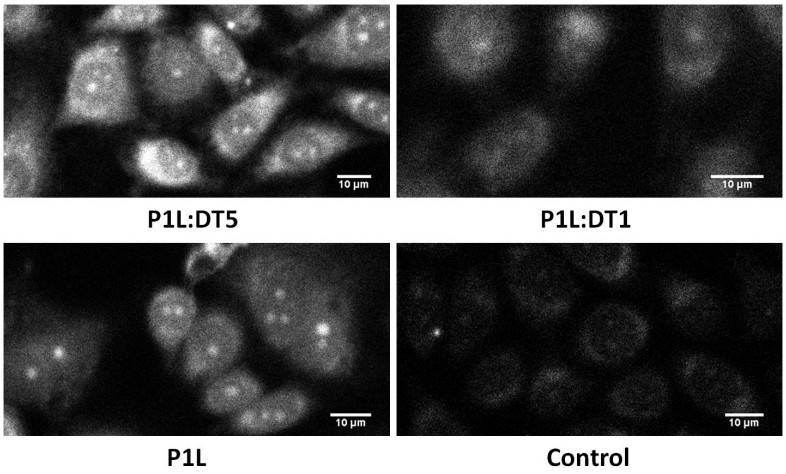

Figure 6.1: DNA targets DT1 and DT5 added via electroporation to CHO cells (top row); methanol fixation of cells and P1L DNA anthracene probe added. The bottom row also undergoes the electroporation and methanol fixation steps but no target added (bottom left) and no target or probe added (bottom right).

The trends previously observed for P1L and match/mismatch DNA targets (Chapter 3) are reproduced in confocal microscope cell images. The GMM analysis (Section 5.5.3) results are given in Table 6.1, quantifying the percentage changes between cell images. Figure 6.1 images confirm that the DNA anthracene probe is able to find a target in a fixed cell that was also present in the prior live cell environment. The next step is similar but the live cell produces the target itself before fixation.

Table 6.1: Comparison of the base-discriminating fluorescence exhibited in CHO cells relative to fluorescence titrations. Image refers to the confocal microscope image treated with probe-only or probe-DNA sequentially. (x_0'-x_0) are the peak centre differences from GMM. The (x_0'-x_0) values between images can yield percentage change and s.e.m. values. These can be compared to the percentage change values from previous cuvette titration studies.

Image	(x_0'-x_0)/A.U.	% change (GMM)	% change (titrations)
P1L	1016	0	0
P1L:DT1	432	-57±1	-43
P1L:DT5	1601	+58±3	+168

6.3 Plasmid method

Chapter 2 contains the full experimental detail for this section. The plasmid design and synthesis shall be described here.

The plasmid (mp71 retroviral vector) contains CRT5-svFc linked to a truncated human CD34 protein (surface expression) by a 2A linker (Figure 6.2). The 2A linker ensures the equal molar expression of both proteins. [203]

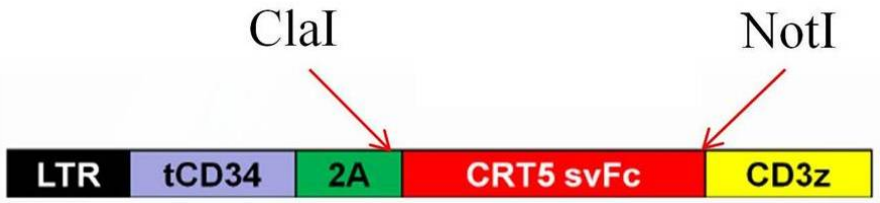

Figure 6.2: Schematic of plasmid (mp71 retroviral vector) region of interest. The CRT5-svFc is linked to a truncated human CD34 by a 2A linker.

The CRT5-svFc can be replaced with an insert using ClaI and NotI enzyme digestion. A schematic diagram shows how the double stranded plasmid is cut and an insert added (Figure 6.3).

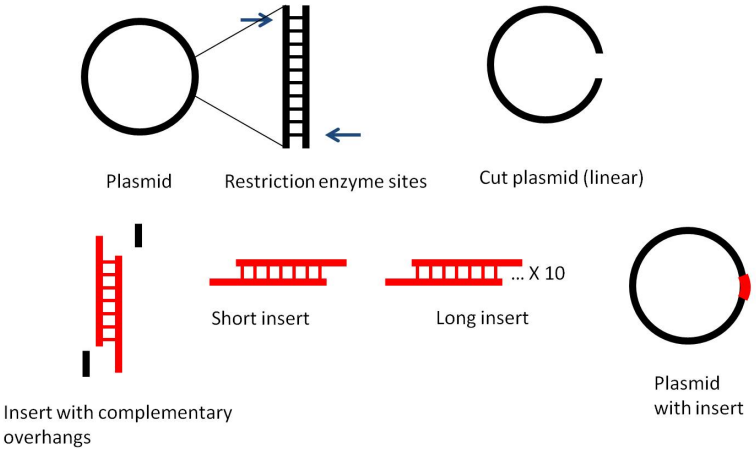

Figure 6.3: Schematic of double stranded plasmid cut to become linear. A region of plasmid is discarded and double stranded DNA replaces it. There are two insert choices: a 15 base sequence and a ten times repeat of that sequence i.e. 150 base sequence. The DNA insert is ligated into the plasmid.

A total of four plasmids were designed and synthesised, each with a different insert. Table 6.2 lists the final plasmid names and their corresponding inserts. PSDT1 and PSDT5 are the match and mismatch 15 base sequences described in Chapter 3. Ten times repeat of these targets, i.e. 150 base sequences, were also synthesised (PLDT1 and PLDT5) since target availability in cells can be problematic. [204] For control purposes, a non-specific plasmid is also included in the studies. This plasmid was provided by the Bicknell group. All plasmids then undergo bacterial transformation in order to amplify the plasmid (Figure 6.4).

Table 6.2: List of plasmids with their corresponding insert sequences (n is the number of repeats; n = 10 throughout). The inserts are double stranded and annealed to their complementary strand. Underlined are the overhangs for insertion into the plasmid.

Plasmid	Insert Sequence (5' to 3')
PSDT1	CGATCTAG(CATTGAGAGAGTCCA)GC
PLDT1	CGATCTAG(CATTGAGAGAGTCCA)nGC
PSDT5	CGATCTAG(CATTGAGAAAGTCCA)GC
PLDT5	CGATCTAG(CATTGAGAAAGTCCA)nGC

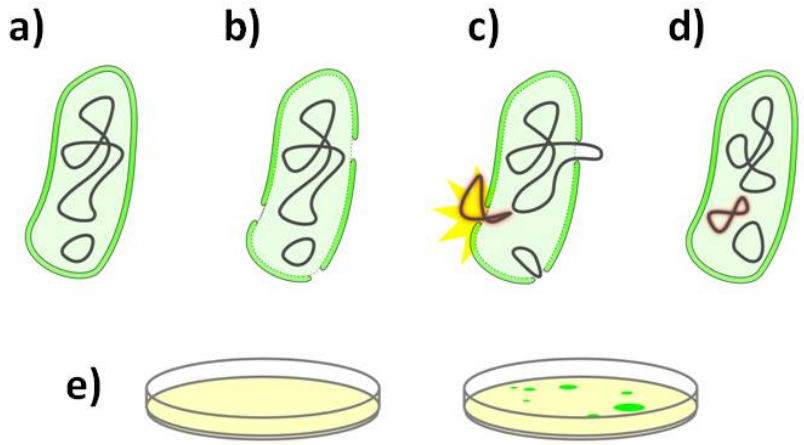

Figure 6.4: Schematic of bacterial transformation. a) *E. coli.* bacterium; b) extreme cold causes pores to appear in bacterial membrane; c) pores allow plasmid DNA to pass through into the bacteria; d) upon heating some bacteria have plasmid DNA inside them (these are the transformed bacteria); e) the untransformed bacteria (no plasmid inside) can be filtered out by growing all the bacteria in an antibiotic-containing medium. Untransformed bacteria are killed by the antibiotic in the medium. The transformed bacteria grow though since the plasmids are antibiotic-resistant. Schematic adapted from http://2012.igem.org.

The plasmids are ampicillin (Amp) resistant. The next stage is to determine which colony contains the plasmid construct with the correct insert. Commonly the plasmid enzyme digestion can be repeated to check which contains the correct insert (based on gel band size). However, since the insert is so small compared to the overall plasmid, this route was unsuitable. PCR by colony can be used as an alternative verification method (Figure 6.5).

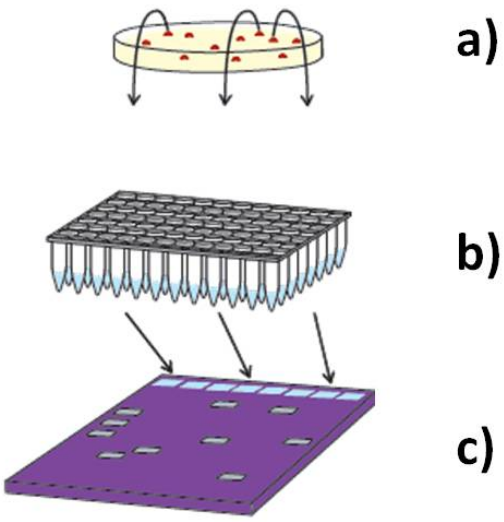

Figure 6.5: Schematic of PCR by colony. a) Pick a colony into a microcentrifuge tube; b) Perform PCR with primers designed specifically to target the insert DNA; c) Analyse by gel electrophoresis. Schematic adapted from http://www.epibio.com/images.

This involved designing primers that specifically target the insert DNA. PCR amplicon presence or absence will determine if the insertion was successful. Likely plasmid candidates are selected from gel electrophoresis of PCR samples and a size marker (for example, Figure 6.6).

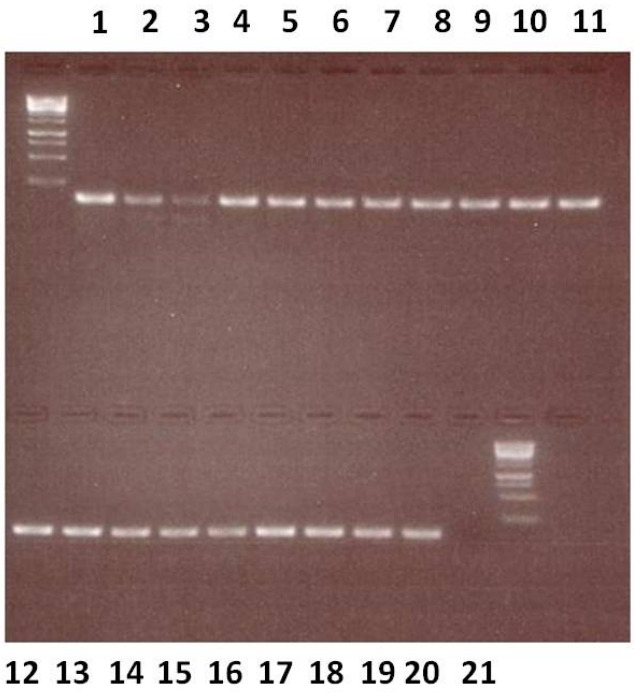

Figure 6.6: PCR by colony gel example (PSDT1). Lanes 17 and 18 were chosen for sequencing (lanes 2 and 3 show impurities). Lane 21 is the negative control. 1kB ladder (GeneRuler, Thermo Scientific) on both rows.

Plasmid samples are sequenced where the insert sequence can be checked. Once the plasmid is confirmed as correct, the plasmid can be grown in large-scale suspension and purified. The plasmid is now ready for future experiments.

6.4 Flow cytometry

PEI transfection was carried out in order to add the plasmids into cells. The cells were analysed by flow cytometry to determine if the transfection had been successful. Flow cytometry is a biophysical technology used to analyse a high number of cells in flow for purposes such as cell counting, cell sorting, or in this case, biomarker detection. Figure 6.7 gives a schematic of flow cytometry.

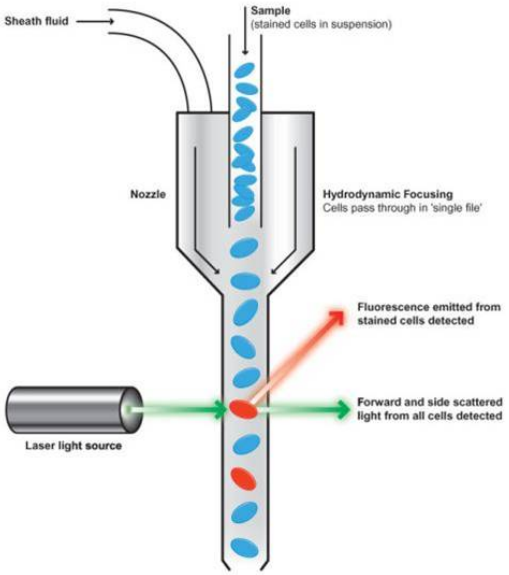

Figure 6.7: Schematic of flow cytometry. Cells flow into to a single stream and are then excited by a laser. Scattered light and fluorescence (often wavelength filtered) is then collected. Schematic adapted from http://www.andor.com.

If cells have been successfully transfected then not only will mRNA be expressed, but also the surface expressed human CD34 (Figure 6.2). Fluorescent-tagged antibodies are added to the transfected cells which are able to bind to the cell surface expressed human CD34 (which correlates with mRNA/protein expression). Therefore, if a shift in fluorescence intensity is detected for transfected cells, compared to controls, it can be confirmed that the desired mRNA target is being produced. A confocal image of the antibodies and cells is given in Figure D.2.

The flow cytometry results for each plasmid transfection into HeLa cells, including controls, is given in Figure 6.8.

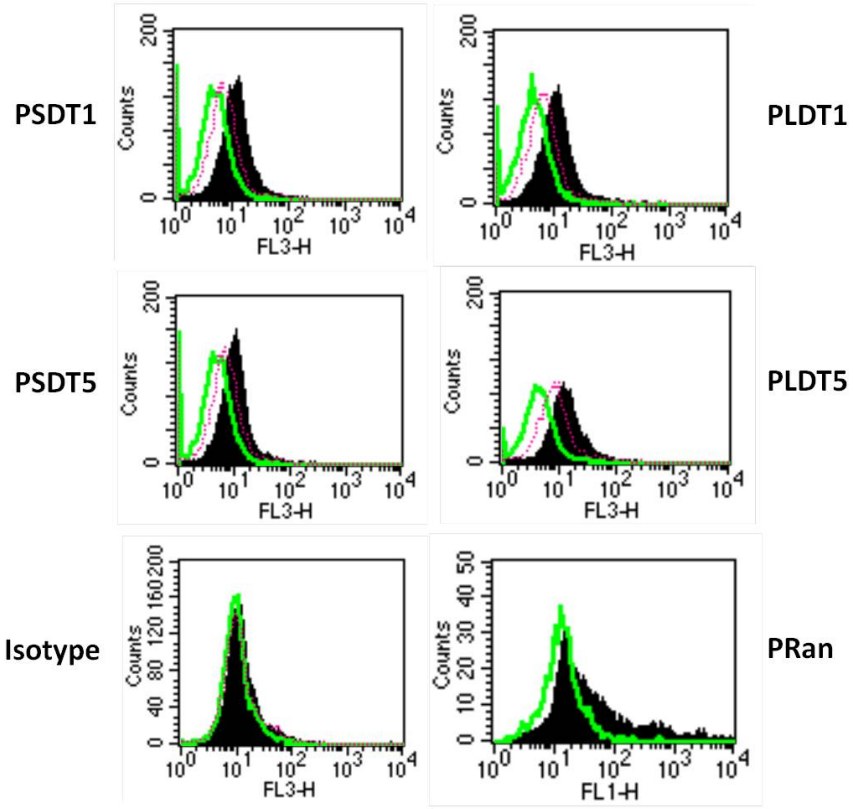

Figure 6.8: Summary of Hela cell plasmid flow cytometry results. Black represents the transfected cells; green line represents control cells and pink line represents mock transfected cells. The isotype control involved a non-specific fluorescent antibody. The non-specific plasmid (PRan) is targeted with appropriate antibodies to ensure its successful transfection.

HeLa cells were found to be the best in terms of transfection efficiency and viability. Other cell types were also tested (Figure D.3): CHO cells were not successful, whereas HEK cells transfected the most efficiently (viability issues later arose during methanol fixation and imaging). The flow cytometry results in Figure 6.8 show successful transfection and therefore mRNA production for the complete set of plasmids (Table 6.2). In all cases a shift in fluorescence intensity (x-axis) is observed for the transfected cells (black) compared to the control and mock transfected cells (green and pink outlines respectively). Overall transfection efficiency could be improved in the fu-

ture by using a retroviral route. The isotype control was a non-specific antibody with the same fluorescent tag (Cy5). It proves that the shifts observed in the plasmid transfected cells are genuine. The non-specific plasmid is targeted with specific antibodies to prove its successful transfection.

6.5 Confocal imaging

Transfected cells, shown to be producing RNA by flow cytometry, were methanol fixed and DNA anthracene probe added as described in Chapter 5. The plasmids were designed to produce match and mismatch targets RT1 and RT5, which give ON/OFF sensing with DNA anthracene probe P1L (Chapter 3). P1L was added to methanol fixed cells expressing RT1, RT5, 10x RT1 and 10x RT5. Confocal microscopy images corresponding to PSDT1/PSDT5 and PLDT1/PLDT5 are given in Figures 6.9 and 6.10 respectively. Control cells and mock transfected cells are given in Figure 6.11. To demonstrate specificity, a random plasmid (PRan) was tested (Figure 6.12) and a random sequence 1L DNA anthracene probe (P1LRan, sequence in Appendix G) added (Figure 6.13), respectively.

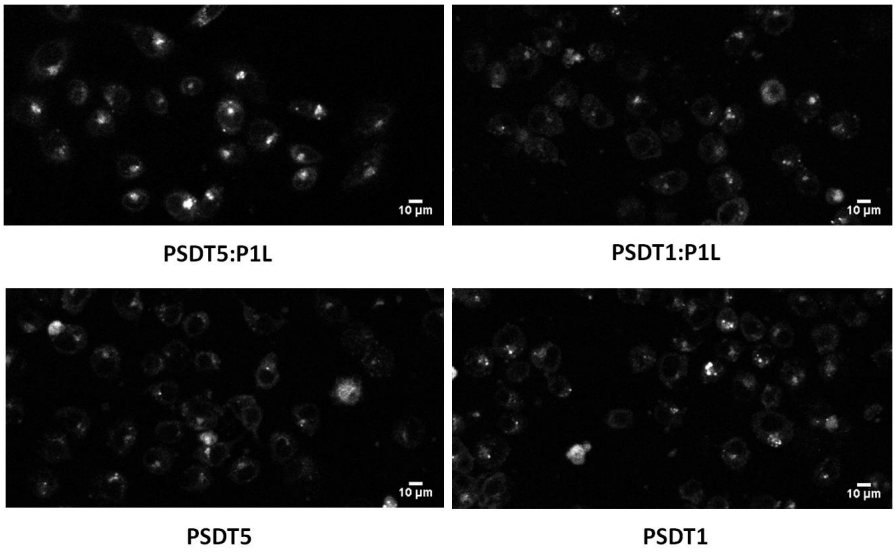

Figure 6.9: PSDT1 and PSDT5 (15mer) plasmids transfected into HeLa cells. The top images are methanol-fixed and P1L added.

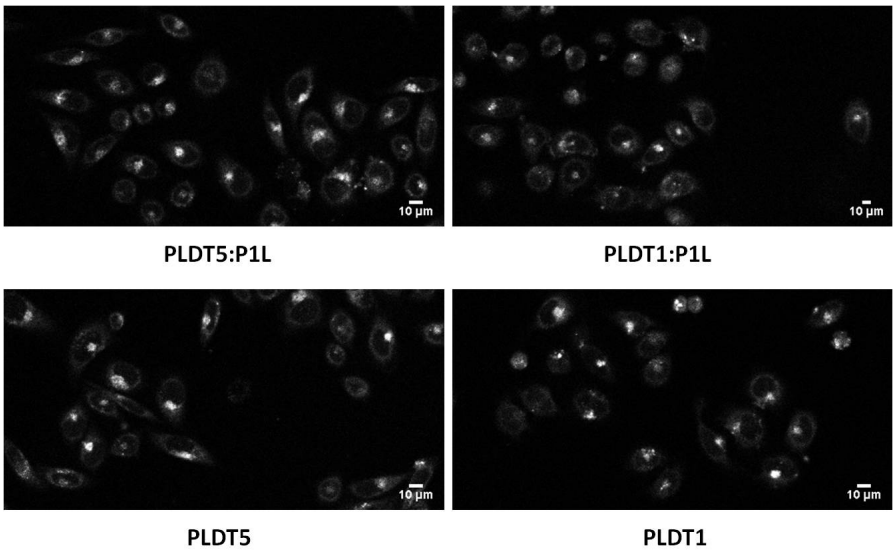

Figure 6.10: PLDT1 and PLDT5 (150mer) plasmids transfected into HeLa cells. The top images are methanol-fixed and P1L added.

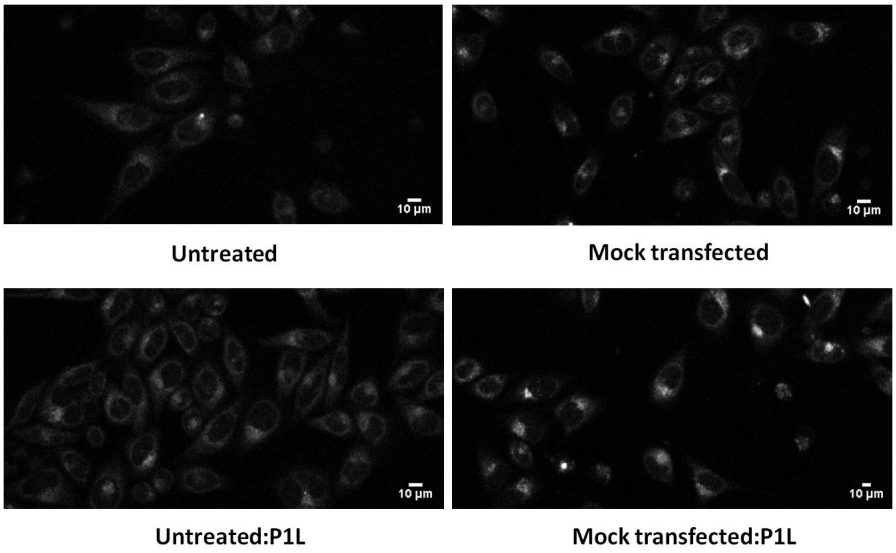

Figure 6.11: Untreated and mock transfected HeLa cells. The bottom images are methanol-fixed and P1L added.

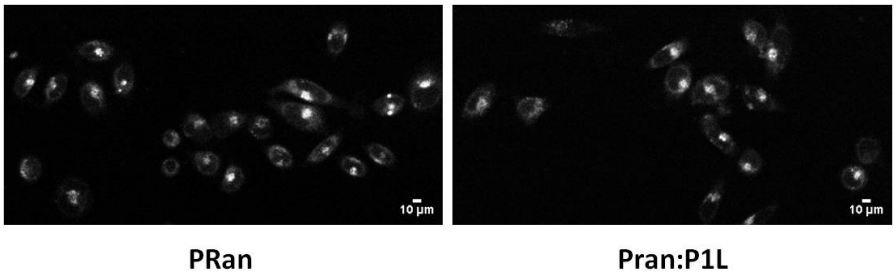

Figure 6.12: PRan transfected into HeLa cells. Left image shows transfected cells only; right image shows transfected cells methanol-fixed and P1L added.

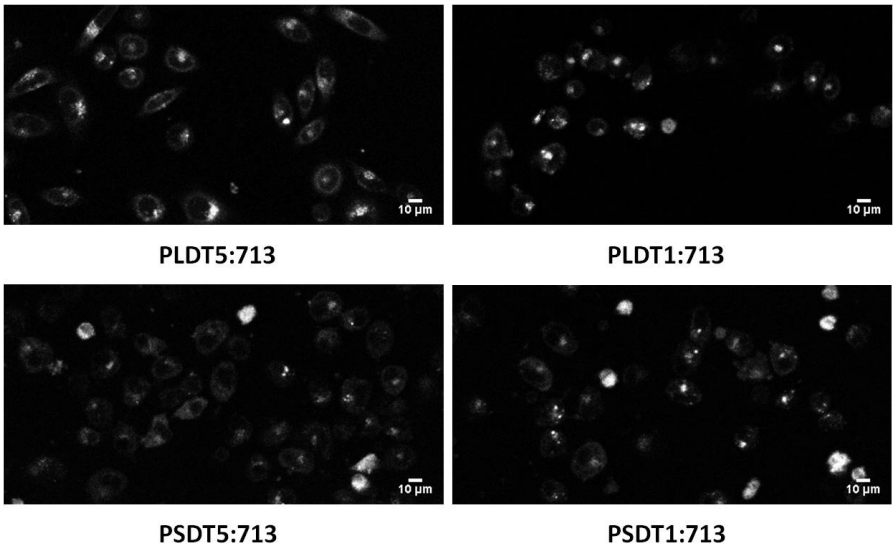

Figure 6.13: Plasmids transfected into HeLa cells and methanol-fixed. A non-specific 1L DNA anthracene probe (P1LRan) is then added.

In the cases where P1L is added to cells expressing RT1 and RT5, it is observed that the RT5 cells are brighter overall than the RT1 cells. This is what would be expected from the trend observed in fixed cells (Chapter 5) and cuvette studies (Chapter 3). Due to the increased number of transcripts, it would be expected that the PLDT1/PLDT5 would give better correlation to the cuvette trends than PSDT1/PSDT5. The mean intensities of the images above were extracted using image analysis, as in Chapter 5, and full results are given in Table D.1, Appendix D. The emission intensities for PSDT1 and PSDT5 were shown to agree within error. However, PLDT5 had a mean emission intensity greater than PLDT1. It is expected for all the plasmids in Table 6.2, that the RNA targets produced will be in excess to the DNA anthracene probe added, reducing high levels of background noise due to unbound probe. Despite this, the initial results suggests that an increased transcript number is beneficial for sensing.

The fluorescence distribution in the cells is non-uniform and appears as bright spots. A fluorescence pattern of punctate speckles has previously been used to describe fluorescent probes targeting endogenous RNA in fixed cells. [10, 115] The localisation,

number and size of fluorescent spots varies depending on the target. [71] The punctate fluorescence indicates specific binding since there is only homogeneous fluorescence due to unhybridised probe in the controls given in Figure 6.11.

The bright spots also appear in the case when P1L is not added. It is therefore clear that the plasmid PEI transfection has an effect on the cells. The control cells display a uniform fluorescence upon addition of P1L whereas the mock transfected cells have more localised fluorescence incidences (Figure 6.11). A stable transfection using retrovirus could provide 100% transfection efficiency and deem PEI transfection each time unnecessary.

When non-specific 1L DNA anthracene probe is added to methanol-fixed cells (Figure 6.13), the level of fluorescence is consistent for all expressing cells. The DNA anthracene probe would not be expected to bind to any target within the cell, and therefore only the level of probe-only emission would be observed. The level of fluorescence is therefore similar to the mock-transfected cells with P1L added (Figure 6.11).

A further test of specificity was to PEI transfect a random plasmid (PRan) into cells and, once methanol fixed, add P1L DNA anthracene probe (Figure 6.12). The level of fluorescence is similar to both the non-specific DNA anthracene probe and the mock-transfected cells with DNA anthracene probe.

6.6 Conclusion

Plasmids were designed to induce the production of mRNA targets in cells differing by a single base. The chosen targets give ON/OFF sensing on the addition of P1L DNA anthracene probe (Chapter 3). The plasmids were successfully synthesised and shown to have correct inserts by sequencing. Plasmids were PEI transfected into HeLa cells and transfection efficiency monitored via flow cytometry. Successfully transfected cells were methanol fixed and P1L DNA anthracene probe added. Confocal microscopy was

carried out to gather images for each plasmid type including appropriate controls. Initial P1L plasmid microscope images demonstrate specificity and emission trends replicated from cuvette/fixed cell studies.

Fluorescence emission from cells may be variable since the amount of hybridisable mRNA changes with time (a 'snapshot' is taken when cells are fixed). In general, the fixation process makes the mRNA more accessible, so the hybridisation should be better than live cell studies. It would be interesting to add the DNA anthracene probe to live transfected cells. If the distribution of fluorescence is shown to be the same as for methanol fixed cells, it would be further proof of specific hybridisation. [10]

Repeating these studies with the CDKN1A gene SNP sensing (Chapter 3) would be an exciting future possibility. The results could be compared to extracted human CDKN1A gene expressing cells and/or tissue. An alternative target could be a common endogenous target such as poly(A)+ or transcription site, which could be compared to literature results. [114]

Finally, there are future possibilities such as combining SNP sensing with sub-cellular localisation studies. [71] Increasing the number of repeats from 10 in the future could help with resolution (although ultimately limited by microscope quality).

Chapter 7

Dual fluorophore (Cy3/anthracene) probe for SNP sensing

7.1 Introduction

Motivation for a new probe was caused by issues concerning the anthracene in the DNA anthracene probe. Despite its unique SNP sensing capabilities, anthracene emits at a short wavelength, which conflicts with regions of autofluorescence in *in vitro* studies. The addition of a second fluorophore to the DNA anthracene probe allows longer wavelength and ratiometric sensing.

The concept of FRET was described in Chapter 1 and fluorophore-tagged DNA in Chapter 4. FRET probes are commonly used in nucleic acid hybridisation studies [114, 164] as well as in the detection of SNPs. [96, 163] This chapter describes a newly designed FRET probe which can detect SNPs using changes in fluorescence emission.

Ratiometric studies monitor emission at two separate wavelengths, and provide a more accurate measure of change compared to measuring intensity changes at one

wavelength. This is because the ratio is less sensitive to experimental fluctuations and less dependent on concentration (Section 1.7). [111, 130]

The aim of the work described in this chapter is to design a probe with anthracene as the donor fluorophore, and retain its SNP sensing capabilities. The anthracene can therefore transfer energy to a longer wavelength emitting fluorophore, Cy3. The probes are studied using UV-vis, fluorescence, circular dichroism and lifetime measurements. The probes are optimised in terms of FRET efficiency between the two fluorophores, which involves varying the relative positions of the two fluorophores. Hybridisation studies with the probe and targets varying by a single base shall be carried out. The probe was also optimised in terms of its discriminatory ability between targets. Emission was monitored at both the donor and acceptor wavelengths, but ratiometric measurements were also made.

7.2 Design, synthesis and purification

The dual fluorophore probe is modified with anthracene (donor) and Cy3 (acceptor). Cy3 was chosen as the acceptor fluorophore since its excitation spectra overlaps with the anthracene emission spectra. This suggests the pair of fluorophores will be capable of FRET. Cy3 is a commonly used fluorophore, especially for FRET purposes. Chapter 4 describes its use in DNA FRET hybridisation studies. Cy3 can be tagged to DNA easily and when added to the terminus has freedom to move and stack with the probe, minimising the effect on target binding. [205]

DNA anthracene probes and unmodified oligonucleotide strands were prepared by automated solid phase synthesis using conventional phosphoramidite chemistry (full details in Chapters 2 and 3). The anthracene monomer with carbon linker $n = 1$ and stereochemistry L was focussed on in these studies. Cy3 phosphoramidites (Glen Research) were tagged to the $5'$ termini (Figure 7.1). A 5L probe was also synthesised for

comparison and will be discussed briefly.

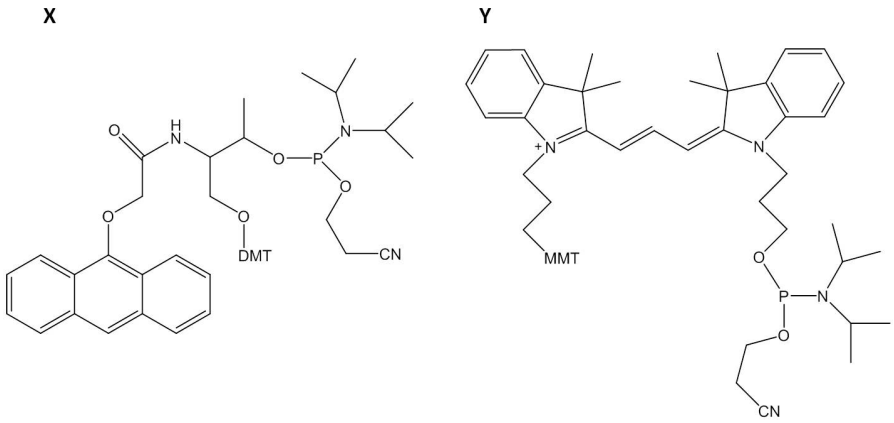

Figure 7.1: **X**: Synthesised anthracene phosphoramidite [86] **Y**: Commercially available Cy3 phosphoramidite (Glen Research). In this study Cy3 is added to the 5′ termini of the oligonucleotide.

Table 7.1 lists the oligonucleotides used in the studies described in this section. A full list of oligonucleotides is given in Table G.1. The sequence used is a 15 base non-biological sequence used throughout this thesis. Single fluorophore probes were designed with either an anthracene or Cy3 modification. Dual fluorophore probes were designed to have both anthracene and Cy3 modifications. Oligonucleotides were purified by RP-HPLC and characterised by mass spectrometry (Appendix F). Standard ultramild treatment with potassium carbonate in methanol failed to fully deprotect the cyanoethyl groups on the dual fluorophore probes nucleotides. It was found that an additional DEA wash for 10 minutes prior to removal from the column successfully removed the cyanoethyl groups. The MMT protecting group was then removed from the Cy3 (Glen Research).

Cy3 was only added to the 5′ of the P1L probe because it would intercalate if incorporated within the structure, and reduce its availability to participate in FRET. [206] The sequence was altered in cases by moving the original central trimer (CXC) closer, denoted by (c), and further (f) from the 5′ termini with and without Cy3 (Figure 7.2).

Table 7.1: Oligonucleotide sequences synthesised. X denotes the anthracene monomer (1L or 5L). Cy3 denotes the cyanine 3 tag.

Oligonucleotide	Sequence (5' to 3')
DN	TGGACTCTCTCAATG
P1L	TGGACTCXCTCAATG
cP1L	TGGCXCACTTCAATG
fP1L	TGGACTTCACXCATG
P5L	TGGACTCXCTCAATG
Cy3	Cy3-TGGACTCTCTCAATG
cCy3	Cy3-TGGCTCACTTCAATG
fCy3	Cy3-TGGACTTCACTCATG
Cy3/P1L	Cy3-TGGACTCXCTCAATG
cCy3/P1L	Cy3-TGGCXCACTTCAATG
fCy3/P1L	Cy3-TGGACTTCACXCATG
Cy3/P5L	Cy3-TGGACTCXCTCAATG
DT1	CATTGAGAGAGTCCA
DT5	CATTGAGAAAGTCCA
DT6	CATTGAAAGAGTCCA
DT7	CATTGAGATAGTCCA
DT8	CATTGAGACAGTCCA
cDT1	CATTGAAGTGAGCCA
cDT5	CATTGAAGTGAACCA
cDT6	CATTGAAGTAAGCCA
fDT1	CATGAGTGAAGTCCA
fDT5	CATGAATGAAGTCCA
fDT6	CATAAGTGAAGTCCA

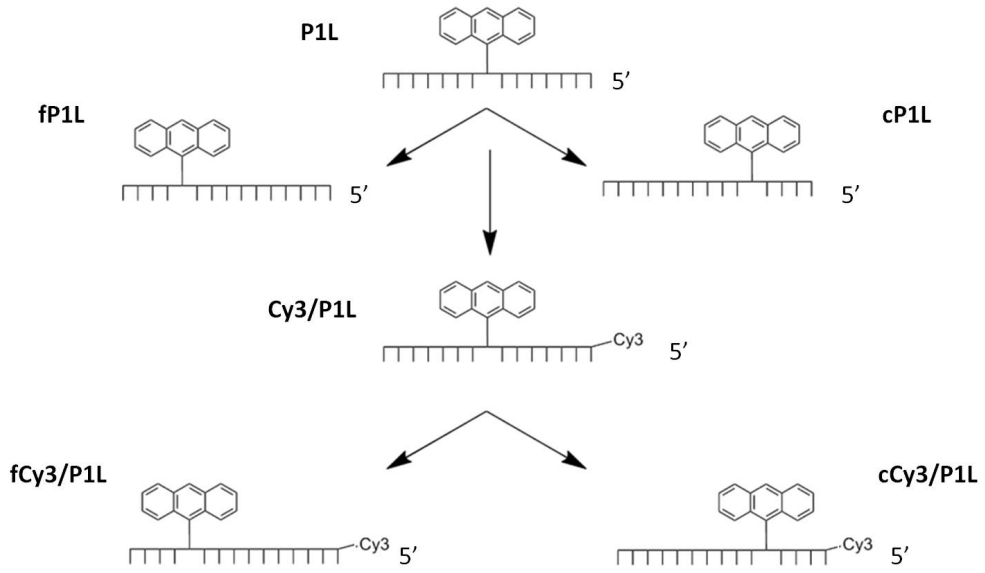

Figure 7.2: Design schematic of the new DNA anthracene probes and dual fluorophore probes.

This was carried out in order to eliminate the effect of changing the adjacent bases on the fluorescent properties of anthracene. Moving the anthracene and Cy3 modifications closer and further apart on the DNA can impact the FRET efficiency since FRET is distance dependent. Inspiration for the design of the FRET probe was taken from Kato *et al.* [207] The positions of FRET pair pyrene and perylene were varied systematically along a 21 base pair DNA duplex. Kato *et al.* [207] compares the FRET efficiency between a theoretical model and experimental values. The theoretical model suggests FRET should drop off dramatically at certain base pair separations between fluorophores, which is due to the fluorophores becoming distanced through a turn (rotation) in the helical duplex. In practice, experimental results show that the FRET efficiency remains high at these base pair separations. The final probe designs chosen for this study included 4, 7 and 10 base pair separations between the fluorophores (Table 7.2)- which all show high theoretical and experimental FRET efficiency from Kato *et al.* [207]

Table 7.2: Distances and orientation between the fluorophores on the duplex. Values calculated using CalcTool (http://www.calctool.org/CALC/prof/bio/dna).

Probe	Distance (bases)	Distance (Angstrom)	Rotation (turns of the helix)
Cy3/P1L	7	23.1	0.67
cCy3/P1L	4	13.2	0.39
fCy3/P1L	10	33	0.96

7.3 Melting studies

All melting studies show the modified probes give stable duplexes with the DNA targets at room temperature (see Appendix E for full results). By moving the anthracene modification closer to the DNA termini the disruption to the structure causes 'fraying' effects which reduced the melting temperatures slightly compared to P1L in the match case (Table 7.3). Table 7.4 shows all the P1L probes have lower melting temperatures in the mismatch case, compared to their respective match case.

The addition of the Cy3 tag on the 5′ end of the unmodified DN probe causes increased melting temperatures (Tables 7.5 and 7.6). This is caused by the Cy3 π-stacking on top of the duplex since Cy3 has a flexible carbon linker between the dye and the DNA backbone. [208] In the case of the cCy3- and fCy3-only probes, the uninterrupted sequence of complementary base pairs and the added stabilisation of the π-stacking Cy3 on the 5′ end causes high melting temperatures. The difference in T_M's between the DT1 and DT5 duplexes are similar regardless of the probe.

Table 7.3: Melting temperatures (°C) of DNA anthracene probes (P1L) and matching target DT1. 5 μM DNA, 100 mM NaCl, 10 mM pH 7.0 sodium phosphate buffer.

Duplex	T_M (°C)
P1L:DT1	53
cP1L:cDT1	52
fP1L:fDT1	51.5

Table 7.4: Melting temperatures (°C) of DNA anthracene probes (P1L) and mismatching target DT5. 5 μM DNA, 100 mM NaCl, 10 mM pH 7.0 sodium phosphate buffer.

Duplex	T_M (°C)
P1L:DT5	46
cP1L:cDT5	41
fP1L:fDT5	47.5

Table 7.5: Melting temperatures (°C) of Cy3-only probes and matching target DT1. 5 μM DNA, 100 mM NaCl, 10 mM pH 7.0 sodium phosphate buffer.

Duplex	T_M (°C)
Cy3:DT1	57
cCy3:cDT1	61
fCy3:fDT1	61

Table 7.6: Melting temperatures (°C) of Cy3-only probes and mismatching target DT5. 5 μM DNA, 100 mM NaCl, 10 mM pH 7.0 sodium phosphate buffer.

Duplex	T_M (°C)
Cy3:DT5	43.5
cCy3:cDT5	48
fCy3:fDT5	47

Table 7.7: Melting temperatures (°C) of Cy3/P1L probes and matching target DT1. 5 μM DNA, 100 mM NaCl, 10 mM pH 7.0 sodium phosphate buffer.

Duplex	T_M (°C)
Cy3/P1L:DT1	49.5
cCy3/P1L:cDT1	53
fCy3/P1L:fDT1	54.5

Table 7.8: Melting temperatures (°C) of Cy3/P1L probes and mismatching target DT5. 5 μM DNA, 100 mM NaCl, 10 mM pH 7.0 sodium phosphate buffer.

Duplex	T_M (°C)
Cy3/P1L:DT5	42
cCy3/P1L:cDT5	42.5
fCy3/P1L:fDT5	42.5

The cCy3- and fCy3-only T_M's help to explain the higher melting temperatures of the cCy3/P1L and fCy3/P1L compared to their respective P1L probes (Tables 7.7 and 7.8). Clearly the stabilising Cy3 overcomes the destabilising anthracene in these dual fluorophore probes.

In the case of the dual fluorophore probe Cy3/P1L, the melting temperatures show less stability compared to the single fluorophore probe duplexes (Table 7.9). There is no obvious trend to the low Cy3/P1L duplex T_M's but it may be due to a conformational change not allowing the anthracene to intercalate as much into the duplex. Intercalation must still be present and causing some stabilisation though since the T_M difference between DT1 and DT5 is similar to that of P1L. This was in agreement with CD studies which are discussed in Section 7.6. Dye-dye and dye-nucleotide interactions could also be a contributing factor to lower melting temperatures (Section E.1.1). [209]

Previous studies into SNP sensing with P1L probes showed that the anthracene was able to stabilise a mismatch being on the 5′ side of the modification. [33] The T_M between P1L and mismatching target DT5 is 1.5 °C greater than P1L with DT6 (mismatch

Table 7.9: Melting temperatures (°C) of central DNA anthracene (P1L), Cy3-only and dual fluorophore probes and targets, plus controls. 5 μM DNA, 100 mM NaCl, 10 mM pH 7.0 sodium phosphate buffer.

Probe/Target	DT1	DT5	$\triangle$(DT1-DT5)
DN	55	42	13
P1L	53	46	7
Cy3	57	43.5	13.5
Cy3/P1L	49.5	42	7.5

Table 7.10: Melting temperatures (°C) of DNA anthracene probes (P1L) and mismatching target DT6. 5 μM DNA, 100 mM NaCl, 10 mM pH 7.0 sodium phosphate buffer.

Duplex	T_M (°C)
P1L:DT6	44.5
cP1L:cDT6	42
fP1L:fDT6	47.5

on $3'$ side of the modification). This small change causes there to be only ON/OFF fluorescence sensing in the case of DT5. The target DT6 was tested here to compare FRET efficiencies with DT5 in the dual fluorophore probe study. Finally, other mismatches were considered such as targets DT7 (G to T mismatch) and DT8 (G to C mismatch). All cases showed duplexes were stable at room temperature (Appendix E). Previous studies show that all the mismatch target T_M's were similar with unmodified DNA probe (DN) but there were differences with P1L, which is reproduced here. [33]

Despite the DT6 causing destabilisation to the P1L duplex, the opposite is true for the corresponding cP1L and fP1L cases (Table 7.10). This trend extends to all the dual fluorophore probes since DT6 yields higher melting temperatures than DT5. It is even the case for the Cy3-only probe duplexes. The hypothesis is that the DT5, compared to DT6, causes an unfavourable conformational change combined with the Cy3. This shall be further discussed with fluorescence results.

7.4 Fluorescence studies

7.4.1 Single fluorophore probes (single stranded)

P1L probes were described in Chapter 3 and their fluorescence properties discussed. Emission spectra of the cP1L and fP1L probes are given in Figure 7.3 alongside P1L.

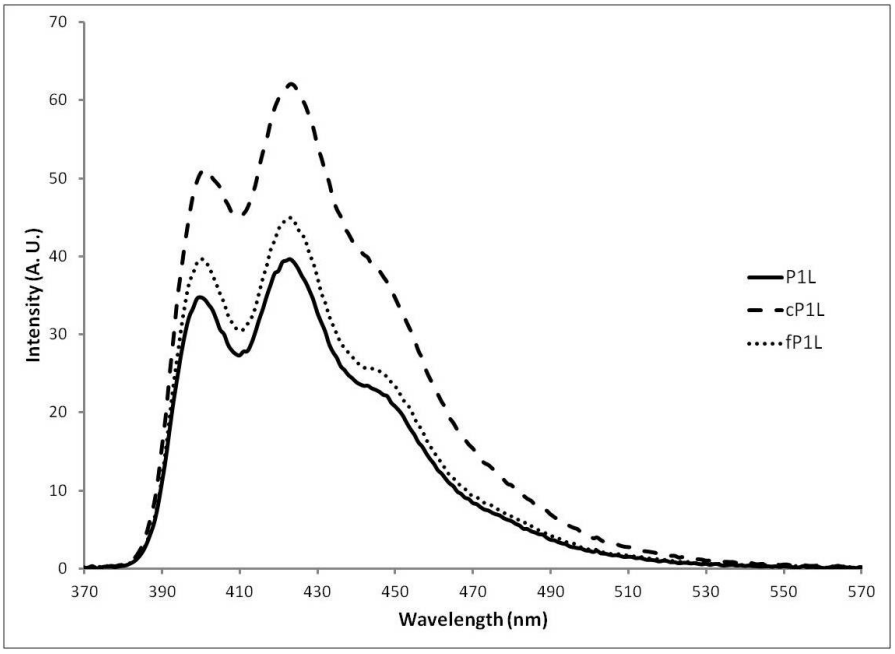

Figure 7.3: Fluorescence spectra showing the emission spectra of DNA anthracene probes P1L, cP1L and fP1L respectively. 1 μM DNA, 100 mM NaCl, 10 mM pH 7.0 sodium phosphate buffer, λ_{ex} = 350 nm.

All the probes give characteristic anthracene emission with a λ_{max} of 426 nm, however the cP1L and fP1L are more emissive than P1L (60% and 15% respectively at λ_{em} = 426 nm). This is borne out by different quantum yields (Table 7.11), which is due to the anthracene being in different environments. The base opposite system was also considered with the P5L probe (Section 3.3.4, Chapter 3). The central anthracene modification was not moved and the P5L fluorescence emission spectra is given in Figure E.4, Appendix E.

Cy3-only tagged probes were shown to have minimal emission when excited at

Table 7.11: Quantum yields of single stranded DNA anthracene probes. 1 μM DNA, 100 mM NaCl, 10 mM pH 7.0 sodium phosphate buffer, $\lambda_{ex} = 350$ nm. Quantum yields were determined relative to quinine sulphate ($\Phi_f = 0.546$)

Probe	Quantum Yield
P1L	0.075
cP1L	0.127
fP1L	0.081

.

350 nm (excitation at 550 nm is given in Figure 7.5). Emission spectra is given in Figure 7.4 and peak emission is monitored at 570 nm. The quantum yields, upon 350 nm excitation, are given in Table 7.12. The fluorescence QY of Cy3 linked covalently to DNA depends on the type of linkage used for attachment, DNA sequence and secondary structure. [206] Cy3 only probes do not vary significantly in emission upon the movement of the central trimer (CTC) since the Cy3 tag remains on the 5′ terminus.

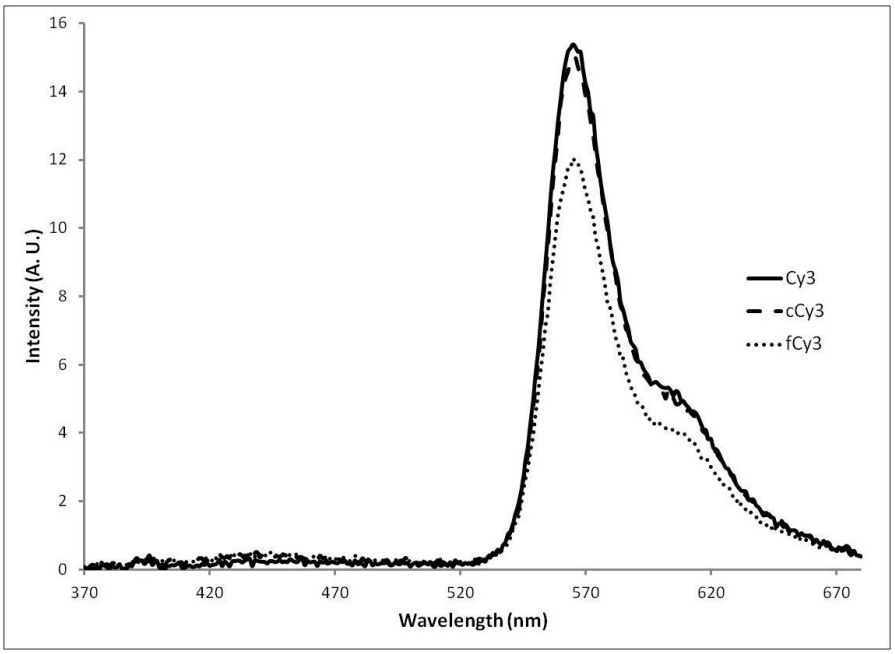

Figure 7.4: Fluorescence spectra showing the emission spectra of Cy3-only probes Cy3, cCy3 and fCy3 respectively. 1 μM DNA, 100 mM NaCl, 10 mM pH 7.0 sodium phosphate buffer, $\lambda_{ex} = 350$ nm.

Table 7.12: Quantum yields of single stranded Cy3-only probes. 1 μM DNA, 100 mM NaCl, 10 mM pH 7.0 sodium phosphate buffer, λ_{ex} = 350 nm. Quantum yields were determined relative to quinine sulphate ($\Phi_f = 0.546$)

Probe	Quantum Yield
Cy3	0.026
cCy3	0.023
fCy3	0.019

.

7.4.2 Dual fluorophore probes (single stranded)

In order to achieve optimum FRET for the dual fluorophore probe, there were two considerations. First, the emission of the donor fluorophore (anthracene) must overlap with the excitation of the acceptor fluorophore (Cy3). However, the overlap is a compromise between enhancing FRET and reducing cross-excitation (also known as cross-talk). Figure 7.5 gives the normalised excitation and emission spectra of the anthracene-only and Cy3-only probes, with the area of overlap labelled. The second consideration was the distance and orientation of the fluorophores. Table 7.2 gives the distance and rotation of the helix between the fluorophores.

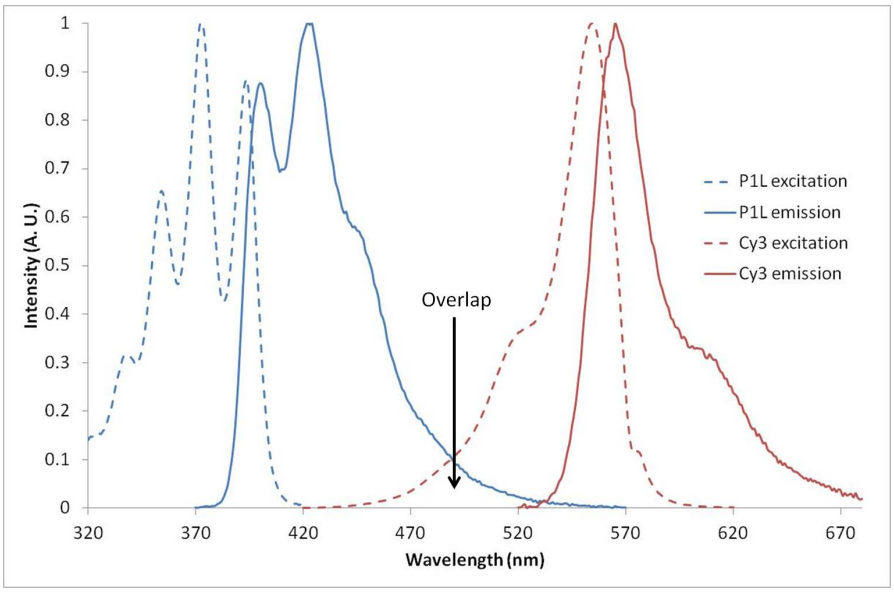

Figure 7.5: Excitation spectra (dashed) and emission spectra (solid) of P1L probes (blue) and Cy3-only probes (red). 1 μM DNA, 100 mM NaCl, 10 mM pH 7.0 sodium phosphate buffer. P1L λ_{ex} = 350 nm and λ_{em} = 426 nm. Cy3 λ_{ex} = 550 nm and λ_{em} = 570 nm. Data is normalised to λ_{max} values.

It can be concluded from the fluorescence emission studies that FRET is able to occur between the anthracene and Cy3 since there is increased Cy3 emission when the anthracene is included in the probe, compared to the Cy3-only probe (Figure 7.6). The emission at 426 nm decreases as emission at 570 nm increases, indicating a transfer of energy. This is the case for the close (Figure 7.7) and far (Figure 7.8) dual fluorophore probes.

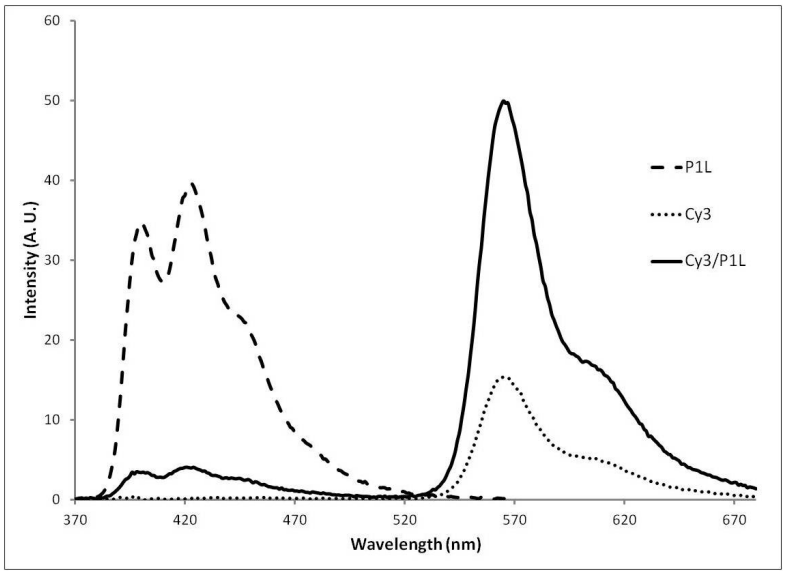

Figure 7.6: Fluorescence spectra showing the emission spectra of P1L, Cy3-only and Cy3/P1L probes respectively. 1 μM DNA, 100 mM NaCl, 10 mM pH 7.0 sodium phosphate buffer, $\lambda_{ex} = 350$ nm.

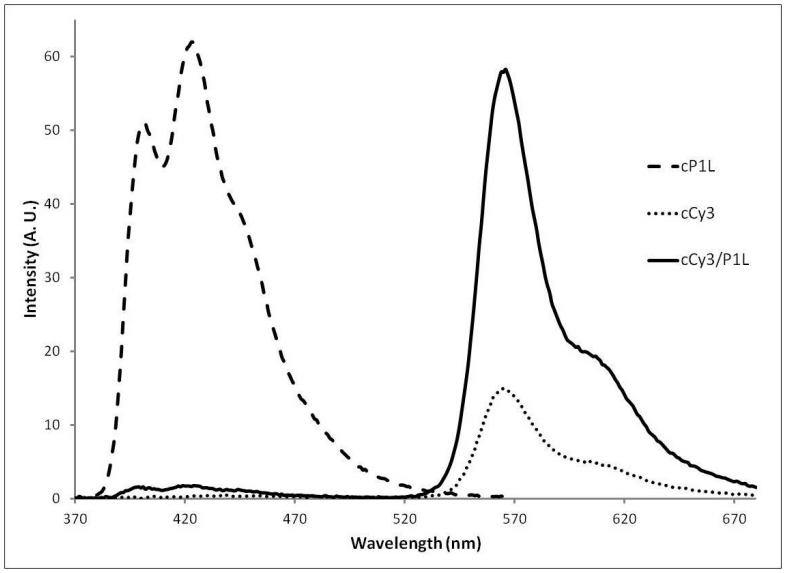

Figure 7.7: Fluorescence spectra showing the emission spectra of cP1L, cCy3-only and cCy3/P1L probes respectively. 1 μM DNA, 100 mM NaCl, 10 mM pH 7.0 sodium phosphate buffer, $\lambda_{ex} = 350$ nm.

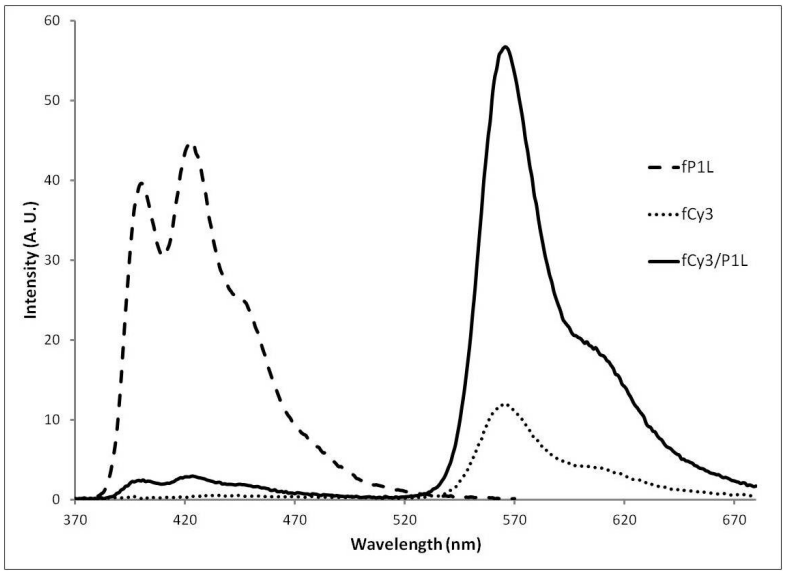

Figure 7.8: Fluorescence spectra showing the emission spectra of fP1L, fCy3-only and fCy3/P1L probes respectively. 1 μM DNA, 100 mM NaCl, 10 mM pH 7.0 sodium phosphate buffer, λ_{ex} = 350 nm.

Figure 7.9 gives the emission spectra of the three dual fluorophore probes upon excitation at 350 nm. The varying distance between the anthracene and Cy3 has little effect on the Cy3 emission at 570 nm. However, there are varying degrees of quenching at 426 nm. Cy3/P5L probe also exhibits FRET between 5L anthracene and Cy3 (Figure E.10).

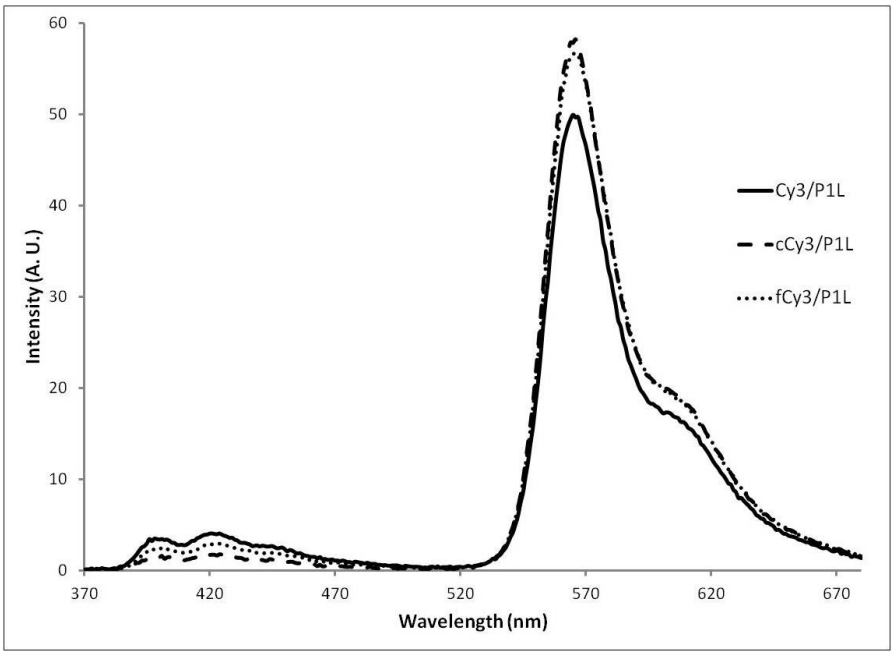

Figure 7.9: Fluorescence spectra showing the emission spectra of Cy3/P1L probes Cy3/P1L, cCy3/P1L and fCy3/P1L respectively. 1 μM DNA, 100 mM NaCl, 10 mM pH 7.0 sodium phosphate buffer, λ_{ex} = 350 nm.

The cCy3/P1L probe has the greatest degree of energy transfer since it has the lowest emission at 426 nm. However, it is not necessarily an efficient energy transfer since the Cy3 emission is no greater than for the fCy3/P1L case. fCy3/P1L would be expected to have lower FRET efficiency than Cy3/P1L due to the distance dependence of FRET. However, the orientation of the fluorophores is important and influenced by the rotation of the DNA helix. In the fCy3/P1L case there is nearly a full helical rotation between the dyes (Table 7.2). The Cy3/P1L probe donates the least energy since it has high and low emission at 426 nm and 570 nm respectively. The quantum yields of the dual fluorophore probes (Table 7.13) are similar to their corresponding DNA anthracene probes, which would be expected if the energy transfer is without significant loss. There is a small difference between the cCy3/P1L and cP1L probes. One factor to consider in the cCy3/P1L probe case is that the two fluorophores are 'too close'. It should be acknowledged that some acceptor emission could be quenched due to the exciton

Table 7.13: Quantum yields of single stranded DNA anthracene and dual fluorophore probes. 1 μM DNA, 100 mM NaCl, 10 mM pH 7.0 sodium phosphate buffer, $\lambda_{ex} = 350$ nm. Quantum yields were determined relative to quinine sulphate ($\Phi_f = 0.546$).

Probe	Quantum Yield
P1L	0.075
cP1L	0.127
fP1L	0.081
Cy3/P1L	0.096
cCy3/P1L	0.091
fCy3/P1L	0.096

coupling between the dyes at close proximity, which has been reported.[84, 210] Kato *et al.* experienced only small levels of FRET efficiency loss in their FRET probe when the fluorophores were separated by one base pair. [207]

7.4.3 Single fluorophore probe in duplex

Cy3-only probes (Cy3, cCy3, fCy3) show a degree of quenching at 570 nm upon hybridisation (Table E.6), however the emission change was the same for all targets (the percentage change values are large since the intensity values are small). Therefore the Cy3-only probes do not partake in base-discrimination sensing. Emission spectra for all the Cy3-only duplexes are given in Appendix E.

P1L probe ON/OFF sensing of targets was described in Chapter 3. Figure 7.10 shows the emission increase on addition of the mismatch target DT5 to P1L, whereas addition of the matching target DT1 causes a decrease in emission.

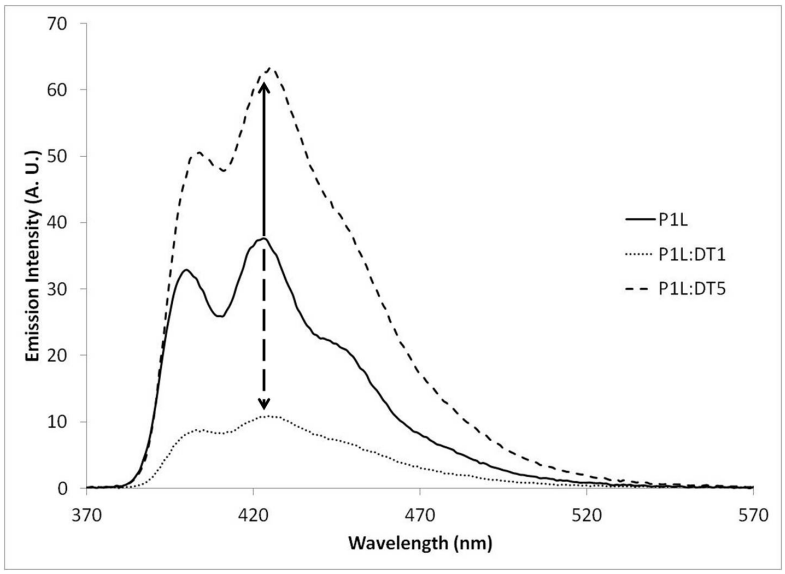

Figure 7.10: Emission spectra showing the change in emission upon hybridisation of anthracene probe P1L with targets DT1 and DT5 respectively. 1 μM DNA, 100 mM NaCl, 10 mM pH 7.0 sodium phosphate buffer, λ_{ex} = 350 nm.

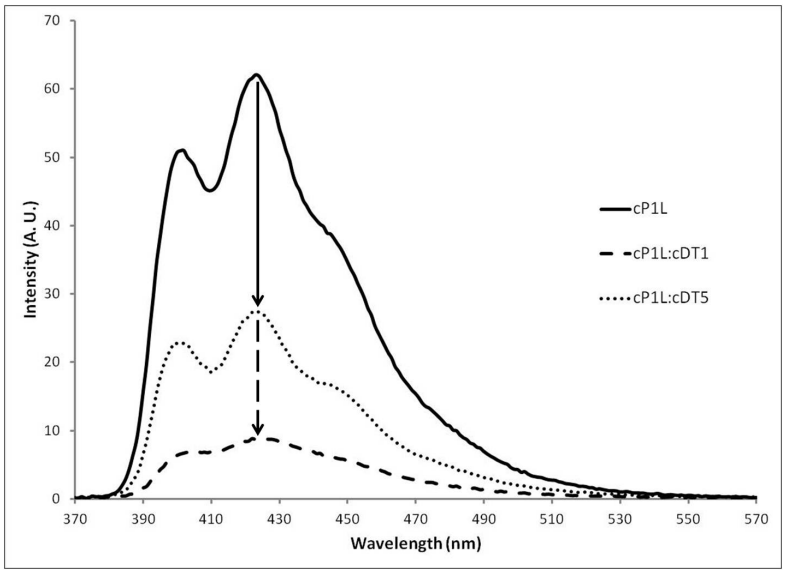

Figure 7.11: Emission spectra showing the change in emission upon hybridisation of anthracene probe cP1L with targets cDT1 and cDT5 respectively. 1 μM DNA, 100 mM NaCl, 10 mM pH 7.0 sodium phosphate buffer, λ_{ex} = 350 nm.

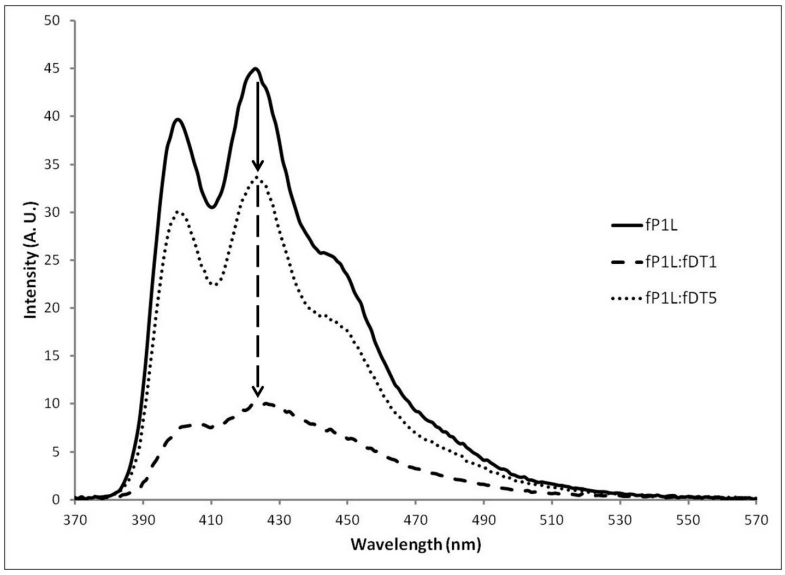

Figure 7.12: Emission spectra showing the change in emission upon hybridisation of anthracene probe fP1L with targets fDT1 and fDT5 respectively. 1 μM DNA, 100 mM NaCl, 10 mM pH 7.0 sodium phosphate buffer, λ_{ex} = 350 nm.

Emission spectra are given for cP1L and fP1L in Figures 7.11 and 7.12 respectively. It is interesting to note that there is no longer ON/OFF sensing, which links to the higher quantum yields (Table 7.13). However, it also alludes to the neighbouring bases and differing structure having an effect on the sensing effect. [33] Despite this the mismatch target DT5 is distinguishable from the matching target DT1, and is consistently higher in emission (Table 7.14). As previously described for the base opposite system (Section 3.3.4) P5L varies in emission depending on the base opposite upon

Table 7.14: Percentage differences in emission at λ_{em} = **426 nm** on addition of DNA targets to DNA anthracene probes, relative to the probe alone. 1 μM DNA, 100 mM NaCl, 10 mM pH 7.0 sodium phosphate buffer, λ_{ex} = 350 nm.

Probe/Target	DT1	DT5
P1L	-70	+77
cP1L	-86	-56
fP1L	-77	-24

hybridisation with DNA targets (Figure E.4).

7.4.4 Dual fluorophore probe in duplex

The dual fluorophore system is capable of FRET as described above, however, hybridisation studies reveal it is capable of SNP discrimination at two different wavelengths. Emission spectra for the dual fluorophore probe duplexes are shown in Figures 7.13, 7.14 and 7.15.

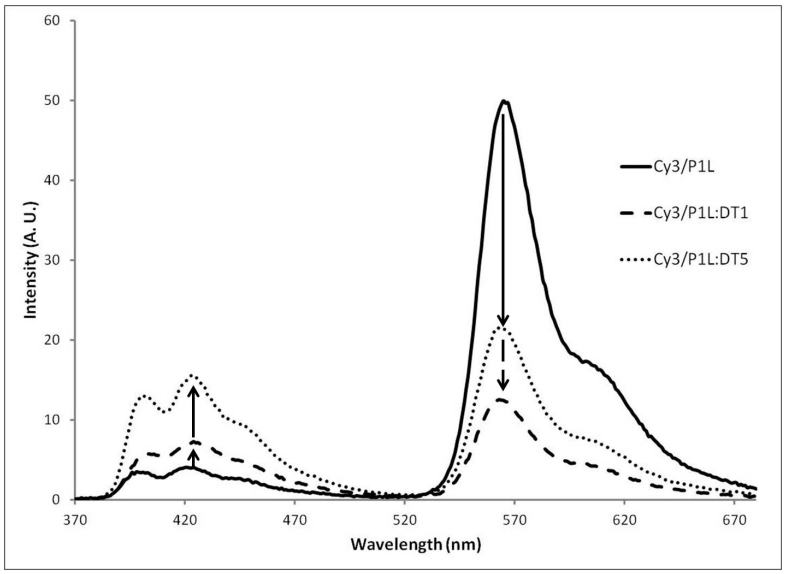

Figure 7.13: Emission spectra showing the change in emission upon hybridisation of Cy3/P1L with targets DT1 and DT5 respectively. 1 μM DNA, 100 mM NaCl, 10 mM pH 7.0 sodium phosphate buffer, λ_{ex} = 350 nm.

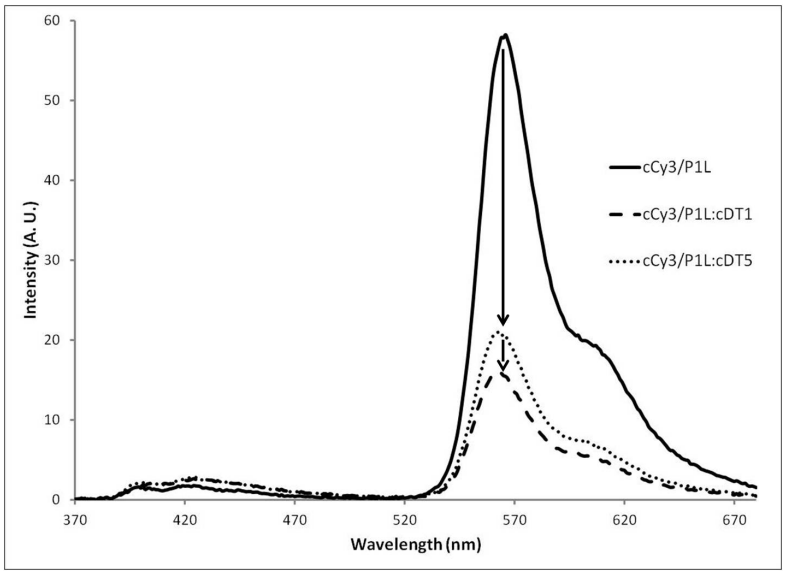

Figure 7.14: Emission spectra showing the change in emission upon hybridisation of cCy3/P1L with targets cDT1 and cDT5 respectively. 1 μM DNA, 100 mM NaCl, 10 mM pH 7.0 sodium phosphate buffer, λ_{ex} = 350 nm.

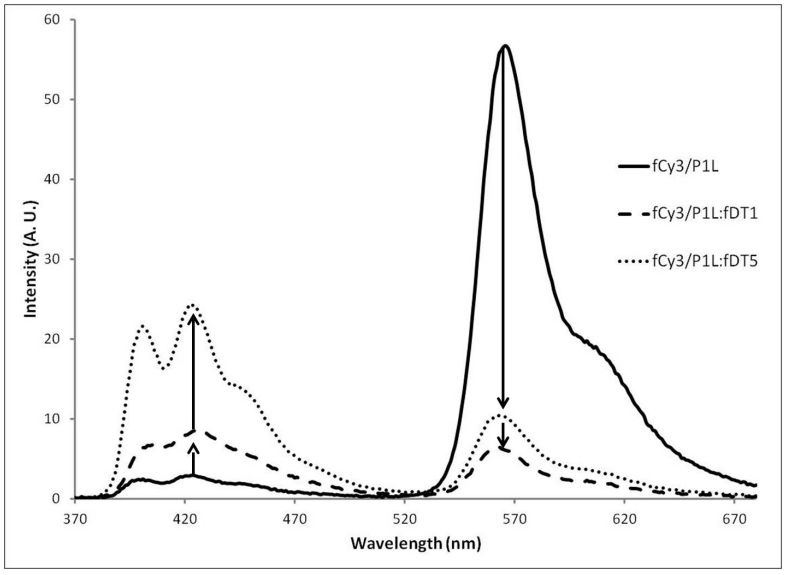

Figure 7.15: Emission spectra showing the change in emission upon hybridisation of fCy3/P1L with targets fDT1 and fDT5 respectively. 1 μM DNA, 100 mM NaCl, 10 mM pH 7.0 sodium phosphate buffer, λ_{ex} = 350 nm.

Titrations of target DNA showed no further change in emission was observed in

the presence of excess target. This indicates the formation of a 1:1 complex, which is consistent with DNA duplex formation. This was applicable for all dual fluorophore probe duplexes. An example of a titration graph is shown in Figure E.9, Appendix E for the Cy3/P1L:DT1 duplex. Figure E.8 shows that the addition of a completely mismatching DNA target (DRan) causes little change in emission for the probes indicating that the sensing is caused by a hybridisation event. Table E.7 gives the percentage change in emission values at 570 nm upon hybridisation of targets. The percentage change in emission values at 426 nm are given in Table E.8, Appendix E (they are very large since the intensity values are small). Hybridised probe quantum yields are given in Table E.9.

For all the dual fluorophore probes there is no ON/OFF sensing at 570 nm but there is discrimination between the targets. In all cases the mismatching target causes the emission at 570 nm to decrease less than the matching target. Therefore, SNP readout is possible at 570 nm, whereas it was not possible with the Cy3-only probe. At 426 nm the anthracene emission generally increases although there is a negligible increase in the case of the cCy3/P1L probe. Despite both targets causing an increase at 426 nm, they are distinguishable since the mismatch target causes a greater increase. Therefore, targets with one base difference are able to undergo sensing at two wavelengths using the dual fluorophore probe.

There are two factors influencing the fluorescence emission: anthracene intercalation and orientation. The increasing anthracene emission at 426 nm for both targets suggests intercalation of the anthracene into the duplex. As found previously with P1L, the anthracene would be expected to intercalate more with the mismatch target (DT5) than the match target (DT1), hence a greater increase in anthracene emission. With DT1, the anthracene is quenched more by its environment and hence less Cy3 emission is observed compared to with DT5. The anthracene intercalates more into the duplex with DT5 and is more emissive, and therefore causes higher Cy3 emission. The FRET efficiency is optimal for the single stranded probes since the anthracene and Cy3 can

align, hence why the Cy3 emission is similar for all dual fluorophore probes. The imposed rigidity of the duplex formation causes a reduction in FRET efficiency. Therefore, the differences in emission caused by the anthracene intercalation is counteracted by the orientation of the two fluorophores upon duplex formation.

DT5 causes higher emission at $\lambda_{em} = 426$ nm than DT6 for the Cy3/P1L, which is consistent with the findings for P1L probe which gives a greater emission for a mismatch on the $5'$ side with respect to the tag. The Cy3 emission at $\lambda_{em} = 570$ nm is slightly higher for DT5 than DT6 (Figure 7.16). The hypothesis is that the anthracene is able to intercalate into the duplex more for DT5 (hence the higher anthracene emission) but is at an orientation which allows it to donate energy to Cy3. When the mismatch is on the other side of the anthracene (DT6), the anthracene can still intercalate into the duplex since T_M values show duplex stabilisation (Table E.1). However, the anthracene is not in an optimum position for FRET and unable to donate as much energy to the Cy3. The same trend is observed for cCy3/P1L:cDT6 and fCy3/P1L:fDT6. The other mismatch targets, DT7 and DT8, give similar results to DT6 for the Cy3/P1L probe.

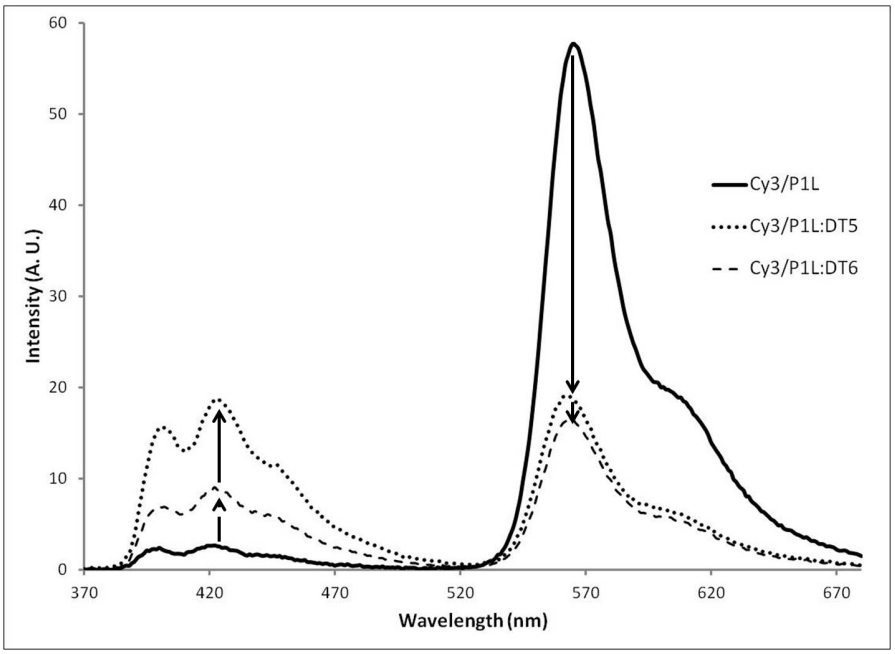

Figure 7.16: Emission spectra showing the change in emission upon hybridisation of Cy3/P1L with targets DT5 and DT6 respectively. 1 μM DNA, 100 mM NaCl, 10 mM pH 7.0 sodium phosphate buffer, λ_{ex} = 350 nm.

The dual fluorophore probe with longer linker anthracene Cy3/P5L also exhibits quenching at 570 nm (Figure E.10). An initial hypothesis for the lack of increased emission at 570 nm upon hybridisation was the restrictive anthracene n = 1 carbon linker, however the same result was observed for the n = 5 carbon linker. It is difficult to discriminate between DNA targets using the Cy3/P5L probe because of less dramatic structural changes, and studies were therefore not continued with this probe.

7.4.5 Ratiometric studies

Table 7.15 gives the ratio of absolute emission intensities at wavelengths 570 nm/426 nm for the dual fluorophore probes and duplexes. Ratiometric studies are beneficial since they contain an internal reference point, meaning that sensing can be obtained despite variable probe concentrations. As long as the probe is completely bound to target DNA, this negates the need for a probe alone measurement prior to target bind-

Table 7.15: Ratio of emission intensity at wavelengths 570 nm/426 nm for dual fluorophore DNA probes and targets. 100 mM NaCl, 10 mM pH 7.0 sodium phosphate buffer, λ_{ex} = 350 nm. Ratios are expressed as mean ± s.e.m. from three repeats.

Probe	Cy3/P1L	cCy3/P1L	fCy3/P1L
Probe only	15.23±3.10	35.74±0.7	20.48±0.35
DT1	1.52±0.12	6.23±0.27	0.65±0.01
DT5	1.17±0.14	7.79±0.23	0.40±0.01

ing. Although the system still involves a measurement at 426 nm (so autofluorescence wavelength regions can not be avoided) it has potential application to areas such as PCR. Figure 7.17 shows that ratio values can also be used for SNP detection purposes since match/mismatch targets can be discriminated. Table E.12 gives the ratios of dual fluorophore probes with other mismatch targets (DT6-DT8). It is found for Cy3/P1L that the DT5 is distinguishable from other adjacent mismatch targets in terms of ratios.

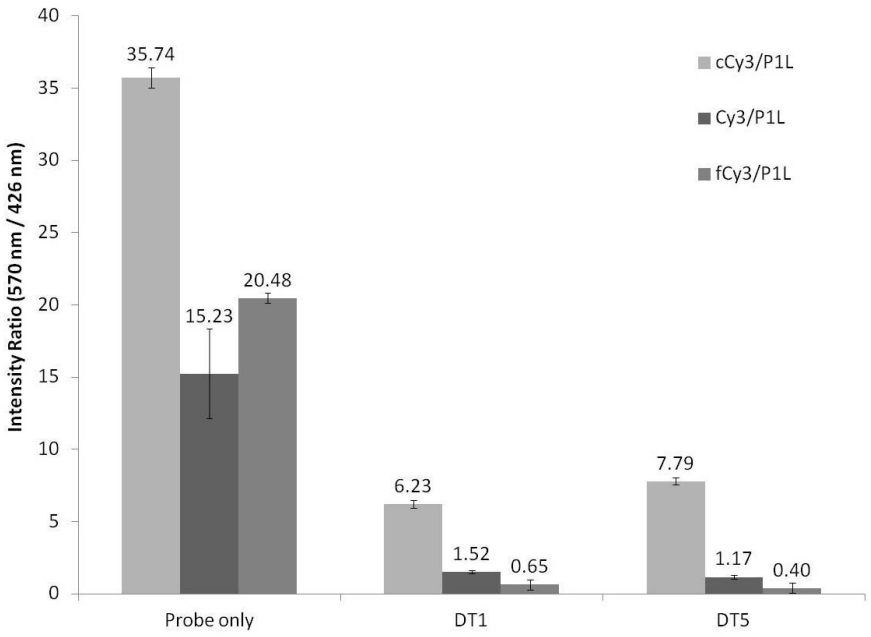

Figure 7.17: Ratio of emission intensity at 570 nm/426 nm for dual fluorophore DNA probes and targets. 100 mM NaCl, 10 mM pH 7.0 sodium phosphate buffer, λ_{ex} = 350 nm. Ratios are expressed as mean ± s.e.m. from three repeats.

A range of concentrations, within the limitations of the equipment, for the Cy3/P1L probe duplex was tested (0.5 - 2 μM). The ratio between emission at 570 nm /426 nm was shown to be consistent within error (Table E.13, Appendix E). This proves that the probe is not aggregating and the sensing results from an intramolecular interaction rather than an intermolecular. Also it demonstrates the principle of ratiometric sensing in that the emission intensity of the probe (and hence its concentration) does not need to be measured or known beforehand, so long as the target is in excess.

7.5 Lifetime studies

Lifetime studies were briefly discussed in Chapter 1 (Section 1.2). Lifetime measurements are particularly relevant and interesting in the base adjacent SNP sensing system. The hypothesis was that the difference in anthracene lifetimes would impact the Cy3 lifetimes in the dual fluorophore probes, causing differences in fluorescence emission.

The P1L probe and most P1L duplexes lifetimes are found to be tri-exponential, consisting of a short (τ1), medium (τ2) and long (τ3) component, suggesting more than one anthracene environment. [211] Conversely, P1L:DT5 can be classed as bi-exponential, although technically due to a very minor sub-ns lifetime, it is tri-exponential. This is only applicable for the mismatch on the 5′ of the modification since P1L:DT6 is tri-exponential. [33] The P1L SNP sensing mechanism was discussed in Chapter 3. The changes in emission are dependent on the match/mismatching bases surrounding the anthracene and how they impact the anthracene environment. It has been previously emphasised that the anthracene is not tightly held in a single configuration, but partitions between different environments. The contribution from the 1L intercalating into the duplex is thought to be greater in the mismatch target (DT5) case. This leads to higher fluorescence emission due to the anthracene being in a hydrophobic environment. τ3 is attributed to the fluorescent emission of anthracene from an environment where it

Table 7.16: Fluorescence lifetimes (ns) of P1L and duplexes. 5 μM DNA, 100 mM NaCl, 10 mM pH 7.0 sodium phosphate buffer, λ_{ex} = 376 nm, λ_{em} = **426 nm**.

	τ1 (Wt %)	τ2 (Wt %)	τ3 (Wt %)	χ^2
P1L	0.61 (12)	2.02 (31)	8.77 (57)	1.252
P1L:DT1	0.62 (38)	1.60 (45)	6.97 (17)	1.175
P1L:DT5	0.43 (2)	2.15 (23)	9.77 (75)	1.354

Table 7.17: Fluorescence lifetimes (ns) of fP1L and duplexes. 5 μM DNA, 100 mM NaCl, 10 mM pH 7.0 sodium phosphate buffer, λ_{ex} = 376 nm, λ_{em} = **426 nm**.

	τ1 (Wt %)	τ2 (Wt %)	τ3 (Wt %)	χ^2
fP1L	0.49 (8)	2.07 (36)	8.37 (56)	1.356
fP1L:fDT1	0.60 (39)	1.48 (56)	6.23 (5)	1.186
fP1L:fDT5	0.41 (6)	2.85 (63)	8.11 (31)	1.245

is closely shielded by nucleobases within the duplex. Previous studies have shown that the P1L with the mismatch target DT5 has a longer lifetime (τ3) than the matching DT1 target. [33]

Table 7.16 gives the lifetime measurements for P1L single-stranded and duplexes, which were re-measured for this thesis (set-up described in Chapter 2) and are similar to those previously measured. [33] Fluorescent decay profiles of P1L single-stranded and duplexes are given in Section E.3, Appendix E.

The lifetimes for fP1L and cP1L are given in Tables 7.17 and 7.18 respectively. They follow a similar trend to that of P1L described above. However, τ3 is reduced, or disappears for cP1L, for the DT1 and DT5 duplexes. This agrees with the hypothesis that the anthracene is not able to intercalate as well in the fP1L and cP1L cases.

The Cy3-only probes lifetimes were measured at 570 nm (Appendix E). For the probes and duplexes, the lifetimes are bi-exponential indicating two different environments. As expected there is little difference between the lifetimes of Cy3-only probes with DT1 and DT5 targets.

Table 7.18: Fluorescence lifetimes (ns) of cP1L and duplexes. 5 μM DNA, 100 mM NaCl, 10 mM pH 7.0 sodium phosphate buffer, λ_{ex} = 376 nm, λ_{em} = **426 nm**.

	τ1 (Wt %)	τ2 (Wt %)	χ^2
cP1L	1.82 (27)	7.86 (73)	1.512
cP1L:cDT1	0.87 (77)	5.16 (23)	1.981
cP1L:cDT5	2.88 (46)	8.61 (54)	1.188

Table 7.19: Fluorescence lifetimes (ns) of dual fluorophore probes and anthracene-only probes. 5 μM DNA, 100 mM NaCl, 10 mM pH 7.0 sodium phosphate buffer, λ_{ex} = 376 nm, λ_{em} = **426 nm**.

	τ1 (Wt %)	τ2 (Wt %)	τ3 (Wt %)	χ^2
P1L	0.61 (12)	2.02 (31)	8.77 (57)	1.252
Cy3/P1L	0.35 (53)	1.42 (29)	8.73 (18)	1.229
fP1L	0.49 (8)	2.07 (36)	8.37 (56)	1.356
fP1L/Cy3	0.29 (50)	1.66 (36)	5.43 (14)	1.226
cP1L	1.82 (27)	7.86 (73)	- (-)	1.512
cCy3/P1L	0.25 (94)	5.83 (6)	- (-)	1.662

The lifetimes of the dual fluorophores were first monitored at 426 nm. τ3 is dependent on anthracene, regardless of any energy transfer, whereas τ2 is influenced mainly by FRET. It is the τ values rather than the weightings which are more important. [207] Due to energy donation, τ2 is expected to be less for the dual fluorophore probe compared to the respective anthracene-only probe when excited at 426 nm. This is true for all the dual fluorophore probes (Table 7.19). τ2 is expected to increase the closer the fluorophores are, which is a trend also observed. As the fluorophores move further apart they tend towards the anthracene-only probe values. cCy3/P1L lifetimes are too short to observe accurately due to the fluorophores high energy transfer and proximity.

Upon duplex formation, it was shown that DT5 causes bi-exponential decay of the Cy3/P1L whereas DT1 remains tri-exponential. This trend was shown to be true for

Table 7.20: Fluorescence lifetimes (ns) of Cy3/P1L duplexes. 5 μM DNA, 100 mM NaCl, 10 mM pH 7.0 sodium phosphate buffer, λ_{ex} = 376 nm, λ_{em} = **426 nm**.

	τ1 (Wt %)	τ2 (Wt %)	τ3 (Wt %)	χ^2
Cy3/P1L:DT1	0.56 (51)	1.45 (43)	7.92 (6)	1.190
Cy3/P1L:DT5	0.79 (16)	2.40 (84)	- (-)	1.208
fCy3/P1L:fDT1	1.50 (85)	2.41 (15)	-(-)	1.596
fCy3/P1L:fDT5	1.37 (32)	3.23 (68)	-(-)	1.505
cCy3/P1L:cDT1	0.33 (-)	5.05 (-)	-(-)	1.576
cCy3/P1L:cDT5	0.19 (70)	5.56 (30)	-(-)	2.041

only the Cy3/P1L probe (Table 7.20). It was also shown that τ2 increases significantly for the DT5 target compared to the DT1 target, except for the cCy3/P1L probe. The increased τ2 indicates more FRET is occurring in the DT5 duplex.

If Cy3 retains the anthracene lifetime trend then DT5 would be expected to have a longer lifetime than DT1 for the Cy3/P1L probe when monitored at 570 nm. There is now a single exponential decay for both targets, however the DT5 causes a significantly longer lifetime due to slower energy transfer than DT1 (excluding the cCy3/P1L case) (Tables 7.21, 7.22 and 7.23). Longer lifetimes are also evident for the fCy3/P1L probe compared to the other dual fluorophore probes due to a slower energy transfer caused by increased distance between the two fluorophores. These results suggest that lifetime differences caused by the anthracene intercalation can be detected by energy transfer to Cy3 at 570 nm. These results are preliminary since some χ^2 values are higher than desirable (>1.4). Future experiments would involve repeating these measurements on tailored equipment.

Changes in fluorescence lifetimes could be measured and visualised using oligonucleotides and appropriate imaging facilities. For example, Tsuji *et al.* was one of the first to use the concept of FRET to target mRNA in the cell. [121] Later FRET was measured using acceptor fluorescence decays. [212] Distinguishing base differences using a

single FRET probe and lifetimes would be a novel method for SNP sensing. This could be further exploited for applications such as fluorescence-lifetime imaging microscopy (FLIM).

Table 7.21: Fluorescence lifetimes (ns) of Cy3/P1L and duplexes. 5 μM DNA, 100 mM NaCl, 10 mM pH 7.0 sodium phosphate buffer, λ_{ex} = 376 nm, λ_{em} = **570 nm**.

	τ1 (Wt %)	τ2 (Wt %)	χ^2
Cy3/P1L	0.71 (26)	1.90 (74)	1.480
Cy3/P1L:DT1	- (-)	1.49 (100)	1.850
Cy3/P1L:DT5	- (-)	2.02 (100)	1.579

Table 7.22: Fluorescence lifetimes (ns) of fCy3/P1L and duplexes. 5 μM DNA, 100 mM NaCl, 10 mM pH 7.0 sodium phosphate buffer, λ_{ex} = 376 nm, λ_{em} = **570 nm**.

	τ1 (Wt %)	τ2 (Wt %)	χ^2
fCy3/P1L	0.61 (21)	2.04 (79)	1.589
fCy3/P1L:fDT1	1.50 (85)	2.41 (15)	1.596
fCy3/P1L:fDT5	1.37 (32)	3.23 (68)	1.505

Table 7.23: Fluorescence lifetimes (ns) of cCy3/P1L and duplexes. 5 μM DNA, 100 mM NaCl, 10 mM pH 7.0 sodium phosphate buffer, λ_{ex} = 376 nm, λ_{em} = **570 nm**.

	τ1 (Wt %)	τ2 (Wt %)	τ3 (Wt %)	χ^2
cCy3/P1L	0.61 (21)	1.81 (79)	-	1.690
cCy3/P1L:cDT1	0.80 (-)	2.66 (-)	3.95 (-)	1.585
cCy3/P1L:cDT5	0.53 (38)	1.32 (62)	-	2.214

7.6 Circular dichroism studies

Circular dichroism (CD) studies give more information on the DNA helical structure and how the anthracene interacts with the duplex. Using CD studies, P1L DNA duplexes

were found to have B-DNA conformation with an induced anthracene signal at approximately 255 nm (Section 3.3.5). Single stranded probes cP1L and fP1L CD spectra are given alongside P1L in Figure 7.18 for comparison, although single stranded DNA tends to give a weak CD signal.

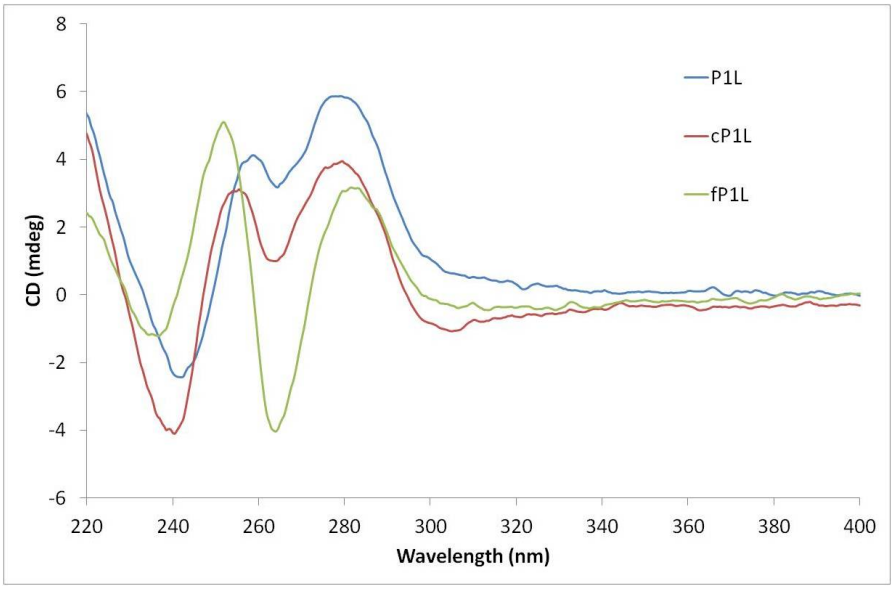

Figure 7.18: Circular dichroism spectra of single stranded P1L DNA probes. 5 μM DNA, 100 mM NaCl, 10 mM pH 7.0 sodium phosphate buffer.

All three anthracene DNA probe duplexes give B-DNA conformations (positive peak at 280 nm and negative peak at 245 nm respectively). The interaction of the anthracene within the different P1L probes becomes more apparent in the duplex CD given in Figures 7.19 and 7.20. The anthracene intercalates most into the P1L duplexes due to strong shoulder peaks at 255 nm. In both the cP1L and fP1L duplexes there is a much reduced shoulder peak at 255 nm, indicating that the anthracene does not interact as strongly due to different orientation upon intercalation. This is understandable for two reasons: the neighbouring bases have altered and the modifications are nearer to the DNA termini which infers less stacking would occur due to 'fraying' effects. This observed lack of anthracene intercalation, which agrees with reduced T_M values, helps

to explain the lack of ON/OFF fluorescence sensing for the cP1L and fP1L probes.

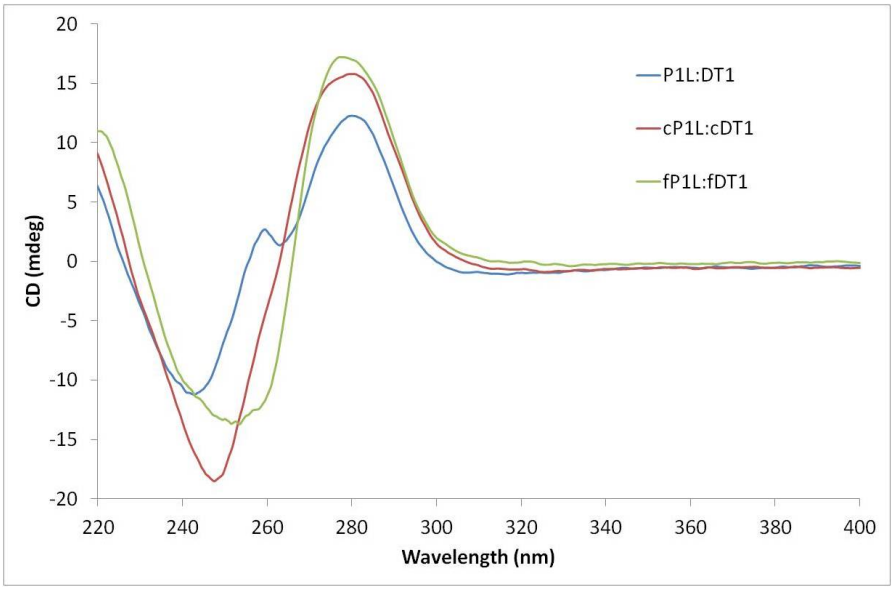

Figure 7.19: Circular dichroism spectra of P1L and DT1 duplexes. 5 μM DNA, 100 mM NaCl, 10 mM pH 7.0 sodium phosphate buffer.

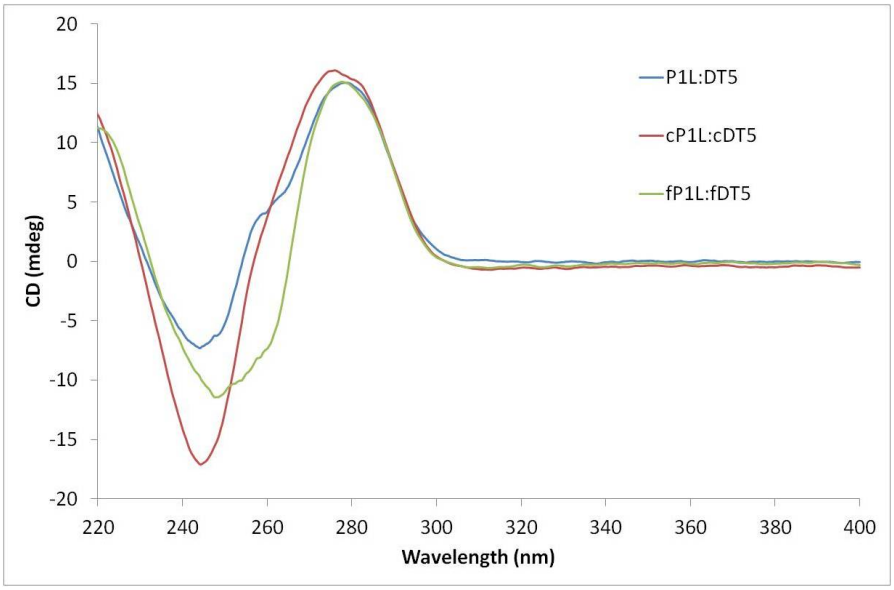

Figure 7.20: Circular dichroism spectra of P1L and DT5 duplexes. 5 μM DNA, 100 mM NaCl, 10 mM pH 7.0 sodium phosphate buffer.

Cy3-only probes and duplexes, have a typical B-DNA conformation plus an ad-

ditional small signal at around 570 nm due to the Cy3 interacting with the duplex. Full CD spectra are given in Appendix E. It is clear that the Cy3 modification does not disrupt the B-DNA conformation of the DNA duplex, and its 5′ stacking is likely to contribute to it. [208, 213]

The full duplex CD spectra for dual fluorophore probes are given in Appendix E. Again, there is a small signal observable for Cy3 at 570 nm showing Cy3 interacts with the DNA duplex. The Cy3 signal does not vary and the shorter wavelength region has more interesting differences. Cy3/P1L CD spectra have similarities with the P1L CD spectra (Figure 7.21). The structure of surrounding base pairs is not disturbed by the introduction of anthracene or Cy3. Cy3/P1L matching/mismatching duplex CD spectra are given in Figures 7.22 and 7.23 respectively.

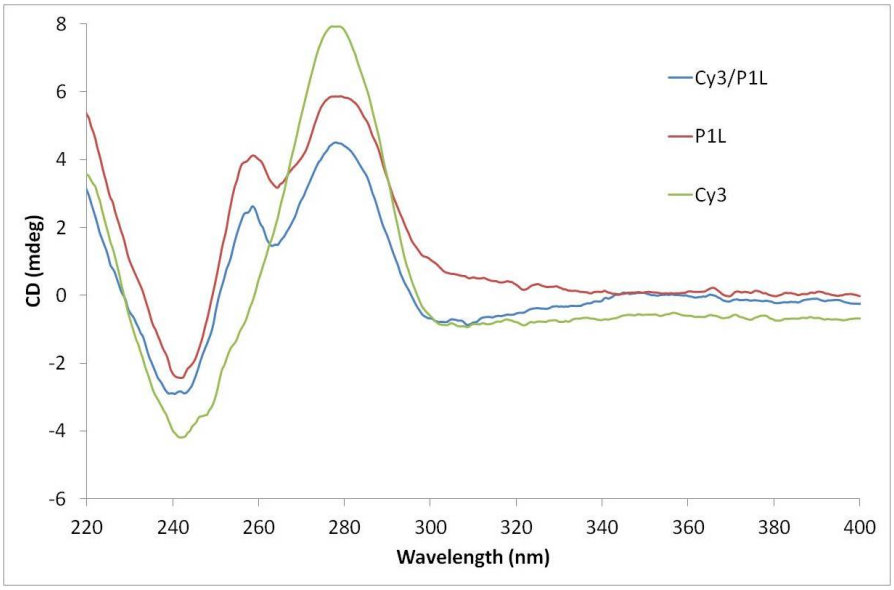

Figure 7.21: Circular dichroism spectra of single stranded P1L, Cy3-only and Cy3/P1L DNA probes. 5 μM DNA, 100 mM NaCl, 10 mM pH 7.0 sodium phosphate buffer.

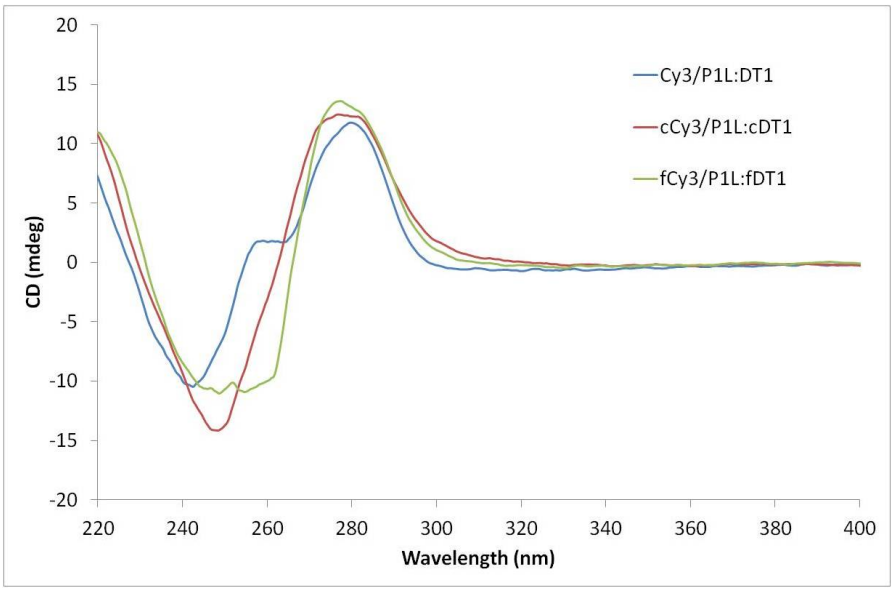

Figure 7.22: Circular dichroism spectra of Cy3/P1L and DT1 duplexes. 5 μM DNA, 100 mM NaCl, 10 mM pH 7.0 sodium phosphate buffer.

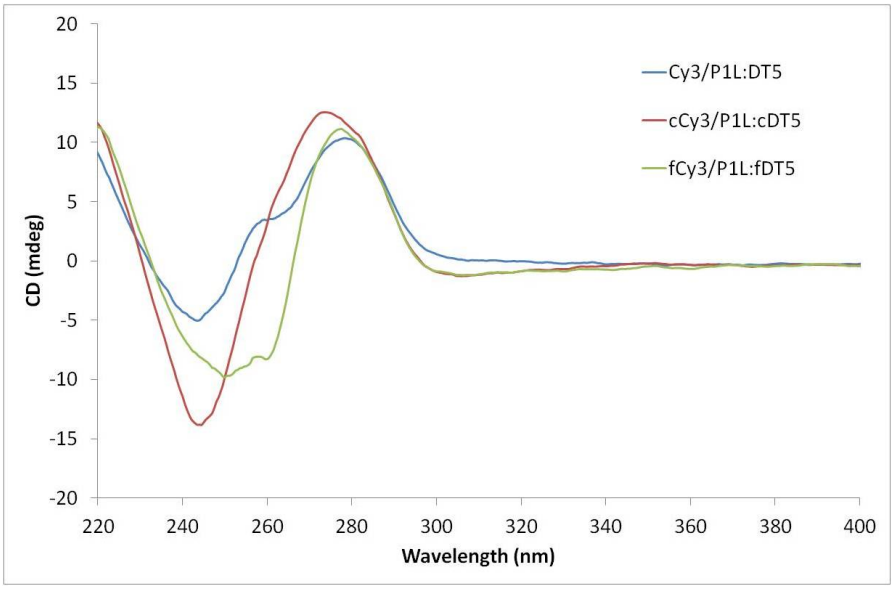

Figure 7.23: Circular dichroism spectra of Cy3/P1L and DT5 duplexes. 5 μM DNA, 100 mM NaCl, 10 mM pH 7.0 sodium phosphate buffer.

The similarities become clear when the DT1 CD spectra are overlaid (Figure 7.24). This is despite a T_M decrease of 3.5 °C between P1L:DT1 and Cy3/P1L:DT1 duplexes.

There are differences between the DT5 CD spectra though (Figure 7.25). The peaks are reduced for the Cy3/P1L:DT5 case, indicating the duplex has diminished helical twist and base stacking. This suggests the duplex is, not surprisingly, disrupted by the two modifications and the mismatch. This links well with the 4 °C decrease in T_M for Cy3/P1L:DT5 compared to P1L:DT5. Despite this, the anthracene is still intercalating significantly more compared to the DT1 target. This agrees with the retention of higher fluorescence emission and longer lifetimes for DT5 versus DT1.

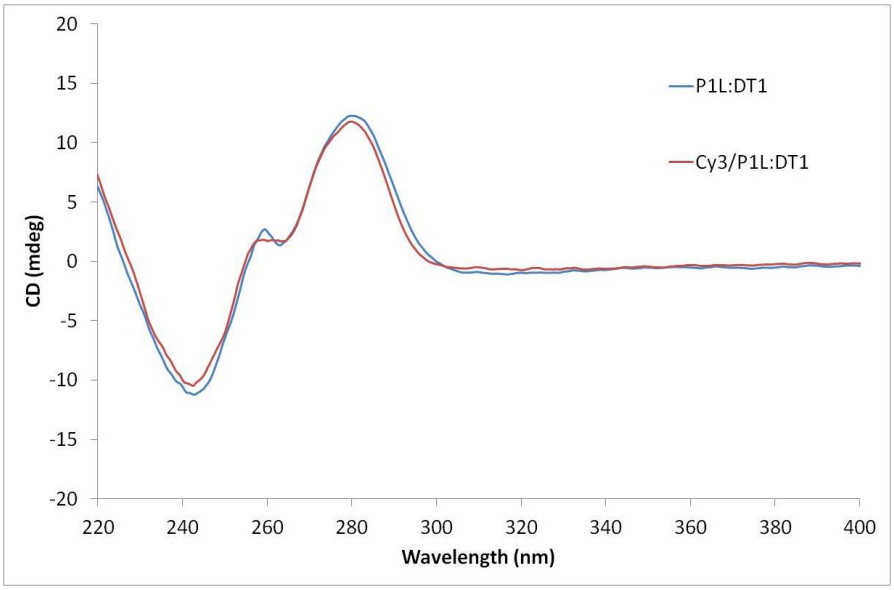

Figure 7.24: Circular dichroism spectra of DT1 duplexes. 5 μM DNA, 100 mM NaCl, 10 mM pH 7.0 sodium phosphate buffer.

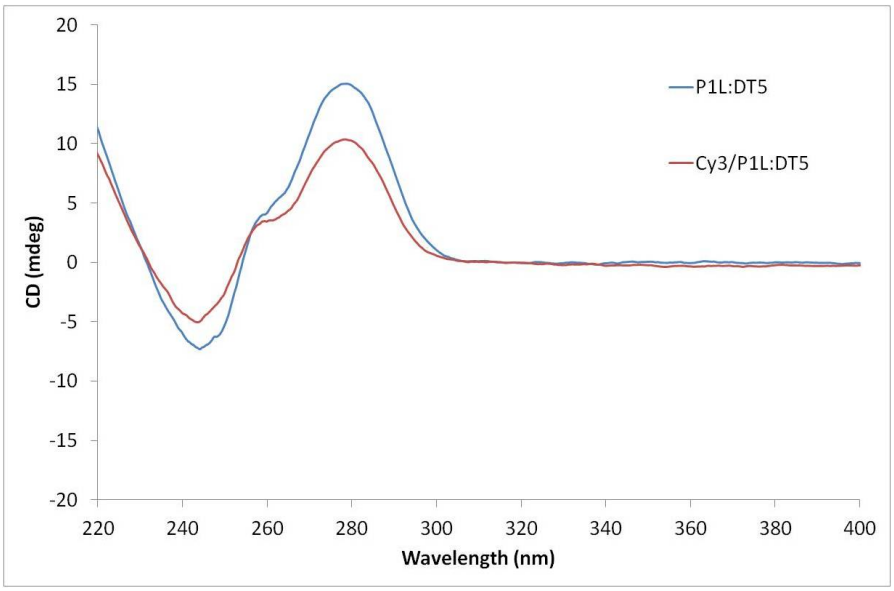

Figure 7.25: Circular dichroism spectra of DT5 duplexes. 5 μM DNA, 100 mM NaCl, 10 mM pH 7.0 sodium phosphate buffer.

cCy3/P1L and fCy3/P1L have similar CD spectra to Cy3/P1L (Figures E.23 and E.24). They both have strong B-DNA conformation due to stretches of unmodified complementary DNA. The fCy3/P1L has a definite lack of anthracene intercalation for both targets, whereas the cCy3/P1L has slightly more anthracene intercalation in the mismatch (DT5) versus the match (DT1) case.

7.7 Conclusion

A next generation DNA anthracene probe was designed to create a ratiometric probe based upon FRET. This was achieved by tagging the fluorophore Cy3 to the 5′ termini of the DNA anthracene probe. Cy3 was chosen since it forms a FRET pair with anthracene and the dual fluorophore probe was shown to successfully display FRET between anthracene as a donor and Cy3 as an acceptor. The probe also exhibited FRET upon hybridisation with targets and differences in emission meant single base discrimination was possible. Discrimination was based solely on the Cy3 emission or using a popular

ratiometric approach, which involves the ratio between the anthracene and Cy3 peak emission intensities. A study to optimise the dual fluorophore probe was undertaken. Since FRET is distance and orientation dependent, the anthracene modification within the DNA sequence was moved closer and further away from the Cy3 modification. All dual fluorophore probes were capable of FRET and again, base discrimination was possible upon target hybridisation. Judging which is the 'best' probe is a difficult task. For SNP sensing purposes, based upon the Cy3 emission only, the Cy3/P1L probe gives the greatest difference in emission between targets. In terms of the ratiometric results, all of the dual fluorophore probes give reliable discrimination between match/mismatch targets. Clearly, P1L remains the best ON/OFF sensing probe.

Overall base discrimination can now be achieved by monitoring emission at a longer wavelength, which is beneficial when considering monitoring at wavelengths removed from regions of cell autofluorescence. [214] Future studies could concentrate on amplifying the differences in emission between targets rather than focussing on achieving ON/OFF sensing. It could be interesting to test the bio-compatibility of the dual fluorophore probes efficiency in cell lysate, fixed cells (Chapters 4 and 5) and DNA/RNA targets extracted from cells.

Further investigation into the effect of the neighbouring bases to the trimer (CXC) is required, or alternatively, FRET probes designed which do not alter the original sequence. Future modelling studies are needed to gain understanding of the Cy3 and anthracene interaction, with each other and surrounding bases. Finally, combining the unique SNP sensing FRET properties of the probe with lifetime measurements could lead to exciting opportunities with time-resolved spectroscopy and FLIM.

Chapter 8

Conclusions and future work

DNA anthracene probes developed by the Tucker group have been shown to have a unique discrimination of single bases based upon emission differences and not relying solely on hybridisation. The two sensing strategies were described in Chapter 3. Both SNP sensing strategies were extended to RNA and 2′OMe RNA targets. ON/OFF sensing was observed for SNP sensing in an RNA sequence associated with Alzheimer's disease. Quantitative measurements could also be made from mixtures of two targets, which is important for future SNP screening applications. These fundamental oligonucleotide studies were carried out with a view to extending the DNA anthracene probe to target RNA in cells.

Additionally, a fundamental study took place to optimise the stability of DNA strands and duplexes in a cellular environment. This was carried out by testing various cell delivery techniques such as chemical transfection, using Cy3-Cy5-tagged DNA and FRET measurements (Chapter 4). It was found that fixed cells and cell delivery techniques which avoided the endocytosis pathway ensured intact DNA and duplexes.

DNA anthracene probes were initially tested in fixed/permeabilised cells since it would not be degraded upon delivery or by nucleases. It was found that the ON/OFF sensing trends of the DNA anthracene probe with DNA and RNA targets were repli-

cated in a cellular environment. Fluorescence emission intensities were extracted from images using a novel application of Gaussian Mixture Modelling (GMM), which allowed quantitative comparisons of changes in emission intensities.

Having established that 1) RNA SNP sensing was possible with the DNA anthracene probe, and 2) DNA anthracene probe SNP sensing trends were replicated in a cellular environment, the DNA anthracene probe could be used in cells to target endogenous RNA. This involved synthesis of plasmids which, upon transfection into cells, over-express mRNA sequences differing by a single base. DNA anthracene probe was added to successfully transfected and fixed cells. Initial microscope images of the DNA anthracene probe targeting mRNA in cells, show differences in emission intensity which correspond to previously observed SNP sensing trends (Chapter 3).

Finally, alongside all the knowledge and experience gained from developing DNA anthracene probes for SNP sensing in cells, a new DNA probe has emerged. Chapter 7 describes the Cy3/anthracene-tagged DNA probe which is able to detect SNPs using FRET and ratiometric measurements. This enables more reliable measurements at a longer wavelength.

This project was always just the beginning of DNA anthracene probes being introduced into a biological setting; there are many exciting prospects. The addition of a fluorophore (which does not spectrally interact with anthracene) to the DNA anthracene probe could provide quantitative information in terms of uptake of probe to cells. Replacing anthracene with a more emissive, longer wavelength emitting fluorophore would be interesting, but it must be able to still fulfil its ON/OFF sensing. Therefore, a fluorophore which is not too bulky and capable of intercalation e.g. BODIPY, could be a good choice. Time-course imaging could be undertaken to monitor localisation of the DNA anthracene probe upon addition to cells. Plus the addition of the DNA anthracene probe to live cells (over-expressing RNA target) using techniques such as microinjection or electroporation to avoid degradation would also help in localisation studies. Targeting

an accessible high copy number endogenous RNA target would further demonstrate the biological compatibility of the DNA anthracene probes.

Appendix A

DNA and RNA SNP sensing with DNA anthracene probes

A.1 DNA sensing

Table A.1 shows the single-stranded DNA anthracene probe quantum yield values. Table A.2 shows percentage differences in emission for DNA anthracene probes and DNA target duplexes. Table A.3 shows the melting temperatures for the same duplex combinations.

A.2 RNA sensing

Figure A.2 and Figure A.3 show titration graphs from emission studies for P1L and P6D respectively with RNA targets. Table A.4 shows percentage differences in emission for DNA anthracene probes and RNA target duplexes. Table A.5 shows the melting temperatures for the same duplex combinations.

Table A.1: Quantum yield of single stranded DNA anthracene probes P(n)(L/D). 1 μM DNA, 100 mM NaCl, 10 mM pH 7.0 sodium phosphate buffer, $\lambda_{ex} = 350$ nm. Quantum yields were determined relative to quinine sulphate ($\Phi_f = 0.546$)

Probe	Quantum Yield
P1L	0.075
P1D	0.21
P3L	0.027
P3D	0.040
P4L	0.036
P4D	0.029
P5L	0.009
P5D	0.039
P6L	0.043
P6D	0.041
P7L	0.041
P7D	0.052

.

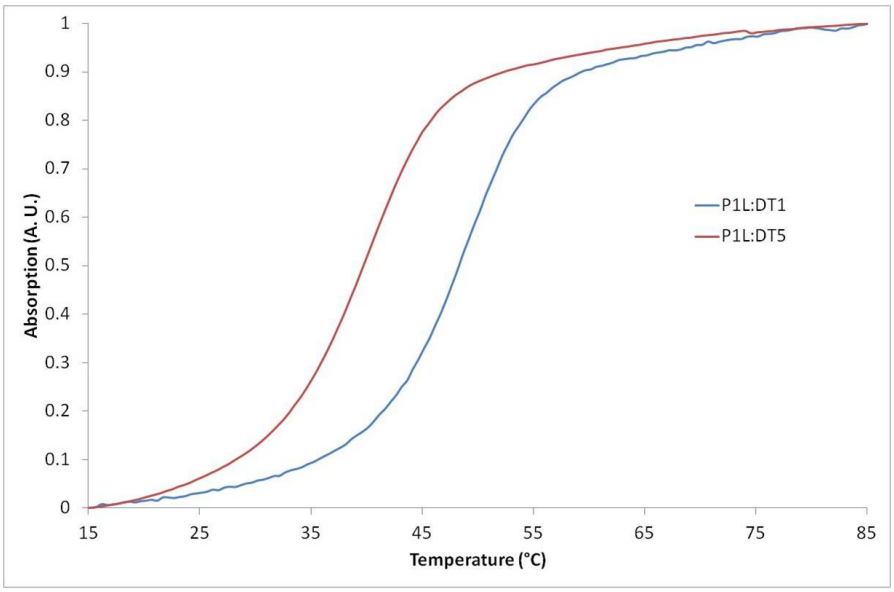

Figure A.1: Absorption spectra of P1L duplexes at varying temperatures. 5 μM DNA, 100 mM NaCl, 10 mM pH 7.0 sodium phosphate buffer.

Table A.2: Percentage differences in emission on addition of DNA targets to DNA anthracene probes, relative to the probe alone. Percentage change in emission is calculated at λ_{em} = 426 nm, compared to the probe alone. 1 μM DNA, 100 mM NaCl, 10 mM pH 7.0 sodium phosphate buffer, λ_{ex} = 350 nm.

Probe/Target	DT1	DT2	DT3	DT4	DT5
P1L	-70	-63	-58	-53	+77
P1D	-72	-79	-81	-86	-61
P3L	+52	+10	-43	-52	+32
P3D	+166	+43	-27	-53	+42
P4L	+70	+29	-26	-57	+86
P4D	+161	+98	+22	-43	+25
P5L	+230	+130	-10	-25	+42
P5D	+205	+107	+20	-35	+78
P6L	+139	+88	+35	-34	+48
P6D	+244	+207	+20	-41	+51
P7L	+159	+66	-35	-49	-
P7D	+88	+25	-4	-40	-

Table A.3: Melting temperatures (°C) of DNA targets and DNA anthracene probes. 5 μM DNA, 100 mM NaCl, 10 mM pH 7.0 sodium phosphate buffer.

Probe/Target	DT1	DT2	DT3	DT4	DT5
DN	55	50	46	48	42
RN	53	47.5	41.5	43	36
P1L	53	55	55	55	46
P1D	48	48	46	48	35
P3L	49.5	52	50	50	41
P3D	50.5	48	46.5	47	42
P4L	49	49.5	50	48	39
P4D	50	51.5	51	51	41
P5L	49	48	49.5	49	40
P5D	48	51	50.5	51	41
P6L	49	50.5	50.5	50	39.5
P6D	48.5	50	53	50.5	41
P7L	49	48.5	52	50	-
P7D	49	49.5	51	50	-

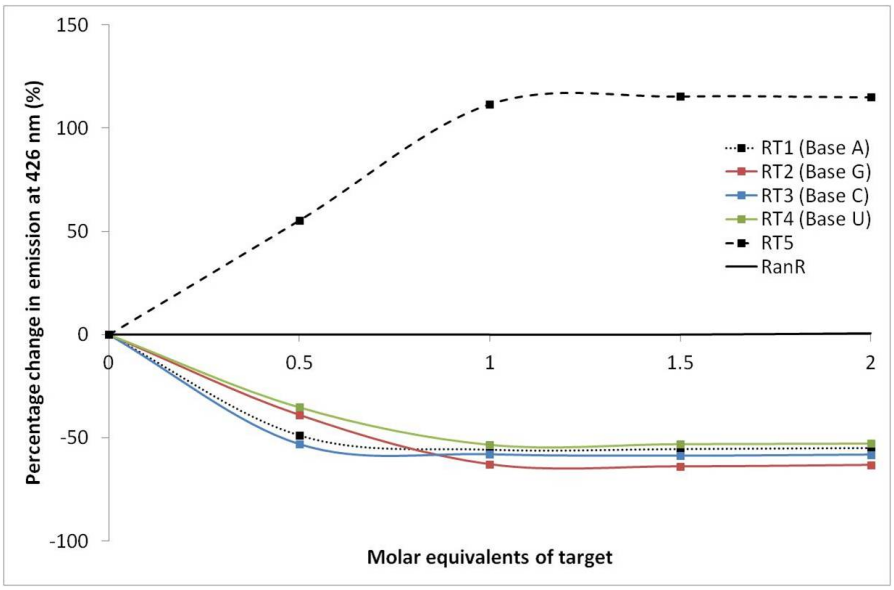

Figure A.2: Fluorescence titrations of up to 2 equivalents of RNA target into probe P1L. The binding is shown to be 1:1 since the emission does not change beyond 1 equivalent of target. The binding is also shown to be specific since there is no change in emission on the addition of a non-complementary target. Percentage change in emission is calculated at λ_{em} = 426 nm, compared to the probe alone. 1 μM DNA/RNA, 100 mM NaCl, 10 mM pH 7.0 sodium phosphate buffer, λ_{ex} = 350 nm.

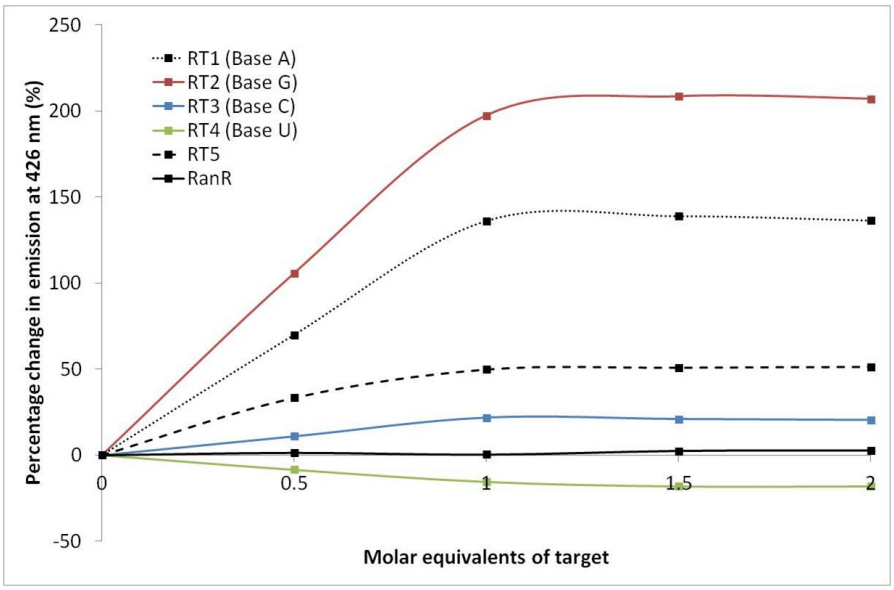

Figure A.3: Fluorescence titrations of up to 2 equivalents of RNA target into probe P6D. The binding is shown to be 1:1 since the emission does not change beyond 1 equivalent of target. The binding is also shown to be specific since there is no change emission on the addition of a non-complementary target. Percentage change in emission is calculated at λ_{em} = 426 nm, compared to the probe alone. 1 μM DNA/RNA, 100 mM NaCl, 10 mM pH 7.0 sodium phosphate buffer, λ_{ex} = 350 nm.

Table A.4: Percentage differences in emission at λ_{em} = 426 nm on addition of RNA targets to DNA anthracene probes, with respect to the probe alone. 1 μM DNA, 100 mM NaCl, 10 mM pH 7.0 sodium phosphate buffer, λ_{ex} = 350 nm.

Probe/Target	RT1	RT2	RT3	RT4	RT5
P1L	-55	-63	-58	-53	+115
P1D	-55	-61	-67	-49	+129
P3L	+34	-20	-26	-43	+143
P3D	+77	+5	+32	+46	+140
P4L	+4	+69	+36	-26	+37
P4D	+15	+19	+10	+2	+45
P5L	+85	+112	+65	-22	+42
P5D	+88	+97	+94	-11	+210
P6L	+23	+187	+13	-14	+50
P6D	+136	+207	+20	-18	+51
P7L	-8	+17	-36	-35	+31
P7D	-17	+17	-40	-26	+37

Table A.5: Melting temperatures (°C) of DNA anthracene probes and RNA targets. 5 μM DNA, 100 mM NaCl, 10 mM pH 7.0 sodium phosphate buffer.

Probe/Target	RT1	RT2	RT3	RT4	RT5
DN	60	56	46	47.5	45
RN	71	66	60	60.5	54
P1L	51	48	51	52	41
P1D	49.5	45.5	45.5	46	38
P3L	47.5	50	49.5	49	-
P3D	45	-	-	-	-
P4L	45	49	48	49	-
P4D	47	42	44	41.5	-
P5L	49	49.5	47	48	-
P5D	47.5	49	49	49	-
P6L	45.5	49	49	48.5	-
P6D	48	49	48.5	48.5	39.5
P7L	46.5	48	47	47	-
P7D	45.5	52	49	48	-

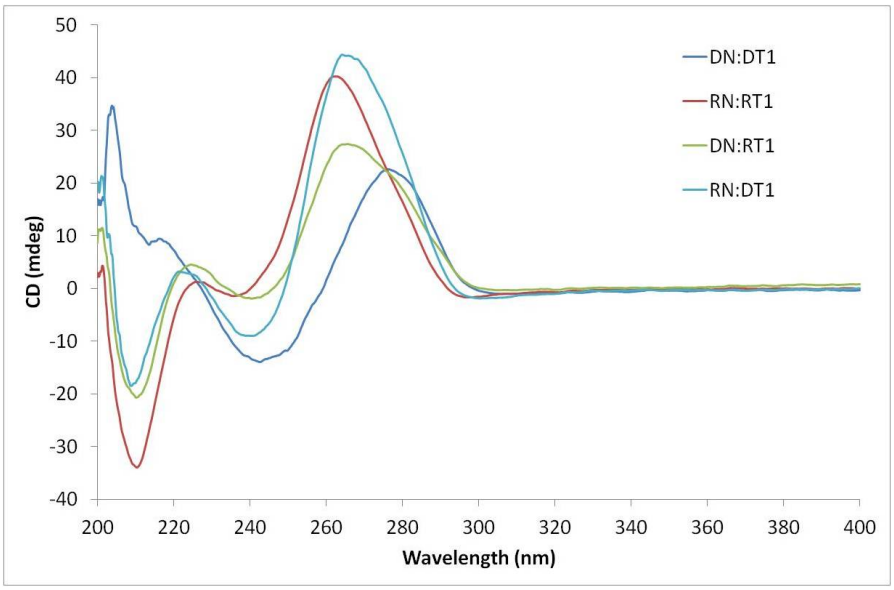

Figure A.4: Circular dichroism spectra of unmodified DNA and RNA duplexes. 5 μM DNA/RNA, 100 mM NaCl, 10 mM pH 7.0 sodium phosphate buffer.

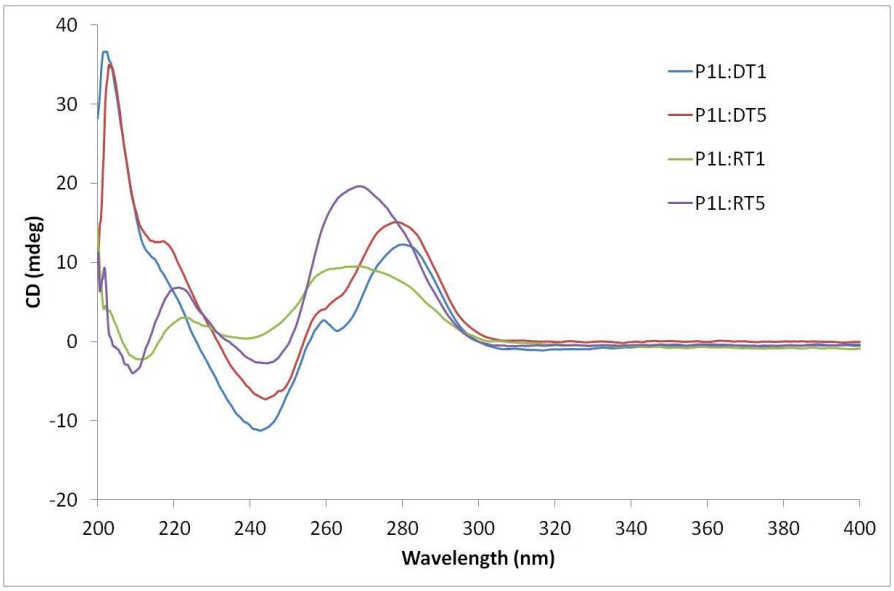

Figure A.5: Circular dichroism spectra of modified (P1L) duplexes with both DNA and RNA targets. 5 μM DNA/RNA, 100 mM NaCl, 10 mM pH 7.0 sodium phosphate buffer.

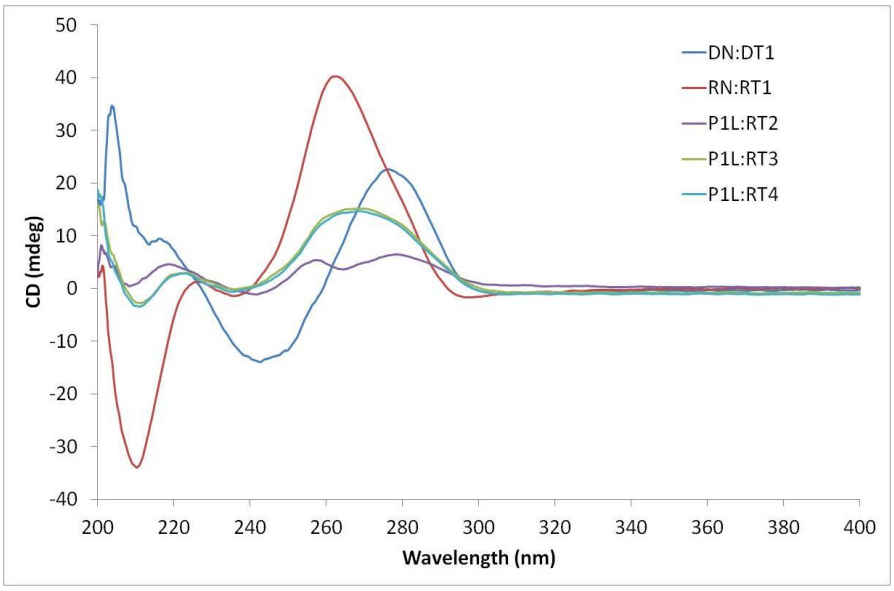

Figure A.6: Circular dichroism spectra of unmodified (DN/RN) and modified (P1L) duplexes. 5 μM DNA/RNA, 100 mM NaCl, 10 mM pH 7.0 sodium phosphate buffer.

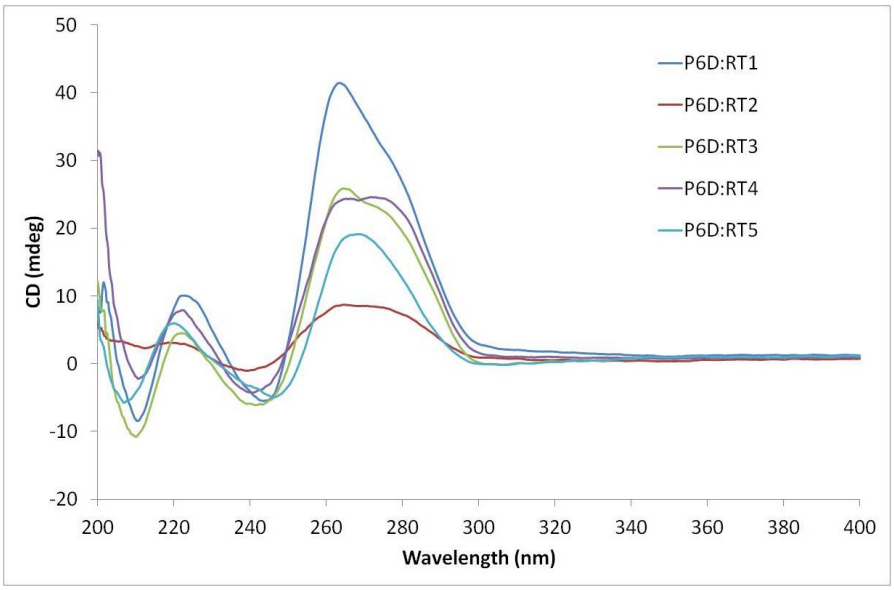

Figure A.7: Circular dichroism spectra of modified (P6D) duplexes with RNA targets. 5 μM DNA/RNA, 100 mM NaCl, 10 mM pH 7.0 sodium phosphate buffer.

A.3 2′OMe RNA sensing

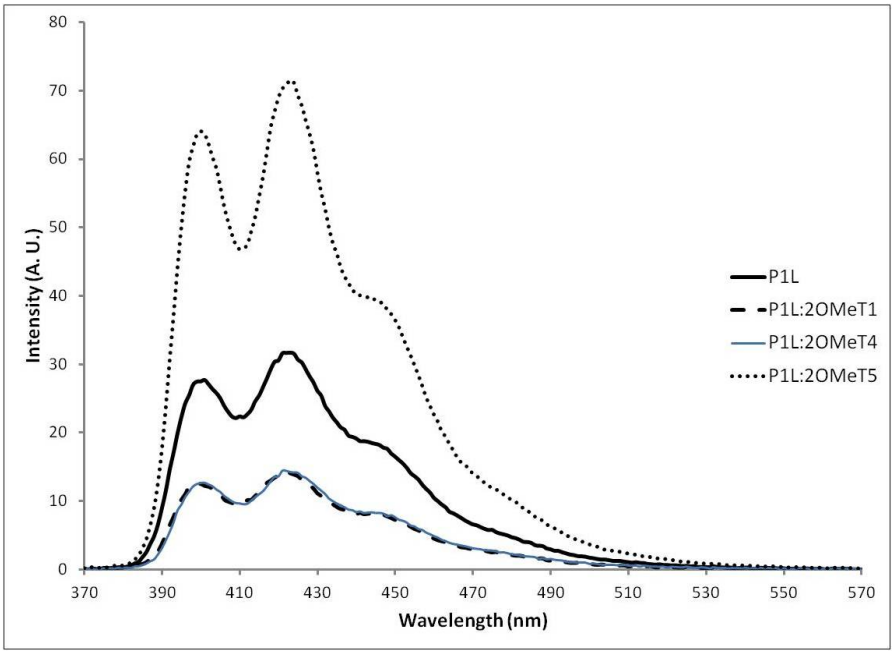

Figure A.8: Fluorescence spectra show the change in emission upon hybridisation of anthracene probe P1L with 2′OMe RNA targets. 1 μM DNA/2′OMe RNA, 100 mM NaCl, 10 mM pH 7.0 sodium phosphate buffer, λ_{ex} = 350 nm.

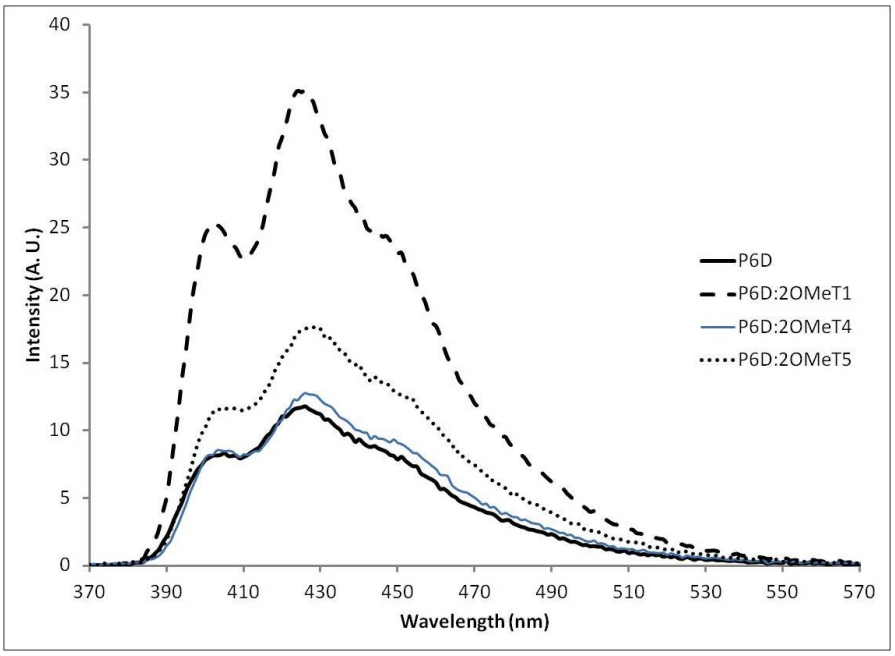

Figure A.9: Fluorescence spectra show the change in emission upon hybridisation of anthracene probe P6D with 2′OMe RNA targets. 1 μM DNA/2′OMe RNA, 100 mM NaCl, 10 mM pH 7.0 sodium phosphate buffer, λ_{ex} = 350 nm.

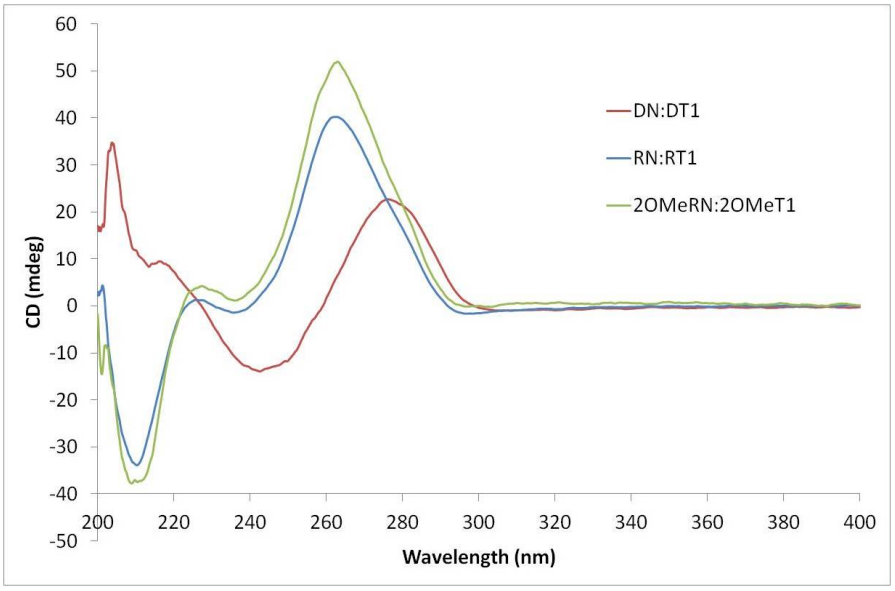

Figure A.10: Circular dichroism spectra of unmodified DNA, RNA and 2′OMe RNA duplexes. 5 μM DNA/RNA, 100 mM NaCl, 10 mM pH 7.0 sodium phosphate buffer.

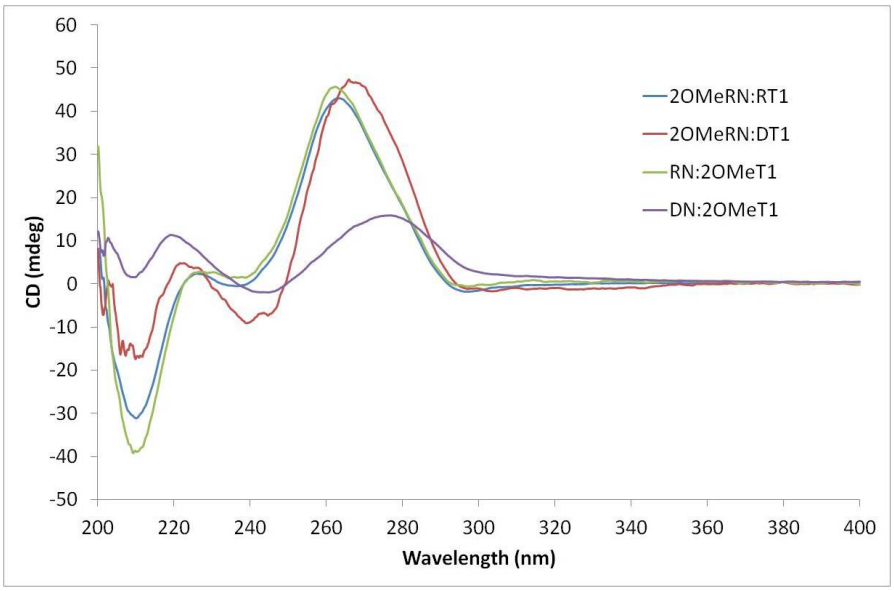

Figure A.11: Circular dichroism spectra of hybrid DNA, RNA and 2′OMe RNA duplexes. 5 μM DNA/RNA, 100 mM NaCl, 10 mM pH 7.0 sodium phosphate buffer.

A.4 CDKN1A gene SNP sensing

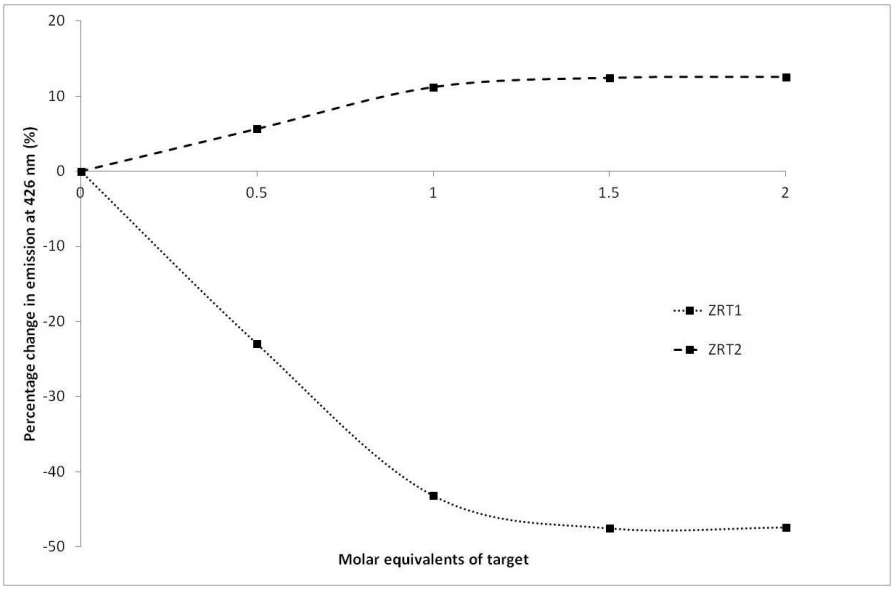

Figure A.12: Fluorescence titrations of up to 2 equivalents of CDKN1A gene RNA targets into probe ZP5L. The binding is shown to be 1:1 since the emission does not change beyond 1 equivalent of target. Percentage change in emission is calculated at λ_{em} = 426 nm, compared to the probe alone. 1 μM DNA/RNA, 100 mM NaCl, 10 mM pH 7.0 sodium phosphate buffer, λ_{ex} = 350 nm.

Table A.6: Percentage differences in emission at λ_{em} = 426 nm on addition of CDKN1A gene RNA targets to DNA anthracene probes, relative to the probe alone. 1 μM DNA, 100 mM NaCl, 10 mM pH 7.0 sodium phosphate buffer, λ_{ex} = 350 nm.

Probe/Target	ZRT1	ZRT2
P1L	-17%	+5
P1D	-28%	-27
P3L	-47%	-2
P3D	-39%	+18
P4L	-45%	0
P4D	-59%	+16
P5L	-47%	+12
P5D	-52%	+4
P6L	-56%	+2
P6D	-53%	+12
P7L	-39%	+14
P7D	-47%	+5

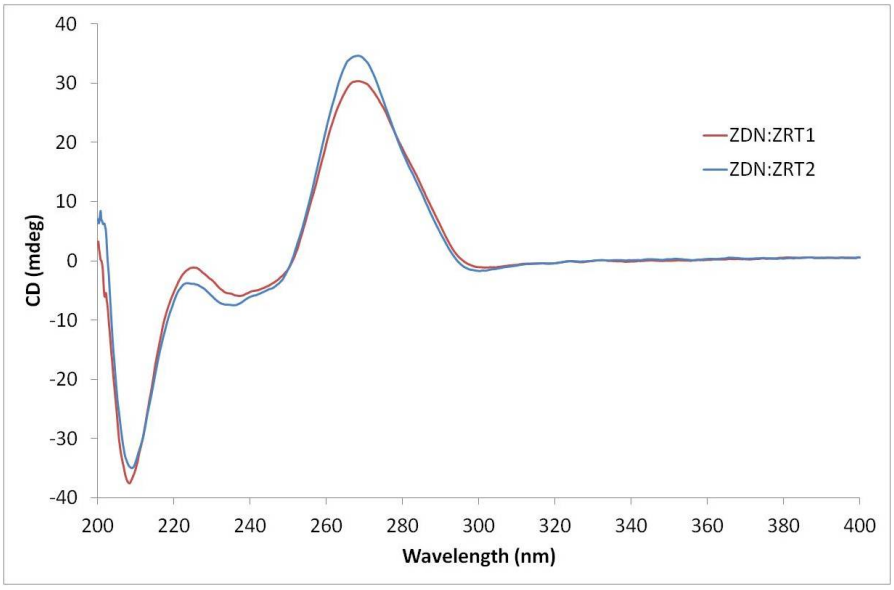

Figure A.13: Circular dichroism spectra of CDKN1A gene DNA anthracene probes and RNA target duplexes. 5 μM DNA/RNA, 100 mM NaCl, 10 mM pH 7.0 sodium phosphate buffer.

Table A.7: Melting temperatures (°C) of CDKN1A gene DNA anthracene probes and RNA targets, plus controls. 5 μM DNA, 100 mM NaCl, 10 mM pH 7.0 sodium phosphate buffer.

Probe/Target	ZRT1	ZRT2
ZDN	70	67
P1L	56	54
P1D	51	52.5
P3L	57.5	54.5
P3D	55.5	56
P4L	57.5	56
P4D	56	56
P5L	57	55.5
P5D	56	55
P6L	56	52.5
P6D	56	56
P7L	56	55
P7D	55	58

Appendix B

Optimising Cy3 and Cy5 tagged DNA delivery to cells

B.1 Random Oligonucleotides

Two further oligonucleotides were synthesised which are not complementary and were used as controls (to show specificity) (Table B.1). All HPLC analytical and mass spectrometry results can be found in Section F.

B.2 Melting Temperatures

Table B.2 shows duplex melting temperatures.

Table B.1: Non-complementary Cy3 and Cy5 tagged DNA sequences synthesised.

Oligonucleotide	Sequence (5' to 3')
Control Cy3 strand (S4)	`Cy3-TTTTTTTTTTTTTTT`
Control Cy5 strand (S5)	`Cy5-CATTGAGTGAGTCCA`

Table B.2: Duplex melting temperatures (10 mM sodium phosphate, 100 mM NaCl, pH 7.0, 5 μM each DNA strand)

Duplex	Melting Temperature (°C)
S1:S2	62
S1:S2 (unmodified)	56.5

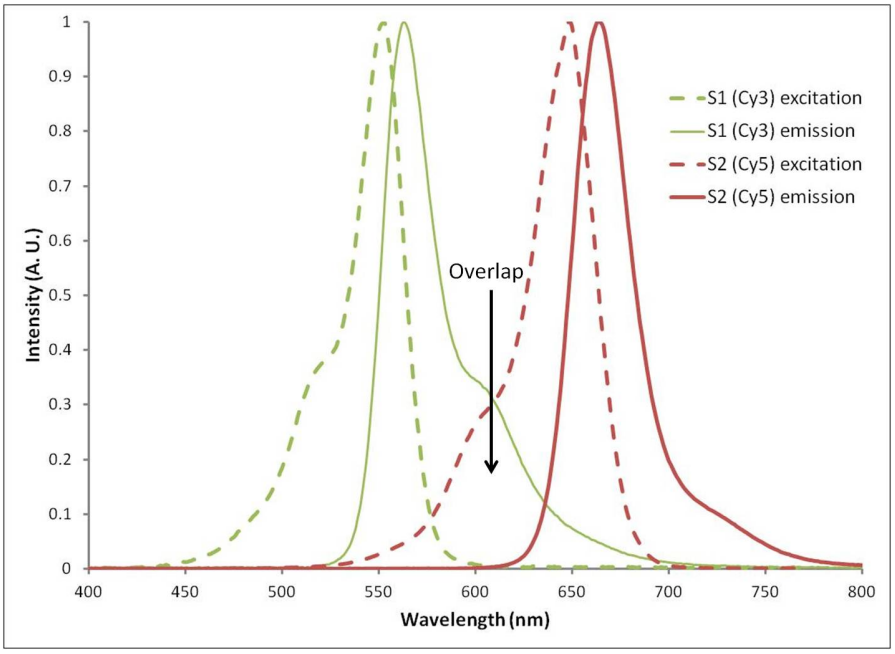

Figure B.1: Excitation spectra (dashed) and emission spectra (solid) of Cy3-tagged DNA (green) and Cy5-tagged DNA (red). 1 μM DNA, 100 mM NaCl, 10 mM pH 7.0 sodium phosphate buffer. S1 (Cy3) λ_{ex} = 554 nm and λ_{em} = 570 nm. S2 (Cy5) λ_{ex} = 650 nm and λ_{em} = 670 nm. Data is normalised to λ_{max} values.

B.3 Cell lysate cuvette studies

The FRET signal from the S1:S2 duplex and S3 were studied in Chinese hamster ovary (CHO) cell lysate at 37 °C in the absence and presence of DNase (Figures B.2 and B.3, respectively).

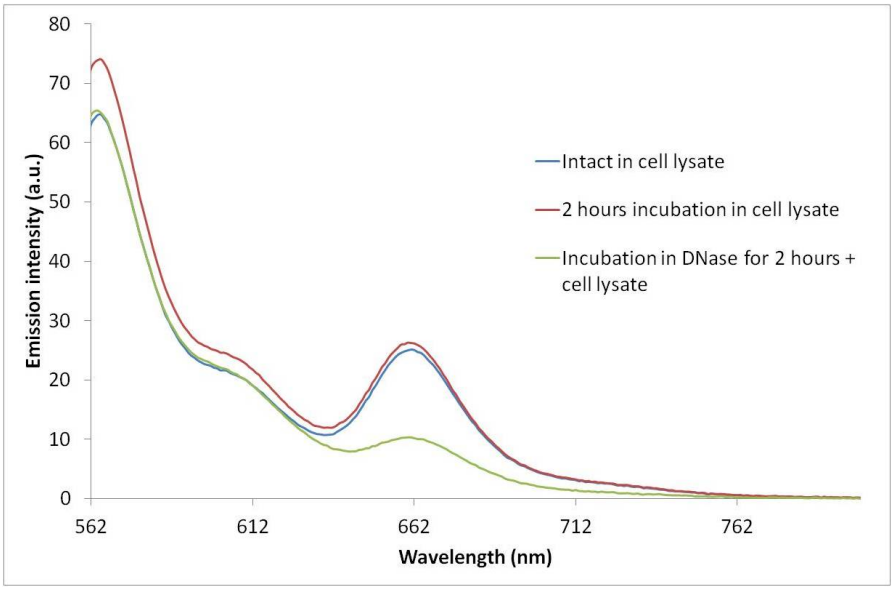

Figure B.2: No change in fluorescence is observed after S1:S2 is incubated in cell lysate at 37 °C for two hours. The FRET peak at approximately 660 nm is reduced significantly after the duplex S1:S2 has been incubated with DNase for two hours. Excitation wavelength 554 nm.

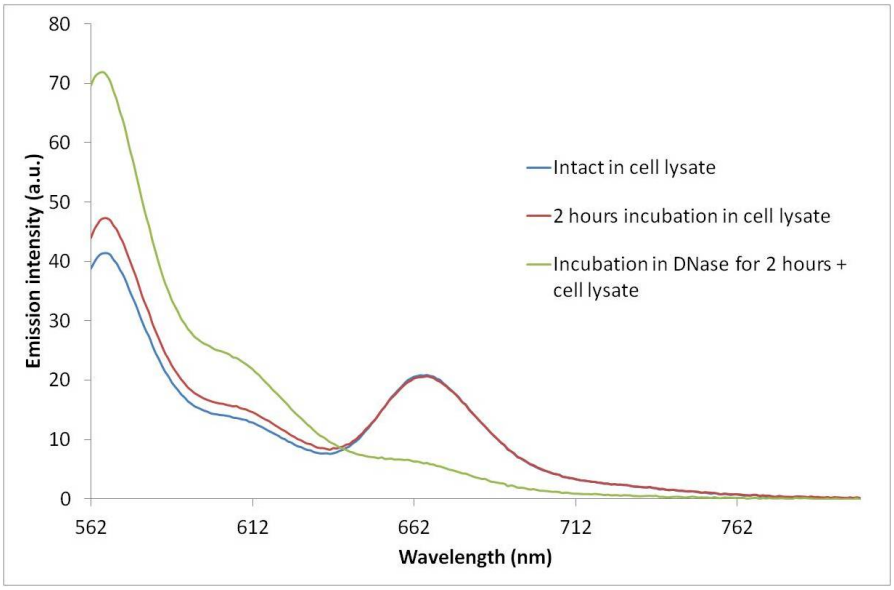

Figure B.3: No change in fluorescence is observed after S3 is incubated in cell lysate at 37 °C for two hours. The FRET peak at approximately 660 nm disappears after S3 has been incubated with DNase for two hours. Excitation wavelength 554 nm.

B.4 Control cell studies

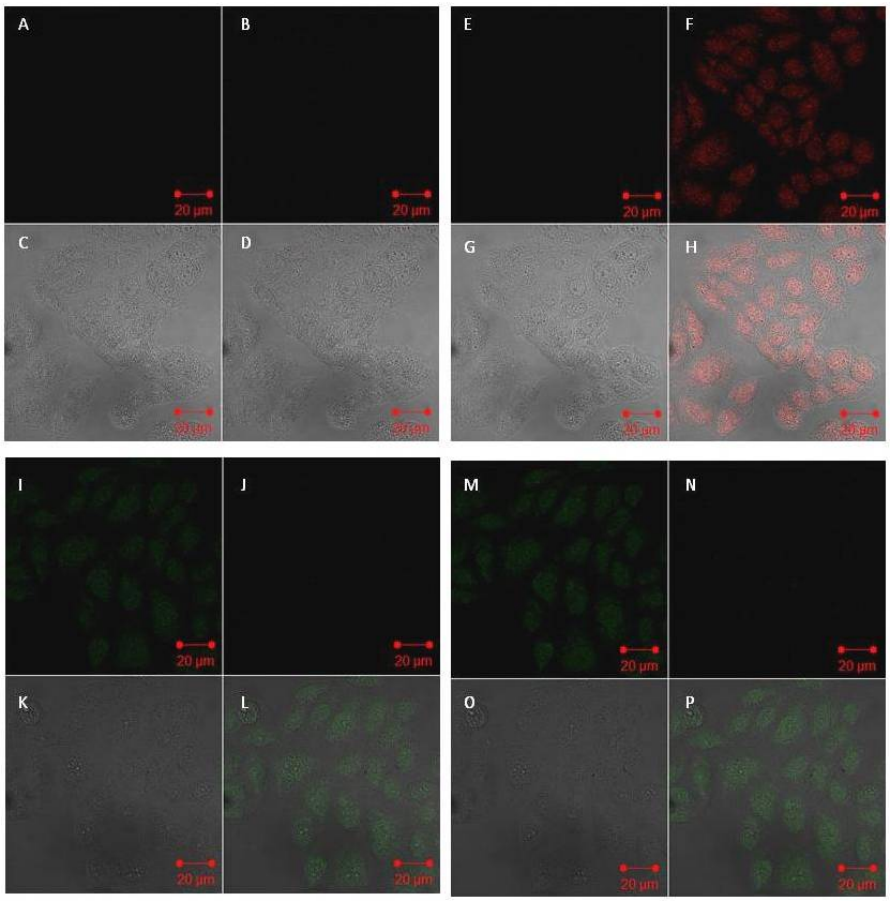

Figure B.4: Images A-H show single stranded Cy5 tagged DNA (S2) added to fixed/permeabilised cells and imaged using confocal microscopy. Images A/E represents the Cy3 channel; B/F the Cy5 channel; C/G the bright field channel and D/H an overlay of all the channels. Images A-D are excited with a 543 nm laser only. Images E-H are excited with both the 543 and 633 nm lasers. Images I-P show single stranded Cy3 tagged DNA (S1) added to fixed/permeabilised cells and imaged using confocal microscopy. Images I/M represents the Cy3 channel; J/N the Cy5 channel; K/O the bright field channel and L/P an overlay of all the channels. Images I-L are excited with a 543 nm laser only. Images M-P are excited with both the 543 and 633 nm lasers.

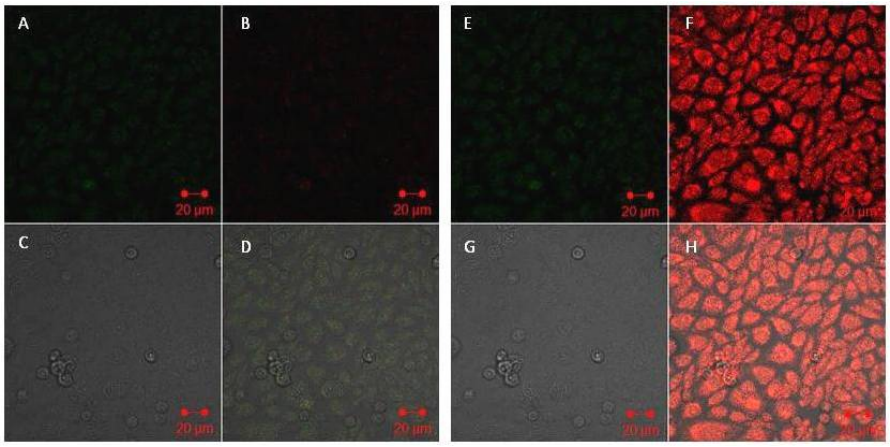

Figure B.5: Images A-H show complementary Cy3 and Cy5 tagged DNA (S1 and S2) added sequentially to fixed/permeabilised cells imaged using confocal microscopy. Images A/E represents the Cy3 channel; B/F the Cy5 channel; C/G the bright field channel and D/H an overlay of all the channels. Images A-D are excited with a 543 nm laser only. Images E-H are excited with both the 543 and 633 nm lasers.

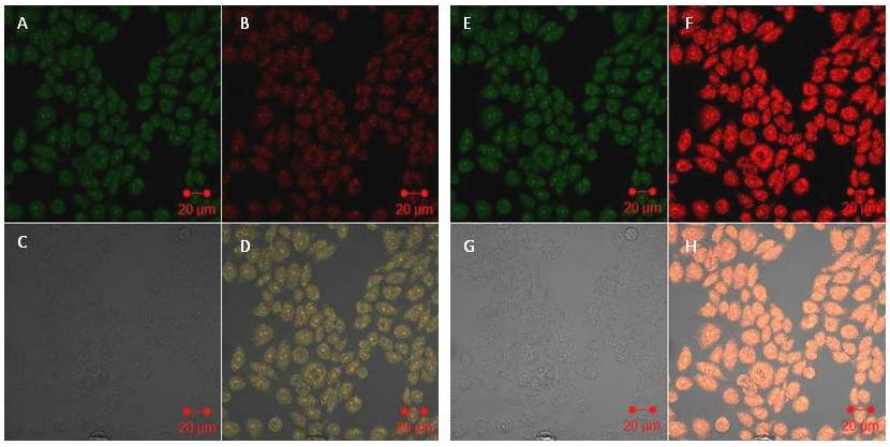

Figure B.6: Images A-H show Cy3 and Cy5 tagged probe DNA (S3) added to fixed/permeabilised cells imaged using confocal microscopy. Images A/E represents the Cy3 channel; B/F the Cy5 channel; C/G the bright field channel and D/H an overlay of all the channels. Images A-D are excited with a 543 nm laser only. Images E-H are excited with both the 543 and 633 nm lasers.

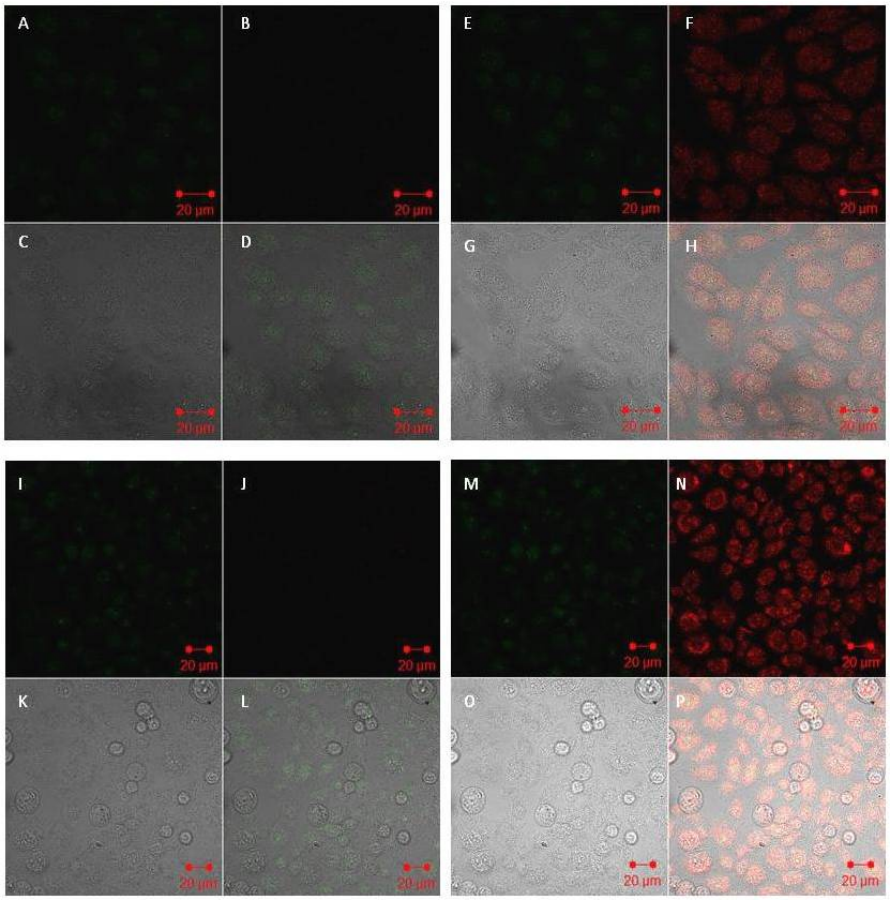

Figure B.7: Images A-H show non-complementary Cy3 and Cy5 tagged DNA (S4:S5) added together to fixed/permeabilised cells and imaged using confocal microscopy. Images A/E represents the Cy3 channel; B/F the Cy5 channel; C/G the bright field channel and D/H an overlay of all the channels. Images A-D are excited with a 543 nm laser only. Images E-H are excited with both the 543 and 633 nm lasers. Images I-P show non-complementary Cy3 and Cy5 tagged DNA (S4 and S5) added sequentially to fixed/permeabilised cells imaged using confocal microscopy. Images I/M represents the Cy3 channel; J/N the Cy5 channel; K/O the bright field channel and L/P an overlay of all the channels. Images I-L are excited with a 543 nm laser only. Images M-P are excited with both the 543 and 633 nm lasers.

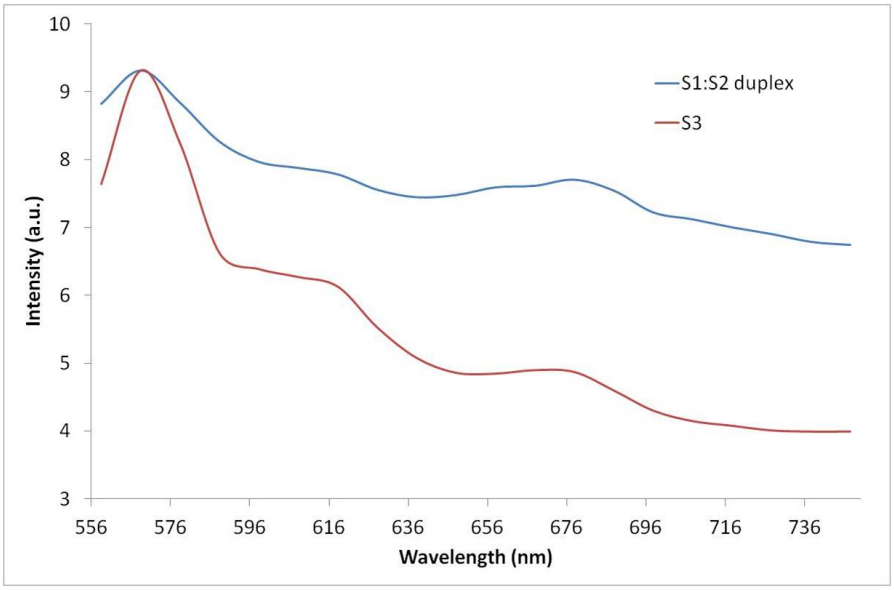

Figure B.8: Mean emission spectra of regions of interest in methanol fixed cells treated with S1:S2 duplex and S3. Cells were excited with 543 nm laser only. Therefore, the peak at ca. 670 nm indicates FRET between the Cy3 and Cy5 fluorophores, hence S1:S2 and S3 are intact. Imaging was carried out using spectral imaging inverted confocal microscopy. Background regions had negligible signal. Minimum of ten cells analysed.

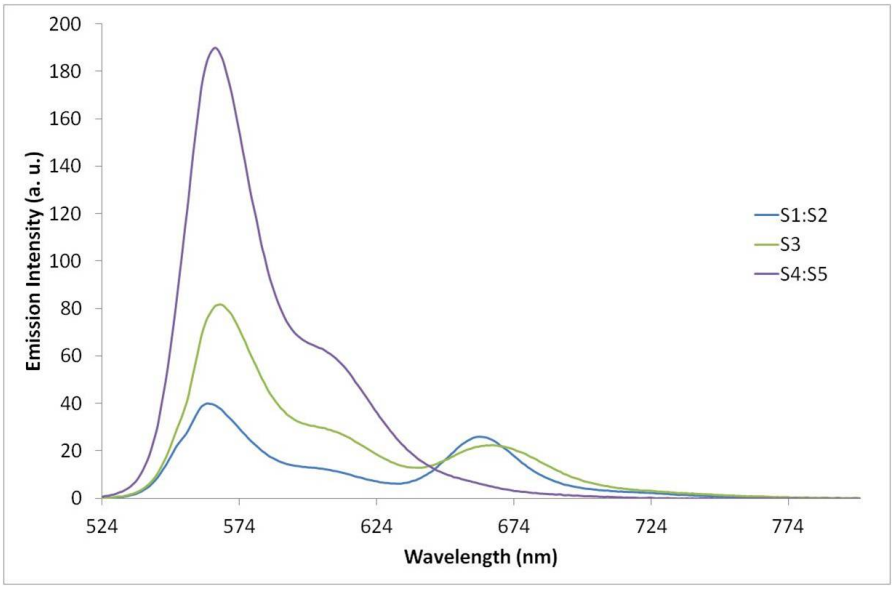

Figure B.9: Emission spectra of tagged DNA after complex formation with lipid based transfection reagent. Both S1:S2 and S3 are shown to FRET in the presence of Lipofectamine. Conditions as for transfection: 100 μM DNA, Opti-MEM medium (Life Technologies) and Lipofectamine RNAiMAX (Life Technologies). Excitation wavelength 554 nm.

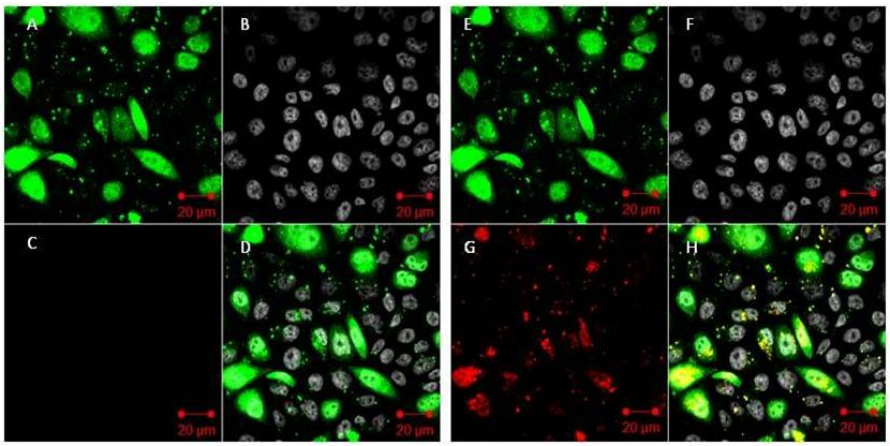

Figure B.10: Images A-H show Cy3 and Cy5 tagged probe DNA (S3) added to cells via lipid based transfection and imaged using confocal microscopy. Images A/E represents the Cy3 channel; B/F the nuclear stain channel; C/G the Cy5 channel and D/H an overlay of all the channels. Images A-D are excited with a 543 nm laser only. Images E-H are excited with both the 543 and 633 nm lasers.

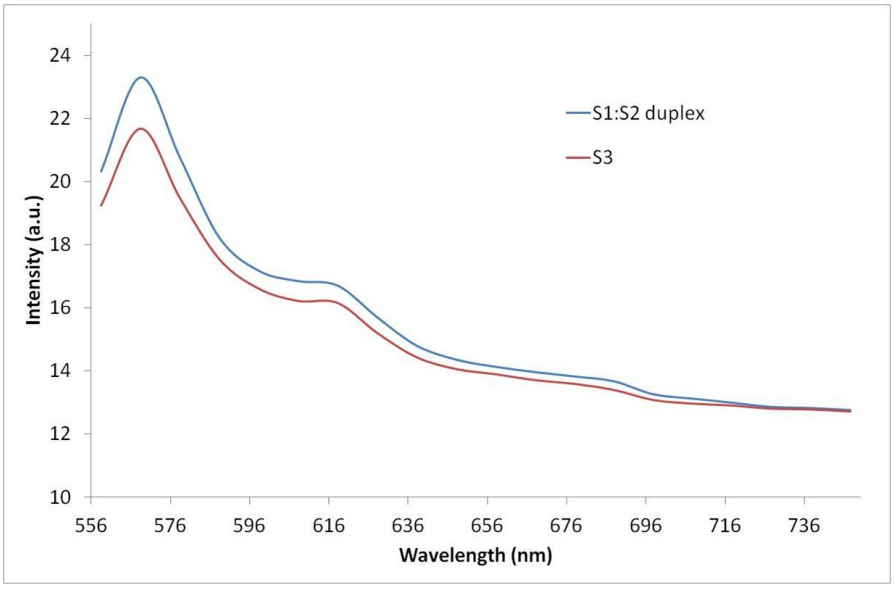

Figure B.11: Mean emission spectra of regions of interest in lipid based transfected cells treated with S1:S2 duplex and S3. Cells were excited with 543 nm laser only. There is no peak at ca. 670 nm which indicates a lack of FRET between the Cy3 and Cy5 fluorophores, hence S1:S2 and S3 are degraded. Imaging was carried out using spectral imaging inverted confocal microscopy. Background regions had negligible signal. Minimum of ten cells analysed.

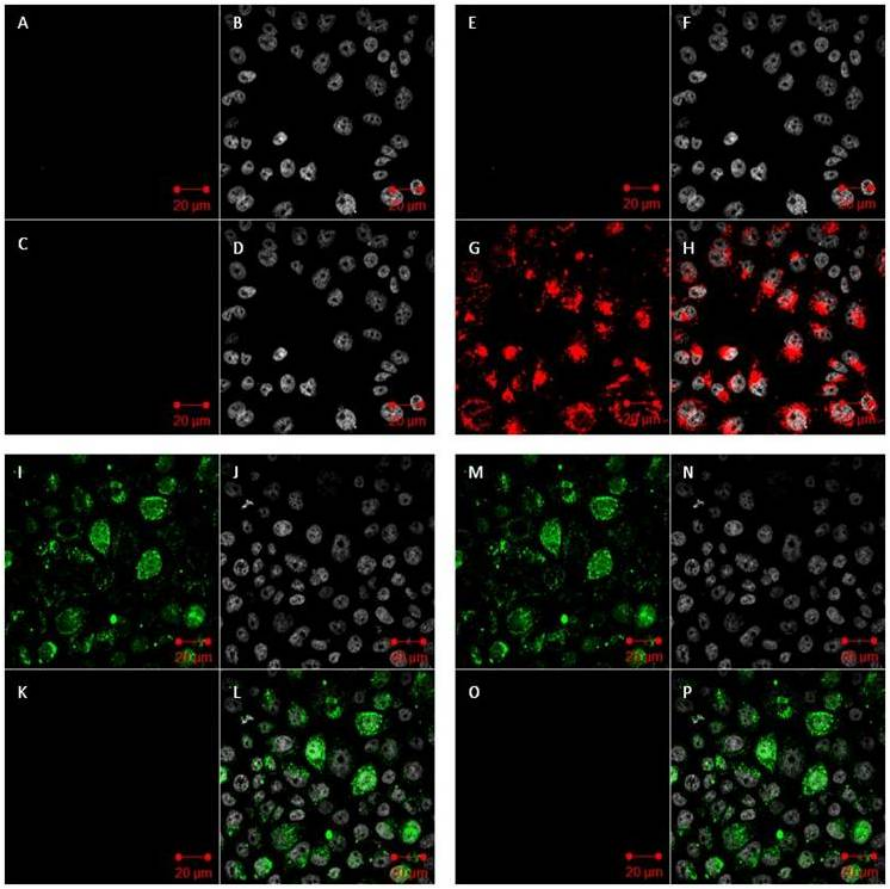

Figure B.12: Images A-H show single stranded Cy5 tagged DNA (S2) added to cells via lipid based transfection and imaged using confocal microscopy. Images A/E represents the Cy3 channel; B/F the nuclear stain channel; C/G the Cy5 channel and D/H an overlay of all the channels. Images A-D are excited with a 543 nm laser only. Images E-H are excited with both the 543 and 633 nm lasers. Images I-P show single stranded Cy3 tagged DNA (S1) added to cells via lipid based transfection and imaged using confocal microscopy. Images I/M represents the Cy3 channel; J/N the nuclear stain channel; K/O the Cy5 channel and L/P an overlay of all the channels. Images I-L are excited with a 543 nm laser only. Images M-P are excited with both the 543 and 633 nm lasers.

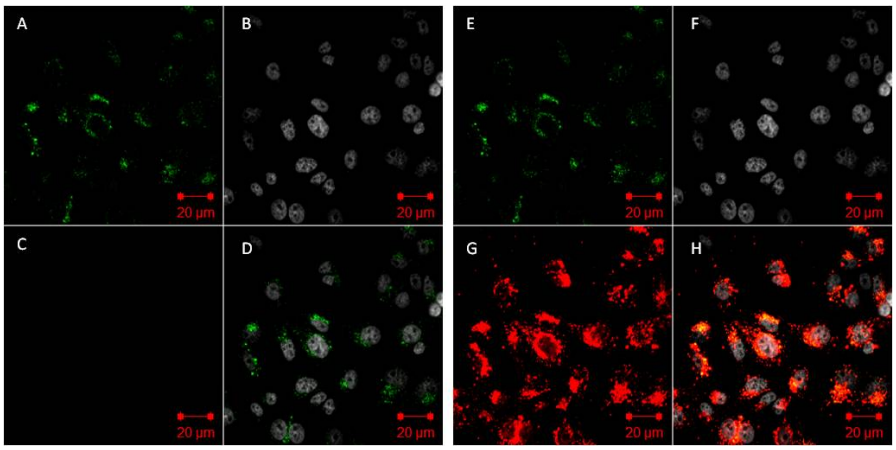

Figure B.13: Images A-H show non-complementary Cy3 and Cy5 tagged DNA (S4:S5) added together to cells via lipid based transfection and imaged using confocal microscopy. Images A/E represents the Cy3 channel; B/F the nuclear stain channel; C/G the Cy5 channel and D/H an overlay of all the channels. Images A-D are excited with a 543 nm laser only. Images E-H are excited with both the 543 and 633 nm lasers.

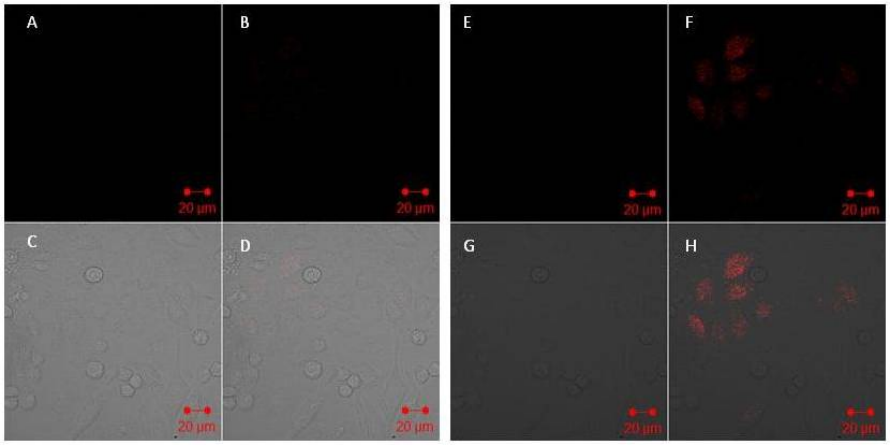

Figure B.14: Images A-H show single stranded Cy5 tagged DNA (S2) added to cells via microinjection and imaged using confocal microscopy. Images A/E represents the Cy3 channel; B/F the Cy5 channel; C/G the bright field channel and D/H an overlay of all the channels. Images A-D are excited with a 543 nm laser only. Images E-H are excited with both the 543 and 633 nm lasers.

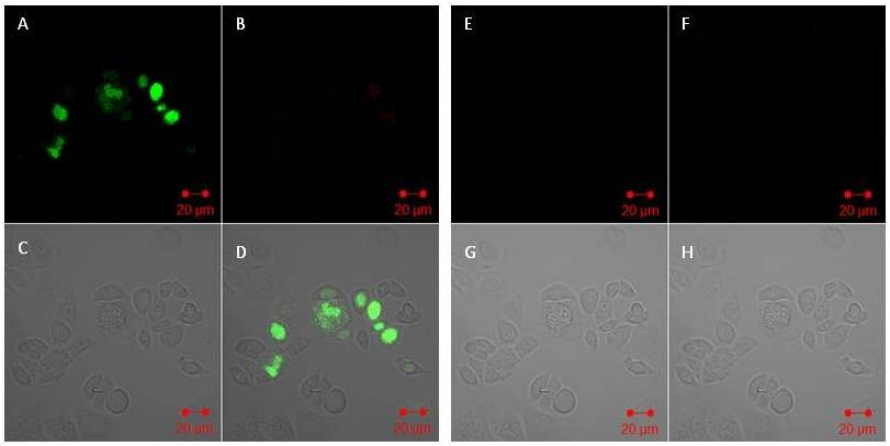

Figure B.15: Images A-H show single stranded Cy3 tagged DNA (S1) added to cells via microinjection and imaged using confocal microscopy. Images A/E represents the Cy3 channel; B/F the Cy5 channel; C/G the bright field channel and D/H an overlay of all the channels. Images A-D are excited with a 543 nm laser only. Images E-H are excited with both the 543 and 633 nm lasers.

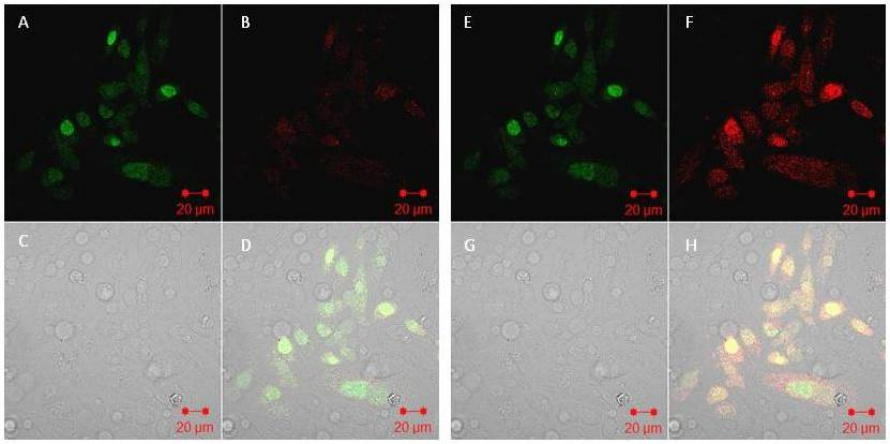

Figure B.16: Images A-H show Cy3 and Cy5 tagged probe DNA (S3) added to cells via microinjection and imaged using confocal microscopy. Images A/E represents the Cy3 channel; B/F the Cy5 channel; C/G the bright field channel and D/H an overlay of all the channels. Images A-D are excited with a 543 nm laser only. Images E-H are excited with both the 543 and 633 nm lasers.

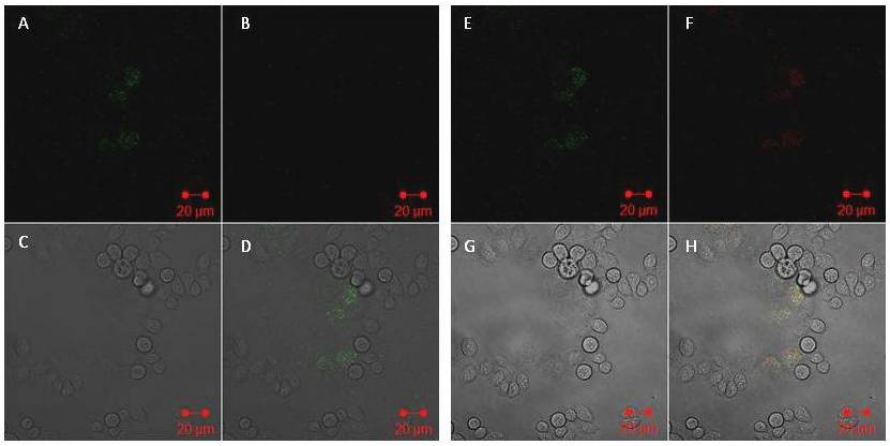

Figure B.17: Images A-H show non-complementary Cy3 and Cy5 tagged DNA (S4:S5) added together to cells via microinjection and imaged using confocal microscopy. Images A/E represents the Cy3 channel; B/F the Cy5 channel; C/G the bright field channel and D/H an overlay of all the channels. Images A-D are excited with a 543 nm laser only. Images E-H are excited with both the 543 and 633 nm lasers.

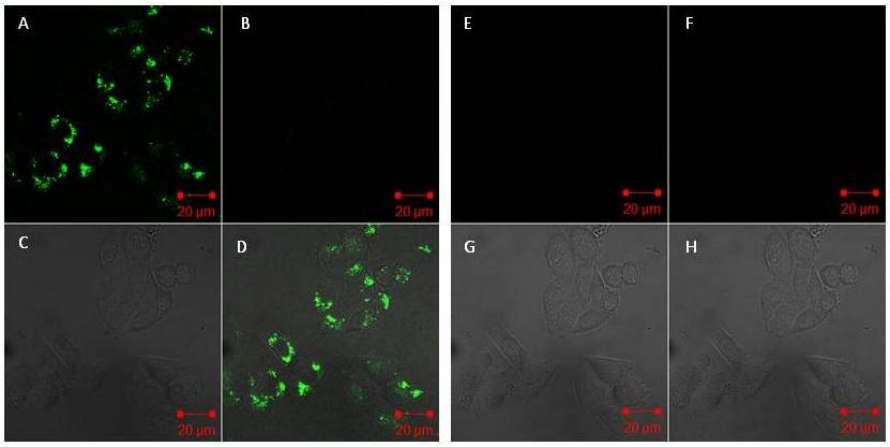

Figure B.18: Images A-H show single stranded Cy3 DNA (S1) added to cells via electroporation and imaged using confocal microscopy. Images A/E represents the Cy3 channel; B/F the Cy5 channel; C/G the bright field channel and D/H an overlay of all the channels. Images A-D are excited with a 543 nm laser only. Images E-H are excited with a 633 nm laser only.

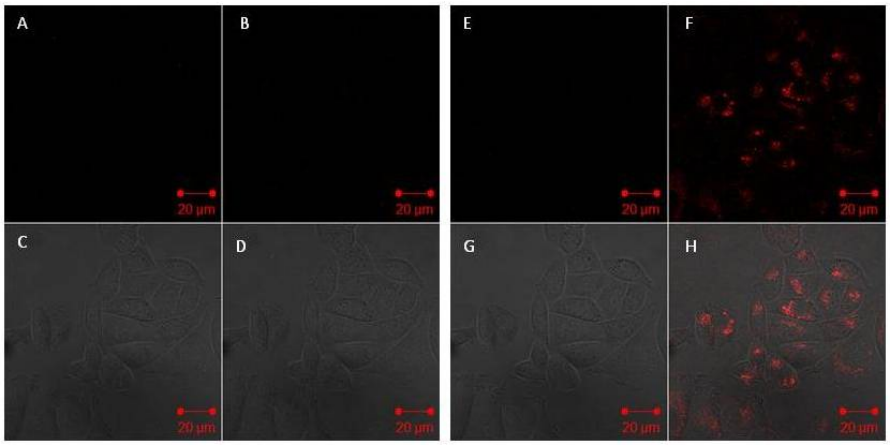

Figure B.19: Images A-H show single stranded Cy5 DNA (S2) added to cells via electroporation and imaged using confocal microscopy. Images A/E represents the Cy3 channel; B/F the Cy5 channel; C/G the bright field channel and D/H an overlay of all the channels. Images A-D are excited with a 543 nm laser only. Images E-H are excited with a 633 nm laser only.

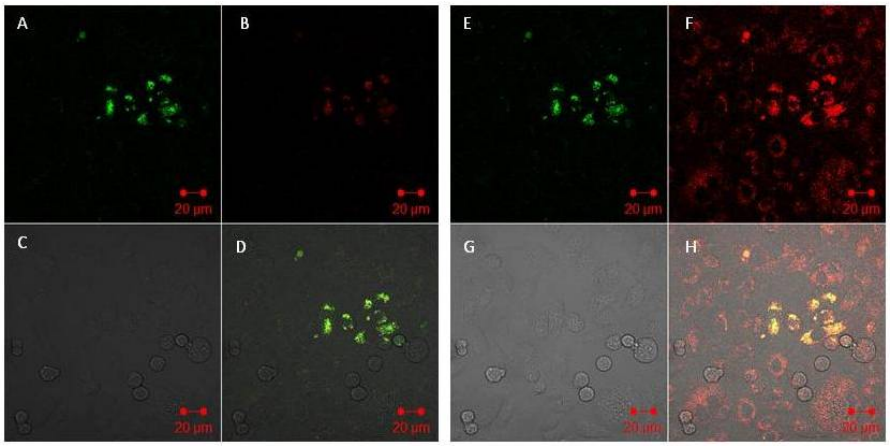

Figure B.20: Images A-H show Cy3 and Cy5 tagged probe DNA (S3) added to cells via electroporation and imaged using confocal microscopy. Images A/E represents the Cy3 channel; B/F the Cy5 channel; C/G the bright field channel and D/H an overlay of all the channels. Images A-D are excited with a 543 nm laser only. Images E-H are excited with both the 543 and 633 nm lasers.

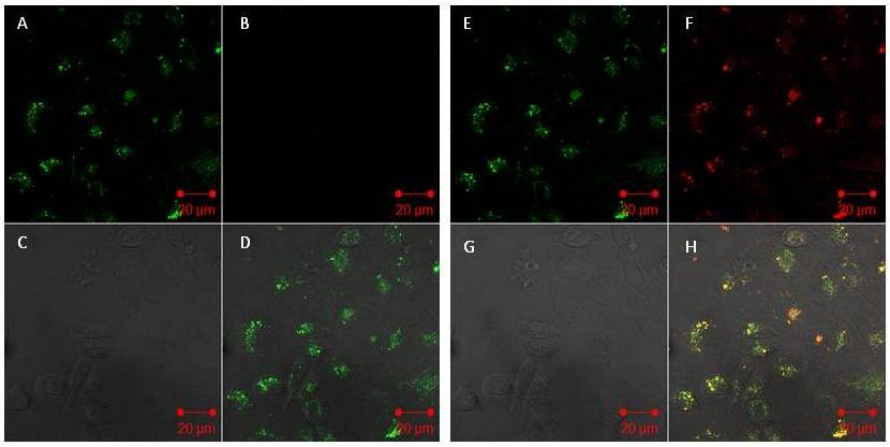

Figure B.21: Images A-H show non-complementary Cy3 and Cy5 tagged DNA (S4:S5) added together to cells via electroporation and imaged using confocal microscopy. Images A/E represents the Cy3 channel; B/F the Cy5 channel; C/G the bright field channel and D/H an overlay of all the channels. Images A-D are excited with a 543 nm laser only. Images E-H are excited with both the 543 and 633 nm lasers.

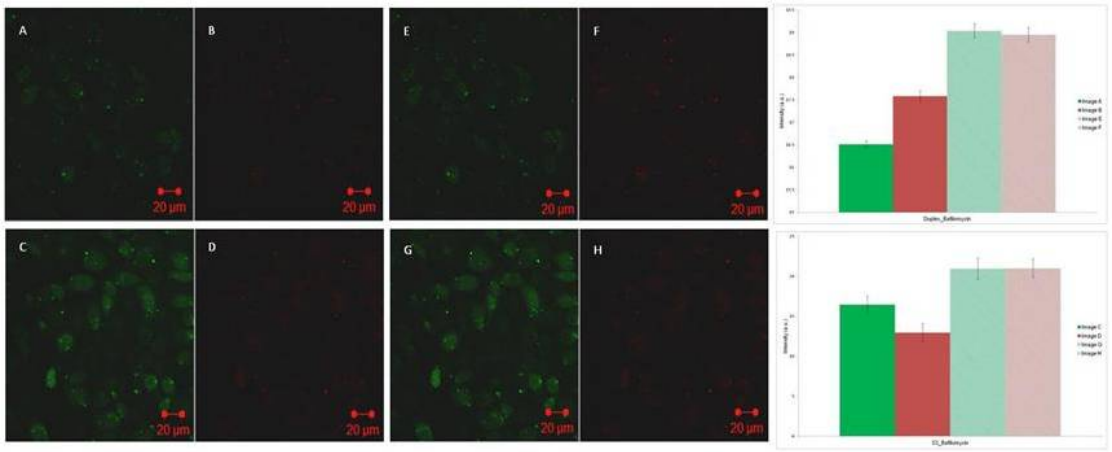

Figure B.22: Cells treated with bafilomycin upon lipid based transfection of S1:S2 duplex and S3, and imaged using confocal microscopy. Images A-D are excited with the 543 nm laser only. Images E-H are excited with both the 543 and 633 nm lasers. The top row cells have been treated with the S1:S2 duplex and the bottom row cells have been treated with S3. Images of the Cy5 channel in B and D clearly show a FRET signal.

Appendix C

Quantification of SNP sensing in a cellular environment with DNA anthracene probes

C.1 DNA acridine probe (PAcr) studies

Figure C.1 shows the titration graph from PAcr emission studies with DNA targets.

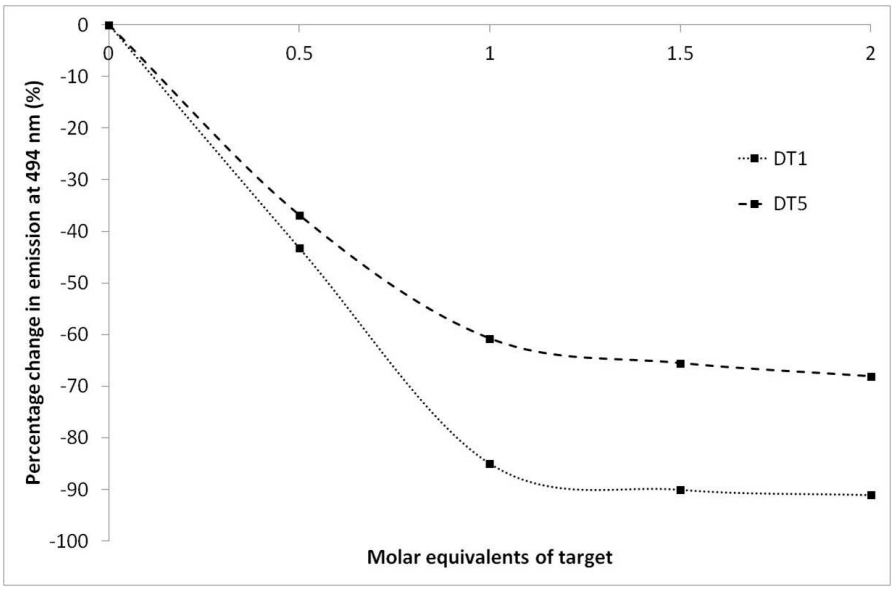

Figure C.1: Titrations of up to 2 equivalents of DNA targets, DT1 and DT5, into probe PAcr. The binding is shown to be 1:1 since the fluorescence does not change beyond 1 equivalent of target. Percentage changes calculated from emission intensity at PAcr = 494 nm. 1 μM DNA, 100 mM NaCl, 10 mM pH 7.0 sodium phosphate buffer, λ_{ex} = 421 nm. Emission range = 440-700 nm.

CD spectra in Figure C.2 shows that PAcr hybridised with complementary target DT1 retains a B-DNA conformation.

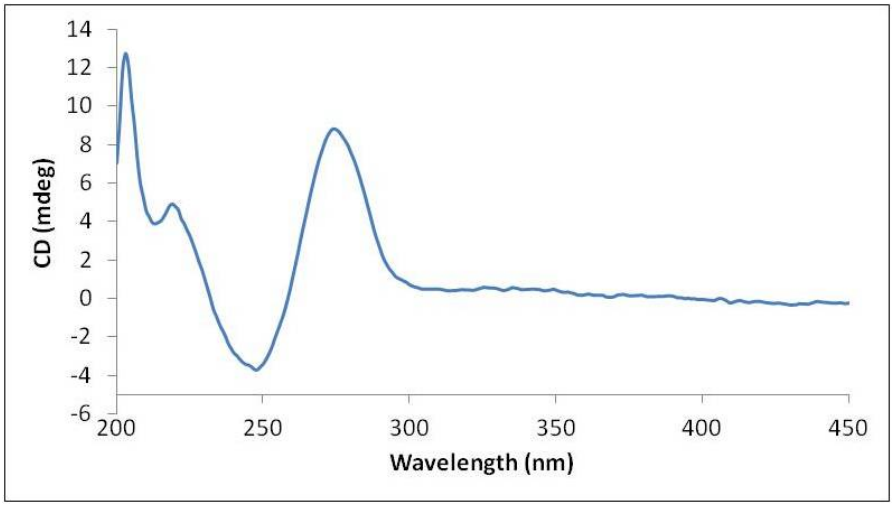

Figure C.2: Circular dichroism spectra of PAcr:DT1 duplex. 5 μM DNA/RNA, 100 mM NaCl, 10 mM pH 7.0 sodium phosphate buffer.

C.2 Z-stack images

Figure C.3 shows an example collection of z-stack images of DNA anthracene probe P1L within cells.

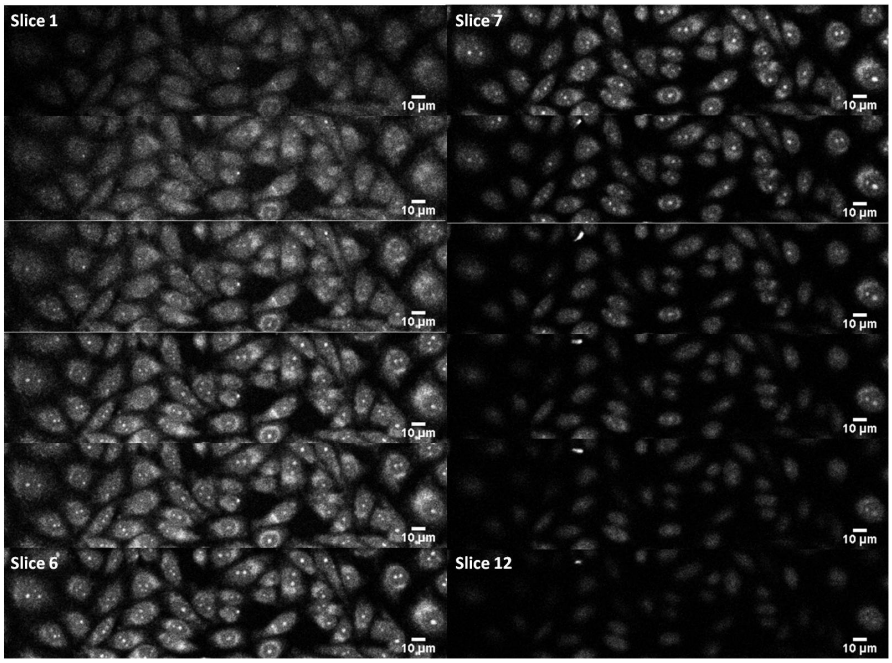

Figure C.3: Confocal microscopy z-stack images show the DNA anthracene probe P1L is within cells. Images were collected at 1 μm intervals. 402 nm laser excitation. Emission range: 425-475 nm.

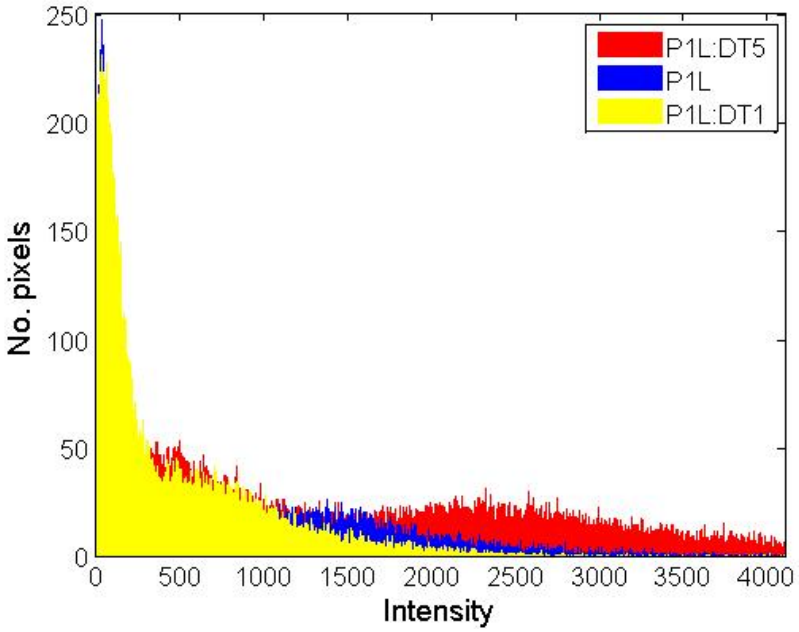

Figure C.4: Overlayed histograms for images displayed in Figure 5.8. A shift in intensity (x-axis) can be seen for images corresponding to different oligonucleotide treatment.

C.3 DNA acridine probe (PAcr) cell images and histograms

Manual inspection of cells treated with DNA acridine probe PAcr with and without targets DT1 and DT5 respectively, suggested the trend found in emission studies had been reproduced (Figure C.5).

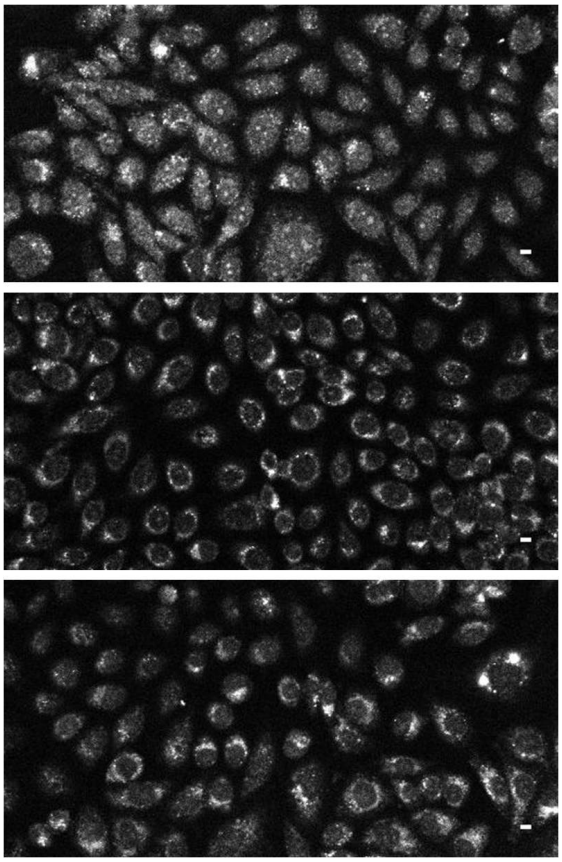

Figure C.5: PAcr; PAcr:DT1; PAcr:DT5 (top to bottom) added to fixed/permeabilised CHO cells and imaged using confocal microscopy. Scale bar 10 μm. 457 nm laser excitation. Emission range: 465-500 nm.

The difference (x_0'-x_0) between the centre of the background and foreground peaks was utilised to compare the intensity between images (Figure C.6).

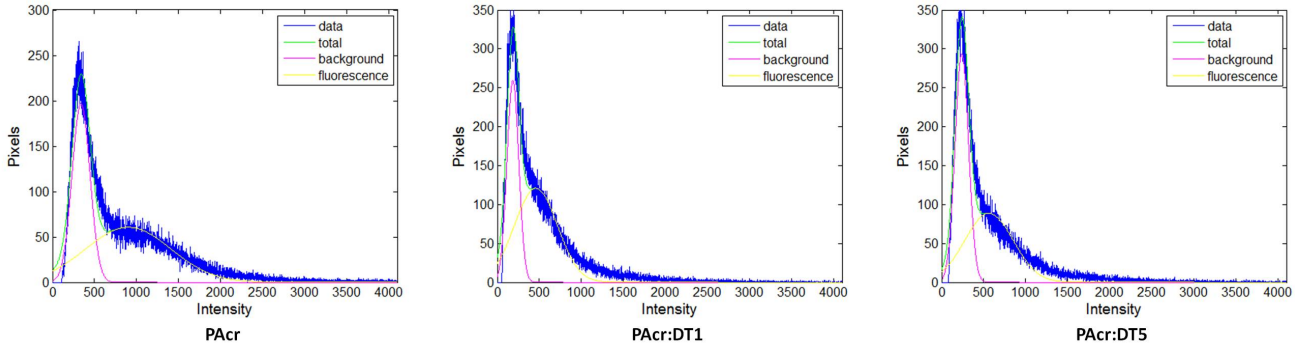

Figure C.6: Histograms with GMM, corresponding to PAcr; PAcr:DT1; PAcr:DT5 (left to right) images. GMM fits two Gaussian distributions corresponding to the background (pink) and fluorescence emission (yellow). The sum of the two Gaussian distributions (green) is shown to fit the outline of the histogram (blue).

C.4 Fixed cell RNA studies

Figure C.7 shows histograms for images of P1L:RNA duplexes added to fixed cell.

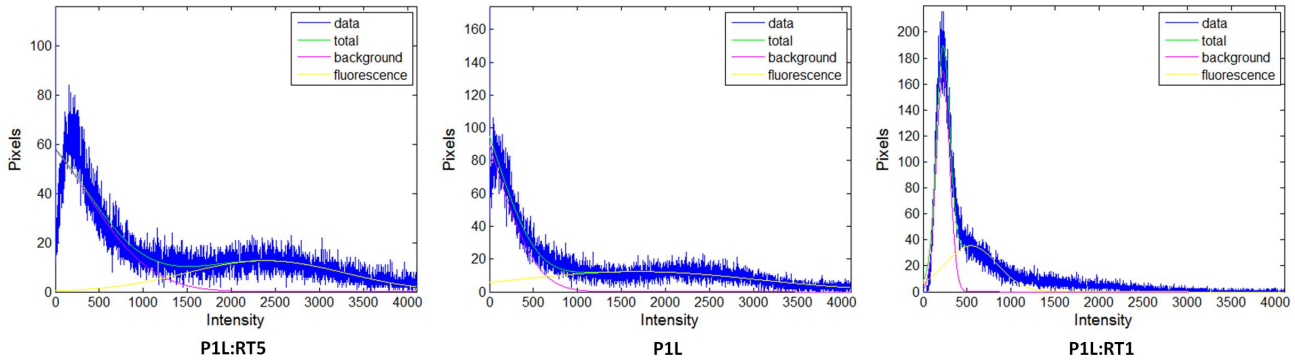

Figure C.7: Histograms with GMM, corresponding to P1L:RT5; P1L; P1L:RT1 (left to right) images. GMM fits two Gaussian distributions corresponding to the background (pink) and fluorescence emission (yellow). The sum of the two Gaussian distributions (green) is shown to fit the outline of the histogram (blue).

Figure C.8 shows histograms for corresponding sequential addition of RNA and P1L fixed cell images.

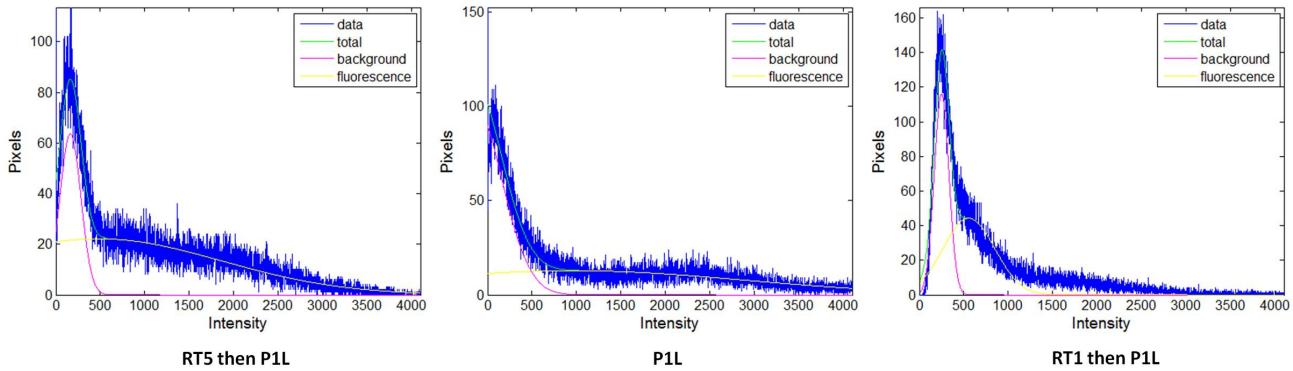

Figure C.8: Histograms with GMM, corresponding to RT5 then P1L; P1L; RT1 then P1L (left to right) images. GMM fits two Gaussian distributions corresponding to the background (pink) and fluorescence emission (yellow). The sum of the two Gaussian distributions (green) is shown to fit the outline of the histogram (blue).

Figure C.9 shows control cell images from RNA studies.

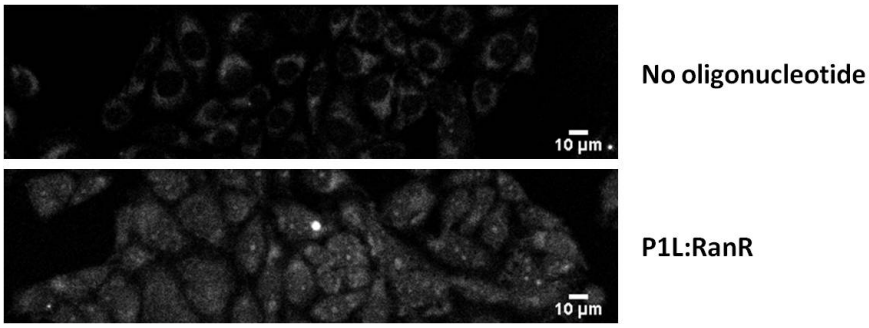

Figure C.9: Top image: No oligonucleotide added; Bottom image: P1L:RanR, added to fixed/permeabilised CHO cells and imaged using confocal microscopy. 402 nm laser excitation. Emission range: 425-475 nm.

C.5 Fixed cell base opposite sensing studies

Figure C.10 shows the confocal microscopy images of fixed cells with P6D duplexes added.

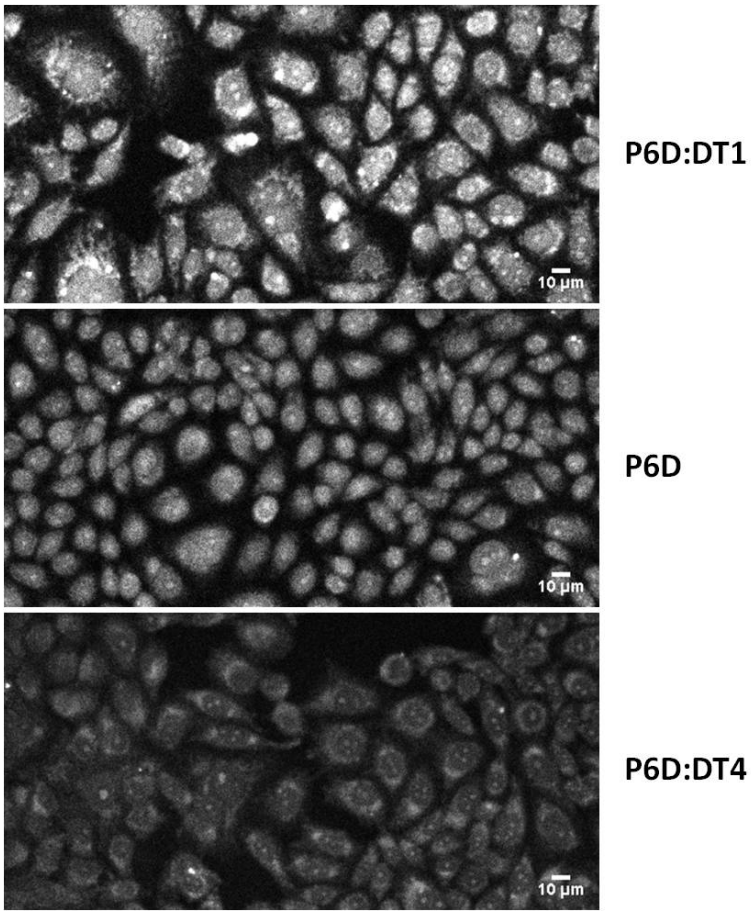

Figure C.10: P6D:DT1; P6D; P6D:DT4 (top to bottom) added to fixed/permeabilised CHO cells and imaged using confocal microscopy. 402 nm laser excitation. Emission range: 425-475 nm.

Figure C.11 shows histograms for corresponding P6D:DNA duplexes in fixed cell images.

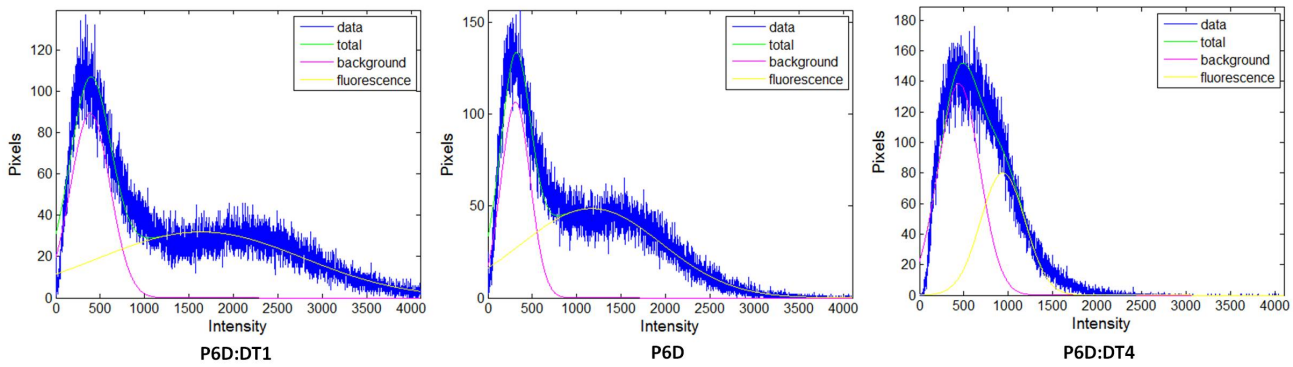

Figure C.11: Histograms with GMM, corresponding to P6D:DT1; P6D; P6D:DT4 (left to right) images. GMM fits two Gaussian distributions corresponding to the background (pink) and fluorescence emission (yellow). The sum of the two Gaussian distributions (green) is shown to fit the outline of the histogram (blue).

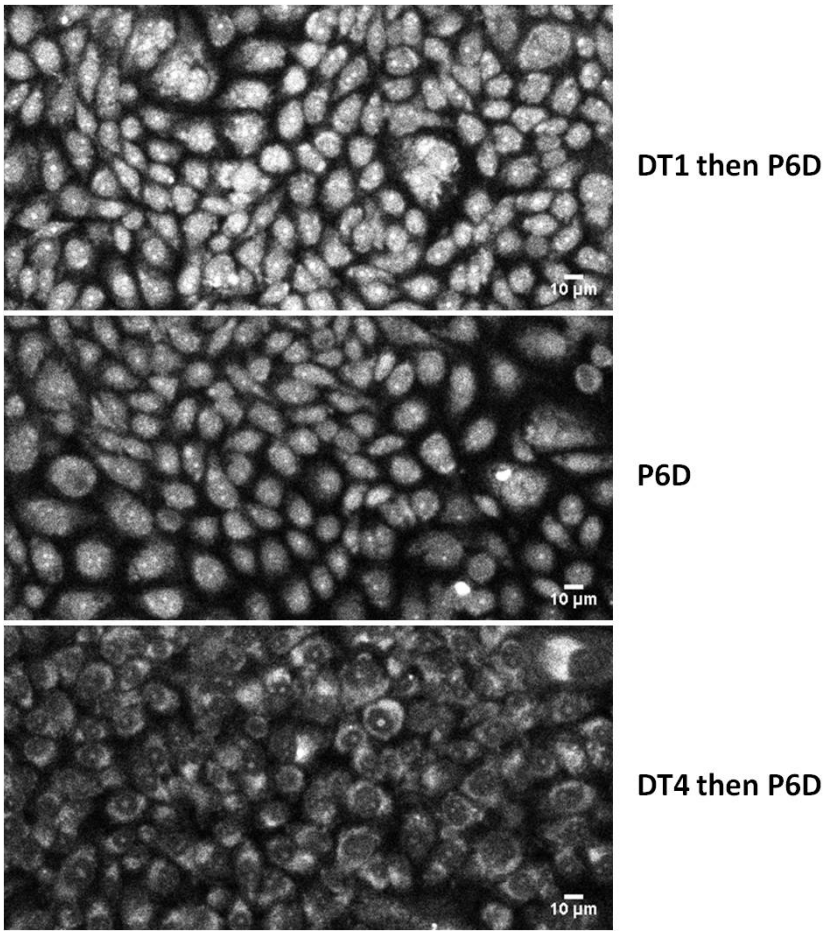

Figure C.12: DT1 then P6D; P6D; DT4 then P6D (top to bottom) added to fixed/permeabilised CHO cells and imaged using confocal microscopy. 402 nm laser excitation. Emission range: 425-475 nm.

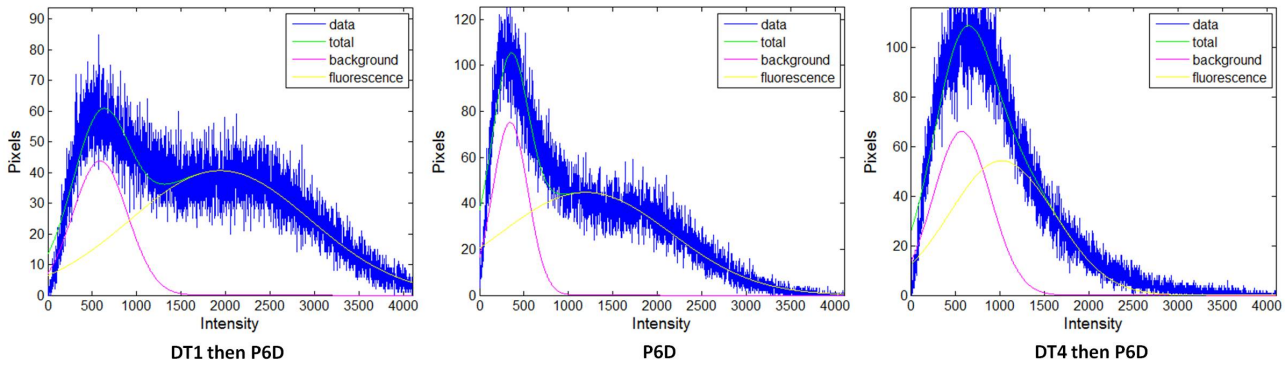

Figure C.13: Histograms with GMM, corresponding to DT1 then P6D; P6D; DT4 then P6D (left to right) images. GMM fits two Gaussian distributions corresponding to the background (pink) and fluorescence emission (yellow). The sum of the two Gaussian distributions (green) is shown to fit the outline of the histogram (blue).

Figure C.14 shows the confocal microscopy images of fixed cells with ZP5L DNA duplexes added.

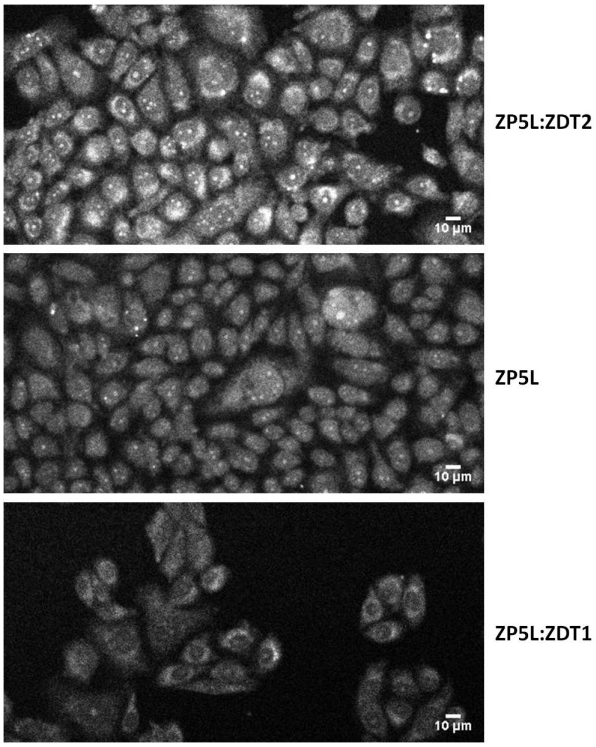

Figure C.14: ZP5L:ZDT2; ZP5L; ZP5L:ZDT1 (top to bottom) added to fixed/permeabilised CHO cells and imaged using confocal microscopy. 402 nm laser excitation. Emission range: 425-475 nm.

Figure C.15 shows histograms for corresponding ZP5L:DNA duplexes in fixed cell images.

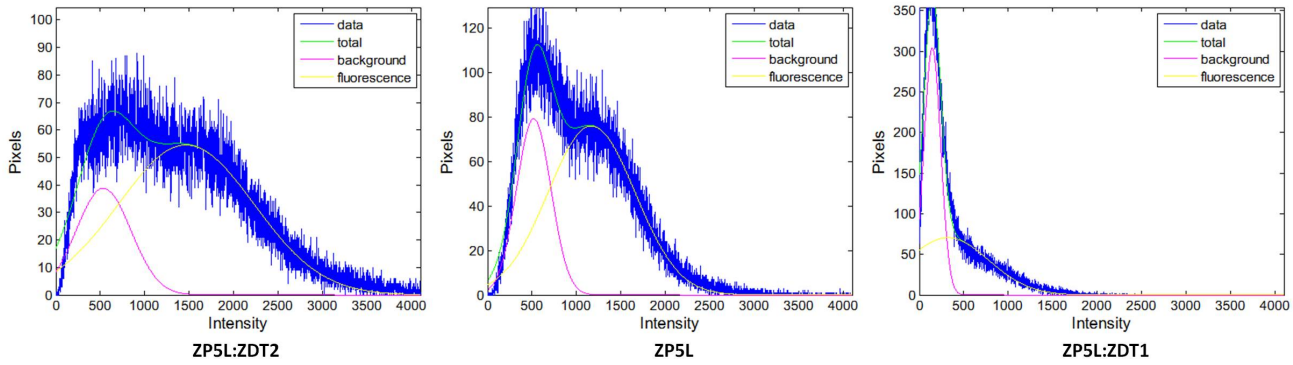

Figure C.15: Histograms with GMM, corresponding to ZP5L:ZDT2; ZP5L; ZP5L:ZDT1 (left to right) images. GMM fits two Gaussian distributions corresponding to the background (pink) and fluorescence emission (yellow). The sum of the two Gaussian distributions (green) is shown to fit the outline of the histogram (blue).

Figure C.16 shows the confocal microscopy images of fixed cells with ZP5L RNA duplexes added.

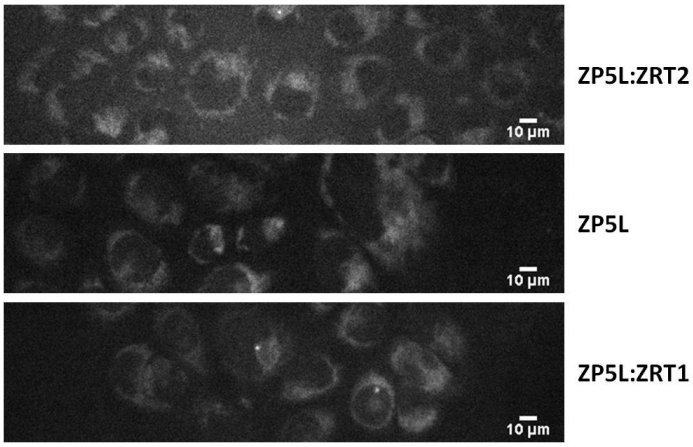

Figure C.16: ZP5L:ZRT2; ZP5L; ZP5L:ZRT1 (top to bottom) added to fixed/permeabilised CHO cells and imaged using confocal microscopy. 402 nm laser excitation. Emission range: 425-475 nm.

Figure C.17 shows histograms for corresponding ZP5L:RNA duplexes in fixed cell images.

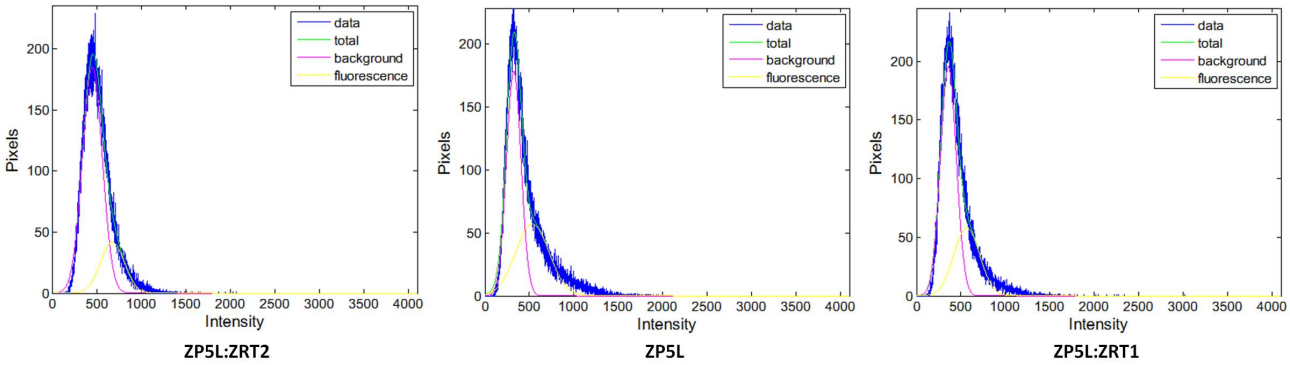

Figure C.17: Histograms with GMM, corresponding to ZP5L:ZRT2; ZP5L; ZP5L:ZRT1 (left to right) images. GMM fits two Gaussian distributions corresponding to the background (pink) and fluorescence emission (yellow). The sum of the two Gaussian distributions (green) is shown to fit the outline of the histogram (blue).

C.6 Computational analysis

C.6.1 Particle Swarm Optimisation (PSO) algorithm

Non-linear fitting can be achieved computationally with evolutionary algorithms, which find the minimum error between the fit and the data, by adjusting the parameters in Equation 5.5. There are six unknown parameters to fit: the peak heights A and A′, coordinates of the peak centres x_0 and x_0', and the peak widths σ and σ' (Figure C.18).

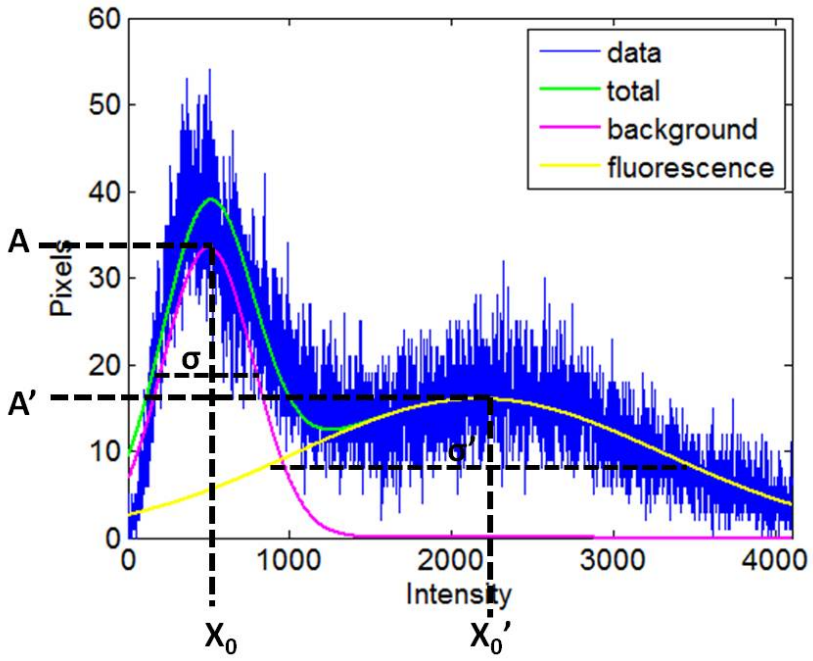

Figure C.18: The outline of the histogram (blue) has two Gaussian curves fitted (yellow and pink) corresponding to the background and fluorescence emission contributions respectively. The unknown parameters are labelled: the peak heights A and A′, coordinates of the peak centres x_0 and x_0', and the peak widths σ and σ'. Using Gaussian Mixture Modelling (GMM) these parameters can be solved using a Particle Swarm Optimisation (PSO) algorithm.

Particle Swarm Optimisation (PSO) was the evolutionary algorithm used to find the parameters. The central paradigm of an evolutionary algorithm is to find the lowest error between the fit and the raw data, in a Darwinistic manner. The PSO algorithm

is analogous to birds flocking; each member, or particle, of the population knows its own best position, and the best position the population has found. Here, the position is defined as the least-squares error between the parameters and the data, thus, the best position is the one of lowest error which is the ultimate target for the PSO algorithm.

Appendix D

SNP sensing with plasmids in a cellular environment

D.1 Anthracene DNA probe chemical transfection

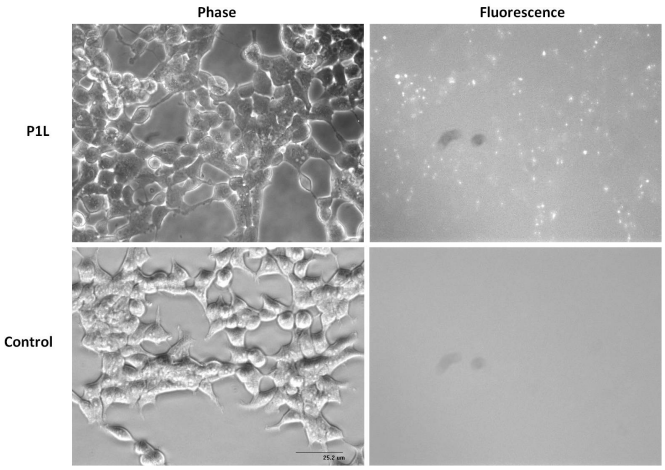

Figure D.1: Chemical transfection confocal microscopy images. Anthracene DNA probe (P1L) added to cells via chemical transfection using Lipofectamine and imaged using confocal microscopy. The left column gives the phase images and right column the fluorescence images. The top row cells were chemically transfected with P1L, and the bottom row cells were untreated. Images were acquired with an inverted fluorescent microscope (Olympus) using a UV filter cube. Scale bar = 25.2 μm.

D.2 Antibody confocal images

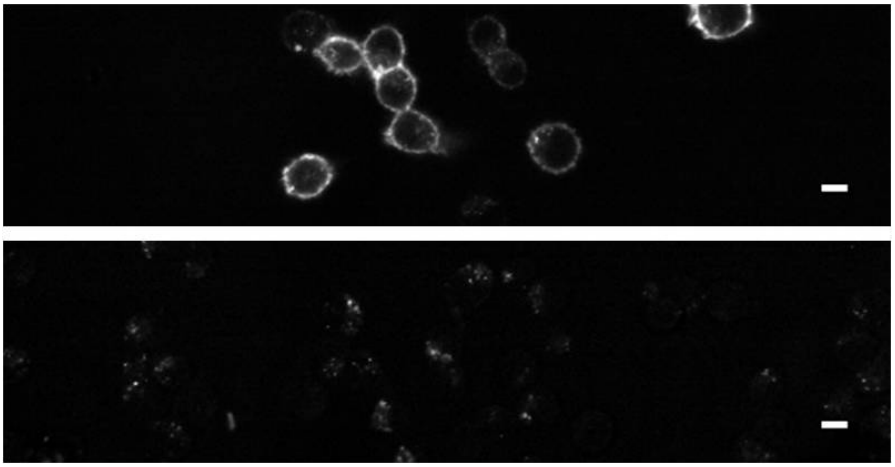

Figure D.2: Antibody with Cy5 fluorophore tag is imaged with cells that have been transfected with plasmid (top) versus untreated cells (bottom). The antibody binds to a surface receptor which ensures equal molar expression of both proteins. Scale bar represents 10 μm.

D.3 Flow cytometry

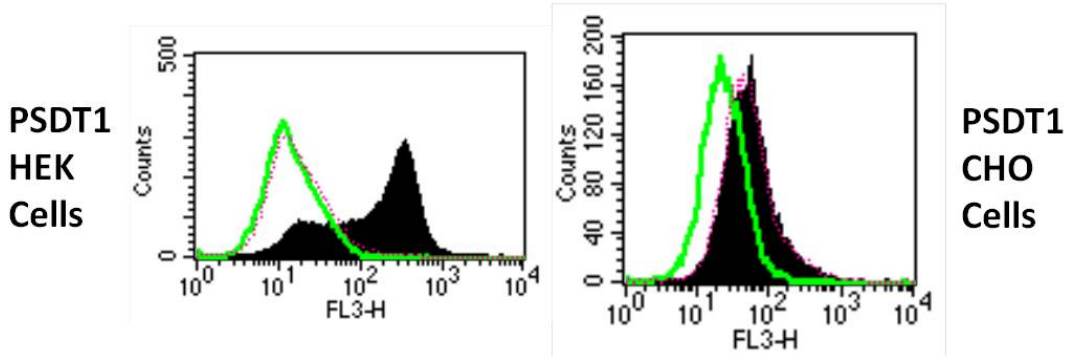

Figure D.3: Example of HEK (left) and CHO (right) cell plasmid flow cytometry results. Black represents the transfected cells; green line represents control cells and pink line represents mock transfected cells.

D.4 Plasmid image analysis

Table D.1: Mean intensity values from ImageJ analysis are calculated from the intensity mean± s.e.m. from at least 24 cells (p=0.01 to 0.05). Image refers to the confocal microscope image of HeLa cells treated with P1L duplexes. **P1L λ_{ex} = 402 nm.** Emission ranges: P1L = 425-475 nm.

Image	Mean intensity (ImageJ)
PSDT1	471±28
PSDT5	460±17
PLDT1	310±31
PLDT5	422±29

Appendix E

Dual fluorophore (Cy3/anthracene) probe for SNP sensing

E.1 Melting studies

Table E.1: Melting temperatures (°C) of central DNA anthracene (P1L), Cy3-only and dual fluorophore probes and targets, plus controls. 5 μM DNA, 100 mM NaCl, 10 mM pH 7.0 sodium phosphate buffer.

Probe/Target	DT1	DT5	DT6	DT7	DT8
DN	55	42	42.5	42.5	41.5
P1L	53	46	44.5	39.5	40.5
Cy3	57	43.5	45.5	45.5	43
Cy3/P1L	49.5	42	43.5	39.5	40

Table E.2: Melting temperatures (°C) of close DNA anthracene (cP1L), cCy3-only and dual fluorophore probes and targets, plus controls. 5 μM DNA, 100 mM NaCl, 10 mM pH 7.0 sodium phosphate buffer.

Probe/Target	cDT1	cDT5	cDT6
cP1L	51.5	41	42
cCy3	61	48	46
cCy3/P1L	53	42.5	44

Table E.3: Melting temperatures (°C) of far DNA anthracene (fP1L), fCy3-only and dual fluorophore probes and targets, plus controls. 5 μM DNA, 100 mM NaCl, 10 mM pH 7.0 sodium phosphate buffer.

Probe/Target	fDT1	fDT5	fDT6
fP1L	52	40.5	47.5
fCy3	61	47	47
fCy3/P1L	54.5	42.5	51

Table E.4: Melting temperatures (°C) of central DNA anthracene (P5L), Cy3-only and dual fluorophore probes and targets, plus controls. 5 μM DNA, 100 mM NaCl, 10 mM pH 7.0 sodium phosphate buffer.

Probe/Target	DT1	DT2	DT3	DT4	DT5	DT6
DN	55	50	46	48	42	42.5
P5L	49	48	49.5	49	40	38.5
Cy3	57	55	55.5	54	43.5	45.5
Cy3/P5L	51.5	53	53.5	51.5	42.5	42

E.1.1 Dye-dye and dye-nucleotide interactions

Low T_M's for multiply labelled probes can be associated with dye-dye and dye-nucleotide interactions. UV-vis melting studies allowed dye-dye interactions to be monitored as Randolph *et al.* carried out. [209] The isobestic point of the single stranded Cy3/P1L was found to be 543 nm in a temperature dependence study (absorption spectra shown in Figure E.1). By choosing to monitor at this wavelength during melting studies of Cy3/P1L duplexes, the change in absorbance of the dyes should be due to conformational changes in the DNA rather than due to the effect of changes in temperature upon the dye itself. The melting temperatures of all the dual fluorophore probes demonstrate that the fluorophores do interact but distance/orientation has little influence (Table E.5). Figure E.2 demonstrates the transition from duplex to single-stranded DNA is reflected in the absorbance curve of the dye as well as the oligonucleotide absorbance at 260 nm. Unmodified duplex (DN:DT1) and anthracene only duplexes (P1L:DT1) do not have a T_M value which is to be expected since there is no Cy3 to interact with.

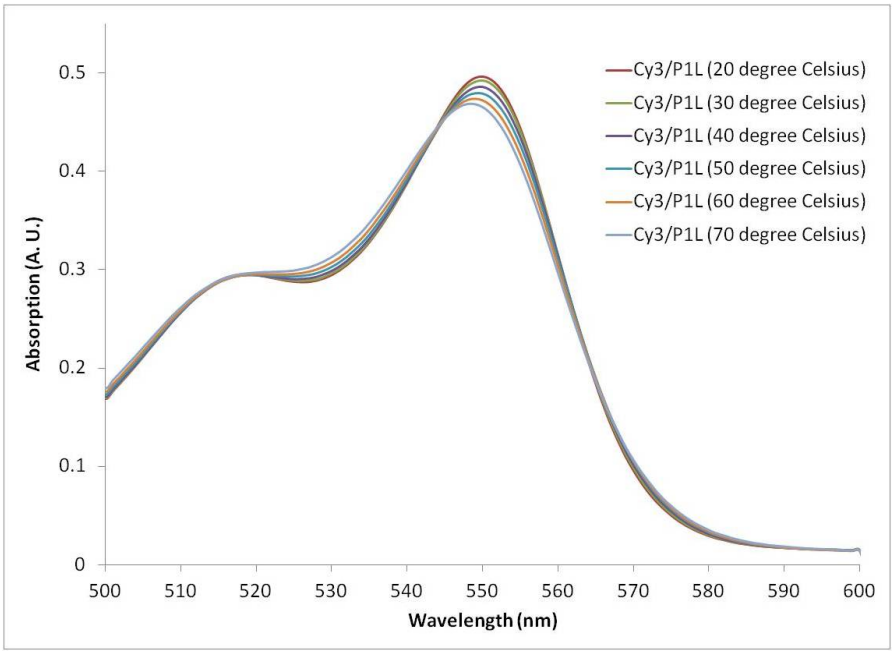

Figure E.1: Absorption spectra of single stranded Cy3/P1L probe at varying temperatures. 5 μM DNA, 100 mM NaCl, 10 mM pH 7.0 sodium phosphate buffer.

Table E.5: Melting temperatures (°C) of dual fluorophore probe duplexes. 5 μM DNA, 100 mM NaCl, 10 mM pH 7.0 sodium phosphate buffer. Absorption measured at **543 nm** wavelength.

Probe/Target	DT1
Cy3/P1L	38
cCy3/P1L	41.5
fCy3/P1L	41.5
Cy3	34

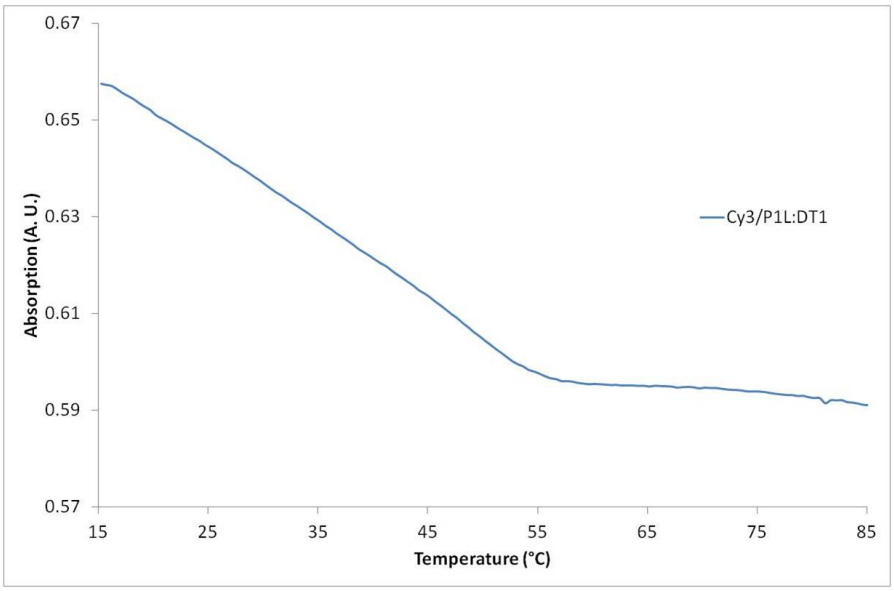

Figure E.2: Melting curve of Cy3/P1L:DT1 duplex monitored at **543 nm**. 5 μM DNA, 100 mM NaCl, 10 mM pH 7.0 sodium phosphate buffer.

Dye-nucleotide interactions cause a shoulder peak at 310 nm in the Cy3/anthracene absorption spectra. Since there is no shoulder peak (Figure E.3) it is assumed that Cy3 does not perturb the bases but stacks on the end of the duplex (which is evident from increased Tm's). Therefore the dual fluorophore probe destabilisation compared to its equivalent single fluorophore probes is contributed to by dye-dye interactions. If the anthracene and Cy3 are interacting physically to the detriment of the probe function, the tether link of the Cy3 could be reduced (ethyl).

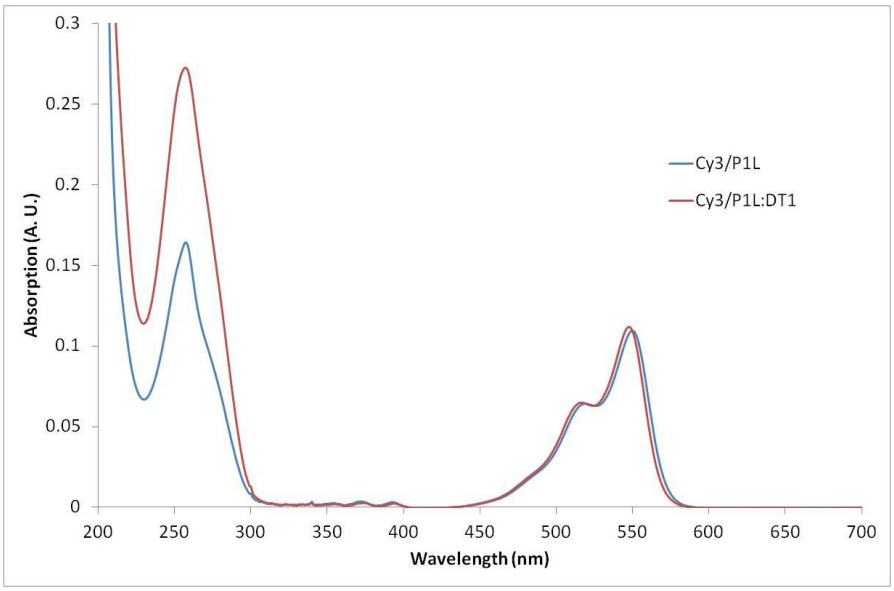

Figure E.3: Absorption spectra of single stranded Cy3/P1L probe and Cy3/P1L:DT1 duplex. 1 μM DNA, 100 mM NaCl, 10 mM pH 7.0 sodium phosphate buffer.

E.2 Fluorescence Studies

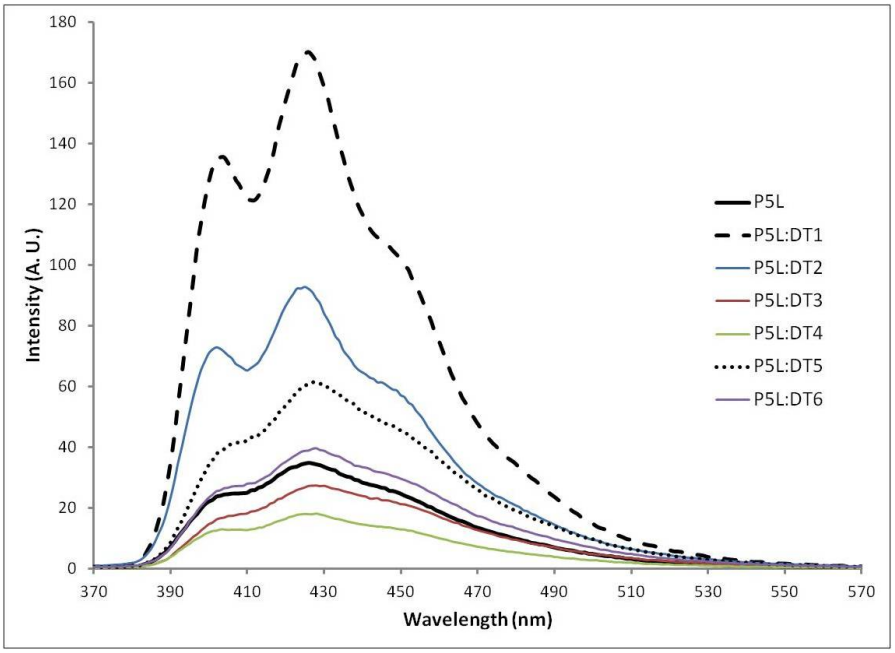

Figure E.4: Fluorescence spectra showing the emission spectra of anthracene probe P5L and DNA targets. 1 μM DNA, 100 mM NaCl, 10 mM pH 7.0 sodium phosphate buffer, λ_{ex} = 350 nm.

Table E.6: Percentage differences in emission at λ_{em} = **570 nm** on addition of DNA targets to Cy3-only probes, relative to the probe alone. 1 μM DNA, 100 mM NaCl, 10 mM pH 7.0 sodium phosphate buffer, λ_{ex} = 350 nm.

Probe/Target	DT1	DT5
Cy3	-62	-57
cCy3	-69	-68
fCy3	-60	-59

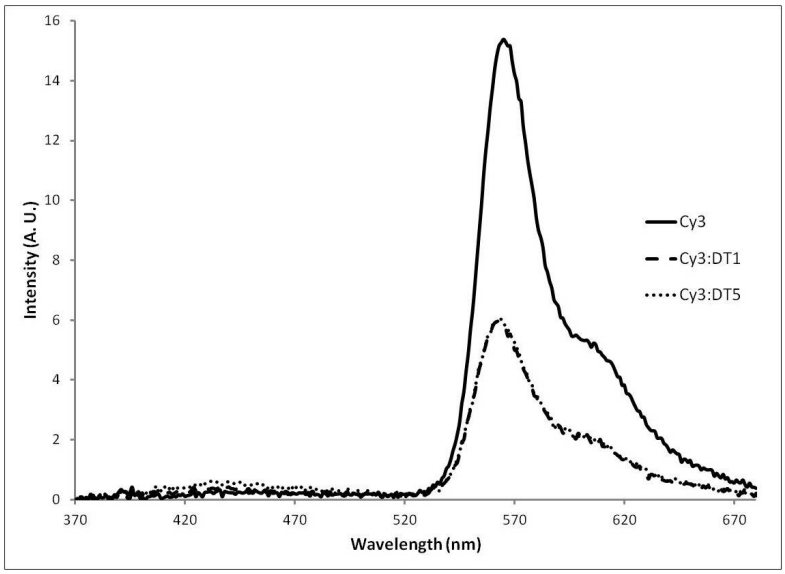

Figure E.5: Emission spectra showing the change in emission upon hybridisation of Cy3-only probe with targets DT1 and DT5 respectively. 1 μM DNA, 100 mM NaCl, 10 mM pH 7.0 sodium phosphate buffer, $\lambda_{ex} = 350$ nm.

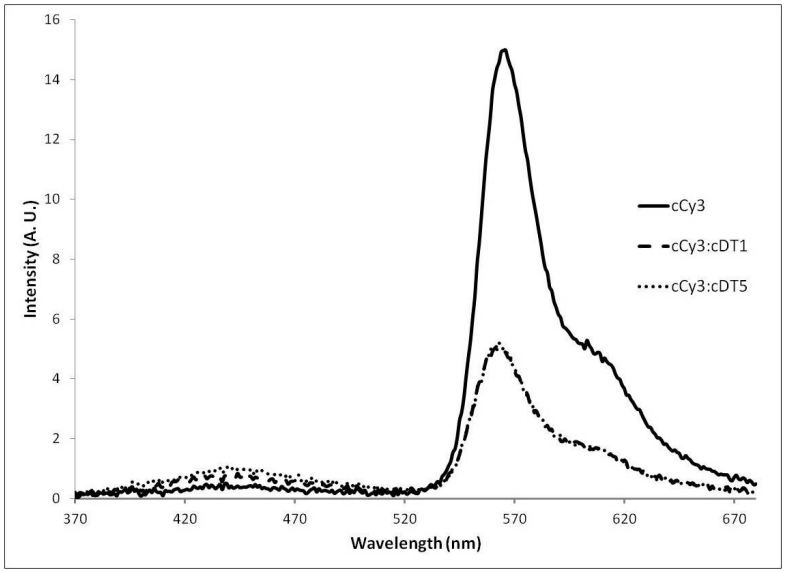

Figure E.6: Emission spectra showing the change in emission upon hybridisation of cCy3-only probe with targets cDT1 and cDT5 respectively. 1 μM DNA, 100 mM NaCl, 10 mM pH 7.0 sodium phosphate buffer, $\lambda_{ex} = 350$ nm.

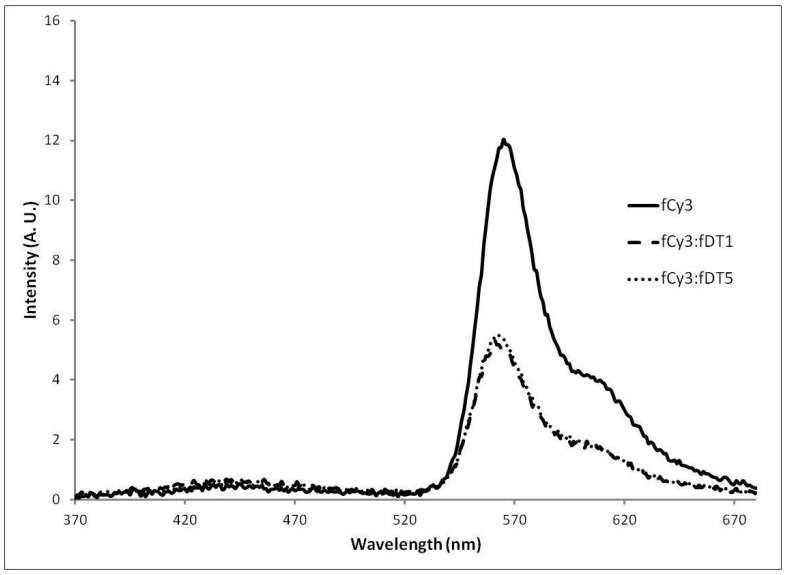

Figure E.7: Emission spectra showing the change in emission upon hybridisation of fCy3-only probe with targets fDT1 and fDT5 respectively. 1 μM DNA, 100 mM NaCl, 10 mM pH 7.0 sodium phosphate buffer, λ_{ex} = 350 nm.

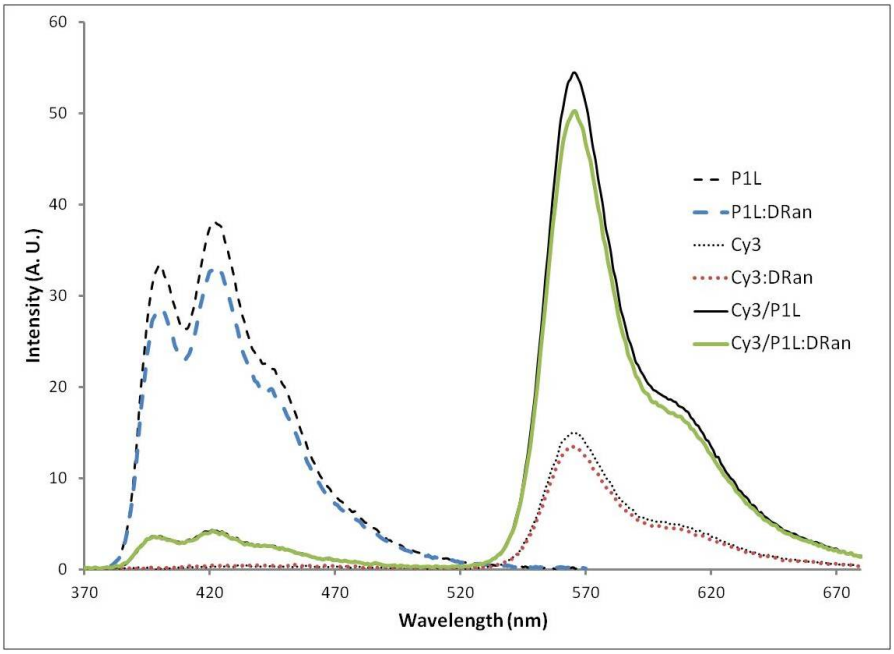

Figure E.8: Emission spectra showing the change in emission upon hybridisation of P1L, Cy3 and Cy3/P1L with random DNA target, DRan. 1 μM DNA, 100 mM NaCl, 10 mM pH 7.0 sodium phosphate buffer, λ_{ex} = 350 nm.

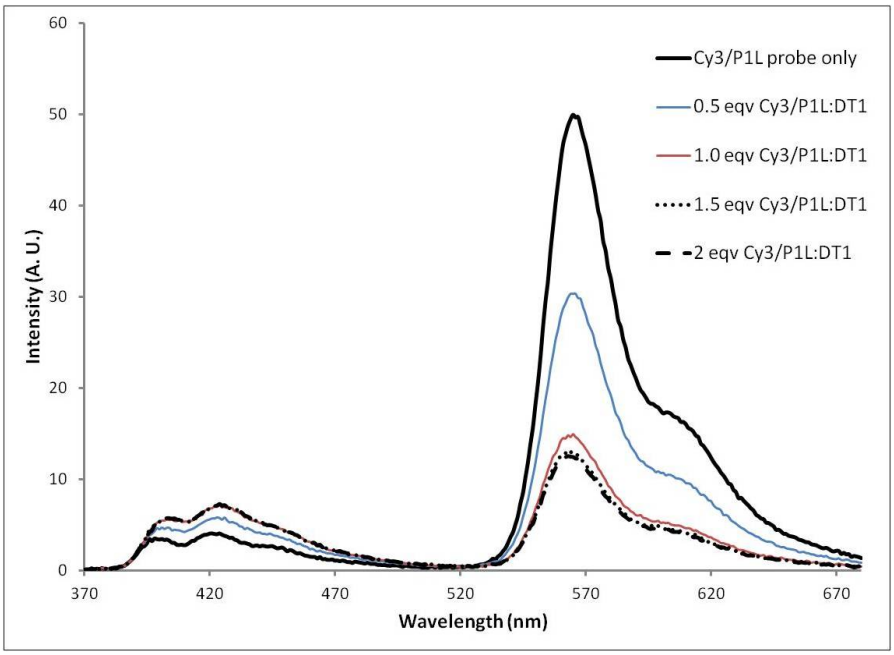

Figure E.9: Fluorescence titrations of up to 2 equivalents of DNA target DT1 into probe Cy3/P1L. The binding is shown to be 1:1 since the emission does not change beyond 1 equivalent of target. 1 μM DNA, 100 mM NaCl, 10 mM pH 7.0 sodium phosphate buffer, λ_{ex} = 350 nm.

Table E.7: Percentage differences in emission at λ_{em} = **570 nm** on addition of DNA targets to Cy3/P1L probes, relative to the probe alone. 1 μM DNA, 100 mM NaCl, 10 mM pH 7.0 sodium phosphate buffer, λ_{ex} = 350 nm.

Probe/Target	DT1	DT5	DT6
Cy3/P1L	-76	-58	-73
cCy3/P1L	-75	-66	-86
fCy3/P1L	-90	-83	-86

Table E.8: Percentage differences in emission at λ_{em} = **426 nm** on addition of DNA targets to Cy3/P1L probes, relative to the probe alone. 1 μM DNA, 100 mM NaCl, 10 mM pH 7.0 sodium phosphate buffer, λ_{ex} = 350 nm.

Probe/Target	DT1	DT5	DT6
Cy3/P1L	+89	+298	+250
cCy3/P1L	+48	+59	-76
fCy3/P1L	+198	+739	-86

Table E.9: Quantum yields of hybridised DNA anthracene probes, Cy3-only probes and dual fluorophore probes. 1 μM DNA, 100 mM NaCl, 10 mM pH 7.0 sodium phosphate buffer, λ_{ex} = 350 nm. Quantum yields were determined relative to quinine sulphate (Φ_f = 0.546).

Probe	Quantum Yield
P1L:DT1	0.030
P1L:DT5	0.17
Cy3:DT1	0.018
Cy3:DT5	0.019
Cy3/P1L:DT1	0.046
Cy3/P1L:DT5	0.087
Cy3/P5L:DT1	0.08
Cy3/P5L:DT5	0.047

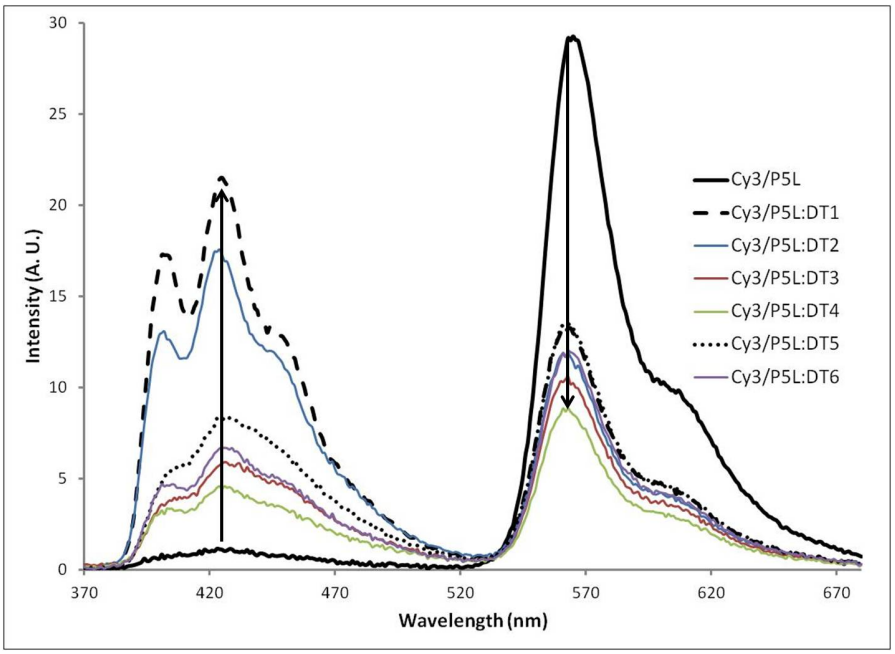

Figure E.10: Emission spectra showing the change in emission upon hybridisation of dual fluorophore probe Cy3/P5L with DNA targets. 1 μM DNA, 100 mM NaCl, 10 mM pH 7.0 sodium phosphate buffer, λ_{ex} = 350 nm.

Table E.10: Percentage differences in emission at λ_{em} = **426 nm** on addition of DNA targets to the Cy3/P5L probe, relative to the probe alone. 1 μM DNA, 100 mM NaCl, 10 mM pH 7.0 sodium phosphate buffer, λ_{ex} = 350 nm.

Probe/Target	DT1	DT2	DT3	DT4	DT5	DT6
Cy3/P5L	+1990	+1562	+480	+351	+708	+555

Table E.11: Percentage differences in emission at λ_{em} = **570 nm** on addition of DNA targets to the Cy3/P5L probe, relative to the probe alone. 1 μM DNA, 100 mM NaCl, 10 mM pH 7.0 sodium phosphate buffer, λ_{ex} = 350 nm.

Probe/Target	DT1	DT2	DT3	DT4	DT5	DT6
Cy3/P5L	-58	-63	-67	-72	-57	-62

Table E.12: Ratio of emission intensity at 570 nm/426 nm for dual fluorophore DNA probes and targets. 100 mM NaCl, 10 mM pH 7.0 sodium phosphate buffer, λ_{ex} = 350 nm. Ratios are expressed as mean ± s.e.m from three repeats.

Probe	Cy3/P1L	cCy3/P1L	fCy3/P1L
Probe only	15.23±3.10	35.74±0.7	20.48±0.35
DT1	6.23±0.27	1.52±0.12	0.65±0.01
DT5	7.79±0.23	1.17±0.14	0.40±0.01
DT6	1.72±0.20	4.07±0.13	0.57±0.03
DT7	1.41±0.19	-	-
DT8	1.49±0.26	-	-

Table E.13: Ratio of emission intensity at 570 nm/426 nm for dual fluorophore DNA probes and targets, at varying concentrations. 100 mM NaCl, 10 mM pH 7.0 sodium phosphate buffer, λ_{ex} = 350 nm. Ratios are expressed as mean ± s.e.m from three repeats.

Concentration/Duplex	Cy3/P1L:DT1	Cy3/P1L:DT5
2	1.14±0.006	0.82±0.013
1.5	1.12±0.020	0.82±0.001
1	1.11±0.016	0.84±0.010
0.5	1.11±0.010	0.88±0.004

E.3 Lifetime studies

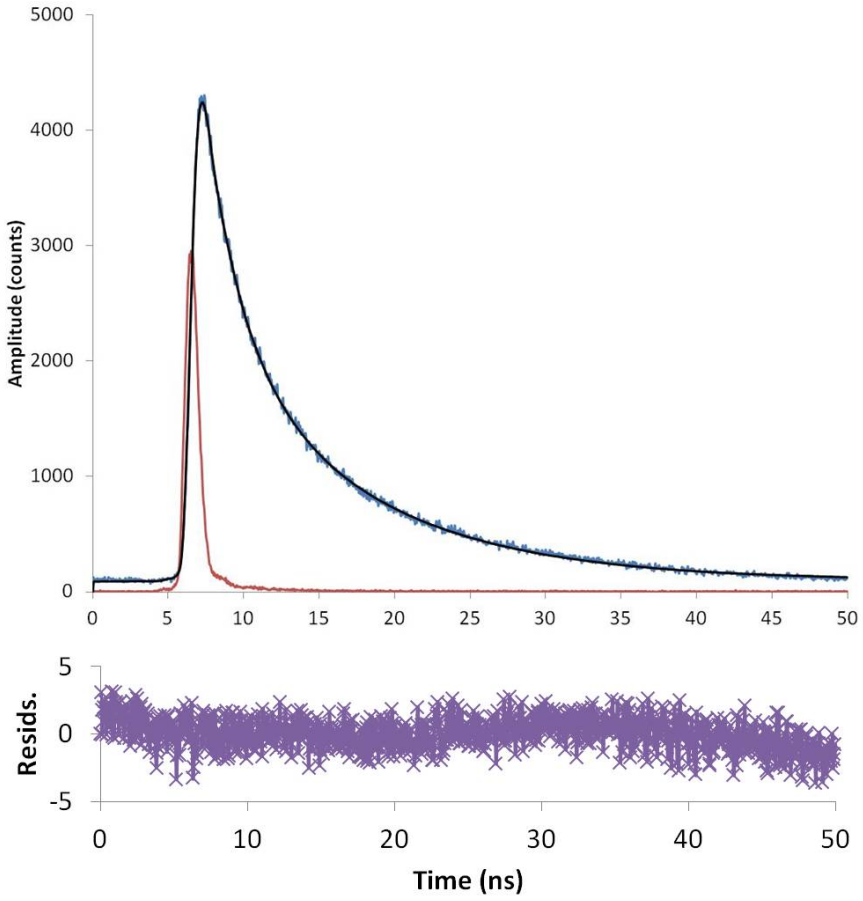

Figure E.11: Fluorescent decay profile of P1L:DT5 duplex (blue). The exponential data fit (black) and IRF (red) are also given. 5 μM DNA, 100 mM NaCl, 10 mM pH 7.0 sodium phosphate buffer, λ_{ex} = 376 nm, λ_{em} = **426 nm**.

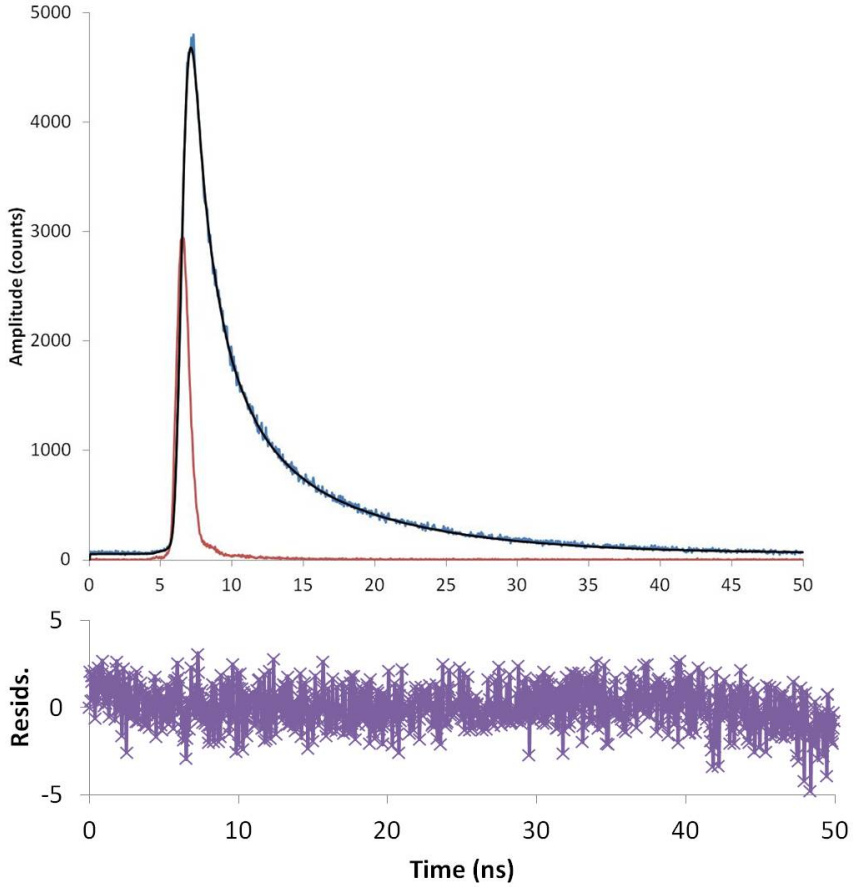

Figure E.12: Fluorescent decay profile of P1L (blue). The exponential data fit (black) and IRF (red) are also given. 5 μM DNA, 100 mM NaCl, 10 mM pH 7.0 sodium phosphate buffer, λ_{ex} = 376 nm, λ_{em} = **426 nm**.

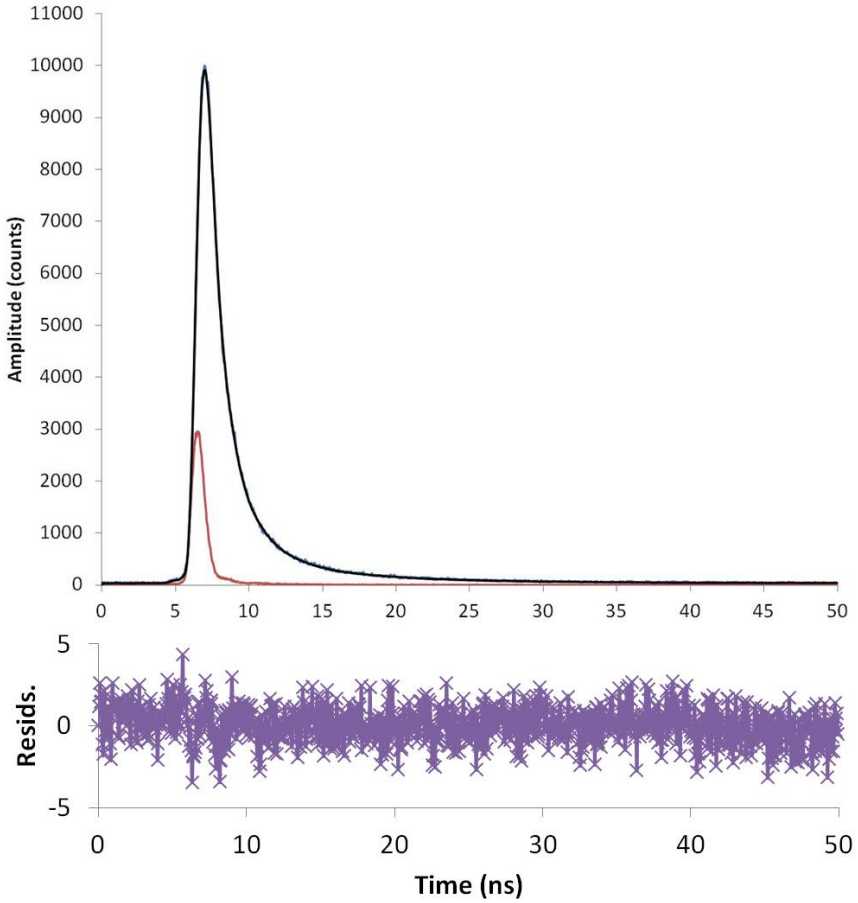

Figure E.13: Fluorescent decay profile of P1L:DT1 duplex (blue). The exponential data fit (black) and IRF (red) are also given. 5 μM DNA, 100 mM NaCl, 10 mM pH 7.0 sodium phosphate buffer, λ_{ex} = 376 nm, λ_{em} = **426 nm**.

Table E.14: Fluorescence lifetimes (ns) of Cy3-only and duplexes. 5 μM DNA, 100 mM NaCl, 10 mM pH 7.0 sodium phosphate buffer, λ_{ex} = 376 nm, λ_{em} = **570 nm**.

	$\tau 1$ (Wt %)	$\tau 2$ (Wt %)	χ^2
Cy3	0.59 (26)	1.91 (74)	1.576
Cy3:DT1	0.52 (52)	1.60 (48)	1.617
Cy3:DT5	0.6 (44)	1.89 (56)	1.582

Table E.15: Fluorescence lifetimes (ns) of fCy3-only and duplexes. 5 μM DNA, 100 mM NaCl, 10 mM pH 7.0 sodium phosphate buffer, λ_{ex} = 376 nm, λ_{em} = **570 nm**.

	τ1 (Wt %)	τ2 (Wt %)	χ^2
fCy3	0.49 (19)	1.91 (81)	1.619
fCy3:fDT1	0.40 (43)	1.23 (57)	2.382
fCy3:fDT5	0.40 (44)	1.31 (56)	2.251

Table E.16: Fluorescence lifetimes (ns) of cCy3-only and duplexes. 5 μM DNA, 100 mM NaCl, 10 mM pH 7.0 sodium phosphate buffer, λ_{ex} = 376 nm, λ_{em} = **570 nm**.

	τ1 (Wt %)	τ2 (Wt %)	χ^2
cCy3	0.59 (19)	2.33 (81)	1.529
cCy3:cDT1	0.41 (44)	1.25 (56)	2.504
cCy3:cDT5	0.43 (49)	1.41 (51)	1.918

Table E.17: Fluorescence lifetimes (ns) of fCy3/P1L and duplexes. 5 μM DNA, 100 mM NaCl, 10 mM pH 7.0 sodium phosphate buffer, λ_{ex} = 376 nm, λ_{em} = **426 nm**.

	τ1 (Wt %)	τ2 (Wt %)	τ3 (Wt %)	χ^2
fP1L/Cy3	0.29 (50)	1.66 (36)	5.43 (14)	1.226
fCy3/P1L:fDT1	0.75 (61)	1.96 (39)	- (-)	1.287
fCy3/P1L:fDT5	0.37 (7)	2.50 (69)	5.58 (24)	1.132

Table E.18: Fluorescence lifetimes (ns) of cCy3/P1L and duplexes. 5 μM DNA, 100 mM NaCl, 10 mM pH 7.0 sodium phosphate buffer, λ_{ex} = 376 nm, λ_{em} = **426 nm**.

	τ1 (Wt %)	τ2 (Wt %)	χ^2
cCy3/P1L	0.25 (94)	5.83 (6)	1.662
cCy3/P1L:cDT1	0.33 (-)	5.05 (-)	1.576
cCy3/P1L:cDT5	0.19 (70)	5.56 (30)	2.041

E.4 Circular dichroism studies

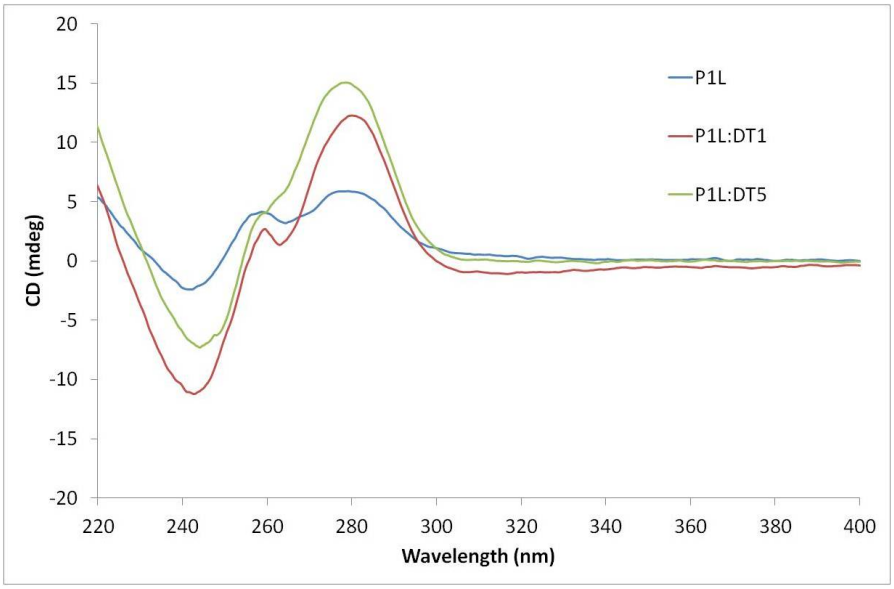

Figure E.14: Circular dichroism spectra of P1L DNA duplexes. 5 μM DNA, 100 mM NaCl, 10 mM pH 7.0 sodium phosphate buffer.

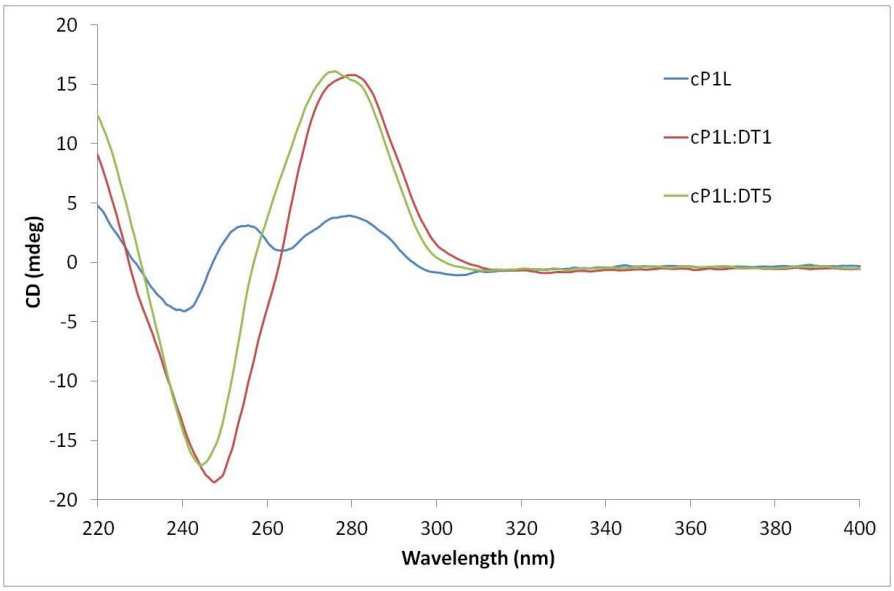

Figure E.15: Circular dichroism spectra of cP1L DNA duplexes. 5 μM DNA, 100 mM NaCl, 10 mM pH 7.0 sodium phosphate buffer.

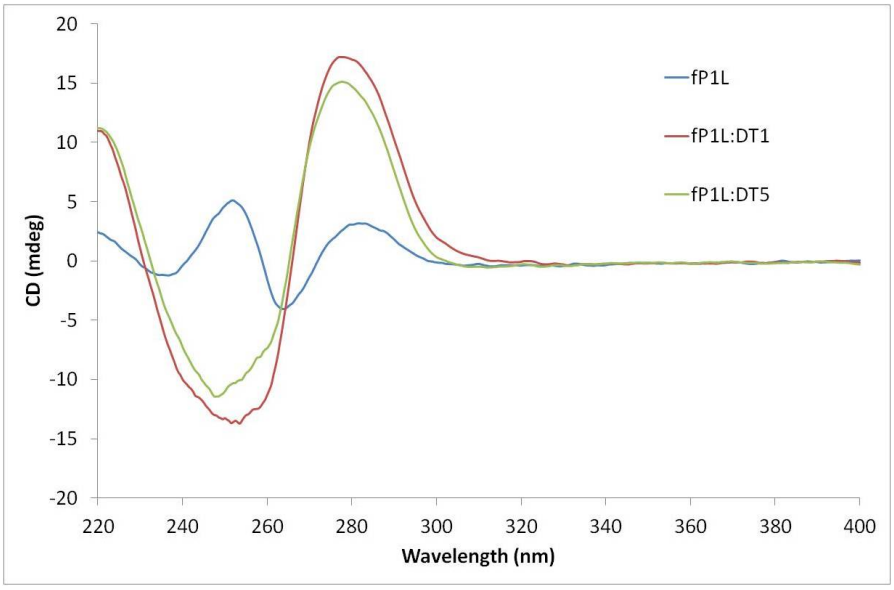

Figure E.16: Circular dichroism spectra of fP1L DNA duplexes. 5 μM DNA, 100 mM NaCl, 10 mM pH 7.0 sodium phosphate buffer.

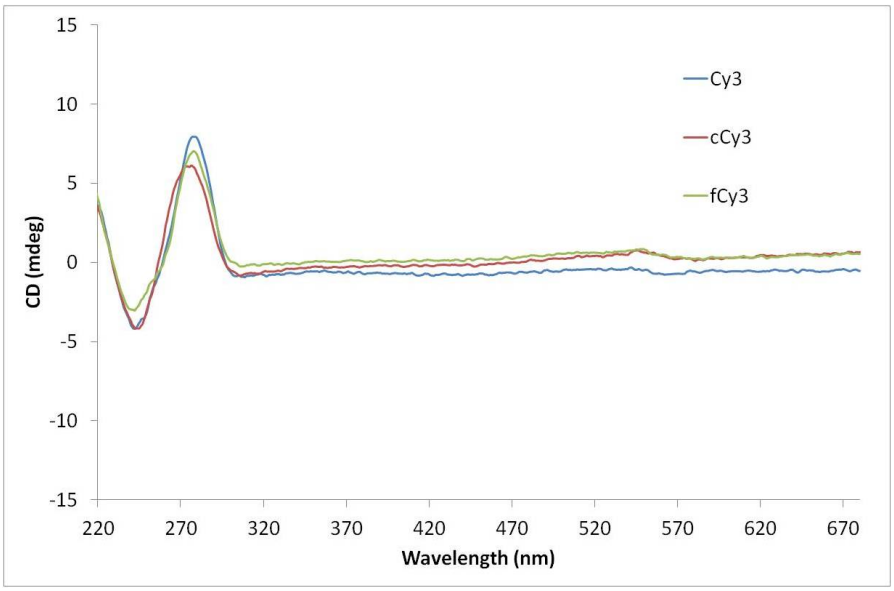

Figure E.17: Circular dichroism spectra of single stranded Cy3-only DNA probes. 5 μM DNA, 100 mM NaCl, 10 mM pH 7.0 sodium phosphate buffer.

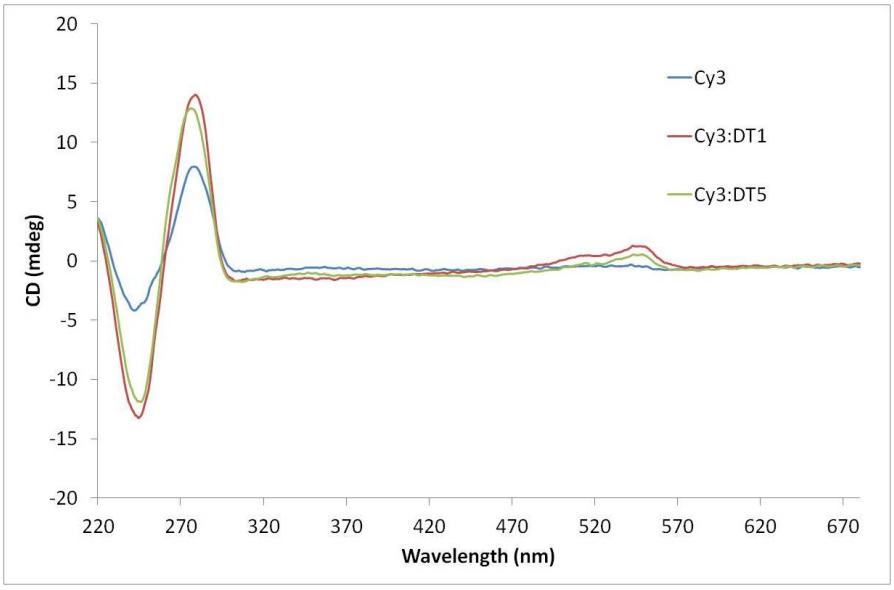

Figure E.18: Circular dichroism spectra of Cy3-only DNA duplexes. 5 μM DNA, 100 mM NaCl, 10 mM pH 7.0 sodium phosphate buffer.

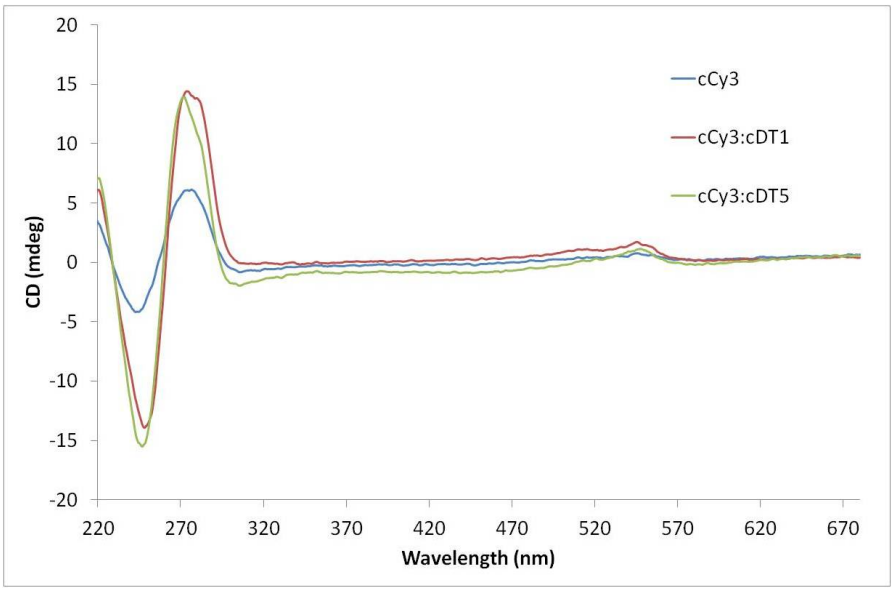

Figure E.19: Circular dichroism spectra of cCy3-only DNA duplexes. 5 μM DNA, 100 mM NaCl, 10 mM pH 7.0 sodium phosphate buffer.

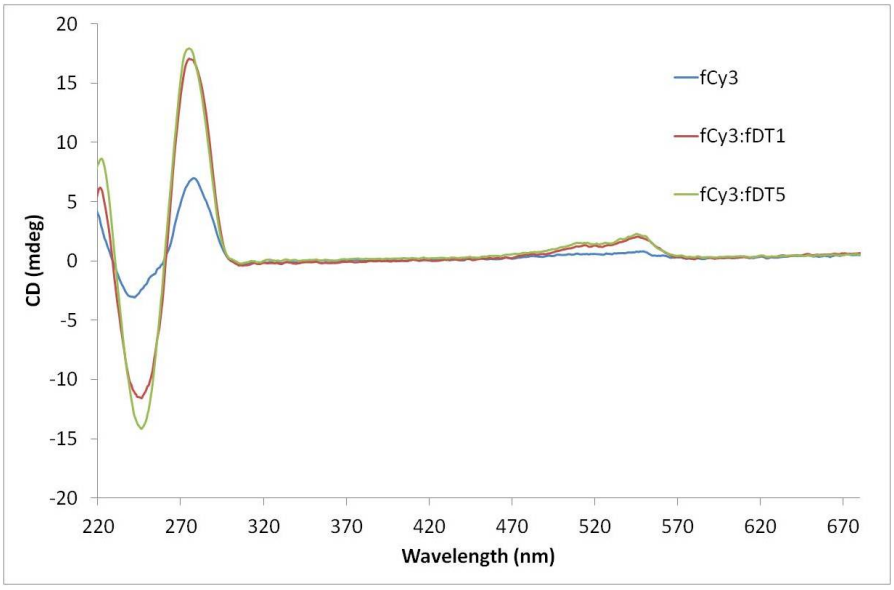

Figure E.20: Circular dichroism spectra of fCy3-only DNA duplexes. 5 μM DNA, 100 mM NaCl, 10 mM pH 7.0 sodium phosphate buffer.

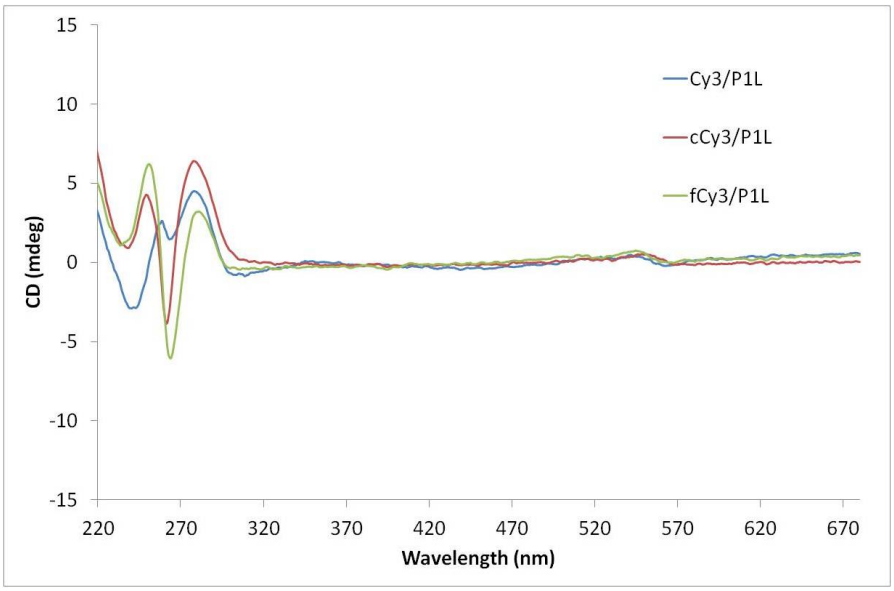

Figure E.21: Circular dichroism spectra of single stranded Cy3/P1L DNA probes. 5 μM DNA, 100 mM NaCl, 10 mM pH 7.0 sodium phosphate buffer.

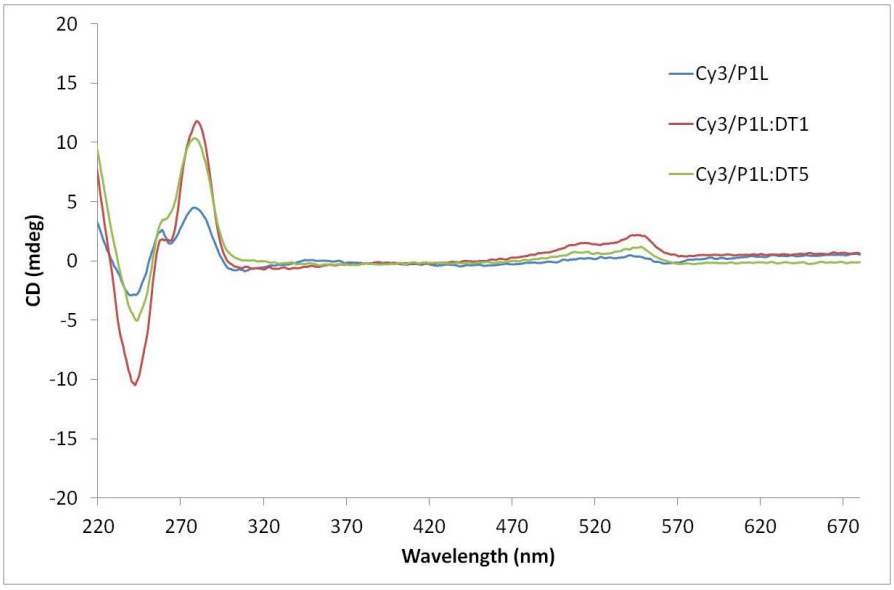

Figure E.22: Circular dichroism spectra of Cy3/P1L DNA duplexes. 5 μM DNA, 100 mM NaCl, 10 mM pH 7.0 sodium phosphate buffer.

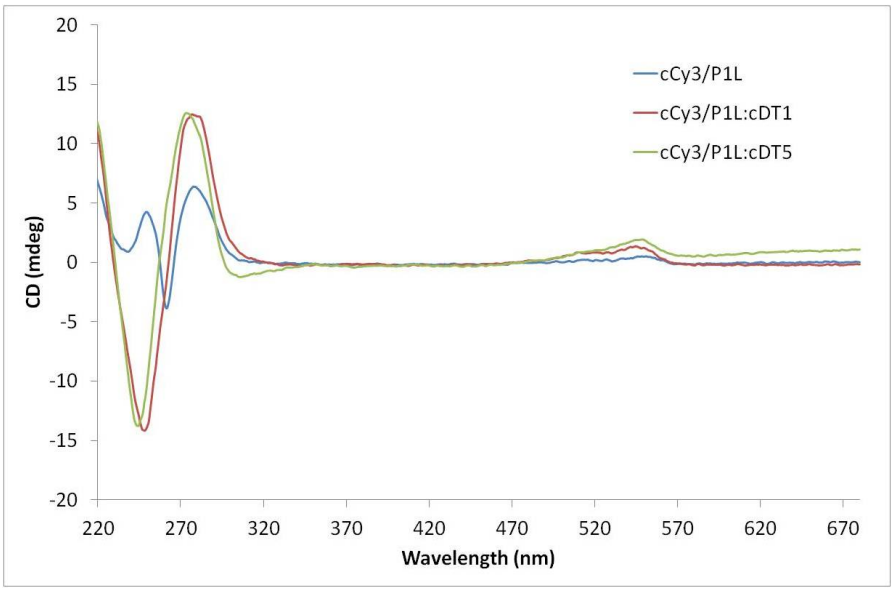

Figure E.23: Circular dichroism spectra of cCy3/P1L DNA duplexes. 5 μM DNA, 100 mM NaCl, 10 mM pH 7.0 sodium phosphate buffer

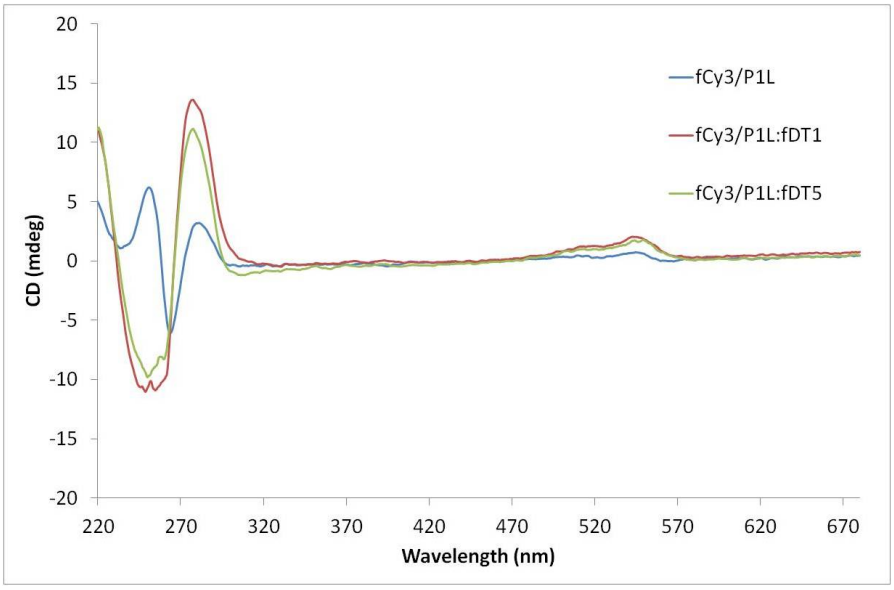

Figure E.24: Circular dichroism spectra of fCy3/P1L DNA duplexes. 5 μM DNA, 100 mM NaCl, 10 mM pH 7.0 sodium phosphate buffer

Appendix F

HPLC and mass spectrometry

HPLC preparative purification was carried out using a Dionex UVD1705 with Phenomenex Clarity 5u Oligo-RP column 150 x 10 mm. HPLC analytical purification was carried out using a Shimadzu UFLC with Phenomenex Clarity 5u Oligo-RP column 150 x 4.6 mm.

30 μl oligo samples, ca. 70 μM were auto injected. Flow rate, 1.0 ml/min, monitored at 260 nm.

TEAA: glacial acetic acid, triethyl amine, HPLC-grade water

Conditions (Thiol method): Solvent system C: MeCN; Solvent system D: 0.1 M TEAA pH 7.0. Gradient (linear increase): 0-25 mins, 5%-25% C; 25-35 mins, 25% C hold; 35-40 mins, 100% C; 40-50 mins, 5% C.

Conditions (Oligo 60 method): Solvent system A: 5% MeCN, 0.1 M TEAA pH 7.0; Solvent system B: 15% MeCN, 0.1 M TEAA pH 7.0; Solvent system C: MeCN. Gradient (linear increase): 0 - 25 mins, 30% B - 50% B; 35 - 45 mins, 0% - 100% C; 45 - 55 mins, 100% C hold; 55-60 mins, 30% B.

Conditions (DMT method): Solvent system B: 15% MeCN, 0.1 M TEAA pH 7.0; Solvent system C: MeCN. Gradient (linear increase): 0 - 10 mins, 100% B; 20 - 25 mins, 70% B; 25 - 35 mins, 100% C hold; 35 -36 mins, 100% B; 36 - 41 mins, 100% B hold.

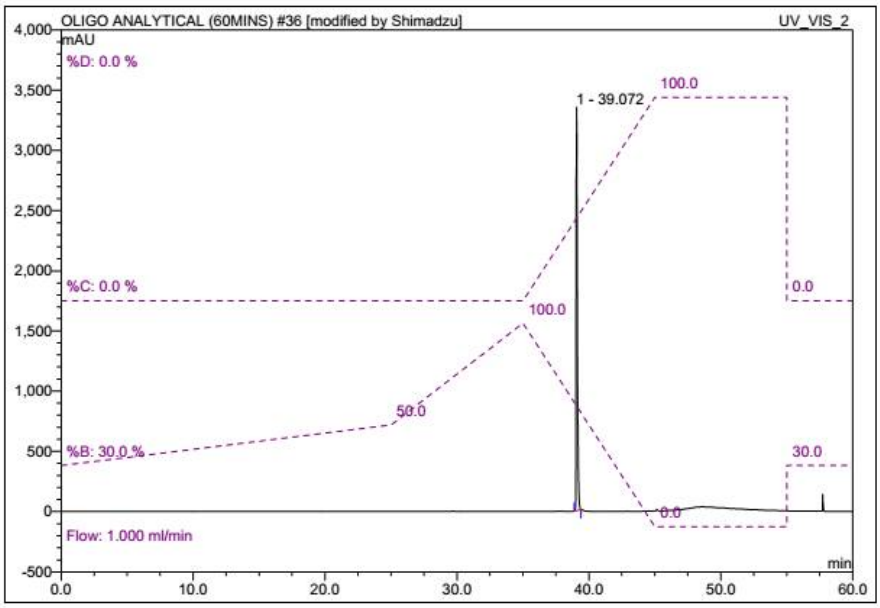

Figure F.1: P1L HPLC analytical

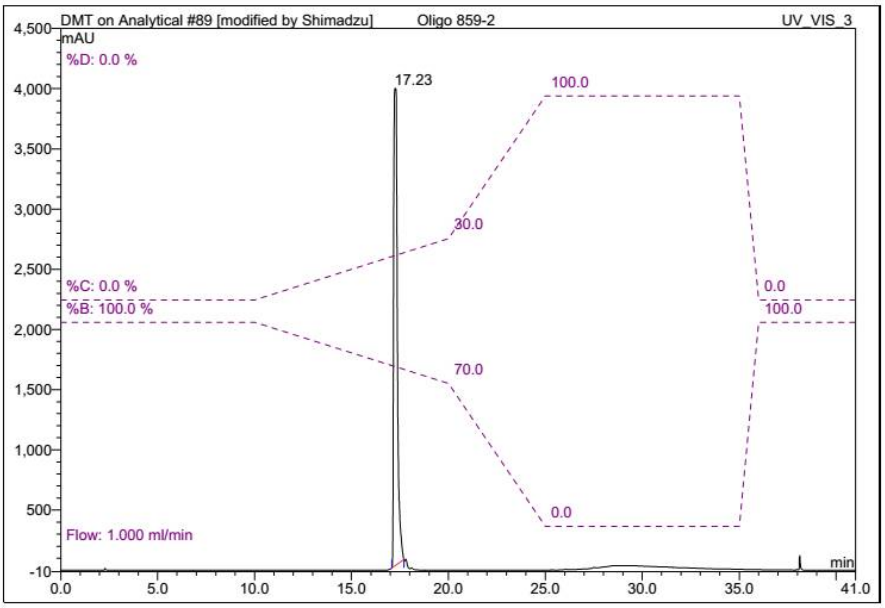

Figure F.2: P6D HPLC analytical

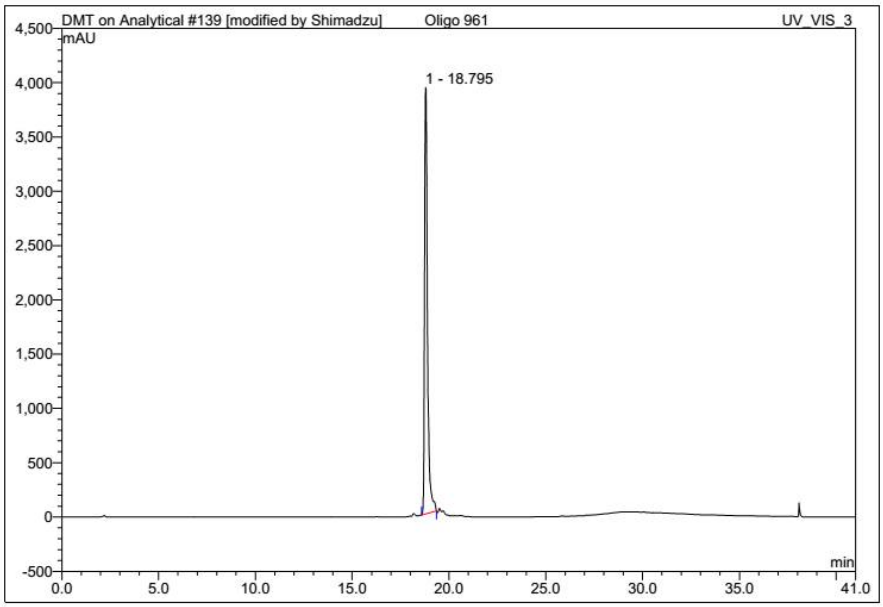

Figure F.3: S1 HPLC analytical

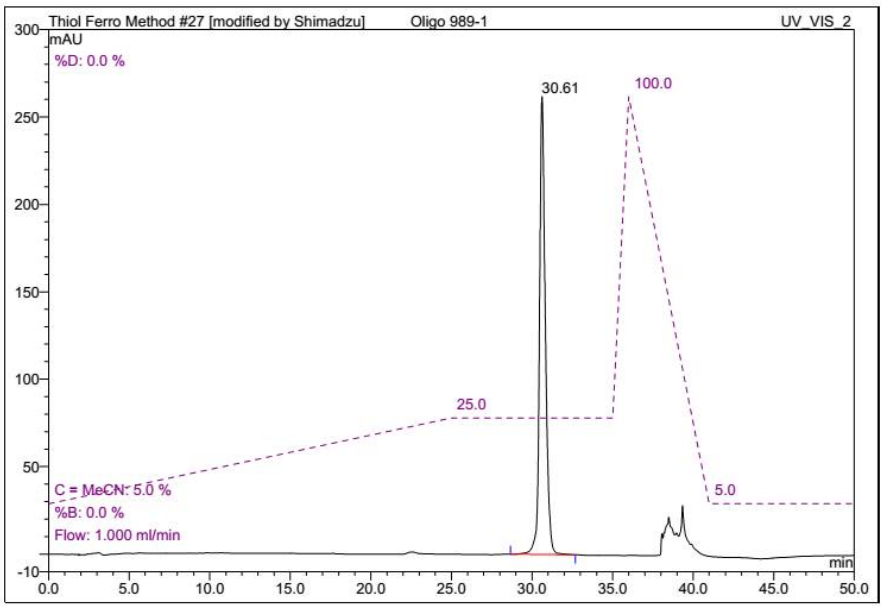

Figure F.4: S2 HPLC analytical

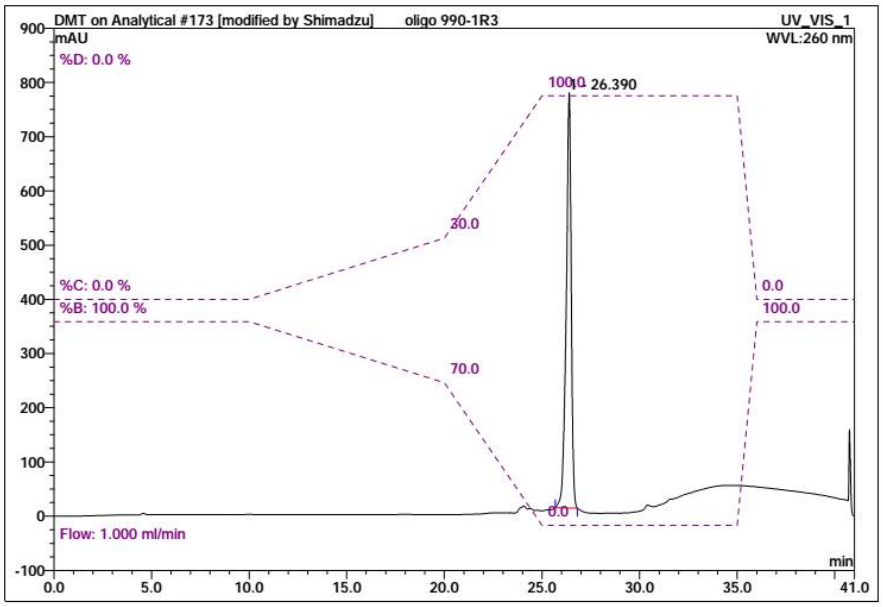

Figure F.5: S3 HPLC analytical

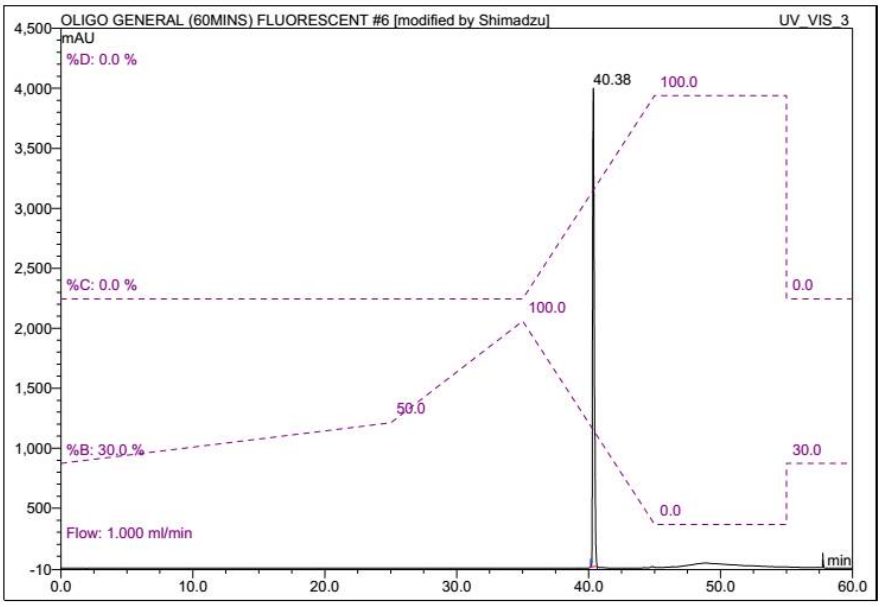

Figure F.6: S4 HPLC analytical

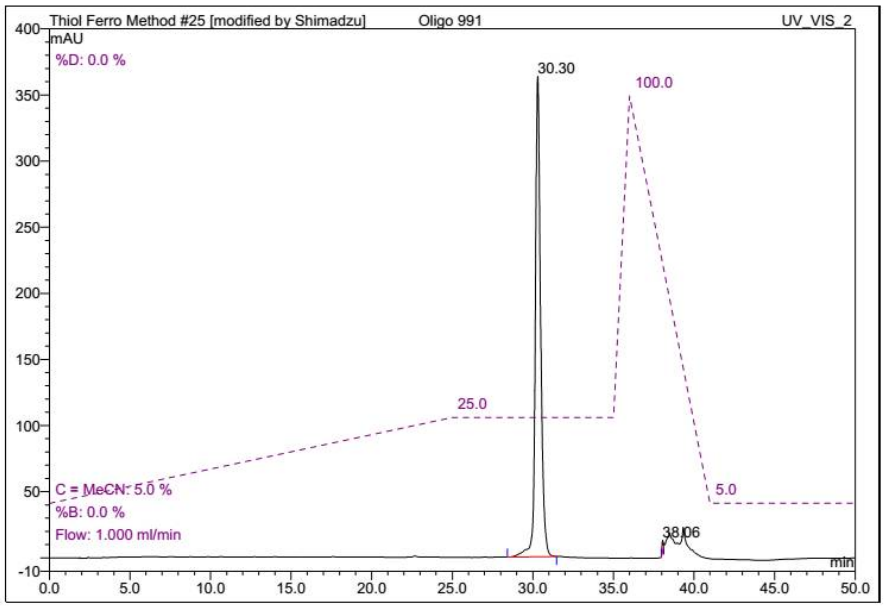

Figure F.7: S5 HPLC analytical

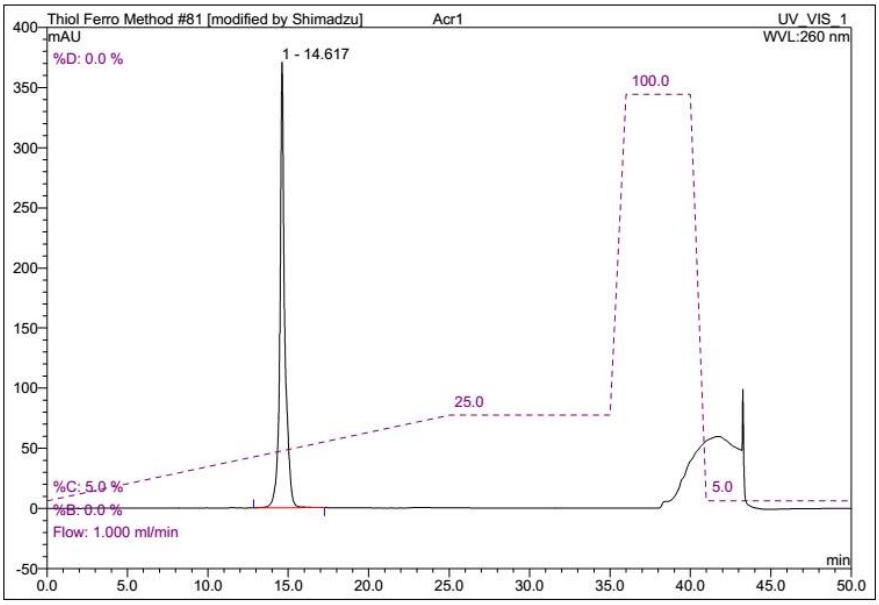

Figure F.8: PAcr HPLC analytical

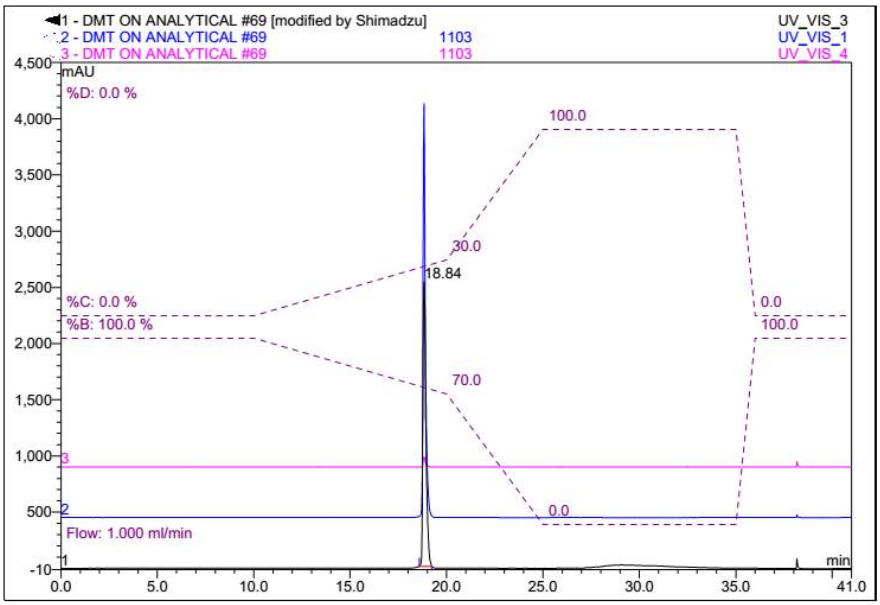

Figure F.9: Cy3/P1L HPLC analytical

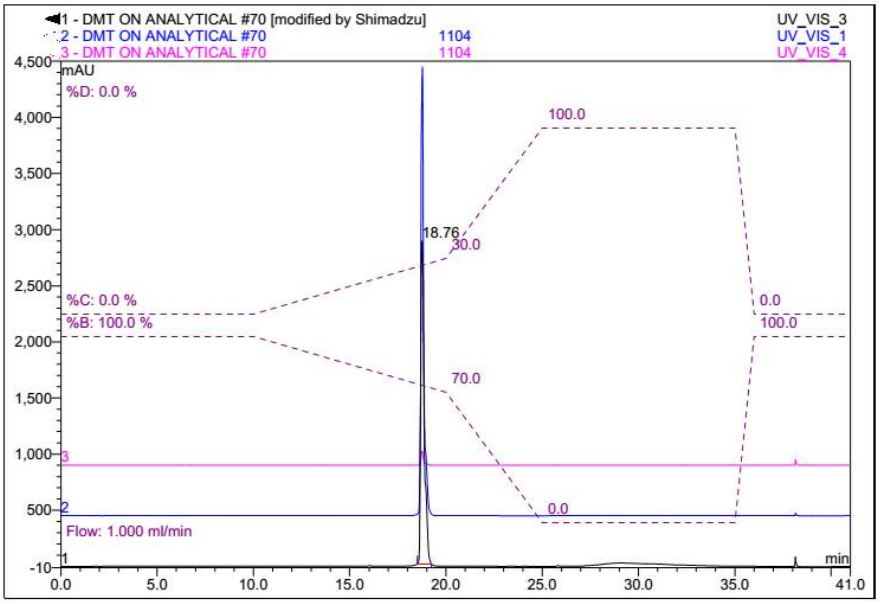

Figure F.10: cCy3/P1L HPLC analytical

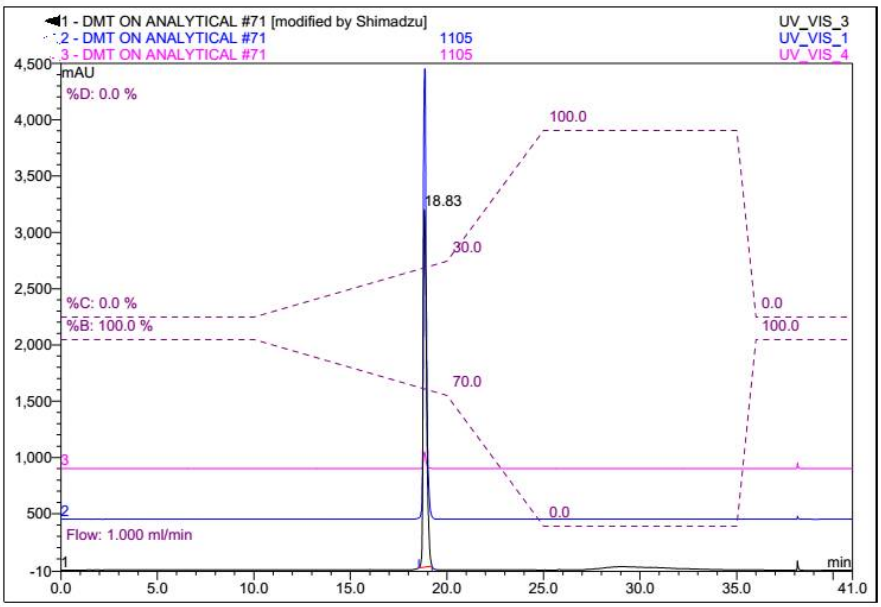

Figure F.11: fCy3/P1L HPLC analytical

Table F.1: HPLC retention times

Oligonucleotide	Sequence (5' to 3')	Retention time (mins)	HPLC Method
DN	TGGACTCTCTCAATG	24.480	Oligo40
RN	UGGACUCUCUCAAUG	16.45	Oligo60
P1L	TGGACTCXCTCAATG	39.072	Oligo60
P5L	TGGACTCXCTCAATG	16.32	DMT
P6D	TGGACTCXCTCAATG	17.23	DMT
P1LRan	GTATTCCXCTGGGAA	38.89	Oligo60
DT1	CATTGAGAGAGTCCA	20.246	Oligo40
DT2	CATTGAGGGAGTCCA	20.48	Oligo40
DT3	CATTGAGCGAGTCCA	21.61	Oligo40
DT4	CATTGAGTGAGTCCA	21.88	Oligo40
DT5	CATTGAGAAAGTCCA	21.083	Oligo40
DT6	CATTGAAAGAGTCCA	21.34	Oligo40
DT7	CATTGAGATAGTCCA	25.61	Oligo60
DT8	CATTGAGACAGTCCA	24.89	Oligo60
RT1	CAUUGAGAGAGUCCA	10.29	Thiol
RT2	CAUUGAGGGAGUCCA	10.11	Thiol
RT3	CAUUGAGCGAGUCCA	10.41	Thiol
RT4	CAUUGAGUGAGUCCA	10.72	Thiol
RT5	CAUUGAGAAAGUCCA	10.45	Thiol
RanR	CAUAAGAAGACCCUU	10.27	Thiol
RanD	GTATTCCTCTGGGAA	32.597	Oligo60
ZDN	AGTCGCGTCTCAGCT	26.24	Oligo60
ZP5L	AGTCGCGXCTCAGCT	16.47	DMT
ZDT1	AGCTGAGCCGCGACT	20.90	Oligo60
ZDT2	AGCTGAGACGCGACT	18.94	Oligo60
ZRT1	AGCUGAGCCGCGACU	10.97	Thiol
ZRT2	AGCUGAGACGCGACU	10.24	Thiol
2OMeRN	UGGACUCUCUCAAUG	15.00	Thiol
2OMeT1	CAUUGAGAGAGUCCA	15.53	Thiol
2OMeT4	CAUUGAGUGAGUCCA	15.08	Thiol
2OMeT5	CAUUGAGAAAGUCCA	15.61	Thiol
S1	Cy3-TGGACTCTCTCAATG	18.795	DMT
S2	Cy5-CATTGAGAGAGTCCA	30.614	Thiol
S3	Cy5-TGGACTCTCTCAATG-Cy3	21.323	DMT
S4	Cy3-TTTTTTTTTTTTTTTT	40.384	Oligo60
S5	Cy5-CATTGAGTGAGTCCA	30.303	Thiol
PAcr	TGGACTCYCTCAATG	14.617	Thiol
cP1L	TGGCXCACTTCAATG	37.69	Oligo60
fP1L	TGGACTTCACXCATG	38.13	Oligo60
Cy3	Cy3-TGGACTCTCTCAATG	18.795	DMT
cCy3	Cy3-TGGCTCACTTCAATG	18.71	DMT
fCy3	Cy3-TGGACTTCACTCATG	18.76	DMT
Cy3/P5L	Cy3-TGGACTCXCTCAATG	19.926	DMT
Cy3/P1L	Cy3-TGGACTCXCTCAATG	18.84	DMT
cCy3/P1L	Cy3-TGGCXCACTTCAATG	18.90	DMT
fCy3/P1L	Cy3-TGGACTTCACXCATG	18.83	DMT
cDT1	CATTGAAGTGAGCCA	29.61	Oligo60
cDT5	CATTGAAGTGAACCA	27.33	Oligo60
cDT6	CATTGAAGTAAGCCA	23.18	Oligo60
fDT1	CATGAGTGAAGTCCA	29.35	Oligo60
fDT5	CATGAATGAAGTCCA	27.35	Oligo60
fDT6	CATAAGTGAAGTCCA	23.26	Oligo60

Table F.2: Mass spectrometry predicted and actual values

Oligonucleotide	Sequence (5' to 3')	Predicted mass	Actual mass
DN	TGGACTCTCTCAATG	4543	4543
RN	UGGACUCUCUCAAUG	4713	4715
P1L	TGGACTCXCTCAATG	4640	4640
P5L	TGGACTCXCTCAATG	4708	4708
P6D	TGGACTCXCTCAATG	4710	4710
P1LRan	GTATTCCXCTGGGAA	4679	4680
DT1	CATTGAGAGAGTCCA	4601	4601
DT2	CATTGAGGGAGTCCA	4617	4618
DT3	CATTGAGCGAGTCCA	4577	4578
DT4	CATTGAGUGAGTCCA	4592	4593
DT5	CATTGAGAAAGTCCA	4585	4585
DT6	CATTGAAAGAGTCCA	4585	4585
DT7	CATTGAGATAGTCCA	4576	4576
DT8	CATTGAGACAGTCCA	4561	4561
RT1	CAUUGAGAGAGUCCA	4799	4799
RT2	CAUUGAGGGAGUCCA	4814	4814
RT3	CAUUGAGCGAGUCCA	4774	4775
RT4	CAUUGAGUGAGUCCA	4775	4776
RT5	CAUUGAGAAAGUCCA	4783	4783
RanR	CAUAAGAAGACCCUU	4742	4743
RanD	GTATTCCTCTGGGAA	4583	4583
ZDN	AGTCGCGTCTCAGCT	4544	4544
ZP5L	AGTCGCGXCTCAGCT	4696	4697
ZDT1	AGCTGAGCCGCGACT	4578	4577
ZDT2	AGCTGAGACGCGACT	4601	4602
ZRT1	AGCUGAGCCGCGACU	4790	4790
ZRT2	AGCUGAGACGCGACU	4814	4814
2OMeRN	UGGACUCUCUCAAUG	4963	4963
2OMeT1	CAUUGAGAGAGUCCA	5021	5021
2OMeT4	CAUUGAGUGAGUCCA	5012	5012
2OMeT5	CAUUGAGAAAGUCCA	5005	5005
S1	Cy3-TGGACTCTCTCAATG	5050	5050
S2	Cy5-CATTGAGAGAGTCCA	5134	5133
S3	Cy5-TGGACTCTCTCAATG-Cy3	5583	5182
S4	Cy3-TTTTTTTTTTTTTTT	5312	5312
S5	Cy5-CATTGAGTGAGTCCA	5125	5124
PAcr	TGGACTCYCTCAATG	4689	4690
cP1L	TGGCXCACTTCAATG	4640	4641
fP1L	TGGACTTCACXCATG	4640	4641
Cy3	Cy3-TGGACTCTCTCAATG	5050	5050
cCy3	Cy3-TGGCTCACTTCAATG	5050	5051
fCy3	Cy3-TGGACTTCACTCATG	5050	5051
Cy3/P5L	Cy3-TGGACTCXCTCAATG	5203	5203
Cy3/P1L	Cy3-TGGACTCXCTCAATG	5147	5148
cCy3/P1L	Cy3-TGGCXCACTTCAATG	5147	5148
fCy3/P1L	Cy3-TGGACTTCACXCATG	5147	5148
cDT1	CATTGAAGTGAGCCA	4601	4601
cDT5	CATTGAAGTGAACCA	4585	4585
cDT6	CATTGAAGTAAGCCA	4585	4585
fDT1	CATGAGTGAAGTCCA	4601	4601
fDT5	CATGAATGAAGTCCA	4585	4586
fDT6	CATAAGTGAAGTCCA	4585	4585

Appendix G

List of oligonucleotides

Table G.1 summarises all oligonucleotides and their sequences used throughout. P (n)(L/D) refers to the modified probe where n is the carbon linker length and L/D is the stereochemistry. Within the sequence, X identifies the position of the modification.

Table G.1: Oligonucleotide Sequences. X denotes the anthracene monomer. Y denotes the acridine monomer. n is the carbon linker length and L/D denotes the stereochemistry.

Oligonucleotide	Sequence (5' to 3')
DN	TGGACTCTCTCAATG
RN	UGGACUCUCUCAAUG
P(n)(L/D)	TGGACTCXCTCAATG
P1LRan	GTATTCCXCTGGGAA
DT1	CATTGAGAGAGTCCA
DT2	CATTGAGGGAGTCCA
DT3	CATTGAGCGAGTCCA
DT4	CATTGAGTGAGTCCA
DT5	CATTGAGAAAGTCCA
DT6	CATTGAAAGAGTCCA
DT7	CATTGAGATAGTCCA
DT8	CATTGAGACAGTCCA
RT1	CAUUGAGAGAGUCCA
RT2	CAUUGAGGGAGUCCA
RT3	CAUUGAGCGAGUCCA
RT4	CAUUGAGUGAGUCCA
RT5	CAUUGAGAAAGUCCA
RanR	CAUAAGAAGACCCUU
RanD	GTATTCCTCTGGGAA
ZDN	AGTCGCGTCTCAGCT
ZP(n)(L/D)	AGTCGCGXCTCAGCT
ZDT1	AGCTGAGCCGCGACT
ZDT2	AGCTGAGACGCGACT
ZRT1	AGCUGAGCCGCGACU
ZRT2	AGCUGAGACGCGACU
2OMeRN	UGGACUCUCUCAAUG
2OMeT1	CAUUGAGAGAGUCCA
2OMeT4	CAUUGAGUGAGUCCA
2OMeT5	CAUUGAGAAAGUCCA
S1	Cy3-TGGACTCTCTCAATG
S2	Cy5-CATTGAGAGAGTCCA
S3	Cy5-TGGACTCTCTCAATG-Cy3
S4	Cy3-TTTTTTTTTTTTTTT
S5	Cy5-CATTGAGTGAGTCCA
PAcr	TGGACTCYCTCAATG
PSDT1	CATTGAGAGAGTCCA
PLDT1	CATTGAGAGAGTCCA x10 repeats
PSDT5	CATTGAGAAAGTCCA
PLDT5	CATTGAGAAAGTCCA x10 repeats
cP1L	TGGCXCACTTCAATG
fP1L	TGGACTTCACXCATG
Cy3	Cy3-TGGACTCTCTCAATG
cCy3	Cy3-TGGCTCACTTCAATG
fCy3	Cy3-TGGACTTCACTCATG
Cy3/P5L	Cy3-TGGACTCXCTCAATG
Cy3/P1L	Cy3-TGGACTCXCTCAATG
cCy3/P1L	Cy3-TGGCXCACTTCAATG
fCy3/P1L	Cy3-TGGACTTCACXCATG
cDT1	CATTGAAGTGAGCCA
cDT5	CATTGAAGTGAACCA
cDT6	CATTGAAGTAAGCCA
fDT1	CATGAGTGAAGTCCA
fDT5	CATGAATGAAGTCCA
fDT6	CATAAGTGAAGTCCA

Bibliography

[1] J. D. Watson and F. H. C. Crick. Molecular Structure of Nucleic Acids: A Structure for Deoxyribose Nucleic Acid. *Nature*, 171:737–738, 1953.

[2] G. M. Blackburn, M. J. Gait, D. Loakes, and D. M. Williams. *Nucleic Acids in Chemistry and Biology*. RSC Publishing, 2006.

[3] R. W. Roberts and D. M. Crothers. Stability and properties of double and triple helices: dramatic effects of RNA or DNA backbone composition. *Science*, 258:1463–6, 1992.

[4] K. Bondensgaard, M. Petersen, S. K. Singh, V. K. Rajwanshi, R. Kumar, J. Wengel, and J. P. Jacobsen. Structural Studies of LNA:RNA Duplexes by NMR: Conformations and Implications for RNase H Activity. *Chem. - A Eur. J.*, 6:2687–2695, 2000.

[5] F. Darfeuille, J. B. Hansen, H. Orum, C. Di Primo, and J. J. Toulmé. LNA/DNA chimeric oligomers mimic RNA aptamers targeted to the TAR RNA element of HIV-1. *Nucleic Acids Res.*, 32:3101–3107, 2004.

[6] A. Okamoto, Y. Saito, and I. Saito. Design of base-discriminating fluorescent nucleosides. *J. Photochem. Photobiol. C Photochem. Rev.*, 6:108–122, 2005.

[7] R. W. Sinkeldam, N. J. Greco, and Y. Tor. Fluorescent analogs of biomolecular

building blocks: design, properties, and applications. *Chem. Rev.*, 110:2579–619, 2010.

[8] Y. Xie, T. Maxson, and Y. Tor. Fluorescent nucleoside analogue displays enhanced emission upon pairing with guanine. *Org. Biomol. Chem.*, 8:5053–5, 2010.

[9] C. Thibaudeau, J. Plavec, N. Garg, A. Papchikhin, and J. Chattopadhyaya. How Does the Electronegativity of the Substituent Dictate the Strength of the Gauche Effect? *J. Am. Chem. Soc.*, 116:4038–4043, 1994.

[10] C. Molenaar, S. A. Marras, J. C. Slats, J. C. Truffert, M. Lemaître, A. K. Raap, R. W. Dirks, and H. J. Tanke. Linear 2' O-Methyl RNA probes for the visualization of RNA in living cells. *Nucleic Acids Res.*, 29:E89–E89, 2001.

[11] M. Majlessi, N. C. Nelson, and M. M. Becker. Advantages of 2'-O-methyl oligoribonucleotide probes for detecting RNA targets. *Nucleic Acids Res.*, 26:2224–9, 1998.

[12] B. Valeur. *Molecular Fluorescence: Principles and Applications.* Wiley-VCH, 2002.

[13] J. R. Lakowicz. *Principles of Fluorescence Spectroscopy.* Springer, 2006.

[14] T. Ha. Single-molecule fluorescence methods for the study of nucleic acids. *Curr. Opin. Struct. Biol.*, 11:287–292, 2001.

[15] D. Dodd and R. Hudson. Intrinsically Fluorescent Base-Discriminating Nucleoside Analogs. *Mini. Rev. Org. Chem.*, 6:378–391, 2009.

[16] P. Cekan and S. T. Sigurdsson. Single base interrogation by a fluorescent nucleotide: each of the four DNA bases identified by fluorescence spectroscopy. *Chem. Commun.*, 29:3393–3395, 2008.

[17] U. Asseline, M. Chassignol, Y. Aubert, and V. Roig. Detection of terminal mismatches on DNA duplexes with fluorescent oligonucleotides. *Org. Biomol. Chem.*, 4:1949–1957, 2006.

[18] T. Kubota, S. Ikeda, H. Yanagisawa, M. Yuki, and A. Okamoto. Hybridization-sensitive fluorescent probe for long-term monitoring of intracellular RNA. *Bioconjug. Chem.*, 20:1256–61, 2009.

[19] L. Bethge, I. Singh, and O. Seitz. Designed thiazole orange nucleotides for the synthesis of single labelled oligonucleotides that fluoresce upon matched hybridization. *Org. Biomol. Chem.*, 8:2439–2448, 2010.

[20] O. Köhler and O. Seitz. Thiazole orange as fluorescent universal base in peptide nucleic acids. *Chem. Commun. (Camb).*, 23:2938–2939, 2003.

[21] D.-L. Ma, H.-Z. He, K.-H. Leung, H.-J. Zhong, D. S.-H. Chan, and C.-H. Leung. Label-free luminescent oligonucleotide-based probes. *Chem. Soc. Rev.*, 42:3427–40, 2013.

[22] T. Forster. Energiewanderung und Fluoreszenz. *Naturwissenschaften*, 33:166–175, 1946.

[23] B. W. van der Meer, G. Coker III, and S.-Y. S. Chen. *Resonance Energy Transfer: Theory and Data*. VCH, New York, 1994.

[24] A. Iqbal, S. Arslan, B. Okumus, T. J. Wilson, G. Giraud, D. G. Norman, T. Ha, and D. M. J. Lilley. Orientation dependence in fluorescent energy transfer between Cy3 and Cy5 terminally attached to double-stranded nucleic acids. *Proc. Natl. Acad. Sci. U. S. A.*, 105:11176–81, 2008.

[25] A. M. Blanco, L. Rausell, B. Aguado, M. Perez-Alonso, and R. Artero. A FRET-

based assay for characterization of alternative splicing events using peptide nucleic acid fluorescence in situ hybridization. *Nucleic Acids Res.*, 37:e116, 2009.

[26] T. Heinlein, J.-P. Knemeyer, O. Piestert, and M. Sauer. Photoinduced Electron Transfer between Fluorescent Dyes and Guanosine Residues in DNA-Hairpins. *J. Phys. Chem. B*, 107:7957–7964, 2003.

[27] C.-Y. Zhang, H.-C. Yeh, M. T. Kuroki, and T.-H. Wang. Single-quantum-dot-based DNA nanosensor. *Nat. Mater.*, 4:826–831, 2005.

[28] S. A. Uhler, D. Cai, Y. Man, C. Figge, and N. G. Walter. RNA Degradation in Cell Extracts: Real-Time Monitoring by Fluorescence Resonance Energy Transfer. *J. Am. Chem. Soc.*, 125:14230–14231, 2003.

[29] V. B. Pinheiro, A. I. Taylor, C. Cozens, M. Abramov, M. Renders, S. Zhang, J. C. Chaput, J. Wengel, S.-Y. Peak-Chew, S. H. McLaughlin, P. Herdewijn, and P. Holliger. Synthetic Genetic Polymers Capable of Heredity and Evolution. *Science*, 336:341–344, 2012.

[30] J. C. Delaney, P. T. Henderson, S. A. Helquist, J. C. Morales, J. M. Essigmann, and E. T. Kool. High-fidelity in vivo replication of DNA base shape mimics without Watson-Crick hydrogen bonds. *Proc. Natl. Acad. Sci. U. S. A.*, 100:4469–4473, 2003.

[31] R. W. Dirks and H. J. Tanke. Advances in fluorescent tracking of nucleic acids in living cells. *Biotechniques*, 40:489–496, 2006.

[32] B. Armitage, T. Koch, H. Frydenlund, H. Ø rum, and G. B. Schuster. Peptide nucleic acid (PNA)/DNA hybrid duplexes: Intercalation by an internally linked anthraquinone. *Nucleic Acids Res.*, 26:715–720, 1998.

[33] J.-L. H. A. Duprey. *Studies on Anthracene Tagged Oligonucleotides.* PhD thesis, University of Birmingham, 2010.

[34] H. V. Nguyen, Z.-Y. Zhao, A. Sallustrau, S. L. Horswell, L. Male, A. Mulas, and J. H. R. Tucker. A ferrocene nucleic acid oligomer as an organometallic structural mimic of DNA. *Chem. Commun.*, 48:12165, 2012.

[35] H. V. Nguyen, A. Sallustrau, L. Male, P. J. Thornton, and J. H. R. Tucker. 1,1'-homodisubstituted ferrocenes containing adenine and thymine nucleobases: Synthesis, electrochemistry, and formation of H-bonded arrays. *Organometallics*, 30:5284–5290, 2011.

[36] J.-L. H. A. Duprey and J. H. R. Tucker. Metal-Carbon Bonds in Biopolymer Conjugates: Bioorganometallic Nucleic Acid Chemistry. *Chem. Lett.*, 43:157–163, 2014.

[37] B. Nordén, A. Rodger, and T. Dafforn. *Linear Dichroism and Circular Dichroism: A Textbook on Polarized-Light Spectroscopy.* RSC Publishing, 2010.

[38] R. T. Ranasinghe and T. Brown. Fluorescence based strategies for genetic analysis. *Chem. Commun.*, 44:5487–502, 2005.

[39] M. Cargill, D. Altshuler, J. Ireland, P. Sklar, K. Ardlie, N. Patil, N. Shaw, C. R. Lane, E. P. Lim, N. Kalyanaraman, J. Nemesh, L. Ziaugra, L. Friedland, A. Rolfe, J. Warrington, R. Lipshutz, G. Q. Daley, and E. S. Lander. Characterization of single-nucleotide polymorphisms in coding regions of human genes. *Nat. Genet.*, 22:231–8, 1999.

[40] S. Kim and A. Misra. SNP genotyping: technologies and biomedical applications. *Annu. Rev. Biomed. Eng.*, 9:289–320, 2007.

[41] Anthony J Brookes. Single Nucleotide Polymorphism (SNP). In *Encycl. life Sci.* 2009.

[42] K. Nakatani. Chemistry challenges in SNP typing. *Chembiochem*, 5:1623–33, 2004.

[43] D. J. Schaid, J. C. Guenther, G. B. Christensen, S. Hebbring, C. Rosenow, C. A. Hilker, S. K. McDonnell, J. M. Cunningham, S. L. Slager, M. L. Blute, and S. N. Thibodeau. Comparison of microsatellites versus single-nucleotide polymorphisms in a genome linkage screen for prostate cancer-susceptibility Loci. *Am. J. Hum. Genet.*, 75:948–65, 2004.

[44] N. Shenker and J. M. Flanagan. Intragenic DNA methylation: implications of this epigenetic mechanism for cancer research. *Br. J. Cancer*, 106:248–53, 2012.

[45] Z. Nagy. The dysregulation of the cell cycle and the diagnosis of Alzheimer's disease. *Biochim. Biophys. Acta*, 1772:402–8, 2007.

[46] P. Hollingworth, D. Harold, L. Jones, M. J. Owen, and J. Williams. Alzheimer's disease genetics: current knowledge and future challenges. *Int. J. Geriatr. Psychiatry*, 26:793–802, 2011.

[47] P. Y. Kwok and Z. Gu. Single nucleotide polymorphism libraries: Why and how are we building them? *Trends Mol. Med.*, 5:538–543, 1999.

[48] R. M. Twyman. SNP discovery and typing techniques for pharmacogenomics. *Curr. Top. Med. Chem.*, 4:1423–1431, 2004.

[49] T. R. Bhangale, M. J. Rieder, R. J. Livingston, and D. A. Nickerson. Comprehensive identification and characterization of diallelic insertion-deletion polymorphisms in 330 human candidate genes. *Hum. Mol. Genet.*, 14:59–69, 2005.

[50] J. M. Mullaney, R. E. Mills, W. S. Pittard, and S. E. Devine. Small insertions and deletions (INDELs) in human genomes. *Hum. Mol. Genet.*, 19:R131–R136, 2010.

[51] N. J. Greco, R. W. Sinkeldam, and Y. Tor. An emissive C analog distinguishes between G, 8-oxoG, and T. *Org. Lett.*, 11:1115–1118, 2009.

[52] S. Kriaucionis and N. Heintz. The nuclear DNA base 5-hydroxymethylcytosine is present in Purkinje neurons and the brain. *Science*, 324:929–930, 2009.

[53] J. J. McCarthy and R. Hilfiker. The use of single-nucleotide polymorphism maps in pharmacogenomics. *Nat. Biotechnol.*, 18:505–8, 2000.

[54] L. J. Engle, C. L. Simpson, and J. E. Landers. Using high-throughput SNP technologies to study cancer. *Oncogene*, 25:1594–601, 2006.

[55] D. J. French, C. L. Archard, T. Brown, and D. G. McDowell. HyBeacon probes: a new tool for DNA sequence detection and allele discrimination. *Mol. Cell. Probes*, 15:363–374, 2001.

[56] D. M. Kolpashchikov. Binary probes for nucleic acid analysis. *Chem. Rev.*, 110:4709–23, 2010.

[57] K. Okabe, Y. Harada, J. Zhang, H. Tadakuma, T. Tani, and T. Funatsu. Real time monitoring of endogenous cytoplasmic mRNA using linear antisense 2'-O-methyl RNA probes in living cells. *Nucleic Acids Res.*, 39:e20, 2011.

[58] D. J. Kleinbaum and E. T. Kool. Sandwich probes: two simultaneous reactions for templated nucleic acid detection. *Chem. Commun.*, 46:8154–6, 2010.

[59] S. Tyagi and F. R. Kramer. Molecular beacons: probes that fluoresce upon hybridisation. *Nat. Biotechnol.*, 14:303–308, 1996.

[60] P. Zhang, T. Beck, and W. Tan. Design of a Molecular Beacon DNA Probe with Two Fluorophores. 2194:402–405, 2001.

[61] S. Tyagi, D. P. Bratu, and F. R. Kramer. Multicolor molecular beacons for allele discrimination. *Nat. Biotechnol.*, 16:49–53, 1998.

[62] J. F. Hopkins and S. A. Woodson. Molecular beacons as probes of RNA unfolding under native conditions. *Nucleic Acids Res.*, 33:5763–5770, 2005.

[63] J. Guo, J. Ju, and N. J. Turro. Fluorescent hybridization probes for nucleic acid detection. *Anal. Bioanal. Chem.*, 402:3115–25, 2012.

[64] A. K. White, M. Vaninsberghe, O. I. Petriv, M. Hamidi, D. Sikorski, M. A. Marra, J. Piret, S. Aparicio, and C. L. Hansen. High-throughput microfluidic single-cell RT-qPCR. *Proc. Natl. Acad. Sci. U. S. A.*, 108:13999–14004, 2011.

[65] R. S. Cha and W. G. Thilly. Specificity, Efficiency and Fidelity of PCR. *PCR Methods Appl.*, 3:18–29, 1993.

[66] C. Lui, N. C. Cady, and C. A. Batt. Nucleic acid-based detection of bacterial pathogens using integrated microfluidic platform systems. *Sensors*, 9:3713–3744, 2009.

[67] F. E. A. McGuigan and S. H. Ralston. Single nucleotide polymorphism detection: allelic discrimination using TaqMan. *Psychiatr. Genet.*, 12:133–6, 2002.

[68] M. J. Espy, J. R. Uhl, L. M. Sloan, S. P. Buckwalter, M. F. Jones, E. A. Vetter, J. D. C. Yao, N. L. Wengenack, J. E. Rosenblatt, F. R. Cockerill, and T. F. Smith. Real-time PCR in clinical microbiology: applications for routine laboratory testing. *Clin. Microbiol. Rev.*, 19:165–256, 2006.

[69] E. V. Volpi and J. M. Bridger. FISH glossary: an overview of the fluorescence in situ hybridization technique. *Biotechniques*, 45:385–6, 388, 390 passim, 2008.

[70] A. Raj, P. van den Bogaard, S. A. Rifkin, A. van Oudenaarden, and S. Tyagi. Imaging individual mRNA molecules using multiple singly labeled probes. *Nat. Methods*, 5:877–9, 2008.

[71] D. O. Wang, H. Matsuno, S. Ikeda, A. Nakamura, H. Yanagisawa, Y. Hayashi, and A. Okamoto. A quick and simple FISH protocol with hybridization-sensitive fluorescent linear oligodeoxynucleotide probes. *RNA*, 18:166–75, 2012.

[72] L. S. Yilmaz, S. Parnerkar, and D. R. Noguera. MathFISH, a web tool that uses thermodynamics-based mathematical models for in silico evaluation of oligonucleotide probes for fluorescence in situ hybridization. *Appl. Environ. Microbiol.*, 77:1118–1122, 2011.

[73] M. R. Speicher and N. P. Carter. The new cytogenetics: blurring the boundaries with molecular biology. *Nat. Rev. Genet.*, 6:782–792, 2005.

[74] H.-C. Becker and B. Nordén. DNA Binding Mode and Sequence Specificity of Piperazinylcarbonyloxyethyl Derivatives of Anthracene and Pyrene. *J. Am. Chem. Soc.*, 121:11947–11952, 1999.

[75] G. W. Breton and X. Vang. Photodimerization of Anthracene. *J. Chem. Educ.*, 75:81–82, 1998.

[76] Y. Molard, D. M. Bassani, J.-P. Desvergne, N. Moran, and J. H. R. Tucker. Structural effects on the ground and excited-state properties of photoswitchable hydrogen-bonding receptors. *J. Org. Chem.*, 71:8523–31, 2006.

[77] J. Manchester, D. M. Bassani, J.-L. H. A. Duprey, L. Giordano, J. S. Vyle, Z.-Y. Zhao, and J. H. R. Tucker. Photocontrolled binding and binding-controlled photochromism within anthracene-modified DNA. *J. Am. Chem. Soc.*, 134:10791–4, 2012.

[78] Y. Chen and M. D. Barkley. Toward understanding tryptophan fluorescence in proteins. *Biochemistry*, 37:9976–82, 1998.

[79] K. Yamana, R. Aota, and H. Nakano. Oligonucleotides having covalently linked anthracene at specific sugar residue: Differential binding to DNA and RNA and fluorescence properties. *Tetrahedron Lett.*, 36:8427–8430, 1995.

[80] H. Kashida, X. Liang, and H. Asanuma. Rational design of functional DNA with a non-ribose acyclic scaffold. *Curr. Org. Chem.*, 13:1065–1084, 2009.

[81] N. Moran, D. M. Bassani, J.-P. Desvergne, S. Keiper, P. A. S. Lowden, J. S. Vyle, and J. H. R. Tucker. Detection of a single DNA base-pair mismatch using an anthracene-tagged fluorescent probe. *Chem. Commun.*, 48:5003–5, 2006.

[82] H. Kashida, H. Asanuma, and M. Komiyama. Insertion of two pyrene moieties into oligodeoxyribonucleotides for the efficient detection of deletion polymorphisms. *Chem. Commun.*, 1:2768–2770, 2006.

[83] K. Fukui, K. Tanaka, M. Fujitsuka, A. Watanabe, and O. Ito. Distance dependence of electron transfer in acridine-intercalated DNA. *J. Photochem. Photobiol. B Biol.*, 50:18–27, 1999.

[84] H. Asanuma, M. Akahane, N. Kondo, T. Osawa, T. Kato, and H. Kashida. Quencher-free linear probe with multiple fluorophores on an acyclic scaffold. *Chem. Sci.*, 3:3165, 2012.

[85] Y. Saito, Y. Miyauchi, A. Okamoto, and I. Saito. Base-discriminating fluorescent (BDF) nucleoside: distinction of thymine by fluorescence quenching. *Chem. Commun.*, pages 1704–1705, 2004.

[86] J.-L. H. A. Duprey, Z.-Y. Zhao, D. M. Bassani, J. Manchester, J. S. Vyle, and J. H. R. Tucker. Detection of DNA base variation and cytosine methylation at a single nucleotide site using a highly sensitive fluorescent probe. *Chem. Commun.*, 47:6629–31, 2011.

[87] J.-L. H. A. Duprey, D. M. Bassani, E. I. Hyde, C. Ludwig, A. Rodger, J. S. Vyle, J. Wilkie, Z.-Y. Zhao, and J. H. R. Tucker. Anthracene-modified oligonucleotides as fluorescent DNA mismatch sensors: discrimination between various base-pair mismatches. *Supramol. Chem.*, 23:273–277, 2011.

[88] Z.-Y. Zhao, M. San, J.-L. H. A. Duprey, J. R. Arrand, J. S. Vyle, and J. H. R. Tucker. Detection of single nucleotide polymorphisms within a sequence of a gene associated with prostate cancer using a fluorophore-tagged DNA probe. *Bioorg. Med. Chem. Lett.*, 22:129–32, 2012.

[89] O. Köhler, D. V. Jarikote, and O. Seitz. Forced intercalation probes (FIT Probes): Thiazole orange as a fluorescent base in peptide nucleic acids for homogeneous single-nucleotide-polymorphism detection. *ChemBioChem*, 6:69–77, 2005.

[90] F. Hövelmann, L. Bethge, and O. Seitz. Single labeled DNA FIT probes for avoiding false-positive signaling in the detection of DNA/RNA in qPCR or cell media. *Chembiochem*, 13:2072–81, 2012.

[91] H. Asanuma, M. Akahane, R. Niwa, H. Kashida, and Y. Kamiya. Highly Sensitive and Robust Linear Probe for Detection of mRNA in Cells. *Angew. Chemie*, 54:4315–4319, 2015.

[92] S. P. Jonstrup, J. Koch, and J. Kjems. A microRNA detection system based on padlock probes and rolling circle amplification. *RNA*, 12:1747–1752, 2006.

[93] J. Houseley and D. Tollervey. The Many Pathways of RNA Degradation. *Cell*, 136:763–776, 2009.

[94] S. Kummer, A. Knoll, E. Socher, L. Bethge, A. Herrmann, and O. Seitz. Fluorescence imaging of influenza H1N1 mRNA in living infected cells using single-chromophore FIT-PNA. *Angew. Chem. Int. Ed. Engl.*, 50:1931–4, 2011.

[95] E. Socher, A. Knoll, and O. Seitz. Dual fluorophore PNA FIT-probes- extremely responsive and bright hybridization probes for the sensitive detection of DNA and RNA. *Org. Biomol. Chem.*, 10:7363, 2012.

[96] L. Dahan, L. Huang, R. Kedmi, M. A. Behlke, and D. Peer. SNP Detection in mRNA in Living Cells Using Allele Specific FRET Probes. *PLoS One*, 8:e72389, 2013.

[97] J. M. Levsky and R. H. Singer. Fluorescence in situ hybridization: past, present and future. *J. Cell Sci.*, 116:2833–8, 2003.

[98] M. Nilsson, H. Malmgren, M. Samiotaki, M. Kwiatkowski, B. P. Chowdhary, and U. Landegren. Padlock probes: circularizing oligonucleotides for localized DNA detection. *Science*, 265:2085–8, 1994.

[99] J. Banér, M. Nilsson, M. Mendel-Hartvig, and U. Landegren. Signal amplification of padlock probes by rolling circle replication. *Nucleic Acids Res.*, 26:5073–8, 1998.

[100] S. Bakht and X. Qi. Ligation-mediated rolling-circle amplification-based approaches to single nucleotide polymorphism detection. *Expert Rev. Mol. Diagn.*, 5:111–116, 2005.

[101] C. Larsson, J. Koch, A. Nygren, G. Janssen, A. K. Raap, U. Landegren, and M. Nilsson. In situ genotyping individual DNA molecules by target-primed rolling-circle amplification of padlock probes. *Nat. Methods*, 1:227–32, 2004.

[102] Y. Tanaka, H. Xi, K. Sato, K. Mawatari, B. Renberg, M. Nilsson, and T. Kitamori. Single-molecule DNA patterning and detection by padlock probing and rolling circle amplification in microchannels for analysis of small sample volumes. *Anal. Chem.*, 83:3352–3357, 2011.

[103] S. Boulon, E. Basyuk, J. M. Blanchard, E. Bertrand, and C. Verheggen. Intranuclear RNA trafficking: insights from live cell imaging. *Biochimie*, 84:805–13, 2002.

[104] J. C. Politz, E. S. Browne, D. E. Wolf, and T. Pederson. Intranuclear diffusion and hybridization state of oligonucleotides measured by fluorescence correlation spectroscopy in living cells. *Proc. Natl. Acad. Sci. U. S. A.*, 95:6043–8, 1998.

[105] D. P. Bratu, B.-J. Cha, M. M. Mhlanga, F. R. Kramer, and S. Tyagi. Visualizing the distribution and transport of mRNAs in living cells. *Proc. Natl. Acad. Sci. U. S. A.*, 100:13308–13, 2003.

[106] G. Bao, W. J. Rhee, and A. Tsourkas. Fluorescent probes for live-cell RNA detection. *Annu. Rev. Biomed. Eng.*, 11:25–47, 2009.

[107] A. E. Prigodich, P. S. Randeria, W. E. Briley, N. J. Kim, W. L. Daniel, D. A. Giljohann, and C. A. Mirkin. Multiplexed nanoflares: MRNA detection in live cells. *Anal. Chem.*, 84:2062–2066, 2012.

[108] S. Kummer, A. Knoll, E. Socher, L. Bethge, A. Herrmann, and O. Seitz. PNA FIT-probes for the dual color imaging of two viral mRNA targets in influenza H1N1 infected live cells. *Bioconjug. Chem.*, 23:2051–60, 2012.

[109] T. Kubota, S. Ikeda, and A. Okamoto. Doubly Thiazole Orange-Labeled DNA for Live Cell RNA Imaging. *Bull. Chem. Soc. Jpn.*, 82:110–117, 2009.

[110] G. G. Jayaraj, S. Nahar, and S. Maiti. Nonconventional chemical inhibitors of microRNA: therapeutic scope. *Chem. Commun.*, 51:820–831, 2015.

[111] A. Järve, J. Müller, I.-H. Kim, K. Rohr, C. MacLean, G. Fricker, U. Massing, F. Eberle, A. Dalpke, R. Fischer, M. F. Trendelenburg, and M. Helm. Surveillance of siRNA integrity by FRET imaging. *Nucleic Acids Res.*, 35:e124, 2007.

[112] C. Larsson, I. Grundberg, O. Söderberg, and M. Nilsson. In situ detection and genotyping of individual mRNA molecules. *Nat. Methods*, 7:395–7, 2010.

[113] I. Weibrecht, I. Grundberg, M. Nilsson, and O. Söderberg. Simultaneous visualization of both signaling cascade activity and end-point gene expression in single cells. *PLoS One*, 6, 2011.

[114] A. Okamoto, K. Sugizaki, M. Yuki, H. Yanagisawa, S. Ikeda, T. Sueoka, G. Hayashi, and D. O. Wang. A nucleic acid probe labeled with desmethyl thiazole orange: a new type of hybridization-sensitive fluorescent oligonucleotide for live-cell RNA imaging. *Org. Biomol. Chem.*, 11:362–71, 2013.

[115] T. Kubota, S. Ikeda, H. Yanagisawa, M. Yuki, and A. Okamoto. Sets of RNA repeated tags and hybridization-sensitive fluorescent probes for distinct images of RNA in a living cell. *PLoS One*, 5:e13003, 2010.

[116] R. W. Dirks, C. Molenaar, and H. J. Tanke. Methods for visualizing RNA processing and transport pathways in living cells. *Histochem. Cell Biol.*, 115:3–11, 2001.

[117] R. W. Dirks, C. Molenaar, and H. J. Tanke. Visualizing RNA molecules inside the nucleus of living cells. *Methods*, 29:51–57, 2003.

[118] V. J. LaMorte, J. A. Dyck, R. L. Ochs, and R. M. Evans. Localization of nascent RNA and CREB binding protein with the PML-containing nuclear body. *Proc. Natl. Acad. Sci. U. S. A.*, 95:4991–4996, 1998.

[119] R. M. Martin, H. Leonhardt, and M. C. Cardoso. DNA labeling in living cells. *Cytom. Part A*, 67:45–52, 2005.

[120] F.-S. Du, Y. Wang, R. Zhang, and Z.-C. Li. Intelligent nucleic acid delivery systems based on stimuli-responsive polymers. *Soft Matter*, 6:835–848, 2010.

[121] A. Tsuji, H. Koshimoto, Y. Sato, M. Hirano, Y. Sei-iida, and S. Kondo. Direct Observation of Specific Messenger RNA in a Single Living Cell. *Biophys. J.*, 78:3260–3274, 2000.

[122] B. D. Brown and L. Naldini. Exploiting and antagonizing microRNA regulation for therapeutic and experimental applications. *Nat. Rev. Genet.*, 10:578–585, 2009.

[123] K. Wang, J. Huang, X. Yang, X. He, and J. Liu. Recent Advances of Fluorescent Nucleic Acid Probes for Living Cell Studies. *Analyst*, 138:62–71, 2012.

[124] Z. Wang, K. Zhang, Y. Shen, J. Smith, S. Bloch, S. Achilefu, K. L. Wooley, and J.-S. Taylor. Imaging mRNA expression levels in living cells with PNA:DNA binary FRET probes delivered by cationic shell-crosslinked nanoparticles. *Org. Biomol. Chem.*, 11:3159–67, 2013.

[125] A. M. Femino. Visualization of Single RNA Transcripts In Situ. *Science*, 280:585–590, 1998.

[126] C. H. Hansen and A. van Oudenaarden. Allele-specific detection of single mRNA molecules in situ. *Nat. Methods*, 10:869–71, 2013.

[127] Y. Cheng, Z. Li, X. Zhang, B. Du, and Y. Fan. Homogeneous and label-free fluorescence detection of single-nucleotide polymorphism using target-primed branched rolling circle amplification. *Anal. Biochem.*, 378:123–126, 2008.

[128] X. Zhang, Y. Xiao, and X. Qian. A ratiometric fluorescent probe based on FRET for imaging Hg2+ ions in living cells. *Angew. Chemie - Int. Ed.*, 47:8025–8029, 2008.

[129] M. Tian and H. Ihmels. Selective ratiometric detection of mercury(II) ions in water with an acridizinium-based fluorescent probe. *Chem. Commun.*, pages 3175–3177, 2009.

[130] L. Yuan, W. Lin, Y. Xie, B. Chen, and J. Song. Development of a ratiometric fluorescent sensor for ratiometric imaging of endogenously produced nitric oxide in macrophage cells. *Chem. Commun.*, 47:9372–4, 2011.

[131] K. K. Ogilvie, N. Usman, K. Nicoghosian, and R. J. Cedergren. Total chemical synthesis of a 77-nucleotide-long RNA sequence having methionine-acceptance activity. *Proc. Natl. Acad. Sci. U. S. A.*, 85:5764–5768, 1988.

[132] C. V. Kumar, E. H. A. Punzalan, and W. B. Tan. Adenine-Thymine Base Pair Recognition by an Anthryl Probe from the DNA Minor Groove. *Tetrahedron*, 56:7027–7040, 2000.

[133] J. Kypr, I. Kejnovská, D. Renciuk, and M. Vorlícková. Circular dichroism and conformational polymorphism of DNA. *Nucleic Acids Res.*, 37:1713–25, 2009.

[134] A. Rodger, I. S. Blagbrough, G. Adlam, and M. L. Carpenter. DNA binding of a spermine derivative: spectroscopic study of anthracene-9-carbonyl-N1-spermine with poly[d(G-C).(d(G-C)] and poly[d(A-T).d(A-T)]. *Biopolymers*, 34:1583–93, 1994.

[135] S. Wang and E. T. Kool. Origins of the large differences in stability of DNA and RNA helices: C-5 methyl and 2'-hydroxyl effects. *Biochemistry*, 34:4125–32, 1995.

[136] C. L. Clark, P. K. Cecil, D. Singh, and D. M. Gray. CD, absorption and thermodynamic analysis of repeating dinucleotide DNA, RNA and hybrid duplexes [d/r(AC)] 12 [d/r(GT/U)]12 and the influence of phosphorothioate substitution. *Nucleic Acids Res.*, 25:4098–4105, 1997.

[137] D. M. Gray and R. L. Ratliff. Circular dichroism spectra of poly[d(AC):d(GT)], poly[r(AC):r(GU)], and hybrids poly[d(AC):r(GU)] and poly[r(AC):d(GT)] in the presence of ethanol. *Biopolymers*, 14:487–98, 1975.

[138] I. Inoue, Y. Hayase, A. Imura, S. Iwai, K. Miura, and E. Ohtsuka. Synthesis and hybridisation studies on two complementary nona(2'-O-methyl)ribonucleotides. *Nucleic Acids Res.*, 15:6131–6148, 1987.

[139] S. Kumar, K. Mapa, and S. Maiti. Understanding the effect of locked nucleic acid and 2'-O-methyl modification on the hybridization thermodynamics of a miRNA-mRNA pair in the presence and absence of AfPiwi protein. *Biochemistry*, 53:1607–15, 2014.

[140] E. A. Lesnik and S. M. Freier. Relative thermodynamic stability of DNA, RNA, and DNA:RNA hybrid duplexes: relationship with base composition and structure. *Biochemistry*, 34:10807–15, 1995.

[141] E. A. Lesnik and S. M. Freier. What affects the effect of 2'-alkoxy modifications? 1. Stabilization effect of 2'-methoxy substitutions in uniformly modified DNA oligonucleotides. *Biochemistry*, 37:6991–7, 1998.

[142] S. M. Freier and K. H. Altmann. The ups and downs of nucleic acid duplex stability: structure-stability studies on chemically-modified DNA:RNA duplexes. *Nucleic Acids Res.*, 25:4429–43, 1997.

[143] M. Kozurková, D. Sabolová, H. Paulíková, L. Janovec, P. Kristian, M. Bajdichová, J. Busa, D. Podhradský, and J. Imrich. DNA binding properties and evaluation of cytotoxic activity of 9,10-bis-N-substituted (aminomethyl)anthracenes. *Int. J. Biol. Macromol.*, 41:415–22, 2007.

[144] N. K. Modukuru, K. J. Snow, B. S. Perrin, J. Thota, and C. V. Kumar. Contributions of a long side chain to the binding affinity of an anthracene derivative to DNA. *J. Phys. Chem. B*, 109:11810–8, 2005.

[145] F. J. Hernandez, K. R. Stockdale, L. Huang, A. R. Horswill, M. A. Behlke, and J. O. McNamara. Degradation of Nuclease-Stabilized RNA Oligonucleotides in

Mycoplasma-Contaminated Cell Culture Media. *Nucleic Acid Ther. (Formerly Oligonucleotides)*, 22:120109070352007, 2012.

[146] M. J. Sø e, T. Mø ller, M. Dufva, and K. Holmstrø m. A sensitive alternative for microRNA in situ hybridizations using probes of 2'-O-methyl RNA + LNA. *J. Histochem. Cytochem.*, 59:661–72, 2011.

[147] M. A. Behlke. Chemical modification of siRNAs for in vivo use. *Oligonucleotides*, 18:305–19, 2008.

[148] T. L. Fisher, T. Terhorst, X. Cao, and R. W. Wagner. Intracellular disposition and metabolism of fluorescently-labeled unmodified and modified oligonucleotides microinjected into mammalian cells. *Nucleic Acids Res.*, 21:3857–65, 1993.

[149] J. P. Leonetti, N. Mechti, G. Degols, C. Gagnor, and B. Lebleu. Intracellular distribution of microinjected antisense oligonucleotides. *Proc. Natl. Acad. Sci. U. S. A.*, 88:2702–6, 1991.

[150] S. Chesnoy and L. Huang. Structure and function of lipid-DNA complexes for gene delivery. *Annu. Rev. Biophys. Biomol. Struct.*, 29:27–47, 2000.

[151] T. Endoh and T. Ohtsuki. Cellular siRNA delivery using cell-penetrating peptides modified for endosomal escape. *Adv. Drug Deliv. Rev.*, 61:704–9, 2009.

[152] N. Nitin, P. J. Santangelo, G. Kim, S. Nie, and G. Bao. Peptide-linked molecular beacons for efficient delivery and rapid mRNA detection in living cells. *Nucleic Acids Res.*, 32:e58, 2004.

[153] C. A. Stein, J. B. Hansen, J. Lai, S. Wu, A. Voskresenskiy, A. Hø g, J. Worm, M. Hedtjärn, N. Souleimanian, P. Miller, H. S. Soifer, D. Castanotto, L. Benimetskaya, H. Ø rum, and T. Koch. Efficient gene silencing by delivery of locked nucleic

acid antisense oligonucleotides, unassisted by transfection reagents. *Nucleic Acids Res.*, 38:e3, 2010.

[154] S. Sixou. Intracellular oligonucleotide hybridisation detected by fluorescence resonance energy transfer (FRET). *Nucleic Acids Res.*, 22:662–668, 1994.

[155] K.'i. Hirano. Detection of Undegraded Oligonucleotides in Vivo by Fluorescence Resonance Energy Transfer. *J. Biol. Chem.*, 271:380–384, January 1996.

[156] E. Neumann. Gene transfer into mouse lyoma cells by electroporation in high electric fields. *EMBO J.*, 1:841–845, 1982.

[157] K. E. Sapsford, L. Berti, and I. L. Medintz. Materials for fluorescence resonance energy transfer analysis: beyond traditional donor-acceptor combinations. *Angew. Chem. Int. Ed. Engl.*, 45:4562–89, 2006.

[158] A. Karadag, M. Riminucci, P. Bianco, N. Cherman, S. A. Kuznetsov, N. Nguyen, M. T. Collins, P. G. Robey, and L. W. Fisher. A novel technique based on a PNA hybridization probe and FRET principle for quantification of mutant genotype in fibrous dysplasia/McCune-Albright syndrome. *Nucleic Acids Res.*, 32:e63, 2004.

[159] J. L. Mergny, A. S. Boutorine, T. Garestier, F. Belloc, M. Rougée, N. V. Bulychev, A. A. Koshkin, J. Bourson, A. V. Lebedev, and B. Valeur. Fluorescence energy transfer as a probe for nucleic acid structures and sequences. *Nucleic Acids Res.*, 22:920–8, 1994.

[160] M. Masuko, S. Ohuchi, K. Sode, H. Ohtani, and A. Shimadzu. Fluorescence resonance energy transfer from pyrene to perylene labels for nucleic acid hybridization assays under homogeneous solution conditions. *Nucleic Acids Res.*, 28:E34, 2000.

[161] P. Jothikumar, V. Hill, and J. Narayanan. Design of FRET-TaqMan probes for

multiplex real-time PCR using an internal positive control. *Biotechniques*, 46:519–24, 2009.

[162] M. Emig, S. Saussele, H. Wittor, A. Weisser, A. Reiter, A. Willer, U. Berger, R. Hehlmann, N. C. Cross, and A. Hochhaus. Accurate and rapid analysis of residual disease in patients with CML using specific fluorescent hybridization probes for real time quantitative RT-PCR. *Leukemia*, 13:1825–32, 1999.

[163] M. M. Mhlanga and L. Malmberg. Using molecular beacons to detect single-nucleotide polymorphisms with real-time PCR. *Methods*, 25:463–71, 2001.

[164] R. A. Cardullo, S. Agrawal, C. Flores, P. C. Zamecnik, and D. E. Wolf. Detection of nucleic acid hybridization by nonradiative fluorescence resonance energy transfer. *Proc. Natl. Acad. Sci. U. S. A.*, 85:8790–4, 1988.

[165] R. M. Clegg, A. I. Murchie, A. Zechel, and D. M. Lilley. Observing the helical geometry of double-stranded DNA in solution by fluorescence resonance energy transfer. *Proc. Natl. Acad. Sci. U. S. A.*, 90:2994–8, 1993.

[166] L. E. Morrison, T. C. Halder, and L. M. Stols. Solution-phase detection of polynucleotides using interacting fluorescent labels and competitive hybridization. *Anal. Biochem.*, 183:231–44, 1989.

[167] S. Dokka and Y. Rojanasakul. Novel non-endocytic delivery of antisense oligonucleotides. *Adv. Drug Deliv. Rev.*, 44:35–49, 2000.

[168] I. H. Pastan and M. C. Willingham. Journey to the center of the cell: role of the receptosome. *Science*, 214:504–9, 1981.

[169] G. M. Barton and R. Medzhitov. Retroviral delivery of small interfering RNA into primary cells. *Proc. Natl. Acad. Sci. U. S. A.*, 99:14943–5, 2002.

[170] M. Dominska and D. M. Dykxhoorn. Breaking down the barriers: siRNA delivery and endosome escape. *J. Cell Sci.*, 123:1183–9, 2010.

[171] N. C. Price and L. Stevens. *Fundamentals of Enzymology: The cell and molecular biology of catalytic proteins*. Oxford University Press, 1999.

[172] H. A. J. Alwan, E. J. J. van Zoelen, and J. E. M. van Leeuwen. Ligand-induced lysosomal epidermal growth factor receptor (EGFR) degradation is preceded by proteasome-dependent EGFR de-ubiquitination. *J. Biol. Chem.*, 278:35781–90, 2003.

[173] A. Yamamoto, Y. Tagawa, T. Yoshimori, Y. Moriyama, R. Masaki, and Y. Tashiro. Bafilomycin A1 prevents maturation of autophagic vacuoles by inhibiting fusion between autophagosomes and lysosomes in rat hepatoma cell line, H-4-II-E cells. *Cell Struct. Funct.*, 23:33–42, 1998.

[174] H. Ginsburg and T. G. Geary. Current concepts and new ideas on the mechanism of action of quinoline-containing antimalarials. *Biochem. Pharmacol.*, 36:1567–1576, 1987.

[175] F. L. Graham and A. J. van der Eb. A new technique for the assay of infectivity of human adenovirus 5 DNA. *Virology*, 52:456–467, 1973.

[176] M. Wigler, S. Silverstein, L. S. Lee, A. Pellicer, Y. C. Cheng, and R. Axel. Transfer of purified herpes virus thymidine kinase gene to cultured mouse cells. *Cell*, 11:223–232, 1977.

[177] P. L. McNeil, R. F. Murphy, F. Lanni, and D. L. Taylor. A method for incorporating macromolecules into adherent cells. *J. Cell Biol.*, 98:1556–1564, 1984.

[178] E. G. Diacumakos. Microsurgically fused human somatic cell hybrids: analysis and cloning. *Proc. Natl. Acad. Sci. U. S. A.*, 70:3382–6, 1973.

[179] M. R. Capecchi. High efficiency transformation by direct microinjection of DNA into cultured mammalian cells. *Cell*, 22:479–88, 1980.

[180] Y. Zhang and L.-C. Yu. Single-cell microinjection technology in cell biology. *BioEssays*, 30:606–610, June 2008.

[181] M.-C. Saleh, R. P. van Rij, A. Hekele, A. Gillis, E. Foley, P. H. O'Farrell, and R. Andino. The endocytic pathway mediates cell entry of dsRNA to induce RNAi silencing. *Nat. Cell Biol.*, 8:793–802, 2006.

[182] B. Gupta, T. S. Levchenko, and V. P. Torchilin. Intracellular delivery of large molecules and small particles by cell-penetrating proteins and peptides. *Adv. Drug Deliv. Rev.*, 57:637–51, 2005.

[183] V. P. Torchilin. Recent approaches to intracellular delivery of drugs and DNA and organelle targeting. *Annu. Rev. Biomed. Eng.*, 8:343–75, 2006.

[184] J. S. Jepsen, M. D. Sø rensen, and J. Wengel. Locked nucleic acid: a potent nucleic acid analog in therapeutics and biotechnology. *Oligonucleotides*, 14:130–46, 2004.

[185] D. L. Sokol, X. Zhang, P. Lu, and A. M. Gewirtz. Real time detection of DNA.RNA hybridization in living cells. *Proc. Natl. Acad. Sci. U. S. A.*, 95:11538–43, 1998.

[186] S. Paillasson, M. Van De Corput, R. W. Dirks, H. J. Tanke, M. Robert-Nicoud, and X. Ronot. In situ hybridization in living cells: detection of RNA molecules. *Exp. Cell Res.*, 231:226–233, 1997.

[187] R. Y. Tsien, L. Ernst, and A. Waggoner. Fluorophores for confocal microscopy: Photophysics and photochemistry. In *Handb. Biol. Confocal Microsc. Third Ed.* Springer, 2006.

[188] R. T. Ranasinghe, T. Brown, and L. J. Brown. Linear fluorescent oligonucleotide

probes with an acridine quencher generate a signal upon hybridisation. *Chem. Commun.*, pages 1480–1481, 2001.

[189] N. Houba-Herin, J. De Graeve, C. M. Calberg-Bacq, and A. Van de Vorst. Characterization of five commercially available samples of acridine yellow. *Stain Technol.*, 58:161–70, 1983.

[190] K. Fukui, K. Iwane, T. Shimidzu, and K. Tanaka. Oligonucleotides covalently linked to an acridine at artificial abasic site: Influence of linker length and the base-sequence. *Tetrahedron Lett.*, 37:4983–4986, 1996.

[191] S. Nafisi, A. A. Saboury, N. Keramat, J.-F. Neault, and H.-A. Tajmir-Riahi. Stability and structural features of DNA intercalation with ethidium bromide, acridine orange and methylene blue. *J. Mol. Struct.*, 827:35–43, 2007.

[192] J. Zhang, Y. Fu, C. V. Conroy, Z. Tang, G. Li, R. Y. Zhao, and G. Wang. Fluorescence Intensity and Lifetime Cell Imaging with Luminescent Gold Nanoclusters. *J. Phys. Chem. C. Nanomater. Interfaces*, 116, 2012.

[193] K. Kawai, Y. Osakada, M. Fujitsuka, and T. Majima. Charge separation in acridine- and phenothiazine-modified DNA. *J. Phys. Chem. B*, 112:2144–9, 2008.

[194] C. A. M. Seidel, A. Schulz, and M. H. M. Sauer. Nucleobase-Specific Quenching of Fluorescent Dyes. 1. Nucleobase One-Electron Redox Potentials and Their Correlation with Static and Dynamic Quenching Efficiencies. *J. Phys. Chem.*, 100:5541–5553, 1996.

[195] D. Weicherding, W. B. Davis, S. Hess, T. von Feilitzsch, M. E. Michel-Beyerle, and U. Diederichsen. Femtosecond time-resolved guanine oxidation in acridine modified alanyl peptide nucleic acids. *Bioorg. Med. Chem. Lett.*, 14:1629–32, 2004.

[196] J. G. Pickering, J. M. Isner, C. M. Ford, L. Weir, A. Lazarovits, E. F. Rocnik, and L. H. Chow. Processing of chimeric antisense oligonucleotides by human vascular smooth muscle cells and human atherosclerotic plaque. Implications for antisense therapy of restenosis after angioplasty. *Circulation*, 93:772–780, 1996.

[197] X. Zhuang, T. Wang, and P. Zhang. A highly robust estimator through partially likelihood function modeling and its application in computer vision. *IEEE Trans. Pattern Anal. Mach. Intell.*, 14:19–35, 1992.

[198] A. Boulmerka, M. Saïd Allili, and S. Ait-Aoudia. A generalized multiclass histogram thresholding approach based on mixture modelling. *Pattern Recognit.*, 47:1330–1348, 2014.

[199] Y.-R. Lai, K.-L. Chung, G.-Y. Lin, and C.-H. Chen. Gaussian mixture modeling of histograms for contrast enhancement. *Expert Syst. Appl.*, 39:6720–6728, 2012.

[200] J.-H. Chang, K.-C. Fan, and Y.-L. Chang. Multi-modal gray-level histogram modeling and decomposition. *Image Vis. Comput.*, 20:203–216, 2002.

[201] E. Bertin and S. Arnouts. SExtractor: Software for source extraction. *Astron. Astrophys. Suppl. Ser.*, 117:393–404, 1996.

[202] Y. Chen, Z.-P. Chen, J. Yang, J.-W. Jin, J. Zhang, and R.-Q. Yu. Quantitative fluorescence spectroscopy in turbid media: a practical solution to the problem of scattering and absorption. *Anal. Chem.*, 85:2015–20, 2013.

[203] G. Trichas, J. Begbie, and S. Srinivas. Use of the viral 2A peptide for bicistronic expression in transgenic mice. *BMC Biol.*, 6:40, 2008.

[204] S. I. Rudnick, J. Swaminathan, M. Sumaroka, S. Liebhaber, and A. M. Gewirtz. Effects of local mRNA structure on posttranscriptional gene silencing. *Proc. Natl. Acad. Sci. U. S. A.*, 105:13787–13792, 2008.

[205] N. Ramsay, A. S. Jemth, A. Brown, N. Crampton, P. Dear, and P. Holliger. CyDNA: Synthesis and replication of highly Cy-Dye substituted DNA by an evolved polymerase. *J. Am. Chem. Soc.*, 132:5096–5104, 2010.

[206] M. Levitus and S. Ranjit. Cyanine dyes in biophysical research: the photophysics of polymethine fluorescent dyes in biomolecular environments. *Q. Rev. Biophys.*, 44:123–51, 2011.

[207] T. Kato, H. Kashida, H. Kishida, H. Yada, H. Okamoto, and H. Asanuma. Development of a robust model system of FRET using base surrogates tethering fluorophores for strict control of their position and orientation within DNA duplex. *J. Am. Chem. Soc.*, 135:741–50, 2013.

[208] D. G. Norman, R. J. Grainger, D. Uhrín, and D. M. Lilley. Location of cyanine-3 on double-stranded DNA: importance for fluorescence resonance energy transfer studies. *Biochemistry*, 39:6317–6324, 2000.

[209] J. B. Randolph and A. S. Waggoner. Stability, specificity and fluorescence brightness of multiply-labeled fluorescent DNA probes. *Nucleic Acids Res.*, 25:2923–9, 1997.

[210] E. Socher, L. Bethge, A. Knoll, N. Jungnick, A. Herrmann, and O. Seitz. Low-noise stemless PNA beacons for sensitive DNA and RNA detection. *Angew. Chemie - Int. Ed.*, 47:9555–9559, 2008.

[211] C. V. Kumar and E. H. Asuncion. DNA binding studies and site selective fluorescence sensitization of an anthryl probe. *J. Am. Chem. Soc.*, 115:8547–8553, 1993.

[212] A. Tsuji, Y. Sato, M. Hirano, T. Suga, H. Koshimoto, T. Taguchi, and S. Ohsuka. Development of a time-resolved fluorometric method for observing hybridization

in living cells using fluorescence resonance energy transfer. *Biophys. J.*, 81:501–15, 2001.

[213] W. Lee, P. H. Von Hippel, and A. H. Marcus. Internally labeled Cy3/Cy5 DNA constructs show greatly enhanced photo-stability in single-molecule FRET experiments. *Nucleic Acids Res.*, 42:5967–5977, 2014.

[214] M. Monici. Cell and tissue autofluorescence research and diagnostic applications. *Biotechnol. Annu. Rev.*, 11:227–56, 2005.